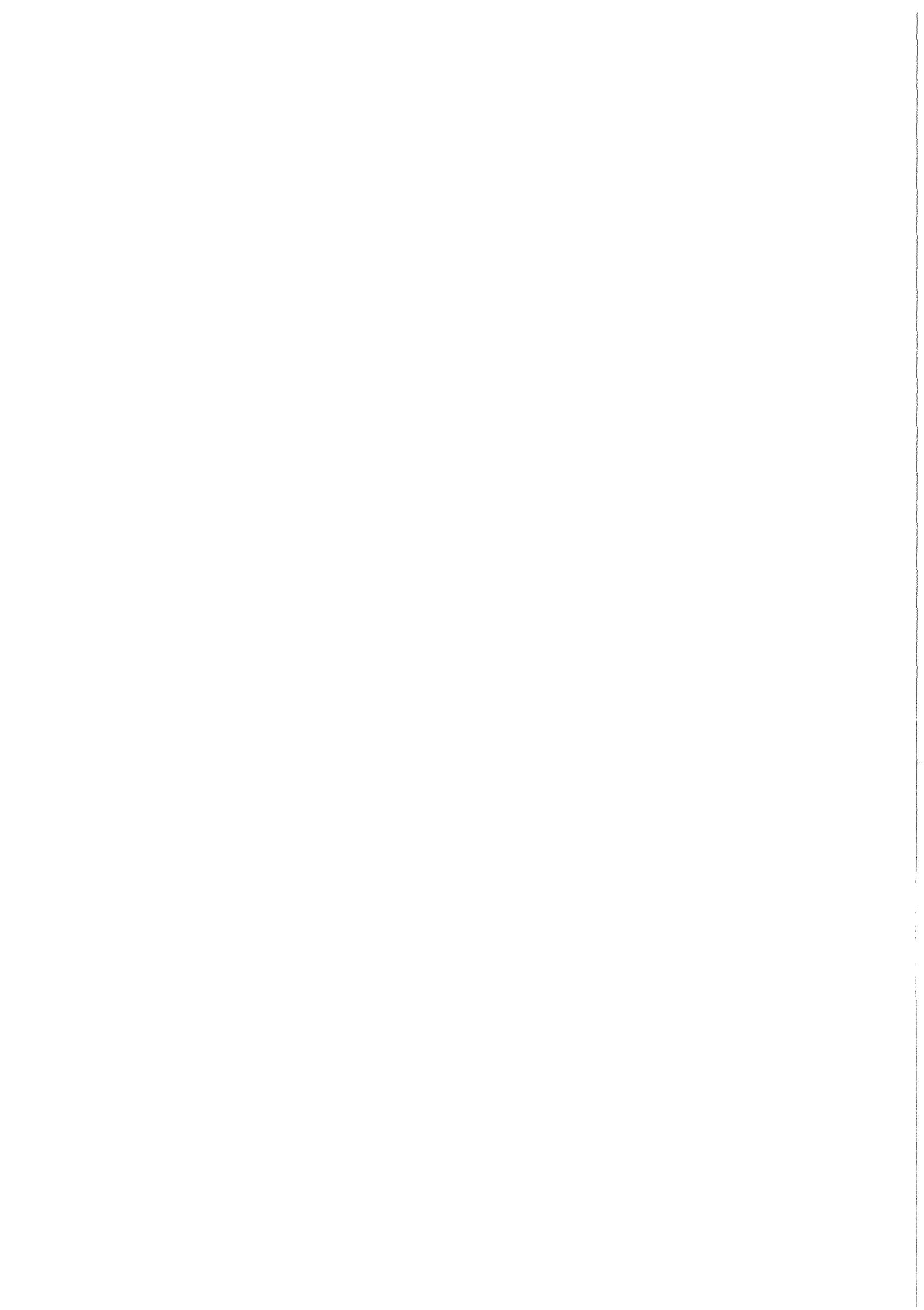# Annual Report on Nuclear Physics Activities

July 1, 1984 - June 30, 1985

Editors:
K. Bekk, P. Doll, Ch. Weddigen
Institut für Kernphysik

Kernforschungszentrum Karlsruhe

KERNFORSCHUNGSZENTRUM KARLSRUHE

Institut für Kernphysik

KfK 3969

ANNUAL REPORT

on

NUCLEAR PHYSICS ACTIVITIES

July 1, 1984 - June 30, 1985

Editors:

K. Bekk, P. Doll, and Ch. Weddigen

Kernforschungszentrum Karlsruhe GmbH, Karlsruhe

Last Annual Reports:

1983/84: KfK 3815 (Oktober 1984)

1982/83: KfK 3621 (November 1983)

1981/82: KfK 3427 (November 1982)

1980/81: KfK 3280 (Februar 1982)

ABSTRACT

This report surveys the activities in basic research from July 1, 1984 to
June 30, 1985 at the Institute for Nuclear Phsysics (IK) of the Kernforschungs-
zentrum Karlsruhe. The research program of this institute comprises laser
spectroscopy, nuclear reactions with light ions, neutron pyhsics, neutrino
physics and physics at medium and high energies.

ZUSAMMENFASSUNG

Der vorliegende Bericht gibt einen Überblick über die Arbeiten am Institut für
Kernphysik (IK) des Kernforschungszentrums Karlsruhe im Zeitraum vom 1. Juli
1984 bis zum 30. Juni 1985. Das Forschungsprogramm umfaßt die Gebiete Laser-
spektroskopie, Kernreaktionen mit leichten Ionen, Neutronenphysik, Neutrino-
Physik, sowie Mittel- und Hochenergiephysik.

PREFACE

This is the fifth annual report on nuclear physics activities at the Kernforschungszentrum Karlsruhe. These activities are carried out in the Institute of Nuclear Research (IK), which consists of three sections (IK I, IK II, IK III). Each section specialises in different energy regions.

Three groups in Section IK I are engaged in work in various fields of nuclear physics and particle physics:

- Fast Neutron Physics: Scattering experiments on very light nuclei are carried out using the polarized neutron beam of the Karlsruhe Cyclotron (POLKA). The main goal is to determine precise phase shifts from experiments with polarized neutrons on unpolarized and also on polarized protons. Moreover, the internal structure and dynamics of the nuclei up to the $A = 5$ system are to be studied. The large-volume polarized proton target has been successfully used for scattering experiments with the polarized neutron beam in a number of experiments.

- High Energy Physics: This group runs the CELLO detector system at the e^+e^- storage ring, PETRA, in Hamburg within the framework of an international collaboration. The detector serves for experiments to study e^+e^- collisions at the highest energies at present attainable. CELLO, with its modern liquid-argon calorimeter, lends itself particularly well to studies of the electromagnetic component in these reactions. This allows, e.g., precise studies of quantum electrodynamics, detailed studies of quark and gluon jets and the search for new quarks. The upgraded detector is working satisfactorily and is strongly involved in the search for a new quark during the continuous energy increases in PETRA. This work, carried out in cooperation with Karlsruhe University, was partly supported by BMFT through the 'Verbund Hochenergiephysik'.

- Neutrino Physics: The newly founded working group is concerned with neutrino physics in the energy range between approximately 10 and 50 MeV, at the Spallation Neutron Source (SNS) under construction at the Rutherford-Appleton Laboratory (RAL) in England. This is a new field of work involving fundamental questions in the fields of elementary particle physics, nuclear physics and astrophysics. The project was proposed by KfK. In the meantime, a bilateral agreement has been signed between KfK and RAL. Several smaller working groups of the University of Oxford (Prof. Dr. N.E. Booth), Queen Mary College of London (Prof. Dr. J.A. Edgington), and University of Erlangen (Prof. Dr. E. Finckh) have meanwhile joined the project. The detector system is being developed at KfK.

It will be installed in a massive blockhouse of iron at the Rutherford SNS until summer of 1986. This work, carried out in cooperation with Karlsruhe University, was partly supported by BMFT through the 'Verbund Mittelenergiephysik'.

Section IK II is mostly working on medium energy physics at CERN and SIN:

- One group, continuing a long tradition in the field of exotic atoms at CERN, has concentrated its activities on the LEAR facility (Low-Energy Antiproton Ring). This instrument, the realization of which was backed very strongly by Karlsruhe, offers unique possibilities for work with slow antiprotons. Antiprotonic X-ray-spectra of selected elements were obtained. They contain new information on the strong interaction of antiproton-nucleon pairs, on the magnetic moment of the antiproton, and on the spin-orbit coupling for antiprotons. Another experiment makes use of the idea of the cyclotron trap proposed by Dr. L.M. Simons, which permits measurements at low gas pressure, where Stark mixing is small. The aim is the study of antiprotonic Hydrogen and Deuterium, the most direct approach to the antiproton-nucleon system. Karlsruhe is involved personally and financially also in a technical upgrading of LEAR, namely the use of electron cooling. A workshop "ECOOL 84", held at KfK, showed the wide interest in this subject. For future LEAR experiments a 4π-detector for both changed and neutral reaction products is being planned in collaboration a number of university groups from Germany, Europe and the U.S.

- The experiments at SIN focus on problems of pion interaction (scattering and absorption) with simple systems consisting of few nucleons. Theoretical assumptions, especially those about the existence of dibaryon states, are verified on the basis of additional information that can be obtained by using polarized targets. Also the low-energy spectrometer LEPS designed by Karlsruhe, which will come into operation in fall of 1985, will mainly be used in studies of very simple systems at energies close to the pion threshold. The Coulomb nuclear interferences have been studied in experiments on Hydrogen and gave results at variance with QCD predictions. Absorption measurements of pion in ^{3}He show an unexpected isospin-dependence of the basic two-nucleon-absorption process and an unexpectedly large contribution of three-pion-absorption. This reaction is of great theoretical significance.

Section IK III is mainly working in the following fields:

- Nuclear astrophysics: Capture cross sections of fast neutrons in the keV to MeV range are measured in order to understand in detail the build-up of heavy elements in stars. Work in this area has concentrated on building up a novel 4π scintillation detector to improve the accuracy of such elements considerably.

- Nuclear reactions: Beams of heavy ions, especially of ^{6}Li, at 26 MeV/nucleon from the Karlsruhe Isochronous Cyclotron are used to study the momentum distribution of nucleons in nuclei via projectile break-up in nuclear collisions. A small magnetic spectrometer specifically designed for the measurement of continuous spectra has come into operation and represents a considerable improvement of our experimental capabilities for this kind of experiments.

- Laser spectroscopy: This technique is applied to sub-ng amounts of radioactive atoms in order to determine hyperfine structure and isotopic shifts of atomic transitions. The results yield information on nuclear moments and on the change of nuclear charge radii due to varying neutron number. At present nuclides of the elements strontium and americium are studied.

- Applied gamma-ray spectroscopy: Here instruments are developed to determine concentration and isotopic composition of fissile material. The instruments make use either of the intrinsic radioactivity or of X-ray absorption and fluorescence. Their main applications are in the safeguards of nuclear fuel and in process control during fabrication and reprocessing.

- Section IK III is also responsible for operating the three accelerators of our institute: The Karlsruhe Isochronous Cyclotron which is mainly used for fast neutron physics and nuclear reaction experiments; the 3.75 MV Van de Graaff accelerator which serves mainly as a source of keV neutrons for the nuclear astrophysics studies; and the new compact cyclotron which is basically a commercial installation to produce radioactive isotopes for nuclear medicine and mechanical engineering.

The institute suffered a severe loss by the unexpected and untimely deaths of both our theoreticians, Dr. Friedrich Dickmann and Dr. Rainer Beck. Their contributions to our work - by their own research as well as by their generous advice on innumerable occasions - will be missed and their frank and engaging personalities will not be forgotten.

(A. Citron)   (G. Schatz)   (B. Zeitnitz)

CONTENTS

1. NUCLEAR PHYSICS

1.1 NUCLEAR ASTROPHYSICS

1.2 NEUTRON PHYSICS

1.   NUCLEAR PHYSICS

1.1   NUCLEAR ASTROPHYSICS

1.1.1   DESTRUCTION OF ^{26}Al IN EXPLOSIVE NUCLEOSYNTHESIS

H.P. Trautvetter[+], H.W. Becker[+], U. Heinemann[+], L. Buchmann[+], C. Rolfs[+],
F. Käppeler, P. Geltenbort[++], F. Gönnenwein[++], M. Baumann[+++],
H. Freiesleben[+++], H.-J. Lütke-Stetzkamp[+++]

The cosmologically short lived isotope ^{26}Al $(t_{1/2} = 7.2 \cdot 10^5$ y) might be useful as a clock for the early solar system. The discovery of a ^{26}Mg excess in the meteorite Allende indicates that this is due to the decay of ^{26}Al which might have been produced by a nearby nova or supernova shortly before the solar system formed. The ^{26}Al(n,p) reaction is important as it influences the destruction rate of this isotope in a neutron rich environment.

We have measured the (n,p) cross section at thermal neutron energies and in the keV region, using neutron spectra which closely resembled the true Maxwellian distributions for kT = 31 keV and kT = 71 keV. An additional measurement was made at E_n = 310 $\pm$ 40 keV.

The reaction may proceed via the ground state of ^{26}Mg or via the 5 first excited states. The respective proton groups P_0 to P_5 are to be expected with different intensity because of different centrifugal barriers. In our measurements we succeeded to detect the most intense P_1-group and also the P_0-group quantitatively. The higher groups were too low in energy and could not be discriminated from the background (except P_2 at thermal energies, where backgrounds were not so severe). The results are summarized in Table 1 and are plotted in Fig. 1.

Table 1 Experimental cross sections for the ^{26}Al(n,p) reaction

		ILL-Reactor	Van de Graaff accelerator		
E_n (keV)		$40 \cdot 10^{-6}$	kT = 31	kT = 71	310 ± 40[a]
(n,p)-cross section (mb)	P_0	26 ± 10	13 ± 6	–	21 ± 8
	P_1	1850 ± 150	124 ± 13	84 ± 14	72 ± 16
	P_2	185	–	–	–

[a] Neutron spectrum ranging from 270 to 350 keV.
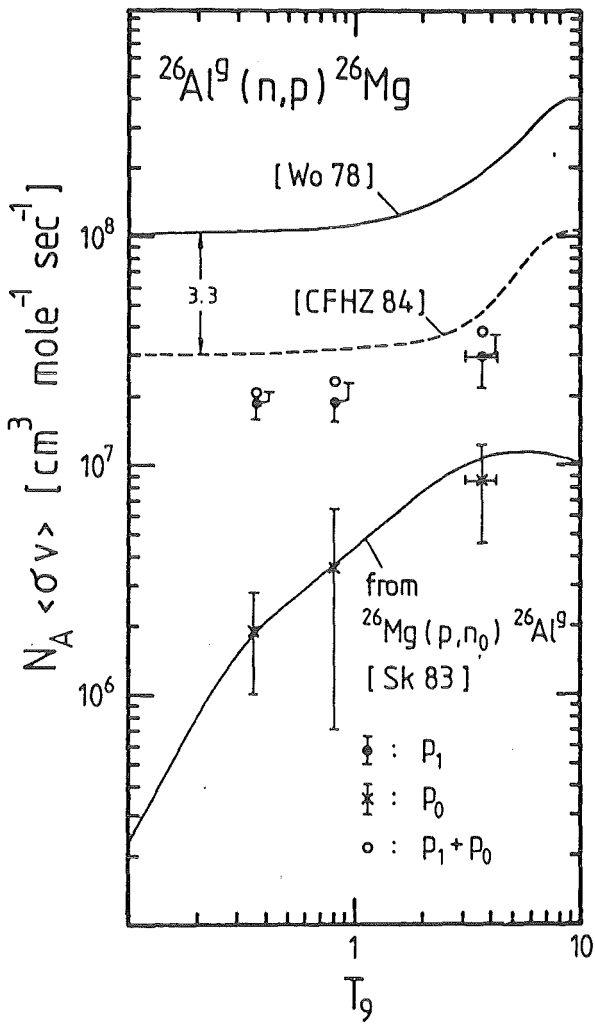
Fig. 1

Comparison of the experimental reaction rates $N_A \langle \sigma v \rangle = N_A \bar{\sigma} v_T$, ($N_A$ = Avogadros number, v_T = mean thermal velocity) with those deduced for the P_0-group from the inverse reaction (1) and with theoretical calculations (2,3).

(1)   R.T. Skelton, R.W. Kavanagh, D.G. Sargood, Ap. J. 271 (1983) 404
(2)   S.E. Woosley, W.A. Fowler, J.A. Holmes, B. Zimmerman,
       Atomic Data and Nuclear Data Tables 22 (1978) 371
(3)   G.R. Caughlan, W.A. Fowler, M.J. Harris, B. Zimmerman,
       Atomic Data and Nuclear Data Tables 32 (1984) 197

+   University of Münster, D-4400 Münster, Federal Republic of Germany
++   Institut Laue-Langevin, Grenoble, France
+++   University of Bochum, D-4640 Bochum, Federal Republic of Germany

1.1.2 THE ^{40}Ar CAPTURE CROSS SECTION AND THE ^{40}Ar SOLAR ABUNDANCE

H. Beer, R.D. Penzhorn[+]

As the natural isotopic abundance of ^{40}Ar is dominated by the radiogenic compo-
nent from the ^{40}K decay the original ^{40}Ar abundance has to be estimated via the
existing concepts of nucleosynthesis. Possibly, the main contribution to the nuc-
leosynthetic ^{40}Ar abundance is due to the s-process (1,2).

In this study a detailed s-process analysis to calculate the ^{40}Ar abun-
dance has been carried out. The synthesis of ^{40}Ar via the seed nuclei ^{40}Ca, ^{39}K,
^{36,38}Ar and ^{35}Cl is illustrated in Fig. 1. The synthesis path is characterized
by complicated branchings caused by radioactive decay and (n,α) and (n,p) reac-
tions on the species ^{41}Ca, ^{40}K, and ^{39}Ar. Among the involved cross sections the
destruction of ^{40}Ar by neutron capture is of primary importance. This cross sec-
tion has been measured by a special activation technique (3,4). The ^{40}Ar sample
for the irradiations was fabricated by chemical fixation of Ar in zeolith 5A (5).
The Maxwellian averaged capture cross section of ^{40}Ar at a thermal energy of kT
= 25 keV was found to be 2.55 ± 0.15 mb.
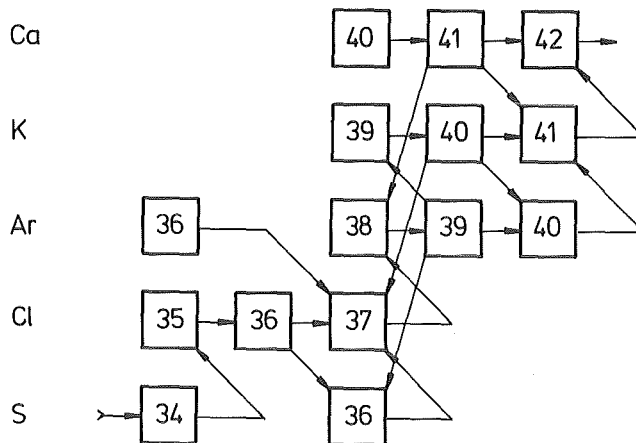
Fig. 1 Section of the reaction network used in calculating the s-process abun-
dance of ^{40}Ar

The s-process calculation was carried out using the neutron exposure distribution derived from a study of s-process abundances for nuclei A>56 (6). For ^{40}Ar an s-process abundance of 4.8 (Si $\equiv 10^6$) has been obtained.

(1)   J.G. Peters, W.A. Fowler, D.D. Calyton, Ap. J. 173, (1972) 637
(2)   A.G.W. Cameron, in Essays in Nucl. Astrophysics Cambridge University Press 1982, p. 23
(3)   H. Beer, F. Käppeler, Phys. Rev. C21 (1980) 534
(4)   H. Beer, F. Käppeler, G. Reffo, G. Venturini, Astrophysics and Space Sci. 97 (1983) 95
(5)   R.D. Penzhorn, G. Walter, H. Beer, Z. f. Naturforschung 38a (1983) 712
(6)   H. Beer, Proc. of the 5th Moriand Astrophysics Meeting, Les Arcs, Savoie 1985

+   Institut für Radiochemie, Kernforschungszentrum Karlsruhe

1.1.3 STELLAR NEUTRON CAPTURE RATES FOR ^{46}Ca AND ^{48}Ca

F. Käppeler, G. Walter, G.J. Mathews[+], (1)

Stellar neutron capture rates for ^{46}Ca and ^{48}Ca have been measured by the activation technique. Both, kT = 25 keV Maxwellian-like incident neutron spectra and non-Maxwellian higher-energy spectra have been utilized to study the possible role of individual capture resonances. Maxwellian averaged (kT = 30 keV) cross sections of 5.7 ±0.5 and 0.95 ±0.09 mb are derived for ^{46}Ca and ^{48}Ca, respectively. The possibility of a neutron capture origin for ^{46}Ca and ^{48}Ca is discussed in the light of these new cross sections as well as a mechanism for the production of the observed isotopic anomalies in inclusion EK-1-4-1 from the Allende meteorite.

(1)   The Astrophys. Journal 291 (1985) 319-327
+   University of California, Lawrence Livermore National Laboratory

1.1.4 MEASUREMENT OF NEUTRON CAPTURE CROSS SECTIONS OF s-ONLY ISOTOPES: ^{70}Ge, ^{86}Se, and ^{87}Sr

G. Walter and H. Beer (1)

In order to improve the s-process data basis in the mass range A < 100 the neutron capture cross sections of ^{86}Sr, ^{87}Sr and, for the first time, ^{70}Ge have been measured by time-of-flight in the energy range from 3.5 to 240 keV. The Maxwellian averaged capture cross sections have been calculated from the data for kT = 20 keV up to kT = 50 keV. At kT = 30 keV we obtained the values 92 ± 5, 74 ± 5, and 100 ± 7 mb for ^{70}Ge, ^{86}Sr, and ^{87}Sr, respectively.
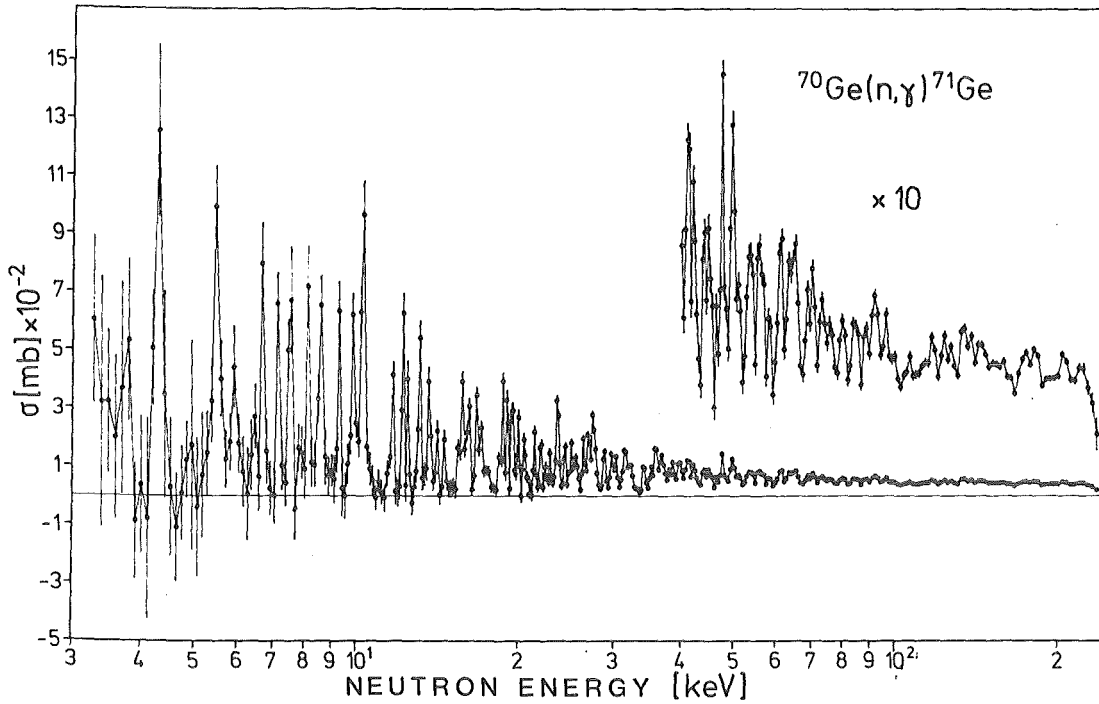
Fig. 1 Capture cross section of ^{70}Ge as a function of neutron energy

(1)   ditto, Astron. Astrophys. 142 (1985) 268

1.1.5 THE s-PROCESS BRANCHING AT ^{85}Kr.

G. Walter, H. Beer, F. Käppeler, R.-D. Penzhorn[+]

We have measured the Maxwellian-average neutron capture cross sections of ^{86}Kr, and ^{85,87}Rb by means of the activation technique at kT = 25 keV. These data combined with results from recent capture cross section measurements of s-only isotopes and others in the mass region of interest allowed us to perform a well-based analysis of the s-process in the mass range 68<A<89 within the classical steady state model with two independent fluence distributions.

The results show that the adopted classical s-process model is capable of describing the solar abundances in the mass region 68<A<89 correctly without overproducing the isotpes with small cross sections at the magic neutron shell N = 50. The analysis of the s-process branching at ^{85}Kr yielded a neutron density for the weak component of

$$n_n^W = (0.9 \pm 0.4) \ 10^8 \ cm^{-3}$$

compatible with the respective value for the main component.

The s-process krypton in a high temperature inclusion of the Murchison meteorite (1) could be interpreted as a mixture of 70% solar system krypton and 30% pure s-process krypton (Fig. 1). It was shown that the weak fluence distribution did not contribute to the pure s-process krypton in this mixture, indi-

cating an independent operation of the two fluence distributions of the classical s-process model.
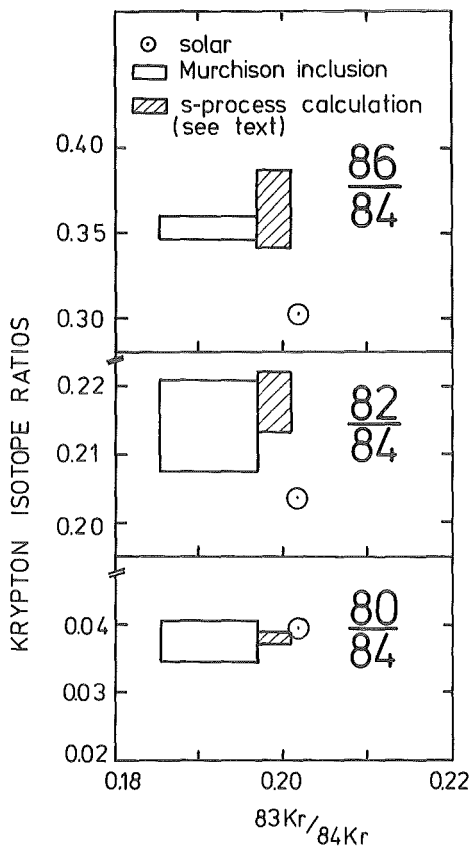
Fig. 1

The anomalous krypton abundances (relative to ^{84}Kr) in a high temperature inclusion of the Murchison meteorite (open boxes, Ref. (1)) and the proposed explanation (shaded boxes, see text). Solar abundance ratios are shown for comparison (circles).

(1)   L. Alaerts, R.S. Lewis, J.-I. Matsuda, E. Anders, Geochim. Cosmichim. Acta 44 (1980) 189

+   Institut für Radiochemie, Kernforschungszentrum Karlsruhe

1.1.6   keV NEUTRON CAPTURE CROSS SECTIONS OF THE Kr ISOTOPES

G. Walter, B. Leugers, F. Käppeler, G. Reffo[+], F. Fabbri[+], Z.Y. Bao[++]

The neutron capture cross sections of the stable krypton isotopes were determined in the energy interval from 4 to 250 keV using a C_6D_6-detector system in conjunction with the time-of-flight technique. The energy resolution of the measurement was 4% at 20 and 6% at 100 keV, and the experimental uncertainties were typically 6 to 10 %. The measurements were complemented by statistical model calculations of all krypton isotopes in the mass range 78<A<86 in order to obtain also reliable cross sections for the unstable nuclei ^{79,81,85}Kr. These calculations were based on local systematics for all relevant parameters, and the uncertainties of the results were estimated to 20-25%. Maxwellian average cross sections were calculated for kT = 30 keV and are compared with previous work in Table 1.
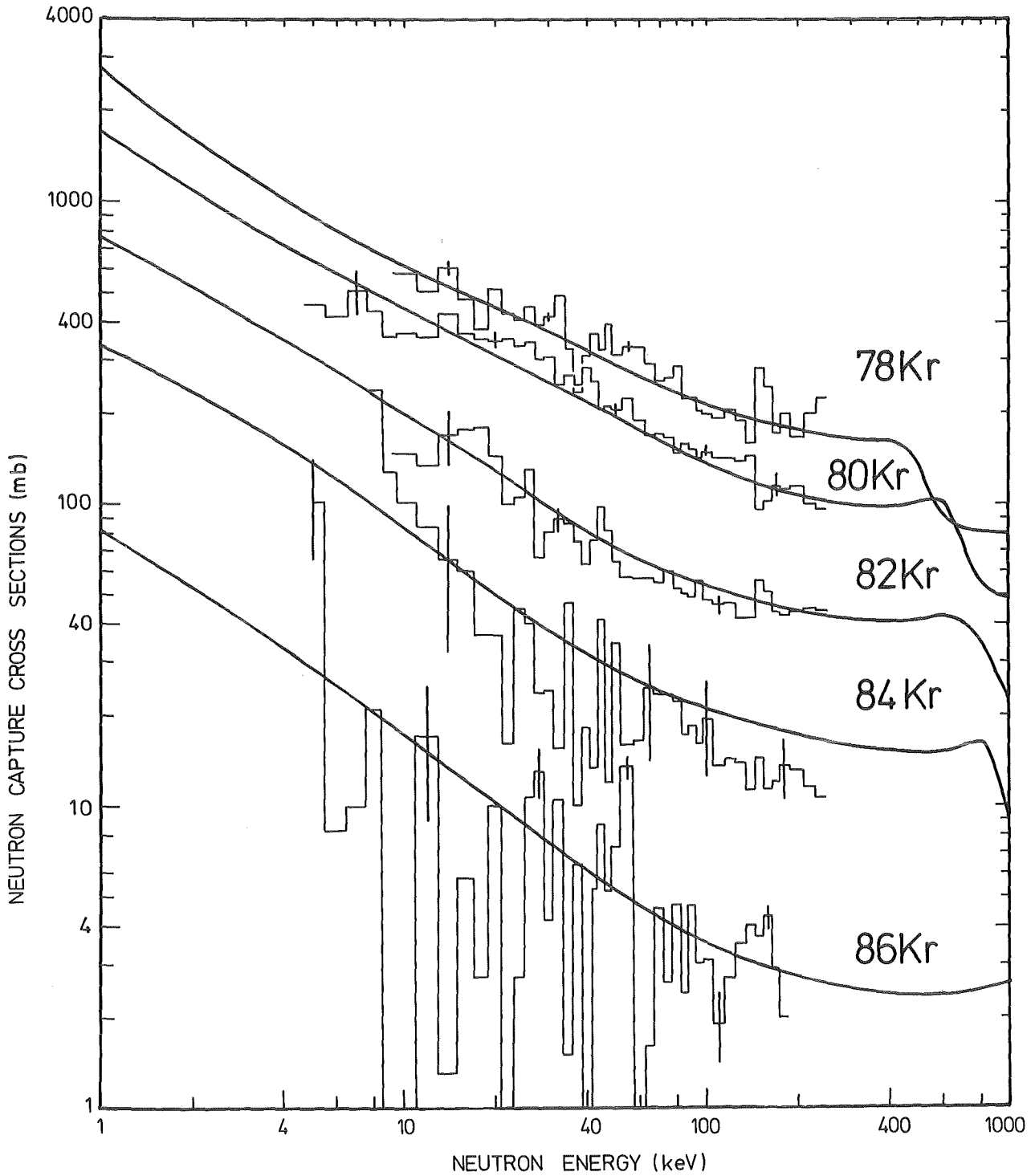
Fig. 1 The averaged experimental cross sections (histograms) together with the calculated values (solid lines) for the even Kr-isotopes.

Table 1 Maxwellian average neutron capture cross sections for kT = 30 keV:
Comparison of present theoretical and experimental values with previous
results

Target Isotope	Maxwellian average cross section (mb) for kT = 30 keV				
	Holmes et al. (1)	Leugers et al.(2)	Harris (3)	this Work calc	exp
^{78}Kr	203	284	253	368	359+44
^{79}Kr	1130	-	-	857	-
^{80}Kr	148	228	156	242	257+15
^{81}Kr	1030	800	994	682	-
^{82}Kr	122	95	79	100	84+6
^{83}Kr	571	345	259	237	251+16
^{84}Kr	25	30	13	40	36.5+4.5
^{85}Kr	155	68	25	67+17	-
^{86}Kr	44	-	3.7	8.0+2.8	5.6+0.7

(1)   J.A. Holmes, S.E. Woosley, W.A. Fowler, and B.A. Zimmerman, Atomic Data
and Nuclear Data Tables 18, (1976) 305
(2)   B. Leugers, F. Käppeler, F. Fabbri, and G. Reffo, Nuclear Cross Sections
and Technology, NBS Spec. Publ. 594 (1980) p. 857
(3)   M.J. Harris, Astrophys. Space Sci. 77, (1981) 357

+   Laboratorio Dati Nucleari, E.N.E.A., Bologna, Italy
++   Institute of Atomic Physics, Academia Sinica, Beijing, Peoples Rep. of
China

1.1.7   s-PROCESS NUCLEOSYNTHESIS BELOW A = 90

H. Beer (1)

In this study a complete s-process analysis of the heavy elements is performed
using the classical model with three exponential exposure distributions as sug-
gested by Ward et al. (2). In addition to the so-called main component which des-
cribes the bulk of heavy elements between A = 90 and 200 a strong component is
introduced to cure problems at the termination of the s-process (3) and a weak
component which allows for a fit of the isotopes below A = 90 towards the iron
seed. The terms strong and weak component were chosen in accordance with the re-
lative strength of the neutron exposure compared to the main component. The s-
process branchings were treated with constant neutron density and temperature.
Different values of these parameters were found for the main and weak component

(4). For the main component also the electron density could be estimated by one of the branchings (5). The global s-process parameters found by an adjustment to isotopes with empirically known s-process abundances are summarized in Table I.

Table I. Parameters for the flux distributions of the main, weak, and
strong components

s-process component	Fraction of solar iron seed abundance	Average time inte-grated neutron flux at kT=30keV	Average number of neutrons per iron seed
Main	(0.048±0.003)%	(0.30±0.01)/mb	11.2±0.7
Weak	(1.6±0.2)%	(0.06±0.01)/mb	1.4±0.4
Strong	$(1.2±0.7)10^{-4}$ %	≥ 6/mb	≥ 150

An important criterion for the consistency of our analysis is that no over-productions of stable isotopes occurs. This requirement is critical if the s-process is the dominant contribution of the solar abundance. In the domain of the main component crucial isotopes are ^{87}Rb, ^{86}Kr, ^{88}Sr, ^{138}Ba, and ^{140}Ce. For the weak s-process certain light isotopes represent a crucial check. They can be easily produced by neutron capture on highly abundant progenitor isotopes which

Table II. Rare neutron rich light isotopes produced preferentially
by the weak s-process via abundant progenitors as seed
nuclei

Seed Nuclei	Nucleus	Abundances[Si=10^6] s-process N	solar N_Θ	N/N_Θ[%]
S32	S33	113.9	3860	3
"	S36	46.2	88	52
Ar36,38	Cl37	396.7	1270	31
" "	K41	21.5	253.7	9
Ca40	Ca42	11.6	395	3
"	Ca43	3.0	82.5	4
Ca40,44	Ca46	0.04	2.17	1.6
" "	Sc45	1.8	33.8	5
Ti48,49	Ti50	13.2	125	10.6
Cr50,52,53	Cr54	52.2	316	16.5
Fe56,57	Fe58	2203	2610	84
Fe56,57,Ni58,60	Ni64	136.1	449	30
" " " "	Cu63	155.2	356	43.6
" " " "	Cu65	120.5	158	76.3
" " " "	Zn67	19.2	51.7	37.1
" " " "	Ga69	10	22.7	44
" " " "	Ge70	13.6	21.7	62.2
" " " "	Ga71	9.3	15.1	61.6

act as seed material. For this seed material solar system composition was assumed. Table II summarizes the studied isotopes. As the comparison with solar abundances shows, there is no case where we have found an overproduction. The most critical case appears to be ^{58}Fe where about 84 % for the solar abundance has to be ascribed to the s-process.

(1)   ditto, 5th Moriond Astrophysics Meeting, Nucleosynthesis and its Implications on Nuclear and Particle Physics, Les Arcs, Savoie 1985
(2)   R.A. Ward, M.J. Newman, D.D. Clayton, Ap. J. Suppl. 31 (1976) 33
(3)   H. Beer, R.L. Macklin, Phys. Rev. C (in press)
(4)   G. Walter, Report KfK 3706 (1984) Kernforschungszentrum Karlsruhe
(5)   H. Beer, G. Walter, R.L. Macklin, Proc. of the 5th Int. Sympl. on Capture Gamma-Ray Spectroscopy and Related Topics, Knoxville 1984

1.1.8   ANALYSIS OF Zr AND Tc ABUNDANCES FROM S-STARS USING THE s-PROCESS WITH AN EXPONENTIAL DISTRIBUTION OF NEUTRON EXPOSURES.

H. Beer and G. Walter (1)

The abundances of Zr, Mo, Tc and Ru from S-stars were studied in the frame of the s-process with an exponential neutron fluence distribution. Estimates for the average time integrated neutron flux and the s-process neutron density and temperature have been derived from the abundances of the Zr-isotopes and from Tc, respectively.

(1)   ditto, M. Jaschek and P.C. Keenan (eds.) Cool Stars with Excesses of Heavy Elements, 373-377 (1985) by D. Reidel Publishing Company.

1.1.9   A STUDY OF THE ^{134}Cs BRANCHING WITH THE PULSED s-PROCESS MODEL

H. Beer

s-Process nucleosynthesis at mass number A = 134 leads to a radioactive isotope, ^{134}Cs, with a terrestrial half life of 2.06 yr. For the currently believed s-process neutron density conditions (1,2) a significant branching of the s-process synthesis path is expected which should be easily detectable via the s-only isotopes ^{134,136}Ba. It is surprising that the experimental data of ^{134,136}Ba (3) do not predict such a branching within quoted uncertainties. Detailed analysis shows that to understand this result there are two possibilities:

- The terrestrial half life is strongly reduced under stellar s-process conditions via fast ß-decay from thermally populated excited states.

- The branching is destroyed through the effect of a pulsed s-process. Significant s-process flow via capture on ^{134}Cs is prevented because ^{134}Cs constantly vanishes by decay in the interpulse phase and has to be

produced again during the next pulse (4).

Investigation of the first possibility shows that the ^{134}Cs half life may be reduced under stellar conditions only moderately to about 1.2 yr due to nuclear structure effects resulting in a retardation of allowed ß- transitions which appear already in the ground state ß-decay.

The second possibility to destroy the ^{134}Cs branching in the pulsed s-process is illustrated in Fig. 1. The σN-value of ^{134}Ba as a function of the exposure per pulse Δτ is plotted and compared with the respective empirical value. The theoretical calculations were carried out with the following input parameters:

Beta decay rate $\lambda(^{134}Cs)$ = (1.8 ± 0.3) 10^{-8}/s

Neutron density n_n = (1.0 ± 0.4) 10^8 cm^{-3} (2)

Thermal energy kT = 25 keV
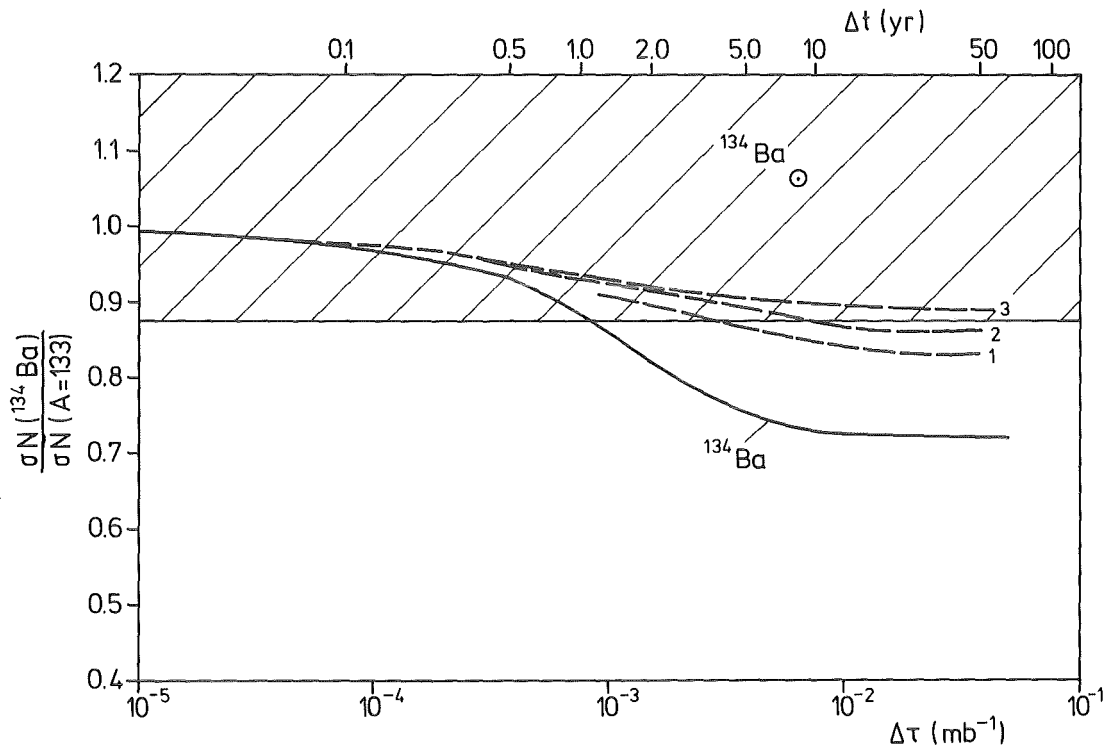
Fig. 1 The analysis of ^{134}Ba located in the ^{134}Cs branching. The σN-value plotted as a function of the exposure Δτ is normalized to σN (A=133) which is identical to σN(^{136}Ba) except for a small correction accounting for non-steady flow. The uncertainty of the theoretical curve is also indicated. Upper error limits are reached at the dashed lines which where calculated using different uncertainties for the ^{134}Cs cross section (1:30%, 2:40%, 3:50%). The hatched area shows the valid range of the empirical ^{134}Ba value.

Capture cross section $\sigma(^{134}Ba) = 221 \pm 35$ mb

For the capture cross section of ^{134}Cs, $\sigma(^{134}Cs) = 597$ mb (5) the uncertainty was varied between 30 and 50 %.

The dashed lines in Fig. 1 indicate the upper limit for the uncertainty of the theoretical curve, where the uncertainty of the ^{134}Cs cross section is assumed to be 30 (1), 40 (2), and 50 % (3), respectively. The intercept of the dashed curves with the lower limit of the empirical ^{134}Ba value provides an upper limit for the pulse duration of the s-process. For a 50 % uncertainty of the ^{134}Cs cross section no restriction of the pulse duration Δt has been performed. In the other two cases, Δt is constrained to values smaller than 9 and 4 yr, respectively.

A more accurate analysis of the ^{134}Cs branching can only be carried out with improved input data.

(1)   H. Beer, G. Walter, R.L. Macklin, P.J. Patchett, Phys. Rev. C30 (1984)464
(2)   R.R. Winters, F. Käppeler, K. Wisshak, G. Reffo, A. Mengoni, KfK 3827 (1984)
(3)   A.R. de L. Musgrove, B.J. Allen, J.W. Boldeman,, R.L. Macklin, Nucl. Phys. A256, (1976) 173
(4)   R.A. Ward, M.J. Newman, Ap. J. 219, (1978) 195
(5)   M.J. Harries, Astrophys. and Space Sci. 77 (1981) 357

1.1.10 MEASUREMENT OF THE ^{139}La CAPTURE CROSS SECTION

H. Beer

The capture cross sections of the isotopes with magic neutron number 82 at the precipice of the σN-curve are of special importance for the adjustment of the main s-process component which describes the bulk of heavy s-process elements ($90 \le A \le 200$).

Previously, measurements on ^{138}Ba, ^{140}Ce (1) and ^{142}Nd (2) have been reported. The measurement of the ^{139}La capture cross section is a continuation of this effort to establish reliable data for this important part of the synthesis path.

The experiment was carried out by the activation method (1) relative to the gold capture cross section. The sample characteristics and the Maxwellian averaged capture cross section are summarized in Table I.

As the new value for ^{139}La deviates considerably from the previously adopted capture cross section $(\sigma(^{139}La) = 54 \pm 5$ mb from Musgrove et al. (3)) a new calculation of the σN-curve with the data of Table II has been carried out. For the time integrated neutron flux $(\tau_o = 0.304 \pm 0.013$ mb$^{-1})$ only a change of 1.5 % was found using the new ^{139}La capture cross section. Therefore, the old

value of τ_o is within the calculated uncertainty consistent with the new value. The derived s-process abundance for ^{139}La of 0.33 ± 0.03 (Si $\equiv 10^6$) is, however, considerably larger than the previous value of 0.23 ± 0.02 (Si $\equiv 10^6$).

Table I   Sample characteristics and Maxwellian averaged capture cross section of ^{139}La

Reaction	$T_{1/2}$	E_γ(keV)	I_γ(%)	$\frac{<\sigma v>}{v_T}$ mb kT = 25 keV
^{139}La(n,γ)^{140}La	40.272 h	1596	95.5 ± 0.3	4.1 ± 2.9
^{197}Au(n,γ)^{198}Au	2.69 d	412	95.52 ± 0.06	657 ± 16

Table II   Neutron capture cross sections of stable nuclei with magic neutron number 82

Nucleus	$<\sigma v>/v_T$ mb	at kT = 30 keV
^{138}Ba	3.96 ± 0.23	Ref. (1)
^{139}La	38.4 ± 2.7	this work
^{140}Ce	10.82 ± 0.53	Ref. (1)
^{141}Pr	119 ± 16	Ref. (3)
^{142}Nd	47 ± 4	Ref. (2)

Note that the capture cross sections in Ref. (1) and (2) had to be normalized due to a change in the Au standard. The most important ^{138}Ba capture cross section is now in excellent agreement with the value $\sigma(^{138}$Ba) = (3.8 ± 0.8) mb reported by Musgrove et al. (4).

(1)   H. Beer, F. Käppeler, Phys. Rev. C21, (1980) 534
(2)   G.J. Mathews, F. Käppeler, Ap. J. 286 (1984) 810
(3)   A.R. de L. Musgrove, B.J. Allen, R.L. Macklin, Aust. J. Phys. 30 (1977) 599
(4)   A.D. de L. Musgrove, B.J. Allen, R.L. Macklin, Aust. J. Phys. 32 (1979) 213

1.1.11 NEUTRON CAPTURE CROSS SECTIONS AND SOLAR ABUNDANCES OF ^{160,161}Dy, ^{170,171}Yb, ^{175,176}Lu, and ^{176,177}Hf FOR THE s-PROCESS ANALYSIS OF THE RADIONUCLIDE ^{176}Lu

H. Beer, G. Walter, R.L. Macklin[+], P.J. Patchett[++] (1)

The neutron capture cross sections and solar abundances of ^{160,161}Dy, ^{170,171}Yb, ^{175,176}Lu, and ^{176,177}Hf have been measured. With this data base s-process studies have been carried out to determine the s-process neutron density and temperature and to investigate the s-process nucleosynthesis of the ^{176}Lu clock. From various branchings the neutron density was found to be $(0.8-1.8) \cdot 10^8$ neutrons per cm³ and the temperature kT to be 18-20 keV. On the basis of the present data, ^{176}Lu proved not to be applicable as a cosmic clock because of the temperature sensitivity of the ^{176}Lu half-life but can be used instead as a stellar thermometer. Constraints for the s-process temperature (kT = 20-28 keV) were found to be in good agreement with the investigated branchings.

(1)　　ditto, Phys. Rev. C 30 (1984) 464

+　　　Oak Ridge National Laboratory
++　　Max-Planck-Institut für Chemie, Mainz

1.1.12 MEASUREMENT OF THE CAPTURE CROSS SECTIONS OF ^{156}Dy and ^{194m,196,198}Pt

H. Beer

The analysis of s-process branchings is a major source of information for important astrophysical parameters like neutron and electron density and the s-process temperature (1). As the various branchings exhibit a different sensitivity to these parameters due to the individual properties of the involved nuclei, it is desirable to analyze as many branchings as possible.

The capture cross section measurements of ^{156}Dy and of the Pt isotopes are intended to contribute to a better analysis of the ^{157}Gd and ^{192}Ir branchings. The measurements were carried out with the activation technique. The experimental arrangement is a standard set up at the Karlsruhe Van de Graaff accelerator and has been described in detail elsewhere (2,3). The decay properties, the induced activities, and the Maxwellian averaged capture cross sections are summarized in Table I.

For branching analyses, the beta decay and the neutron capture rate of the branch point isotope, but also the capture cross section of a stable s-process isotope on one of the branches are of primary importance. This signifies for the ^{157}Gd and ^{192}Ir branchings that improved capture cross sections of ^{158}Dy and ^{192}Pt, respectively, are needed. The measured capture cross sections on ^{156}Dy, ^{194m,196,198}Pb are useful to derive better statistical model parameters

for the individual nuclei in the isotopic chain, especially for ^{158}Dy and ^{192}Pt.

Table I   Decay properties and measured capture cross sections (preliminary)

Reaction	$T_{1/2}$	E_γ (keV)	I_γ (%)	$\dfrac{<\sigma v>}{v_T}$ (mb) $kT = 25$ keV
^{156}Dy$(n,\gamma)^{157}$Dy	8.1 h	326	94 $\pm$ 2	1741
^{194}Pt$(n,\gamma)^{195}$Pt^m	4.02 d	99	11.1 $\pm$ 1.1	31
^{196}Pt$(n,\gamma)^{197}$Pt^m	94.4 min	346	11.1 $\pm$ 0.5	13.2
^{196}Pt$(n,\gamma)^{197}$Pt	18.3 h	77	17 $\pm$ 1	213
^{198}Pt$(n,\gamma)^{199}$Pt	30.8 min	543	15	75.6
^{197}Au$(n,\gamma)^{198}$Au	2.69 d	412	95.5 $\pm$ 0.06	657

(1)   H. Beer, G. Walter, R.L. Macklin, P.J. Patchett, Phys. Rev. C30 (1984)464
(2)   H. Beer, F. Käppeler, Phys. Rev. C21 (1980) 534
(3)   H. Beer, F. Käppeler, G. Reffo, G. Venturini, Astrophys. and Space Sci. 97 (1983) 95

1.1.13 ANALYSIS OF BRANCHINGS WITH A PULSED s-PROCESS MODEL

H. Beer (1)

The classical s-process model as it was successfully applied over the years in reproducing solar abundances (2-5) makes use of exponential neutron exposure distributions and assumes a continuous irradiation over the whole synthesis (6).

On the basis of the works of Ulrich (7), Iben (8-10) and Truran and Iben (11) about s-process nucleosynthesis in the He-shell of a red giant star the exponential exposure distribution is, however, rather the result of a pulsed than a continuous irradiation of s-process material. Therefore, modifications of the classical model are a matter of consistency. The pulsed nature of the s-process shows up directly at the branchings due to the interpulse decay of the radioactive branch point isotopes and the necessary reconstruction during the next pulse.

In this work important s-process branchings were analyzed using the pulsed s-process model of Ward and Newman (12). In this model the classical s-process appears as a limiting case for a large pulse duration ($\Delta\tau \rightarrow \infty$) and the derived neutron density represents a lower limit in the pulsed scenario. A decrease in the pulse duration would require a corresponding increase in neutron density to reproduce a branching.

The investigations of the branchings at ^{151}Sm, ^{163}Dy, ^{170}Tm, ^{185}W and

^{192}Ir showed that realistic pulse durations (7-9) require a solution close to the classical limit. The ^{151}Sm branching which is most sensitive to the pulses provided a lower limit for the pulse duration ($\Delta t \geq 3$ yr.).
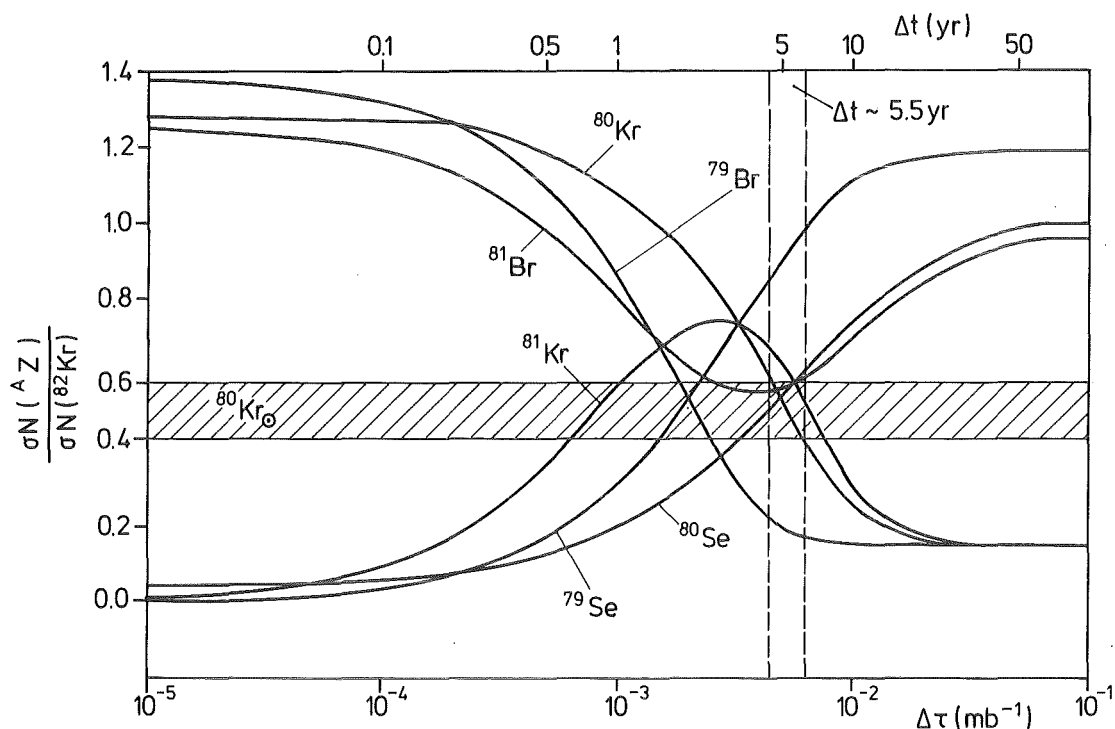
Fig. 1 The analysis of the isotopes located in the ^{79}Se branching is shown. The σN values normalized to ^{82}Kr are plotted as a function of the exposure $\Delta\tau$. The curves for ^{79}Br, ^{80}Kr and ^{79}Se, ^{80}Se reflect the influence of the ^{79}Se branching only. ^{81}Kr and ^{81}Br are in addition strongly determined by the ^{81}Kr branching. The branching at ^{80}Br is of minor influence. For an exposure $\Delta\tau \geq 5 \cdot 10^{-2}$ mb^{-1} the classical steady s-process limit is reached. For ^{80}Kr an empirical value can be given (hatched area). The intercept of the theoretical curve with the empirical value yields a pulse duration of 5.5 yr.

For the ^{63}Ni, ^{79}Se and ^{85}Kr branchings the classical two component s-process cannot reproduce the abundances solely with neutron density and temperature of the main component (5). Such a solution is, however, possible with the pulsed s-process model. A pulse duration around 5.5 yr. is required. Fig. 1 shows the analysis of the ^{79}Se branching. The sum of weak + main s-process component is plotted as a function of the exposure $\Delta\tau$ per pulse. In Fig. 2 the s-process calculation from ^{56}Fe to ^{209}Bi with the pulsed s-process model is displayed. The consistency of neutron density and temperature for the main and weak component

does not necessarily imply a common site of synthesis which was excluded in the classical analysis (5).
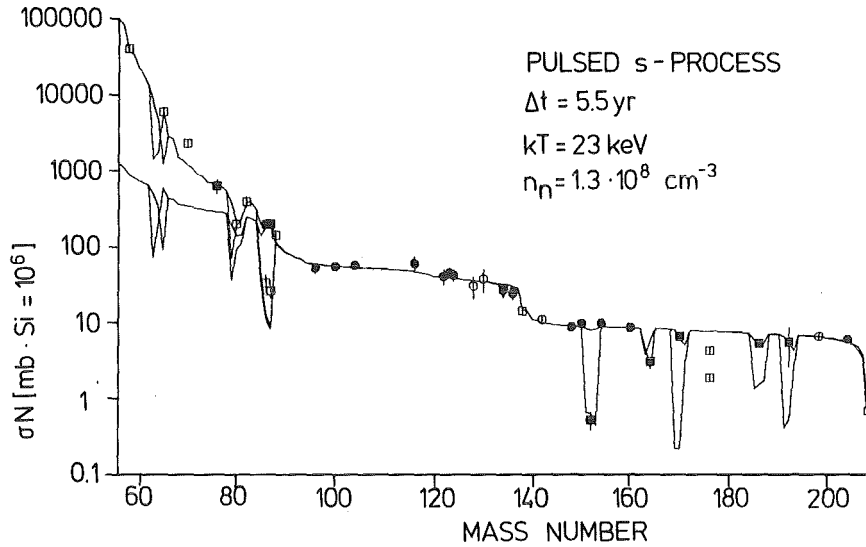
Fig. 2 The product of capture cross section σ and s-process abundance N as a function of mass number. The symbols correspond to empirical data. Significant branchings were identified due to low empirical σN values. Iron seed abundance and average time integrated neutron flux for the various components are the same as in the classical analysis (4). Only the branchings at ^{63}Ni, ^{79}Se and ^{85}Kr turned out to be really influenced by the pulse conditions. The results for the other branchings are practically identical with the classical s-process analysis.

(1)   ditto, "Workshop on Nuclear Astrophysics" Ringberg Castle, Tegernsee, May 20-24, 1985
(2)   P.A. Seeger, W.A. Fowler, D.D. Clayton, Ap. J. Suppl. 11 (1965) 121
(3)   F. Käppeler, H. Beer, K. Wisshak, D.D. Clayton, R.L. Macklin, R.A. Ward, Ap. J. 257 (1982) 821
(4)   H. Beer, G. Walter, R.L. Macklin, P.J. Patchett, Phys. Rev. C30 (1984) 464
(5)   H. Beer, Proc. Conf. on Nucleosynthesis and its Implications on Nucl. and Particle Phys., 5th Moriond Astrophysics Meeting 1985, Les Arcs, Savoie
(6)   R.A. Ward, M.J. Newman, D.D. Clayton, Ap.J. Suppl. 31 (1976) 33
(7)   R.K. Ulrich, in Explosive Nucleosynthesis Austin, Texas 1973, p. 139
(8)   I. Iben jr., Ap. J. 196 (1975) 525
(9)   I. Iben jr., Ap. J. 196 (1975) 549
(10)   I. Iben jr., Ap. J. 217 (1977) 788
(11)   J.W. Truran, I. Iben jr., Ap. J. 216 (1977) 797
(12)   R.A. Ward, M.J. Newman, Ap. J. 219 (1978) 195

1.1.14 s-PROCESS NUCLEOSYNTHESIS - STELLAR ASPECTS AND THE CLASSICAL MODEL

F. Käppeler

The classical s-process model has been shown to be an attractive tool for pheno-menological studies, complementing stellar model calculations: It is easy to handle, contains only a few parameters (seed abundances, mean neutron exposure τ_0), and yields very accurate results (σN-curve, s-process abundances, neutron density, etc.). Corresponding analyses (1,2) are based on a fit of the model parameters to the s-only isotopes along the s-process synthesis path. If the classical model is to be applied to abundance patterns observed in stars, there is the problem that only element abundances can be derived from stellar spectra (except for very cool stars, where isotope assignments can be made via molecular lines). This feature complicates the interpretation of stellar abundances, as the clear s-process signature on the isotopic pattern is washed out by the averaging conversion into element abundances. This is illustrated in Fig. 1 which shows the s-process contributions to solar matter (solid line). The outstanding abundance peaks at the neutron magic isotopes are completely diluted except for barium which is one of the few elements - together with Sr, Y, Zr, and Ce - with practically negligible r-process contributions. These elements are therefore known to be good s-process indicators.

Despite the difficulties of observation and analysis, abundances from red giants are a fascinating alternative to solar matter because of the strong over-abundances of s-processed material, which result most likely from nucleosynthesis in just these stars. While the origin of the solar s-process component is rather unclear, the direct observation of s-enhancements in particular stars provides an immediate link to the s-process site and hence facilitates the comparison to stellar models.
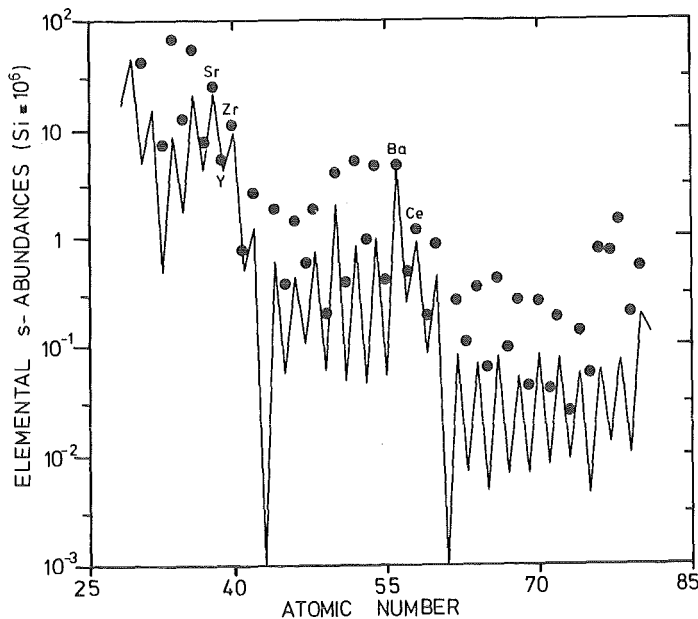
Fig. 1
s-process contribution (solid line) to solar abundances (dots).

An investigation of the sensitivity and the limits of s-process analyses of stellar element distributions with the classical model showed that (i) the present status of input data for the classical s-process model appears to be sufficient with respect to the analysis of stellar abundance patterns, (ii) the effect of s-process branchings (in particular at ^{85}Kr) and the decay of radioactive isotopes cannot be neglected, and (iii) the quality of present observations allows for meaningful estimates of mean neutron exposures and neutron densities, (at least in certain ranges of these parameters) provided the abundance patterns include the important key elements Rb, Sr, Y, Zr, Ba, Ce.

For improvements in this field more accurate and comprehensive observations are called for. Element patterns need to be as complete as possible including not only a few important species. The more elements are determined the better the analysis can be made, including cross checks for consistency of abundance ratios and corrections for the initial envelope composition. For reliable s-process analyses a few complete abundance patterns are certainly of more help than a survey of many stars which includes only a few elements.

(1)   F. Käppeler, H. Beer, K. Wisshak, D.D. Clayton, R.L. Macklin, R.A. Ward, Ap. J., 257 (1982) 821

(2)   G.J. Mathews, R.A. Ward, Reports on Progress in Physics, 1985, in print

1.1.15 BETA-DECAY RATES FOR THE s-PROCESS

K. Yokoi, K. Takahashi[+], (1)

The ß-decay rates under s-process conditions are presented for heavy nuclei in the ranges $26 \leqslant Z \leqslant 83$ and $59 \leqslant A \leqslant 210$. The types of ß-decay processes taken into account in the calculation are continuum-state β^--decay, bound-state β^--decay, bound-electron capture, continuum-electron capture and continuum-state β^+-decay. The rates are calculated at various temperatures ($1 \cdot 10^8 \leqslant T \leqslant 5 \cdot 10^8$ K) and electron number densities ($3 \cdot 10^{26} \leqslant n_e \leqslant 3 \cdot 10^{27}$ cm^{-3}). It is emphasized that the bound-state β^--decay is of importance for the study of s-process nucleosynthesis.

(1)   ditto, KfK-Report 3849 (1985)

+   Lawrence Livermore National Laboratory

1.1.16 THE $T(p,n)^3He$ REACTION FOR MEASUREMENTS OF STELLAR REACTION RATES

F. Käppeler, A.A. Naqvi[+], M. Al-Ohali[+]

It was shown previously (1) that the stellar neutron spectrum at temperatures of about 300 million degrees (corresponding to a thermal energy of kT = 25 keV) can be well simulated by the neutron spectrum from the $^7Li(p,n)^7Be$ reaction. Following the same principle of kinematic collimation near the reaction threshold, we investigated the $T(p,n)^3He$ reaction and found that the angle integrated neutron spectrum for E_p = 1100 keV provides a good representation of a Maxwell-Boltzmann spectrum at kT = 54 keV (Fig. 1). This energy is high enough that the $T(p,n)^3He$ reaction can be used to complement measurements at kT = 25 keV. It allows to assess the energy dependence of the Maxwell-averaged cross sections and to improve the accuracy of the deduced cross sections at the standard s-process environment of kT = 30 keV.
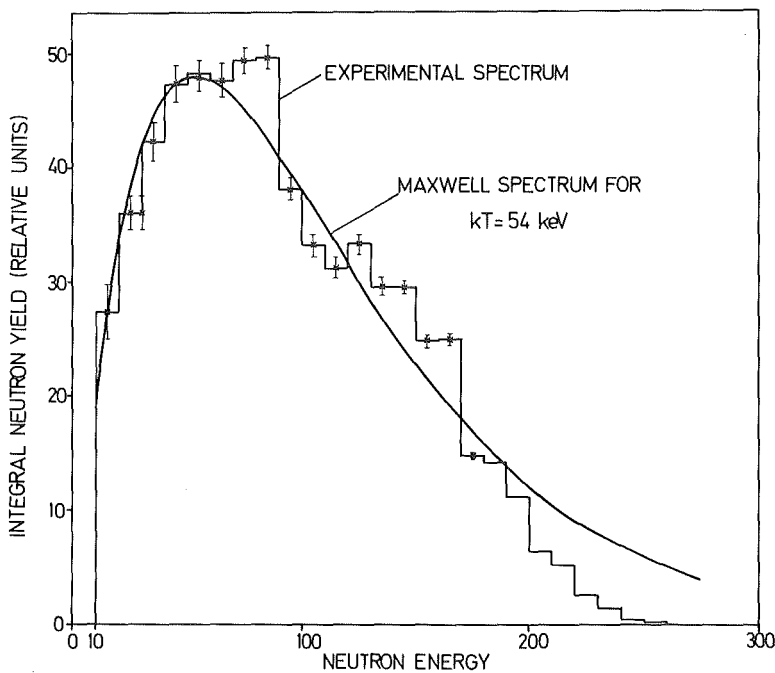
Fig. 1
Angle-integrated neutron yield from the $T(p,n)^3He$ reaction at E_p = 1100 keV (histogram) and the fitted Maxwell-Boltzmann distribution at kT=54 keV.

(1)   H. Beer, F. Käppeler, Phys. Rev. C21 (1980) 534
+   University of Petroleum and Minerals, Dhahran, Saudi Arabia

1.2 NEUTRON PHYSICS

1.2.1 MEASUREMENT OF THE n-p SPIN CORRELATION PARAMETER A_{yy}

P. Doll, V. Eberhard, W. Heeringa, K. Hofmann, H.O. Klages, H. Krupp,

Chr. Maier

At the Karlsruhe polarized neutron facility POLKA (1) the $\vec{n}$-$\vec{p}$ spin correlation parameter A_{yy} has been measured in the energy range from 20 to 50 MeV. The polarized neutrons were obtained utilizing the first beams of polarized deuterons from the new atomic beam ion source PASKA. Beam intensities of up to 150 nA were reached with an average of about 100 nA. A deuteron vector polarization $P_d \sim 0.55$ was achieved. Polarized neutrons were produced in a liquid D_2-target and scattered at a distance of 5 m by the polarized protons of a TiH_2 sample. The "brute-force" nuclear polarization facility KRYPTA (2) was used to cool the sample down to ~ 10 mK in a magnetic field of 9 T. These parameters correspond to a proton polarization of ~ 0.70.

The principal set-up for the A_{yy} measurement has been described in the 1983/84 annual report (3). 5 pairs of neutron detectors with gain monitoring via LED-light pulses are used at 5 angles to detect the scattered neutrons. Multiparameter data acquisition is performed with a CAMAC-LSI 11 system.

The neutron beam polarization was reversed or switched on-off every 10 seconds. The magnetic field of KRYPTA was reversed after ten days of beam time. A special construction (4) inside the cryostat enabled the fast (1 h) interchange of the TiH_2 and a Ti sample. The background of neutrons scattered elastically or inelastically from Ti was determined frequently. The neutron beam intensities before and after the samples were measured with six ΔE-E proton recoil telescopes and two thin plastic scintillator detectors. These systems serve simultaneously as monitors for the neutron flux normalization and as a set-up for the determination of the spin-spin dependence of the total cross section. In the $\vec{n}$-$\vec{p}$ system this corresponds to a measurement of $\int A_{xx} + \int A_{yy}$. A third application is the use of four ΔE-E proton recoil telescopes in the polarized neutron beam for the determination of the analyzing power of the backward angle $\vec{n}$-p scattering. The proton angles of 12.5° and 20° in the lab. system correspond to c.m. angles of 155° and 140° for the scattered neutrons.

About 150 magnetic tapes of data were taken in ~ 400 h of beam time in June/ July 85. These data are being analyzed. Final results will be presented in the near future. We hope that this experiment together with the measurement of the backward angle differential cross section will allow us to put sharper constraints on some NN phase shifts.

(1)   H.O. Klages, H. Dobiasch, P. Doll, H. Krupp, M. Oexner, P. Plischke,
       B. Zeitnitz, F.P. Brady, J.C. Hiebert, Nucl. Instr. Meth. 219 (1984) 269

(2)   R. Aures et al., Nucl. Instr. Meth. 224 (1984) 347

(3)   F.P. Brady, P. Doll, R. Garrett, W. Heeringa, K. Hofmann, H.O. Klages,
       H. Krupp, J. Wilczynski, KfK report 3815 (1984) 22

(4)   W. Heeringa, H. Skacel, KfK report 3815 (1984) 152

1.2.2 BACKWARD ANGLE n-p DIFFERENTIAL CROSS SECTION MEASUREMENTS

P. Doll, G. Fink, R. Garrett, W. Heeringa, K. Hofmann, H.O. Klages,
H. Krupp

In the framework of the neutron scattering programme at POLKA the backward angle elastic n-p differential cross section was measured with high accuracy. The aim was to provide new precise data on n-p scattering observables as input in nucleon-nucleon phase shift analyses. Phase shifts predicted by various potentials (1,2) differ from phase shifts derived from exp. data (3). Especially the $^1P_1$ phase shift and the mixing parameter ε_1, coupling $^3S_1 - ^3D_1$ states, are still not well determined. Sensitivity calculations (4,5) indicate that correlations of $^1P_1$ and ε_1 on data base can be reduced by e.g. a very precise determination of the differential cross section at backward angles.

We employed telescope techniques for charged recoil particles, mainly protons, from a thin polyethylene foil. The telescope systems, each consisting of a 500 μm Si ΔE-detector and a 1" NaI E-detector (6), are set up in an evacuated scattering chamber, providing highly accurate geometrical conditions and also avoiding neutron and proton interaction with air.
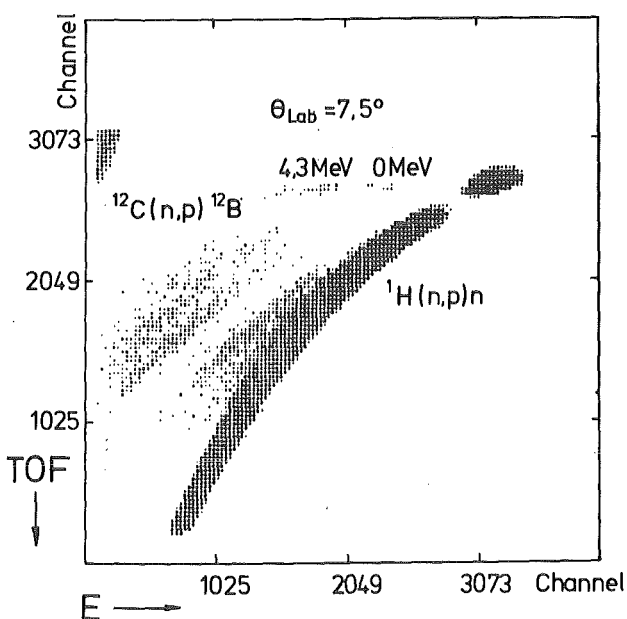
Fig. 1 Total time-of-flight versus energy at Θ_{lab} = 7.5 degrees
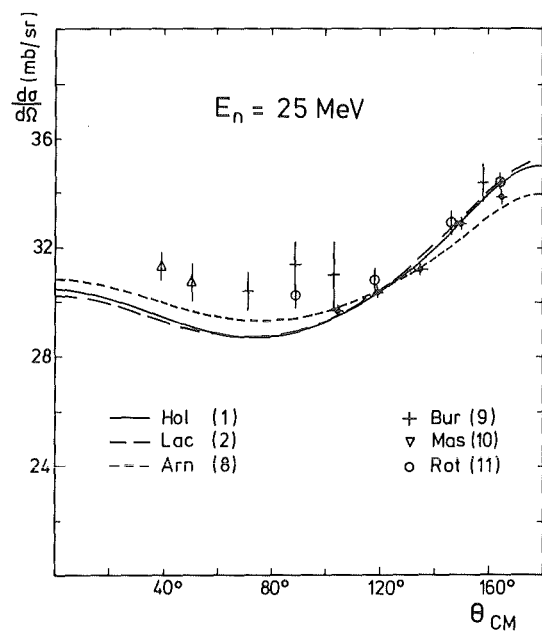
Fig. 2 Differential cross section for n-p scattering at 25 MeV

In fig.1 the total time-of-flight for the neutrons to the polyethylene target plus the protons to the telescopes is plotted versus the energy measured in the NaI-crystal. This matrix was measured at a laboratory angle of $7.5°$. Only the protons were selected for this picture. Fig.1 exhibits an excellent separation between elastic neutron scattering on hydrogen and the charge exchange reaction (n,p) on ^{12}C.

Making use of the continuous energy neutron beam at POLKA we could take data in 8 energy bins in the range from 22 to 50 MeV. 7 angle positions covered the range from $7.5° - 52.5°$ in the lab. system corresponding to $\Theta_{c.m.} = 75° - 165°$ for the scattered neutrons. It is therefore possible to evaluate the cross section shape, especially the ratio $d\sigma(180°)/d\sigma(90°)$, which is a good measure and test for potential predictions (7).

Multiparameter acquisition was performed to separate off-line elastic scattering events from other reaction products. Computer calculations for parameters provide a good possibility in separating and even verifying possible systematic errors in data acquisition and analysing. The data analysis is nearly completed, statistical errors are less than .1% for nearly all measured energies and angles, systematic errors are of the same order or even smaller. First preliminary results are shown in fig.2. Fig.2 shows the differential cross section at 25 MeV as predicted by three models (1,2,8) and measured by previous experiments (9,10,11). Our new data are indicated by small crosses.

(1)   K. Holinde and R. Machleidt, Nucl. Phys. A247 (1975) 495
(2)   M. Lacombe et al., Phys. Rev. C21 (1980) 861
(3)   R.A. Arndt, R.H. Hackman and L.D. Roper, Phys. Rev. C15 (1977) 1021
(4)   R. Bryan and J. Binstock, Phys. Rev. D19 (1974) 72
(5)   J. Wilczynski, KfK report 3781 (1984)
(6)   P. Doll, G. Fink, R. Garrett, H.O. Klages, KfK report 3815 (1984) 140
(7)   A. Bol et al., Few Body Problems in Physics, Vol.2, B. Zeitnitz (editor) Elsevier Science Publishers 1984, p.23
(8)   R.A. Arndt et al., Phys. Rev. D28 (1983) 97
(9)   T.W. Burrows, Phys. Rev. C7 (1973) 1306
(10)   T.G. Masterson, Phys. Rev. C6 (1972) 660
(11)   L.N. Rothenberg, Phys. Rev. C1 (1970) 1226

1.2.3   BACKWARD ANGLE n-d DIFFERENTIAL CROSS SECTION MEASUREMENTS

P. Doll, G. Fink, R. Garrett, W. Heeringa, K. Hofmann, H.O. Klages, H. Krupp

The observables of the n-d system can be calculated in principle exactly with the Faddeev theory (1). For the comparison of this predictions with the measured angular distributions it is necessary to have high precision data over a large energy range. For the elastic differential cross section the data base above 20.0 MeV is very small. The agreement between the calculations and the existing experimental results is, except for the backward angular range, satisfactory. Therefore, we have measured the differential cross section for angles greater than

130°_{cm} in 10°-steps, to see whether these discrepancies are due to the nucleon-nucleon input in the Faddeev calculations or to the experimental data.

We used telescope techniques to detect the charged recoil particles from a thin polyethylene- and deuterated polyethylene foil (47.5 mg/cm^2). The telescopes consist of a ΔE-detector (500 μm Si) and a E-detector (NE 102). We were able to measure the distribution relative to the better known n,p scattering.

The experiment was performed at POLKA in the energy range from 20 to 50 MeV. For monitoring the incident neutron flux a proton recoil monitor system was used.

Fig.1 presents our results together with the distribution of P.Schwarz et al. (squares). The agreement in the minimum is good; but with increasing angles the shape of the new data (circles) is clearly below the previous results.
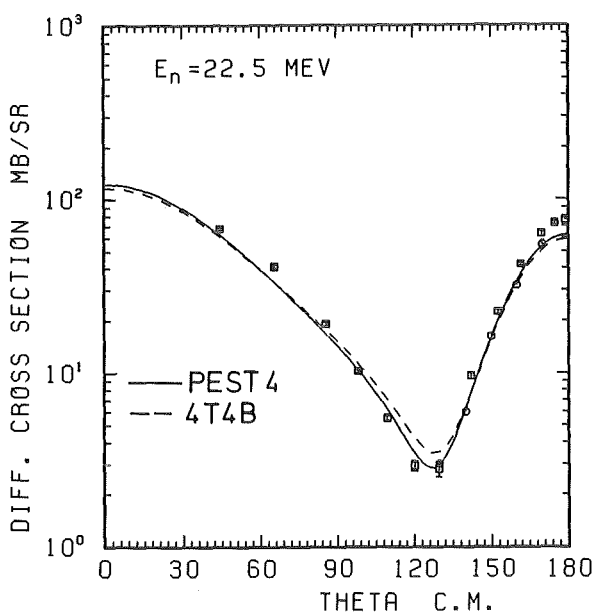
Fig. 1 Differential cross sec-
tion for n-d scattering
at 22.5 MeV
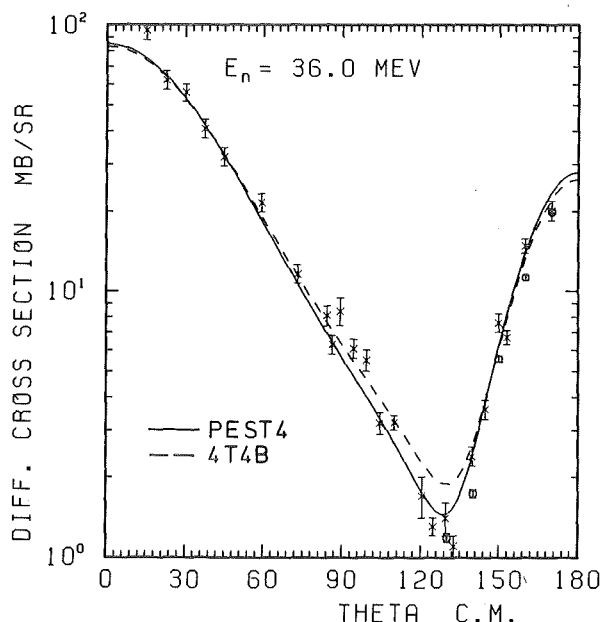
Fig. 2 Differential cross section
for n-d scattering at 36 MeV

For energies below 30 MeV the new data are well described by the Faddeev calculations. To show this, fig.1 contains a prediction with PEST 4 (2) and 4T4B nucleon-nucleon potentials. At higher energies the data points are below the calculations. Fig.2 shows our results with the older exp. distribution of Romero et al. (4) at 36.0 MeV. The agreement between both experiments is very good. For final conclusions it would be necessary to include higher partial waves in the Faddeev code (see contribution 1.2.4).

(1)   L.D. Faddeev, Sov. Phys. IETP 12 (1961) 1014
(2)   J. Haidenbauer and W. Plessas, Phys. Rev. C30 (1984) 1822
(3)   P.Schwarz, H.O. Klages, P. Doll, B. Haesner, J. Wilczynski, B. Zeitnitz,
       Nucl. Phys. A398 (1983) 1
(4)   J.L. Romero, J.A. Jungerman, F.P. Brady, W.J. Knox and Y. Ishizaki,
       Phys. Rev. C2 (1970) 2134

1.2.4 FADDEEV CALCULATIONS WITH VARIOUS SEPARABLE NN POTENTIALS

K. Hofmann, H.O. Klages, Y. Koike[*]

For the n-d-system it is possible to solve the three body problem exactly. Using coupled integral equations in the Faddeev theory it is possible to calculate static and dynamical observables of the three-body system.

We have measured the differential cross section and analyzing power distribution for the elastic n-d scattering in the energy range from 20 to 50 MeV. To compare these results with predictions of Faddeev calculations we installed a three nucleon code at the IBM computer of KfK. This program is based on the non-relativistic AGS form of the Faddeev equations. It is possible to test separable NN-potentials systematically. Included are all partial waves up to $l = 2$ and the coupled $^3S_1 - ^3D_1$ state. The name of the potential refers only to the coupled state.

Potential Name	$^1S_0$	$^3S_1 - ^3D_1$	P and D waves
GRAZ II	GRAZ II	GRAZ II	
PEST 4	PEST	PEST 4	Doleschall
4T4B	Doleschall	Doleschall	

Fig.1 shows the results for the analyzing power at 30 MeV for these three potentials and for the experimental distribution from W.Nitz et al. (1). The best agreement between experiment and predictions is obtained with the GRAZ II potential in the whole energy range.
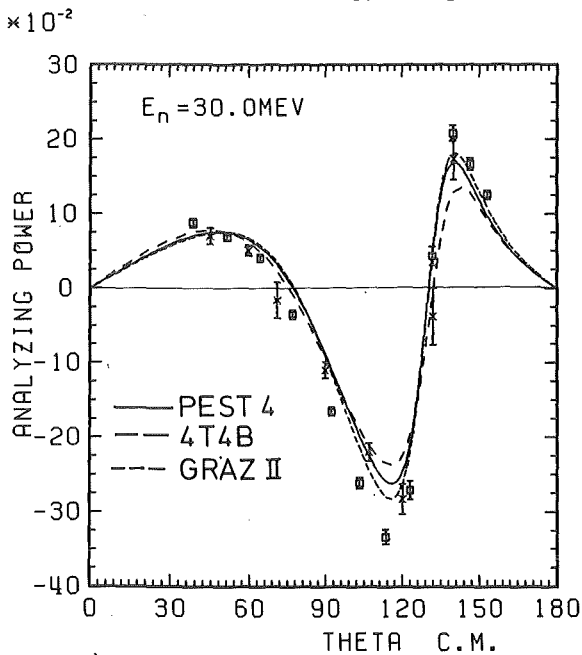
Fig.1 n-d analyzing power at

E_n = 30 MeV
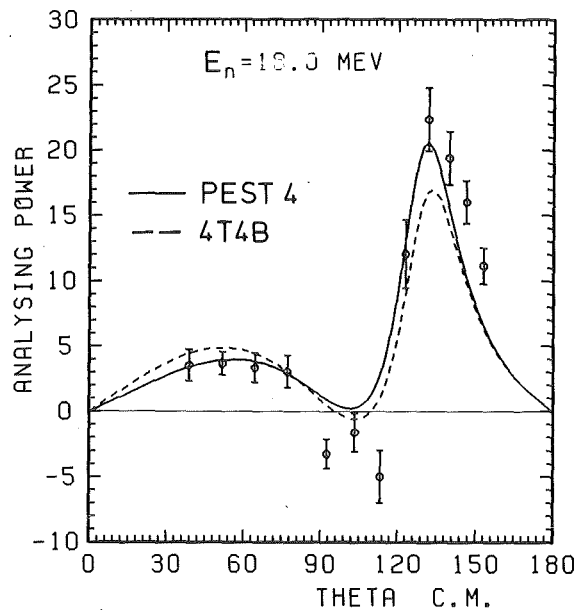
Fig. 2 n-d analyzing power at

E_n = 18 MeV

But there are still discrepancies in the minima and the zero crossing of the A_y-

distribution. A completely unsatisfactory situation is found at lower energies, for example at 18 MeV. Here the experiment yields a zero crossing which is not reproduced by the calculations, see fig.2.

For the cross section the agreement with the data is good up to 30 MeV. For higher energies the shape of the measured cross section is below the predictions in the backward angular range.

For final conclusion it is necessary to include higher partial waves in the three body code. This is possible for the PEST 4 potential. Here J.Haidenbauer and W.Plessas (2) used the EST-method to transform the on- and off-shell properties of the original PARIS potential (3) to a separable form which can in principle be used in the program of Y.Koike. The problem is still the limitation of computer time even with modern computers.

(1)   W. Nitz, Diploma thesis, Univ. Karlsruhe (1985)
(2)   J. Haidenbauer and W. Plessas, Phys. Rev. C30 (1984) 1822
(3)   M. Lacombe, B. Loiseau, J.M. Richard, R. Vinh Mau, J. Cote, B. Pires and
        R. de Tourreil, Phys. Rev. C21 (1980) 861

*   RCNP Osaka, Japan

1.2.5 N-D ANALYZING POWER MEASUREMENT AT 3.5 AND 8 MeV

P. Doll, W. Heeringa, K. Hofmann, P. Jany, H.O. Klages, H. Krupp, G. Völker

In connection with the investigation of the A = 3 system with neutron and deuteron in the entrance channel the analyzing power for the elastic n-d scattering was measured at low neutron energies.

The experiment was performed at the Karlsruhe 3 MV Van-de-Graaff accelerator using polarized neutrons produced by the Be(α,n)C reaction (1,2). This reaction produces two neutron groups, which are well separated in energy, with high polarization at the same angle and α-energy. Thus we had the possibility to measure two energies 3.5 and 8 MeV simultaneously using a pulsed beam of 2.6 MeV α-particles. The polarization of the neutrons was determined by a two-dimensional interpolation (described in 1.2.7) of precise data for the source reaction.

The polarized neutrons passed a superconducting solenoid, used to change the spin direction every ten minutes, and a polyethylene collimator which formed a narrow rectangular beam (3).

As a scattering sample a cylinder filled with the deuterated liquid scintillator NE 213 was used. 14 neutron detectors were set up in symmetric pairs at a distance of 0.27 m from the sample. Angular distributions were measured in the range of 30° lab. to 120° lab..

The uncorrected angular distributions for A_y taken from our data (circles) are shown in fig.1,2 for the two energies. The error bars contain only the statistical

errors, which have been compared to previous experiment at these low energies.
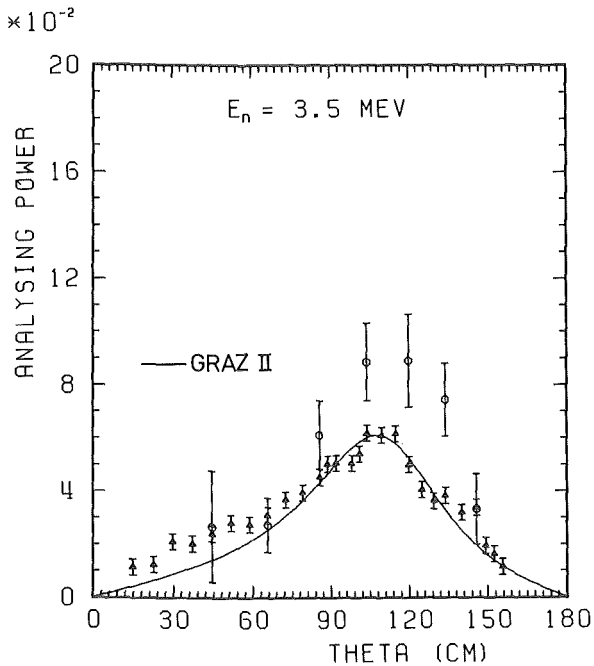
Fig. 1 $\vec{n}$-d and $\vec{p}$-d analyzing
power at 3.5 MeV.
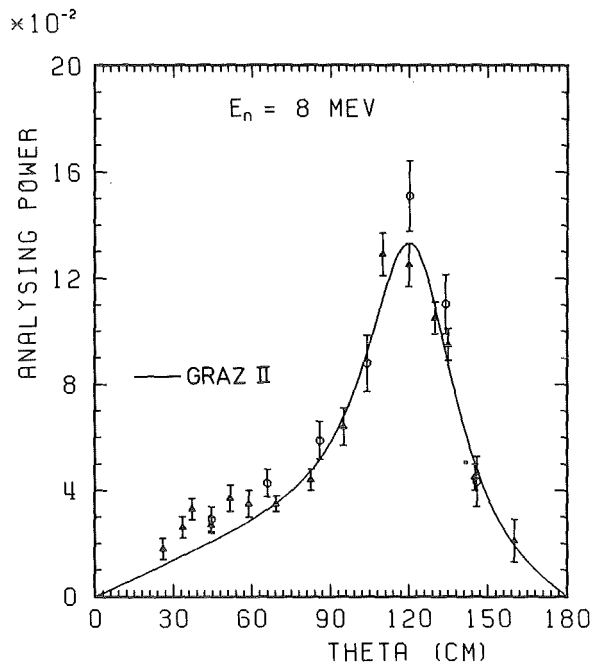
Fig. 2 $\vec{n}$-d and $\vec{p}$-d analyzing power
at 8 MeV.

In the next step these data have to be corrected for multiple scattering and fi-
nite geometry effects by using the program "Muscat" (4,5). These effects are ex-
pected to shift the measured data by 1-3%. The final results will allow compari-
sons to $\vec{p}$-d observables (6,7) (triangles) and three nucleon calculations based
on the three-nucleon code of Y.Koike (8).

(1)   P.B. Dunscombe, R. Maschuw, G. Meyer-Kretschmer, T.G. Miller, P. Suhr,
        B. Zeitnitz, Nucl. Instr. Meth. 120 (1974) 477
(2)   Th. Stammbach, G. Spalek, I. Taylor, R.L. Walter, Nucl. Instr. Meth. 80
        (1970) 304
(3)   P. Jany, Diploma thesis, Univ. Karlsruhe (1985)
(4)   J. Hansmeyer, Diploma thesis, Univ. Karlsruhe (1983)
(5)   W. Nitz, Diploma thesis, Univ. Karlsruhe (1985)
(6)   T.B. Clegg, W. Haeberli, Nucl. Phys. (1967) 608
(7)   R.E. White, W. Gruebler, B. Jenny, V. Koenig, P.A. Schmelzbach, H.R. Buergi,
        Nucl. Phys. A321 (1979) 1
(8)   Y. Koike, private communications

1.2.6   TWO-DIMENSIONAL EVALUATION OF POLARIZATION- AND CROSS SECTION DATA
        P. Jany, H.O. Klages, Chr. Maier, G. Völker

In scattering experiments observables like asymmetries and cross sections are
usually measured as function of parameters like scattering angle and energy. Of-
ten such experiments are performed at discrete scattering angles and discrete en-

ergies. To obtain the observable at any specific parameter value, it is an elegant way to use a computer routine, which allows interpolation between experimental data in full parameter space. Also it is very useful to have the whole information about any parameter dependence in one figure like in a contour plot.

The routine "HKPLOT" (1) enables the presentation of a function of at least two variables by their contour lines. Before "HKPLOT" can be called, the list of the variables and their function values has to be sorted and interpolated between the existing values with the availables subroutines "VORINT" and "MEDINT" (2). After these preparations a function can be shown in dependence to its variables.

In our scattering experiments at the Van-de-Graaff accelerator the polarized neutrons were produced by the $T(p,n)$ ^{3}He reaction. The polarization, which is a function of the energy of the protons and of the angle between tritium-target and the proton-beam, has to be well known at a fixed angle and energy. So the polarization was plotted as function of the energy and the angle. So we could read off the polarization for our experimental conditions from this contour plot (fig.1).
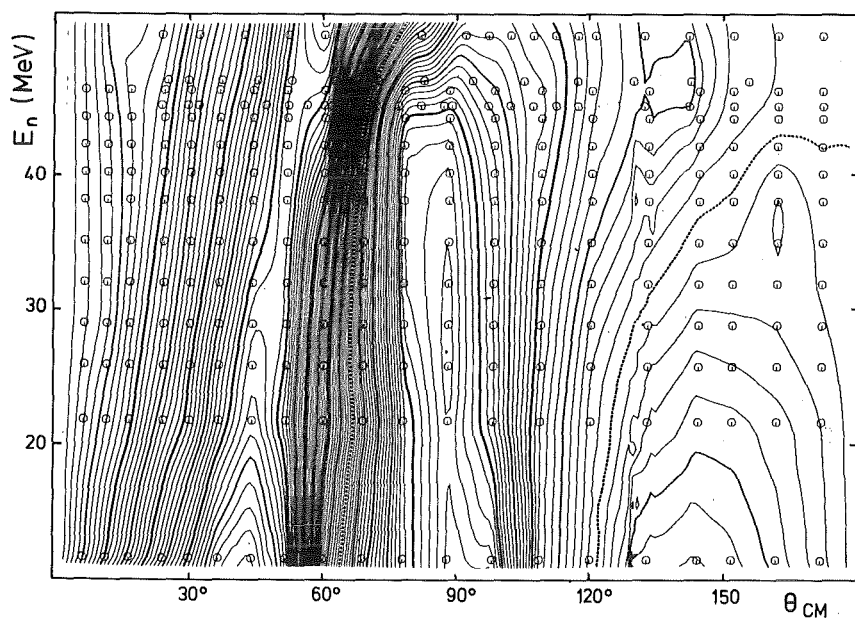
Fig. 1 Analyzing power for $\vec{n}$-^{3}He. Energy versus c.m. angle

In figure 1 the analyzing power of the elastic $\vec{n}$ - ^{3}He scattering was shown in the energy range from 10 to 50 MeV and in the angle range from 0 to 180 degree. This contour plot is based on the following different data sets: at 8., 12. and 17.1 MeV from Lisowski et al. (4), at 10. and 15.3 MeV from Dobiasch et al. (5) and at 16., 18., 20., 22., 24., 27., 30., 33., 36., 40. and 50 MeV from Maier (6). Out of this plot all interpolated values of an observable could be quoted.

(1)   S. Kleinheins, Programmbeschreibung 386 (18.12.81), INR KfK Karlsruhe
(2)   W. Fischer, Programmbeschreibung 344 (16.12.74), INR KfK Karlsruhe
(3)   P. Jany, Diploma thesis, Univ. Karlsruhe (1985)
(4)   L. Lisowski et al., Nucl. Phys. A259 (1976) 61
(5)   H. Dobiasch, Dissertation, Univ. Karlsruhe (1979)
(6)   Chr. Maier, Diploma thesis, Univ. Karlsruhe (1984

1.2.7   FINAL RESULTS OF THE ANALYZING POWER OF THE ELASTIC $\vec{n}$-^{3}He SCATTERING
        AT LOW ENERGIES AND PHASE SHIFT ANALYSIS

G.M. Hale[*], W. Heeringa, K. Hofmann, P. Jany, H.O. Klages, H. Krupp,
Chr. Maier

Analyzing power distributions of the elastic $\vec{n}$-^{3}He scattering have been measured
in the energy range from 0.94 to 2.00 MeV. The measurement was performed at the
Karlsruhe Van-de-Graaff accelerator using the ^{3}H($p,\vec{n}$) source reaction and as
scattering sample a liquid ^{3}He-scintillation detector. The scattered neutrons
were detected by six pairs of neutron detectors at scattering angles from 50° to
160° (c.m.). Multiparameter data acquisition and off-line data analysis were per-
formed.

The data were corrected for the effects of multiple scattering, finite
geometry and the energy distribution in the neutron beam. The corrections were
calculated with the Monte Carlo code "PMS3" which simulates the experiment. This
code needs a phase shift parametrization of the n-^{3}He scattering as input. This
input was taken from a recent R-matrix analysis of the A = 4 system. The agree-
ment of the analyzing power distributions predicted by this R-matrix calculation
and the measured ones is sufficiently good for the corrections.

Due to the multiparameter data acquisition which was enabled by the liquid
^{3}He scintillating scatterer the amount of double scattering ($\sim$ 1.4%) and of back-
ground ($\sim$ 0.9%) were rather small. Therefore, the corrections to A_y were also
small ($\sim$ 0.003).

Fig.1 shows the corrected data compared to the R-matrix predictions and to
results of other authors at comparable energies (1,2).The solid lines are results
of a phase shift analysis performed in this work, in which the existing n-^{3}He
scattering data were parametrized in the energy region from 1.0 to 3.7 MeV. We
calculated the real part of the phase shifts, the absorption parameters and the
mixing parameters up to L, J = 2.

The n-^{3}He data were compared to data of other channels in the A = 4 system
(p-^{3}H, p-^{3}He). The large difference between n-^{3}He and p-^{3}H found at the lowest
energies shows the large influence of the Coulomb interaction. This difference
decreases rapidly with increasing energy. The difference found between n-^{3}He and
p-^{3}He can, apart from the Coulomb interaction, also be attributed to the lacking
of T = 0 levels in the p-^{3}He system. This difference seems to remain up to at
least 50 MeV (3).
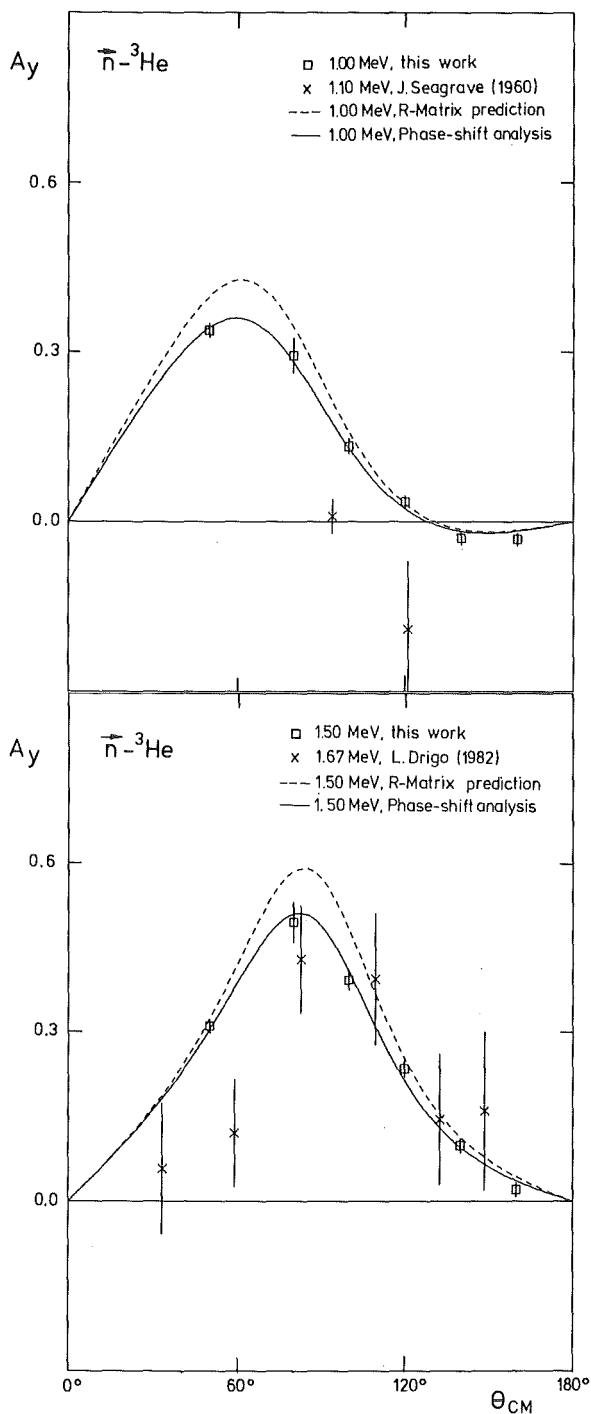
Fig. 1 Comparison of our $\vec{n}$-^{3}He analyzing power results with other data, with R-matrix predictions and with curves from a phase-shift analysis.
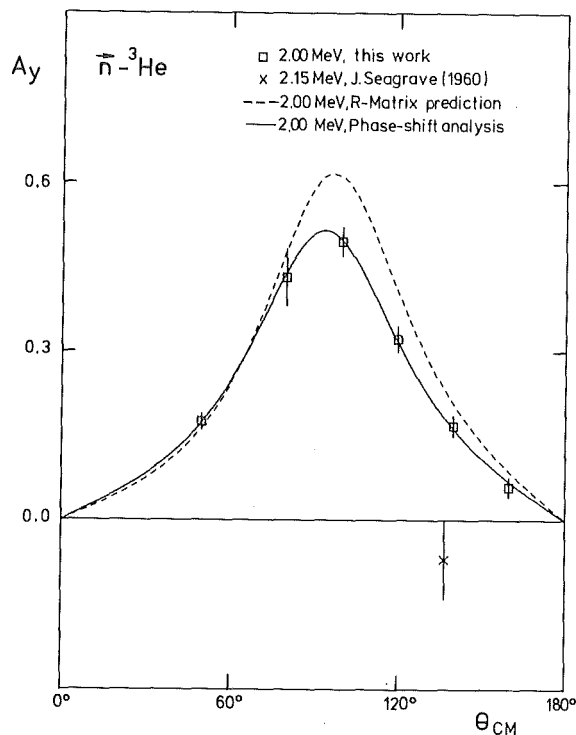
(1)   J.D. Seagrave, L. Cranberg and J.E. Simmons, Phys. Rev. 119 (1960) 1981
(2)   L. Drigo, G. Tornielli and G. Zannoni, Ann. d. Physik 39 (1982) 408
(3)   Chr. Maier, Diploma thesis, Univ. Karlsruhe (1984)

*   Theory Division, LANL, Los Alamos, New Mexico 87545, USA.

1.3   NUCLEAR REACTIONS BY CHARGED PARTICLES

1.3.1   THE NONELASTIC PROJECTILE BREAK UP CROSS SECTION ASSOCIATED WITH γ-RAY EMISSION IN ^{6}Li + ^{40}Ca COLLISIONS AT 156 MeV

R. Planeta[+], H. Klewe-Nebenius[++], J. Buschmann, T. Kozik, H.J. Gils, H. Rebel and K. Grotowski[+]

The continuum part of inclusive particle spectra from nuclear reactions with composite particles often exhibits bell-shaped bumps centered around the energies corresponding to the beam-velocity and dominating the spectra at forward angles. These bumps are readily ascribed to the break up of the projectile into its fragments. This phenomenon is very pronounced for loosely bound projectiles like ^{6}Li, which is of special interest due to the transitional character of ^{6}Li induced nuclear reactions, linking typical light-ion phenomena with features of heavy-ion reactions. In fact, by a series of measurements of the inclusive cross sections for the emission of light charged particles when bombarding various targets by 156 MeV ^{6}Li ions, large yields of light particles have been found. Some more exclusive studies of the break up of ^{6,7}Li reveal the importance of nonelastic break up processes, where one of the fragments interacts inelastically with the target. In particular, a break-up-fusion type process, in which one of the break up fragments is absorbed by the target nucleus, has been shown to play an important role.

The present work explores the nonelastic break up modes in more detail by measuring the γ-ray spectra from the heavy residual nuclei in coincidence with light ejectiles (in particular beam-velocity particles) from bombardment of ^{40}Ca by 156 MeV ^{6}Li ions.

The measurements aim at a determination of the $(^6\text{Li},\alpha\gamma)$, $(^6\text{Li},^3\text{He}\gamma)$, $(^6\text{Li},t\gamma)$, $(^6\text{Li},d\gamma)$ and $(^6\text{Li},p\gamma)$ contributions clarifying more details of the mechanism for the emission of light particles in ^{6}Li-nucleus collisions. As far as nonelastic break up processes are signalled by γ-ray emission from target-like reaction products the results may provide a serious check of theoretical predictions based on the DWBA break up theory. The DWBA analysis of the inclusive charged particle spectra observed for ^{6}Li + ^{40}Ca reactions at E_{Li} = 156 MeV predicts (1) large contributions from nonelastic break up processes.

Fig. 1 compares the inclusive γ-particle spectra at various emission angles with the corresponding spectra measured in coincidence with all observed γ-ray peaks, corrected for the detection efficiency of the γ-ray detector. Contributions by the γ-ray continua adjacent to the lines have been subtracted. At
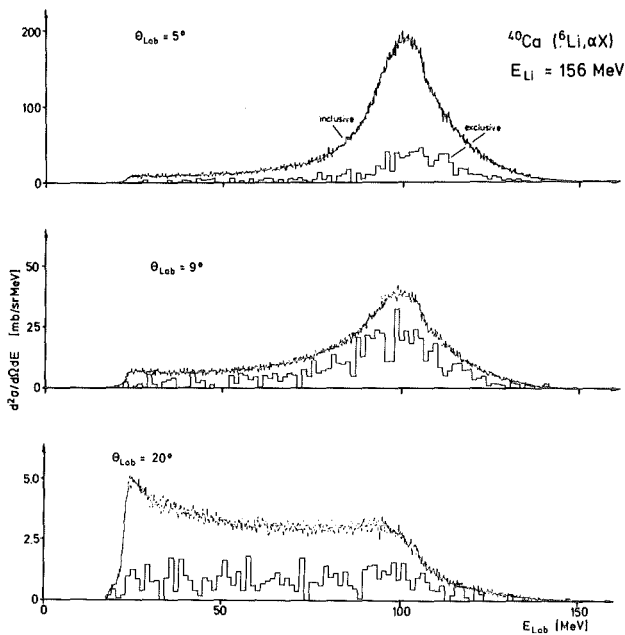
Fig. 1

Inclusive and exclusive energy spectra of α-particles emitted at various angles when bombarding ^{40}Ca by 156 MeV ^{6}Li-ions.
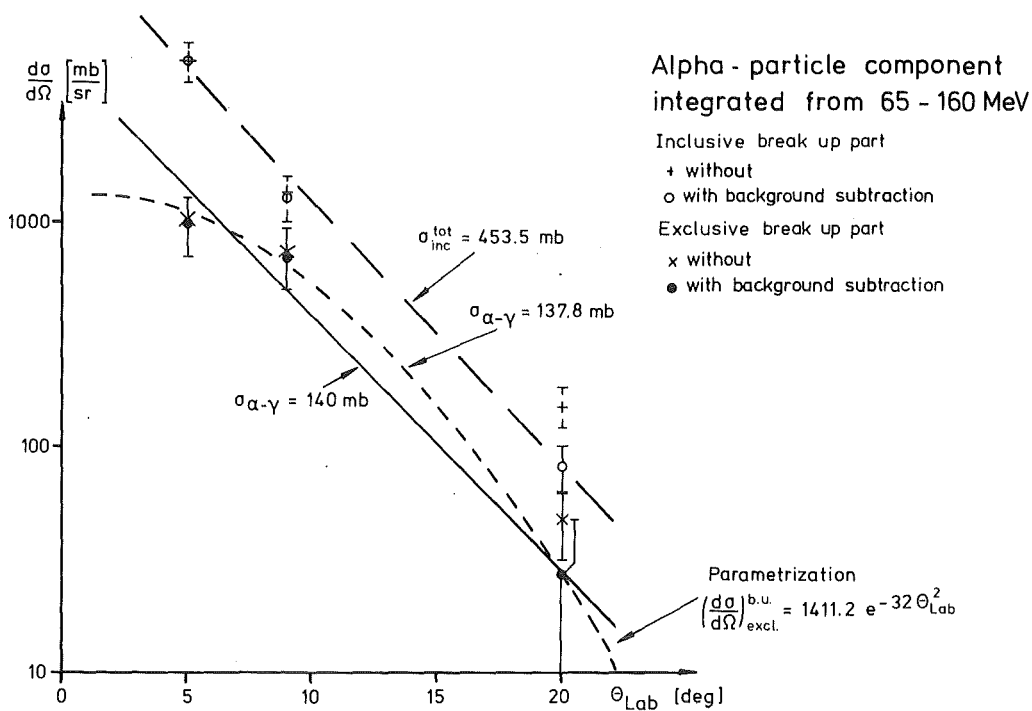
Fig. 2 Angular distributions of the energy-integrated α-particle cross section.

least two different components can be identified in the inclusive and exclusive particle spectra: (i) the bump centered around the beam velocity energy and ascribed to α-particles from the projectile break up and (ii) an evaporation and preequilibrium emission component ("background"). Fig. 2 displays the angular dependence of the inclusive and exclusive cross sections for the α-particle as an example.

For the studied case of the ^{6}Li + ^{40}Ca reaction at E_{Li} = 156 MeV the nonelastic break up contributions comprise a summed-up cross section of σ = 582 ± 110 mb which should be compared with the value σ = 930 ± 115 mb of the total break up cross section.

The differential cross sections for the nonelastic break up are found to be significantly smaller than the values predicted (1) by the DWBA break up theory, which describes a direct break up mode and ignores a possible two-step mechanism ("sequential" break up).

(1)   B. Neumann, H. Rebel, H.J. Gils, R. Planeta, J. Buschmann, H. Klewe-Nebenius, S. Zagromski, R. Shyam and H. Machner, Nucl. Phys. A382 (1982) 296

+   Institute of Physics, Jagellonian University, Cracow, Poland
++   Institut für Radiochemie, Kernforschungszentrum Karlsruhe

1.3.2 MEASUREMENTS OF ^{6}Li BREAK UP FRAGMENTS IN VERY FORWARD DIRECTION

H. Jelitto, J. Buschmann, H.J. Gils, H. Rebel, S. Zagromski, T. Kozik[+], C. Samanta[++]

The break up of ^{6}Li projectiles at E_{Li} = 156 MeV was shown (1) to be dominated by the direct nuclear break up for reaction angles larger than $\Theta_{Lab} \sim 10°$. At smaller angles (larger impact parameters) a change of the reaction mechanism from nuclear to Coulomb break up is expected. It is most interesting to investigate whether this influences the monotonic exponential decrease of the angular distributions of the fragments observed at larger angles (1,2). Also the importance of multi-step processes (sequential break up) and of Coulomb-nuclear interference effects are of considerable interest.

For such experiments, which require the detection of fast break up fragments in very forward direction and an efficient reduction of the background, the recently installed magnetic spectrograph "Little John" is a very suitable instrument.

As a first step of these studies inclusive energy spectra of ^{6}Li fragments ejected from targets of ^{6}Li, ^{12}C, ^{120}Sn, ^{208}Pb have been measured at very small emission angles with the magnetic spectrograph. Since the charged particle spectra are characterized by broad bumps (1) the spectrograph was used in the low

dispersion / high momentum acceptance mode (3) (focal plane 2) in order to measure a large fraction of the spectra with a fixed magnetic field. The momentum acceptance in this mode is $\delta p/p = 9.3$ %. As an example, Fig. 1 shows the inclusive energy spectrum of alphas at $\Theta_{Lab} = 3°$ obtained with two magnetic settings as indicated covering the whole break up region of deuterons and α-particles. For the spectroscopy of protons, tritons, and ^{3}He particles other field settings have to be used. The break up spectra of all these particles have been measured in eight overlapping momentum regions in the angular range $\Theta_{Lab} = 1.5$ to $12°$ in steps of $1°$.
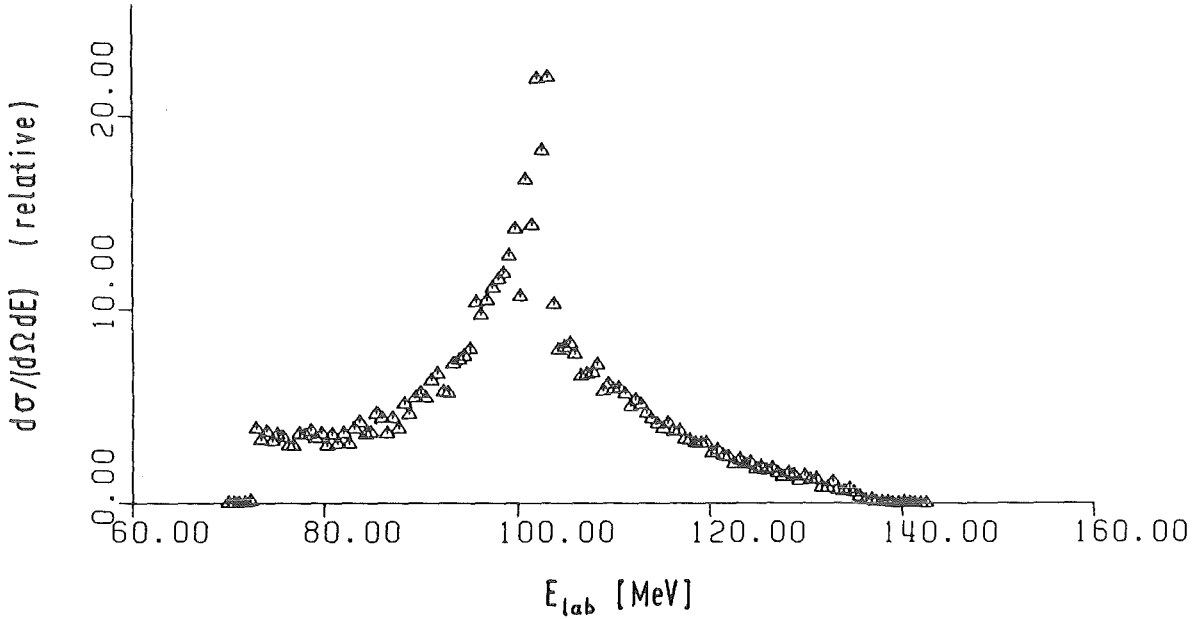
Fig. 1 Inclusive alpha particles from the reaction 156 MeV ^{6}Li + ^{208}Pb at $\Theta_{Lab} = 3°$.

In Fig. 2 the angular distribution of the break up deuterons from ^{208}Pb is displayed together with the elastic ^{6}Li scattering cross sections. The correlated change in the angular behaviour from Coulomb to nuclear effects is clearly indicated, which will be analysed in detail.
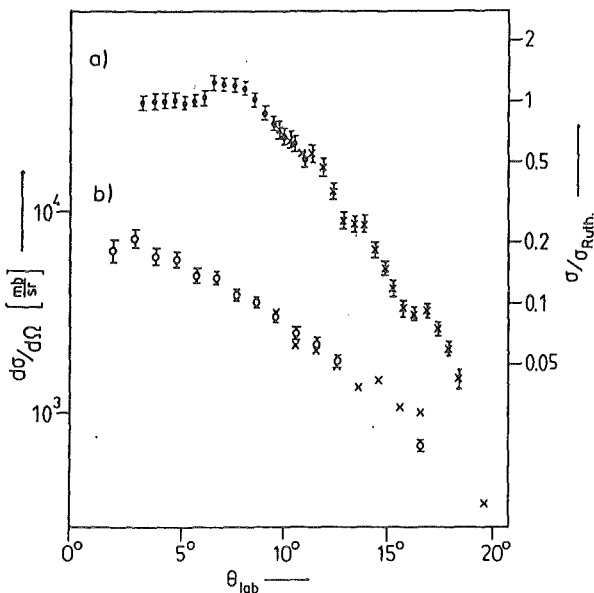
Fig. 2 Differential cross sections of elastic ^{6}Li scattering divided by the Rutherford cross section (a) and of break up alphas from the reaction ^{6}Li + ^{208}Pb at $E_{Li} = 156$ MeV (b) (data from previous measurements are included as crosses)

(1)   B. Neumann, H. Rebel, H.J. Gils, R. Planeta, J. Buschmann, H. Klewe-Nebenius, S. Zagromski, R. Shyam and H. Machner, Nucl. Phys. A382 (1982) 296

(2)   B. Neumann, H. Rebel, J. Buschmann, H.J. Gils, H. Klewe-Nebenius, S. Zagromski; Z. Phys. A296 (1980) 113

(3)   H.J. Gils, KfK-Report 2972 (1980)

+   On leave from Institute of Physics, Jagellonian University, Cracow Poland
++   On leave from Saha Institute of Nuclear Physics, Calcutta, India

1.3.3 A PRIOR INTERACTION DWBA FOR DIRECT BREAK UP OF LIGHT-IONS

D.K. Srivastava[+] and H. Rebel

There are various attempts to describe direct break up processes of a nuclear projectile in the field of an atomic nucleus. The most elaborate theory accounting for the absorption and the distortion by the nuclear field is the post-form DWBA theory worked out by Baur et al. (1) and applied successfully for the analysis of experimental data in a variety of cases. However, the theory rests upon a zero-range approximation which implies an internal momentum distribution of the cluster fragments being constrained to a Lorentzian shape with parameter values fixed by the binding energy. There are experimental indications that this breaks down for ^{6}Li break up e.g. It is definitevely not applicable when the internal cluster motion is not confined to a relative s-state. In fact, the possible access to the internal momentum distribution is one of the most interesting aspects of projectile-break up studies. A full finite-range evaluation of the matrix element for the elastic break up reaction a + A → b + x + A is hardly feasible as the $d\vec{r}_{aA}$ integral converges very slowly, and a straight-forward evaluation may involve integrations up to a few hundred fms.

In the present paper we analyse the possibility to overcome the mentioned drawbacks by a reformulation of the DWBA break up theory on the basis of the prior-form prescription of the T matrix,

$$T_{\vec{q}_a \to \vec{q}_b \vec{q}_x} = \int \chi_b^{(-)*}(\vec{r}_{bA}) \chi_x^{(-)*}(\vec{r}_{xA}) \; [U_{bA}(r_{bA}) + U_{xA}(r_{xA}) - U_{aA}(r_{aA})]$$

$$\phi_a(\vec{r}_{bx}) \; \chi_a(\vec{r}_{aA}) \; d\vec{r}_{aA} \; d\vec{r}_{bx}$$

which is formally equivalent to the post-form expression.

We find that the orbital dispersion effects and the dependence of the spectra on details of the properties of the wave-function can be clearly brought out due to the use of the plane wave expansion technique devised by Robson et al.(2). The explicit appearance of projectile-interaction terms provides a very clear understanding of the reaction mechanism and the theory is thus easily amenable to calculations of more complicated forms of break-up.

In order to test the various aspects of our theory, in particular, the finite range aspect and the automatic inclusion of recoil effects, we have studied in detail, the break up of ^{6}Li at 156 MeV on a ^{6}Li target into alpha and deuteron, for which preliminary experimental data on angular correlation were available. Two alternative descriptions were used for the α-d relative motion wave function in the ground state of the projectile, to get an illustration of the sensitivity of the break up cross section to the details of the internal momentum distribution: (i) a Yukawa type wave function (ii) a (α+d) wave function generated by a Woods-Saxon potential, reproducing the 2s bound state at 1.47 MeV. Fig. 1 compares a measured correlation spectrum of the elastic ^{6}Li→α+d break up with theoretical results, showing the preference of the Woods-Saxon wave function and the sensitivity to finite range effects.

^{6}Li + ^{6}Li ⟶ α + d + ^{6}Li
156 MeV

Θ_α = 5°
Θ_d =-10°

--- x 5. (Yuk)
—— 2 s (WS)
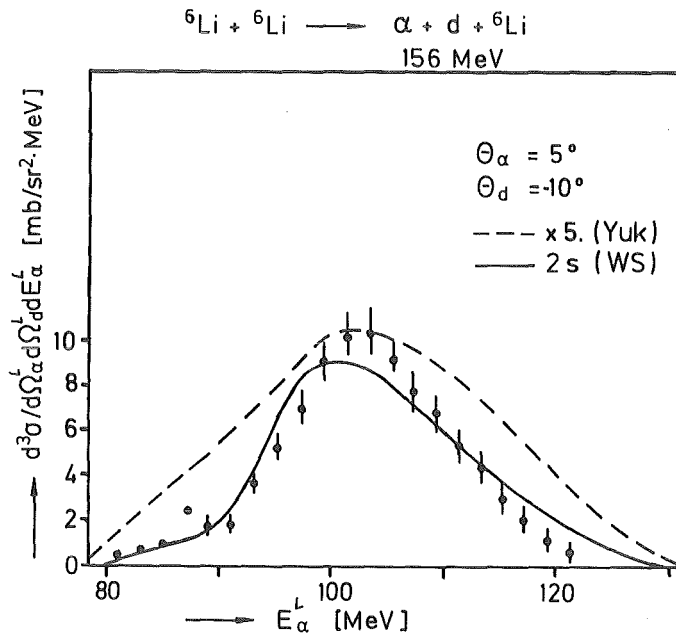
Fig. 1 Triple differential cross section for the elastic break up reaction
^{6}Li+^{6}Li → α+d+^{6}Li

(1)   G. Baur, F. Rösel, D. Trautmann and R. Shyam, Phys. Rev. C111 (1984) 333
(2)   D. Robson and R.D. Koshel, Phys. Rev. C6 (1972) 1125.
        L.A. Charlton, Phys. Rev. C8 (1973) 146.

+   On leave from V.E.C. Centre, Calcutta, India

1.3.4 COULOMB BREAK UP OF LIGHT IONS IN A DIRECT DWBA MODEL

C. Samanta[+], D.K. Srivastava[++] and H. Rebel

Break up processes of nuclear projectiles under the influence of the differential Coulomb field of a heavy target nucleus are of considerable interest, since they provide the possibility to study electromagnetically induced interactions of the projectile constituents. Sequential processes proceeding through the excitation of sufficiently long-living resonance states of the projectile are expected to be well described like Coulomb excitation of bound states. The direct (nonresonant) process involves energy dependent transition matrix elements into the continuum of the fragment system, which might be somewhat distorted by the Coulomb field present at the break up point. However, for fast particles the internal distortion of the relative system of the fragments may be small, so that the direct DWBA break up approach worked out by Baur et al. (1) should provide an adequate description of the situation, even in zero-range approximation.

In applying the direct break-up-DWBA-T matrix element

$$T_{\vec{q}a \to qb,qx} = D_0 \int \chi_b^{(-)x}(\vec{q}_b,\vec{R}) \chi_x^{(-)x}(\vec{q}_x,R) \; \chi_a^{(+)}(\vec{q}_a,R) d\vec{R}$$

for the reaction

$$a + A \to b + x + A$$
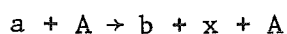
with the usual meaning of the symbols, we have exploited some specific properties of the Coulomb-wave functions which enter as distorted waves. In the case of pure Coulomb waves the radial integrals involved can be brought into an analytical expression, which simplifies the numerical evaluation. A corresponding computer code is in development (2).

In context of our current experimental studies of ^{6}Li$\to\alpha$+d dissociation in the field of ^{208}Pb at E_{Li}=156, we have explored some features of the direct break up in a pure Coulomb potential. Considering a particular value of the laboratory energy E_α^{LAB} of the α-particle fragment coincidently emitted with the corresponding deuteron, we have first studied the angular momentum localization of the reaction. It turns out that like with the nuclear break up, the reaction is fairly well concentrated around the grazing angular momenta of the emerging α-particles and deuterons. This was not obvious before and can lead to further simplifications of the calculations. First calculations of the triple differential cross sections result in unrealistically small values. The origin of this feature is not understood, but it might be due to the unrealistic interaction potential, ignoring any absorption of low partial waves. The necessity to include such effects has been demonstrated in studies of Coulomb break up of the deuteron (3).

(1)   G. Baur, F. Rösel, D. Trautmann and R. Shyam, Phys. Rep. 111C (1984) 333
(2)   C. Samanta, unpublished report, Kernforschungszentrum Karlsruhe 1985
(3)   B. Hoffmann and G. Baur, Phys. Rev. C30 (1984) 247

+   On leave from Saha Institute of Nuclear Physics, Calcutta, India
++   On leave from V.E.C. Centre, Calcutta, India

1.3.5 RESONANT AND NONRESONANT COULOMB BREAK UP - ACCESS TO ELECTROMAGNETIC INTERACTION MATRIX ELEMENTS AT LOW RELATIVE ENERGIES

D.K. Srivastava[+] and H. Rebel

In view of the experimental difficulties in measuring radiative capture reaction cross sections at low relative energies, being of considerable interest for nuclear astrophysics, it has been proposed (1) to investigate the inverse reaction: the electromagnetically induced decay of a nucleus into two fragments, which subsequently emerge with low relative energies, however on a pedestal of sufficiently high laboratory energies, convenient for experimental detection. Such a process is the break up of a complex nuclear projectile, while moving through the Coulomb field of a nucleus, which only acts as a catalyst. In addition to obvious advantages (1), partly arising from the kinematical situation, one expects an enhancement of the dissociation cross section as compared to the photodissociation cross section (directly related by detailed balance to the capture cross section). The enhancement is due to the richness of the virtual photon spectrum, experienced by the projectile of sufficiently large energy. With these aspects, we have analysed the Coulomb break up of light-ion projectiles on the basis of a DWBA approach. We followed Rybicki and Austen (2), assuming the process as evolving from a two-step mechanism: excitation to a nonresonant or resonant continuum state of the fragment-system, describing this "excited projectile" by a distorted wave $\chi_Q(\vec{R})$ in the field of target nucleus. This picture differs from the DWBA approach of Baur et al. (3), where any final state interaction between the fragments is ignored.

In the specific case of the Coulomb break up of ^6Li in $\alpha+d$, the dominant contribution is of multipolarity $L = 2$. For quadrupole transitions the evaluation of the DWBA-transition matrix element can be considerably simplified and the influence of the catalyst-nucleus on the orbital motion is absorbed in a "contact term" C^2, determined by the orbital wave functions $\chi_Q(R)$ at the origin. The triple differential cross section of observing a fragment α-particle in coincidence with the corresponding deuteron in an elastic break up event is given by a simple expression

$$\frac{d^3\sigma}{d\Omega_\alpha d\Omega_d dE_\alpha}(E_\alpha,\theta_\alpha,\theta_d) = \frac{(4\pi)^5 Z_A^2 e^2}{4\hbar(2J_f+1)}\left[\frac{m_{Li}}{2E_{Li}}\right]^{1/2} C^2 b(E2,k,J_i{\rightarrow}J_f)\,\rho$$

where ρ is the three-body phase space and in which the electromagnetic transition probability $b(E2,k)$ from the ^{6}Li ground state to the continuum state with the relative momentum k of the α-d system enters in a transparent way. Fig. 1 displays the theoretical cross section for a particular kinematical situation. For the calculations of the non-resonant cross section the $b(E2,k)$ distribution has been calculated using theoretical wave functions, while for the resonant part the experimental $B(E2;1^+-3_1^+)$ has been adopted.
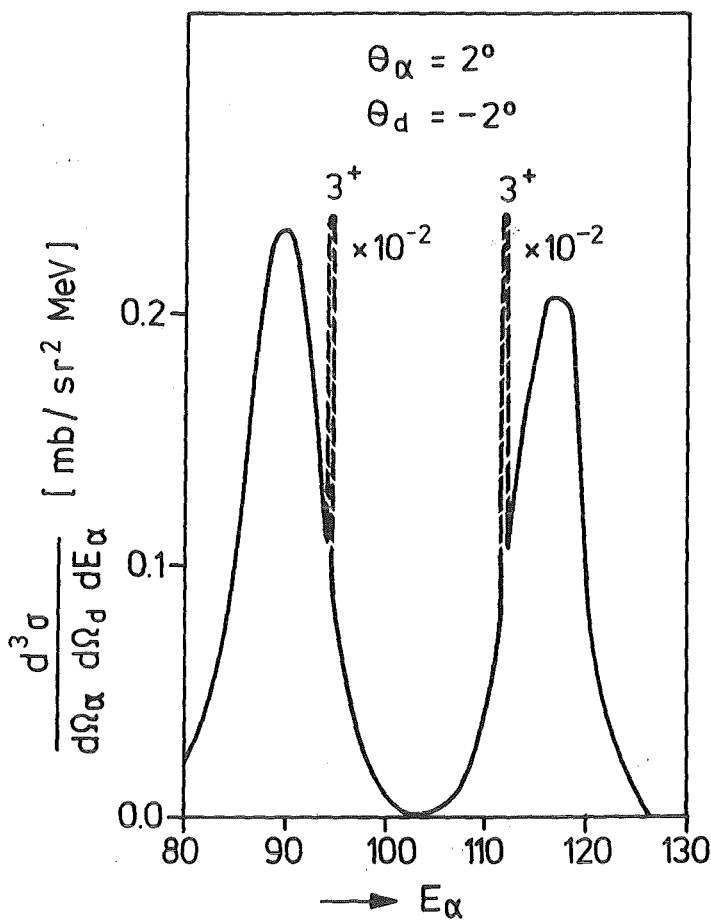
Fig. 1
Triple differential cross section for resonant and nonresonant excitation of the α+d continuum in ^{6}Li projectile break up in the Coulomb field of ^{208}Pb at E_{Li} = 156 MeV

The measurements of the cross sections would sensitively test the theoretical ingredients and possibly provide an acess to the electromagnetic continuum transition elements.

(1)   H. Rebel "Nuclear Reaction Cross Sections of Astrophysical Interest", unpublished Report, Kernforschungszentrum Karlsruhe, February 1985
(2)   F. Rybicki and N. Austen, Phys. Rev. C6 (1972) 1525
(3)   G. Baur, F. Rösel, D. Trautmann and R. Shyam, Phys. Rep. C111 (1984) 333

+   On leave from V.E.C. Centre, Calcutta, India

1.3.6 MASSIVE TRANSFER TO THE PROJECTILE IN ^{6}Li INDUCED NUCELAR REACTIONS AT
E_{Li} = 156 MeV.

T. Kozik[+], J. Buschmann, K. Grotowski[++], H. Klewe-Nebenius[+++], H.J. Gils,
H. Jelitto, R. Planeta[++], H. Rebel and S. Zagromski

Extensive studies of different reaction channels of the ^{6}Li + ^{40}Ca reaction at
156 MeV (1) suggest that strongly damped collisions might contribute with a con-
siderable fraction to the total reaction cross section. In order to investigate
this question we have measured the cross sections for the production of light
("projectile-like") fragments (heavier than ^{6}Li) in ^{6}Li induced reactions with
^{27}Al, ^{46}Ti, ^{50}Ti and ^{58}Ni nuclei. The energy spectra of the reaction products
were observed with two ΔE-E gascounter - Si surface barrier detector telescopes
and one ΔE-E Si surface barrier detector telescope, detecting the ejectiles in
the angular range Θ_{Lab} = 5° - 85°. The spectra (Fig. 1) show no significant
structure, but immediately indicate a large energy dissipation. This is corro-
borated by the exponential shapes of the angular distributions (Fig. 2), which
miss any peak at the grazing angles. The angle integrated charge distributions
show well pronounced odd-even effects, following the binding energy of the final
reaction products.
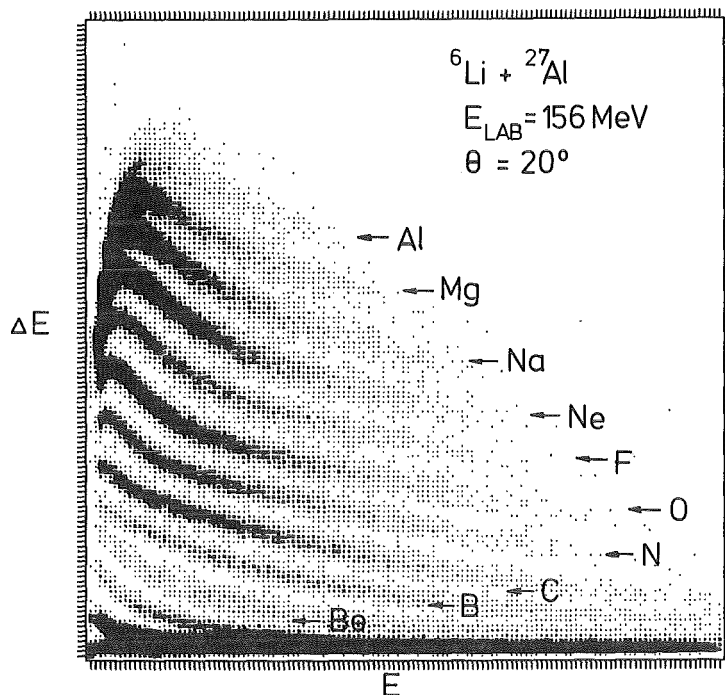
Fig. 1 ΔE-E spectrum measure with a gascounter-Si surface barrier detector
telescope for ^{6}Li + ^{27}Al reactions at E_{Li} = 156 MeV.
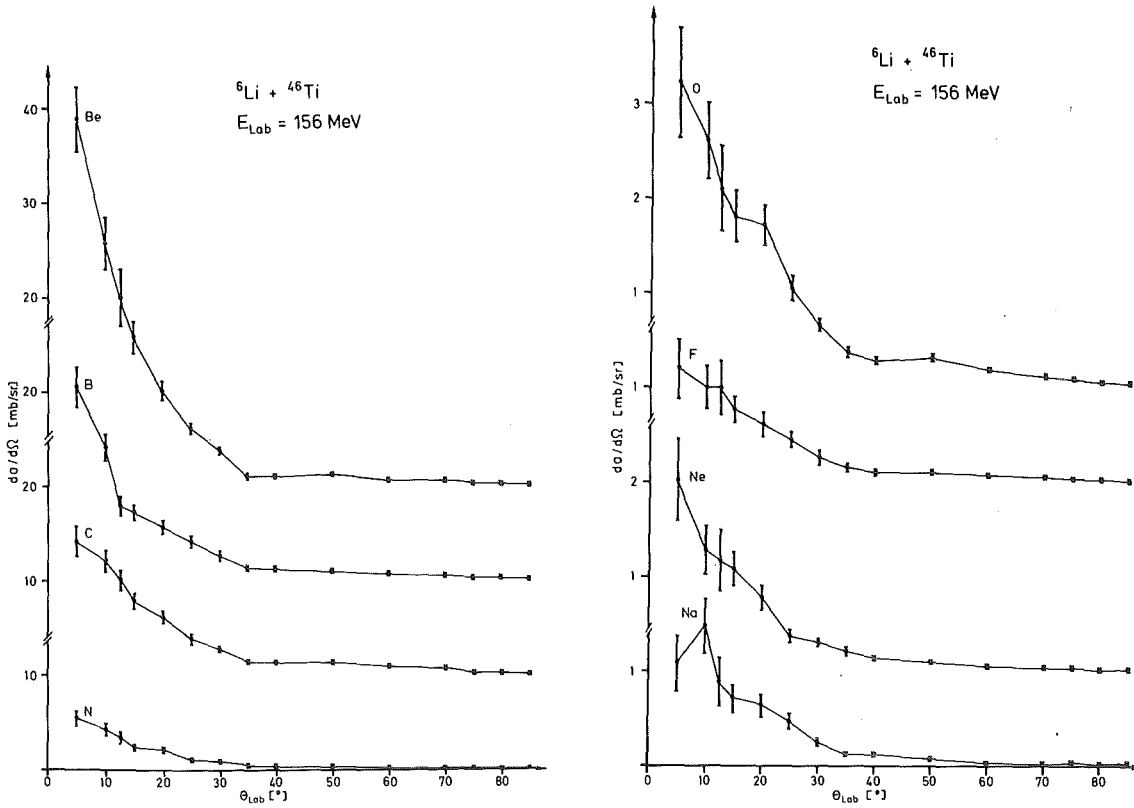
Fig. 2   Angular distributions of projectile-like fragment emission in the
^{6}Li+^{46}Ti reaction at E_{Lab} = 156 MeV.

The total inclusive (energy, angle and Z-integrated) cross section for
Z = 4-11 products amounts to 41 ± 7 mb for the ^{6}Li → ^{46}Ti reaction at 156 MeV.

Assuming basically a reaction mechanism, which leads in an intermediate step
to a non-equilibrated, rotating dinuclear system (2), decaying preferentially in-
to two fragments, the angular distributions can be fairly well described in terms
of the rotational frequency of the primary dinuclear system. The analysis of the
Q-values results in fact in a large energy dissipation of more than 100 MeV
during the processes.

(1)   R. Planeta, H. Klewe-Nebenius, J. Buschmann, H.J. Gils, H. Rebel, S. Za-
       gromski, T. Kozik, L. Freindl and K. Grotowski, Nucl. Phys. A (accepted)
(2)   J. Barette, P. Braun-Munzinger, G.K. Gelbke, H.E. Wegner, B. Zeidman,
       A. Gamp, C. Harrey and Th. Walcher, Nucl. Phys. A279 (1977) 125

+   On leave from Institute of Physics, Jagellonian University Cracow, Poland
++   Institute of Physics, Jagellonian University, Cracow, Poland
+++   Institut für Radiochemie, Kernforschungszentrum Karlsruhe

1.3.7 STATISTICAL ANALYSIS OF THE MOMENTUM TRANSFER IN ^{6}Li INDUCED REACTIONS
WITH ^{46}Ti at E_{Li} = 156 MeV

T. Kozik[+], K. Grotowski[++], H. Klewe-Nebenius[+++] and H. Rebel

In the context of recent experimental studies of massive transfer processes,
leading to the emission to heavy projectile like reaction products (^{7}Li...^{20}Ne)
in collisions of 156 MeV ^{6}Li projectiles with ^{46}Ti, the question arises which
linear momenta are transferred to an intermediate dinuclear system, expected to
be the source for some kind of "preequilibrium" emission of the observed reac-
tion products. The knowledge of the momentum transfer would help to study wheth-
er the ^{6}Li projectile itself forms the intermediate system, or one of the break
up fragments (α-particle or deuteron) after a break up process. In order to ana-
lyse the experimental data with these aspects a statistical reconstruction of
the reaction events has been applied, which is a certain type of a "moving sour-
ce analysis", simplfied by the assumption that transverse momenta are small i.e.
that the source travels along the beam axis. In order to find out the most prob-
able decomposition of the laboratory velocities V_{Lab}, observed for a particular
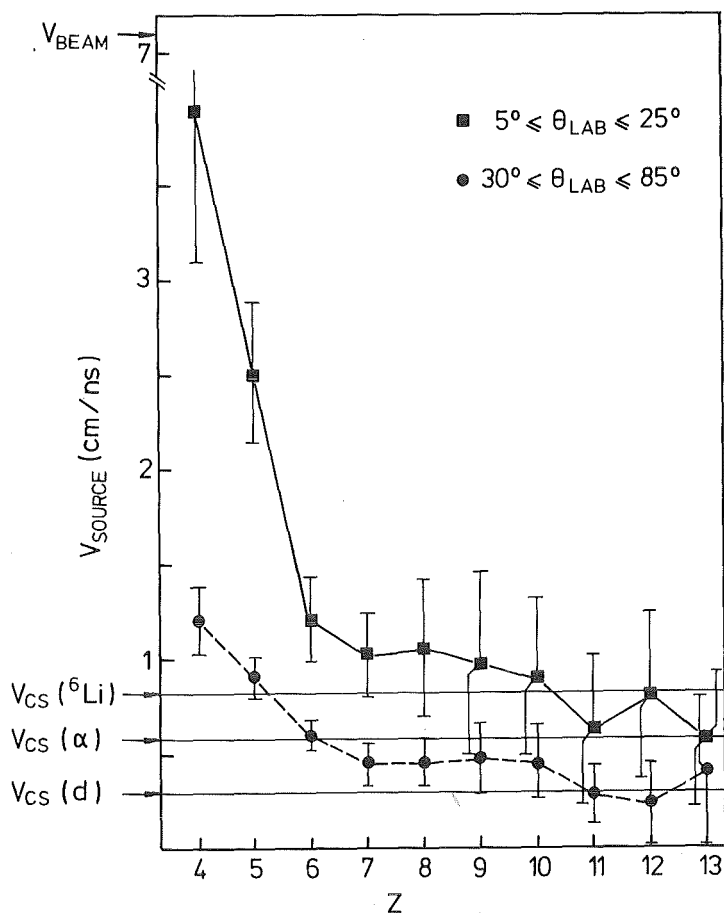
Fig. 1 Velocities of a
moving source emitting the
light fragments with the
atomic number Z. $V_{cs}(^{6}$Li),
$V_{cs}(\alpha)$, $V_{es}(d)$ are calculated
values of a source, resulting
from transfer of the ^{6}Li pro-
jectile or of beam-velocity
fragments (α or d) of ^{6}Li.

Z $(\nu M/2)$ and a particular laboratory angle Θ_{Lab}, into the velocity of the source, V_S, and the c.m. velocity V_{cm} of the ejectile, each small velocity in V_{Lab} $(E_{Lab}, \Theta_{Lab}, Z)$ has been transformed into the c.m. system varying the a-priori unknown c.m. emission angle $\Theta_{c.m.}$ over the full angular range. Separately for each reaction product, all possible (V_S, V_{cm}) combinations were statistically analysed and examined whether they exhibit correlations. The corresponding measured differential cross sections were used as statistical weights. The analysis results in a clear preference of particular values of V_S and V_{cm} (for all laboratory angles), rather well defined with small dispersions.

Fig. 1 shows the resulting source velocities of different light fragments and for two different regions of the laboratory emission angles.

At forward angles the source velocities are considerably higher than the velocity of the composite system, indicating a direct or deep inelastic component transferring nucleons to the projectile. The reaction products (Z>5) emitted in backward direction appear to originate from incompletely fused intermediate systems.

+   On leave from Institute of Physics, Jagellonian University, Cracow, Poland
++   Institute of Physics, Jagellonian University, Cracow, Poland
+++   Institut für Radiochemie, Kernforschungszentrum Karlsruhe

1.3.8 FINITE RANGE DWBA ANALYSIS OF SINGLE NUCLEON TRANSFER REACTIONS IN ^{6}Li + ^{6}Li COLLISIONS AT 156 MeV

S. Micek[+], H. Rebel and D.K. Srivastava[++]

Single nucleon pick-up reactions from ^{6}Li, leading to the unbound systems of ^{5}Li and ^{5}He, provide the possibility to study the nuclear structure of such systems as well as the implications of the reaction mechanism, in particular, the distortion by the optical potentials acting between the observed (stable) ejectile and a metastable system. The case of single nucleon transfer processes in ^{6}Li + ^{6}Li collisions is rather interesting, because it enables to study two such systems: ^{7}Li + ^{5}Li and ^{7}Be + ^{5}He with an identical entrance channel, for which the optical potential has been recently extensively investigated at E_{Li} = 156 MeV (1).

With the aspect of the information about the elastic interaction of unstable systems, otherwise hard to explore, we have analysed experimental differential cross sections for the ^{6}Li(^{6}Li,^{7}Li)^{5}Li$_{gr.}$ and ^{6}Li(^{6}Li,^{7}Be)^{5}Be$_{gr.}$ reactions at E_{Li} = 156 MeV (2). The analysis was based on the finite-range DWBA description of the reactions and endeavoured to reproduce shapes and magnitudes of the measured cross sections, requiring that the spectroscopic factors do not significantly differ from theoretical values. In contrast to the general belief

dσ/dΩ [mb/sr]
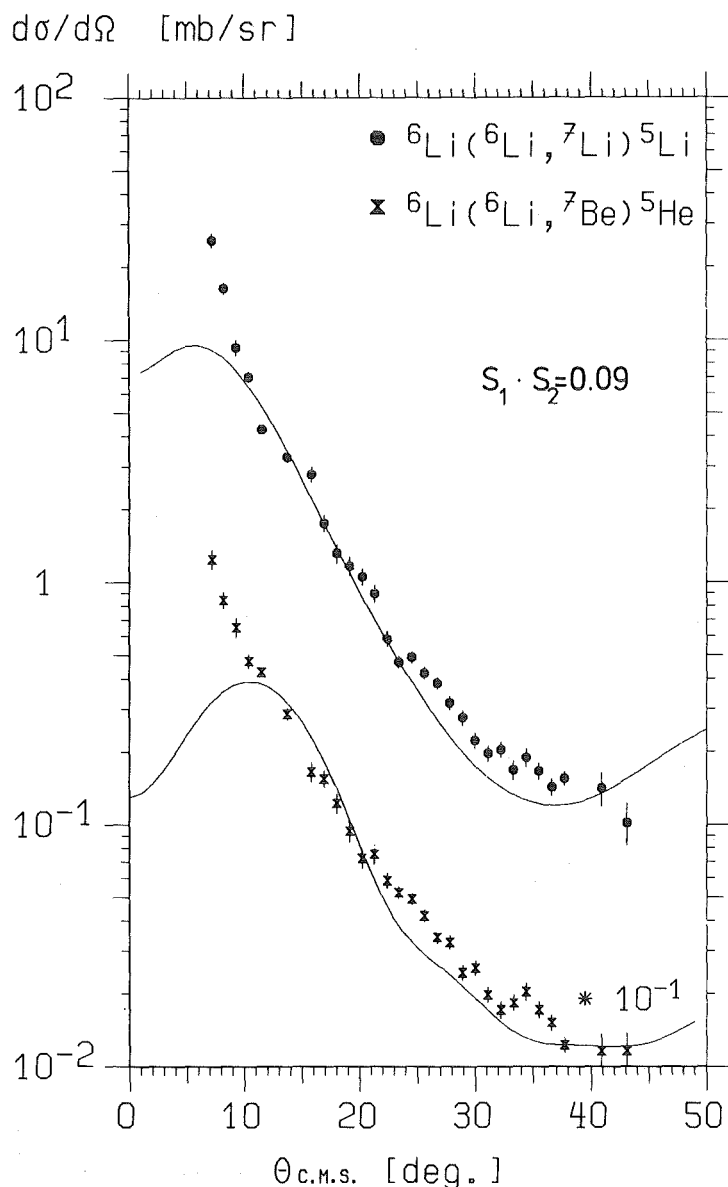
Fig. 1

Results of the FR-DWBA-analyses of the ^{6}Li(^{6}Li,^{7}Li)^{5}Li$_{gr}$ and ^{6}Li(^{6}Li,^{7}Be)^{5}He$_{gr}$ transfer cross sections with values of the spectroscopic factors ($S_1 \times S_2$) approaching theoretical predictions.

that the optical potentials in similar interacting systems should not be very different, the experimental data cannot be reasonably described, if the ^{6}Li+^{6}Li optical potential (1) is used in the exit channel. A readjustment of the ^{7}Be+^{5}He and ^{7}Li+^{5}Li potential parameters is necessary; in particular, the strengths of the real and imaginary parts have to be increased, in order to get a fair agreement between experimental and theoretical cross sections.

These effects arise with the application of a first order conventional DWBA procedure. Higher order processes may account for the remaining deficiencies in describing the data. To which extent two-step processes in the elastic exit channel are just absorbed by the readjusted optical potentials, is a question, which needs a more elaborate description of the reaction mechanism, including more complicated reaction paths.

(1)   S. Micek, Z. Majka, H. Rebel, H.J. Gils, H. Klewe-Nebenius, Nucl. Phys.
        A435 (1985) 621
(2)   S. Micek, H. Rebel, H.J. Gils, H. Klewe-Nebenius, S. Zagromski, and
        D.K. Srivastava, to be published

+   Institute of Physics, Jagellonian University, Cracow, Poland
++   On leave from V.E.C. Centre, Calcutta, India

1.3.9 THE OPTICAL POTENTIAL FOR ^{6}Li + ^{6}Li ELASTIC SCATTERING AT 156 MeV

S. Micek[+], Z. Majka[+], H. Rebel, H.J. Gils and H. Klewe-Nebenius[++] (1)

Elastic scattering of ^{6}Li from ^{6}Li has been studied for the beam energy of 156
MeV. The experimental differential cross section has been analysed on the basis
of the optical model using various phenomenological forms. The spin-orbit inter-
action proves to be less significant. A semi-microscopic double-folding cluster
model which generates the real part of the optical potential by an antisymmetriz-
ed dα cluster wave function of ^{6}Li and αα, dd and dα interactions is well able
to describe the experimental data.

(1)   ditto,Nucl. Phys. A435 (1985) 621

+   Institute of Physics, Jagellonian University, Cracow, Poland
++   Institut für Radiochemie, Kernforschungszentrum Karlsruhe

1.3.10 ^{6}Li BREAK-UP EFFECT ON ELASTIC AND INELASTIC SCATTERING OF ^{6}Li+^{6}Li AT 156 MeV

Y. Sakuragi[+], M. Kamimura[+], S. Micek[++], H. Rebel and H.J. Gils

The double-folding model for the nucleus-nucleus interaction potential has been
proven to be rather successful in reproducing the observed elastic scattering
cross sections for a large number of systems at energies above 5 MeV/amu. In the
cases of ^{6}Li, ^{7}Li and ^{9}Be projectiles, however, the strength of the real part of
the folded potential must be reduced by a renormalization factor $N_R \sim 0.5$ in or-
der to reproduce the measured differential cross sections. This effect has been
interpreted to be a consequence of the high break-up probability of the projec-
tile. In fact, on the basis of a three-body model of the (α+d)+ target system for
^{6}Li scattering, Thompson and Nagarajan (1) and Sakuragi, Yahiro and Kamimura (2)
showed that the coupling to the projectile-break-up channels considerably im-
proves the theoretical descriptions of the observed elastic scattering cross sec-
tions.

Sakuragi et al. (2) calculated explicitly the dynamical polarization po-
tential induced by the coupling of the projectile break up channels; in the sur-
face region which dominantly contributes for the scattering, the potential proves

to be strongly repulsive, and its strength explains quantitatively the magnitude of the renormalization of the folded potential. The coupled channel (CDCC) approach (2) appears to be a rather transparent method since it provides a coherent and consistent description of the scattering and various competing break-up processes (through resonant and nonresonant excited states) on equal footing.

In the present work we study the system $^6Li + ^6Li$ at a projectile energy of 156 MeV. In addition to elastic scattering we consider the inelastic scattering, in particular from the 3_1^+ state at $E_x = 2.19$ MeV. We have measured the differential cross section for ^6Li scattering from this state, and as this state is located above the α-d break-up threshold, the analysis of the experimental data can provide information about the role of resonant continuum states in the break-up of ^6Li and test theoretical predictions. Fig. 1 shows the result of the analysis of the differential cross sections.
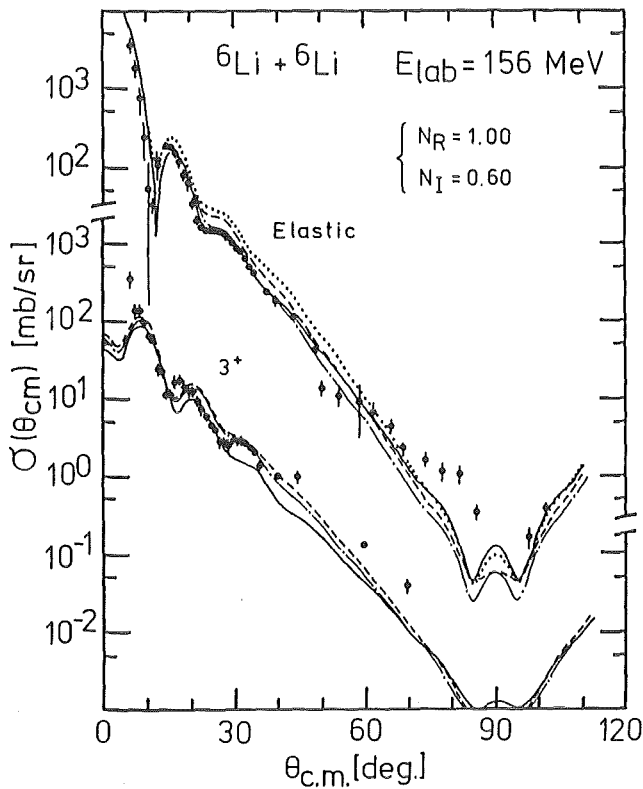
Fig. 1
Experimental and theoretical differential cross sections for elastic and inelastic scattering of 156 MeV ^6Li-ions from ^6Li.

The theoretical calculations of the $^6Li + ^6Li$ scattering are based on the method of CDCC to include resonant and non-resonant break-up states of ^6Li. The only adjustable parameter in the present CDCC calculation is the strength factor N_I of the imaginary part which is taken to be common to all the diagonal and non-diagonal coupling potentials; the radial shape of each imaginary potential is assumed to be the same as that of the corresponding real part which is derived by the double-folding prescription without any renormalization factor. The parameter

N_I is determined by a best fit of the coupled-channel calculation to the elastic scattering cross section. Thus, there are no adjustable parameters left in the calculation of the inelastic cross sections for the 3^+, 2^+ and 1^+ resonance states at 2.19, 4.31 and 5.65 MeV, respectively, as well as for the non-resonant continuum states. The couplings between the break-up channels are found to affect considerably the shape and the magnitude of the elastic and break-up cross sections. A further crucial test would be provided by experimental cross sections for the non-resonant break-up states of ^{6}Li.

(1)   I.J. Thompson and M.A. Nagarajan, Phys. Lett. 106B (1981) 163
(2)   Y. Sakuragi, M. Yahiro and M. Kamimura, Prog. Theor. Phys. 68 (1982) 322; ibid, 70 (1983) 1047

+   Kyushu University, Fukoka 812, Japan
++   Institut of Physics, Jagellonian University, Cracow, Poland

1.3.11 TECHNIQUE OF 0°-MEASUREMENTS WITH THE MAGNETIC SPECTROGRAPH "LITTLE JOHN"

H.J. Gils, H. Jelitto, S. Zagromski, W. Eyrich[+], H. Schlösser[+]

Nuclear reaction experiments requiring the detection of charged particles ejected at 0° with respect to the primary beam axis are of considerable interest in different fields of nuclear structure and reaction mechanism studies [1,2]. In general, such experiments are only possible with a magnetic spectrograph providing – in most cases – a spatial separation of the particles to be detected from the primary beam.

In this contribution we report on the particular technique of 0°-measurements of ^{6}Li break up fragments performed with the magnetic spectrograph "Little John". Looking for the break up deuterons and α particles a magnetic separation of the primary beam is not possible. Therefore, an arrangement as shown in Fig. 1 was used.

The primary beam is stopped in front of the focal-plane (FP) detector in a special Faraday cup consisting of an electrically isolated carbon block as beam stop and an 700 mm long absorber (Lithium paraffine) for fast neutrons produced in the beam stop. Depending on the part of the fragment energy spectrum to be measured the Faraday cup can be placed at any position across the dispersion plane (see Fig. 1). The neutron absorber worked quite efficient in suppressing background events produced by fast neutrons in the FP-detector. This was demonstrated by comparing measurements with beam stops without absorber and with a shorter absorber, respectively.

Most important for 0°-measurements is a careful focusing of the ^{6}Li-beam and a suppression of the beam halo and of slit scattering. Since the final equip-

ment in particular for the beam line is still under construction provisional dia-
phragms between the monochromator magnet and switching magnet (3) and at the en-
trance of the target chamber (see Fig. 1) have been used with good success. The
exact positioning of all movable slits in the beam line and in the spectrograph
was optimized by observing the total countrate in the plastic scintillator of the
FP-detector.
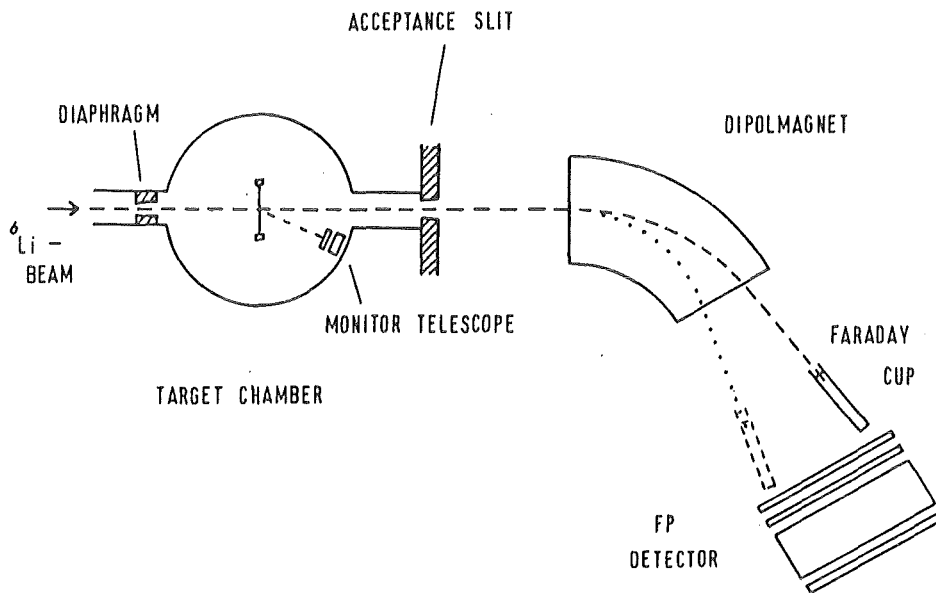
Fig. 1 Arrangement of the magnetic spectrograph and beam stop for 0°-measurements
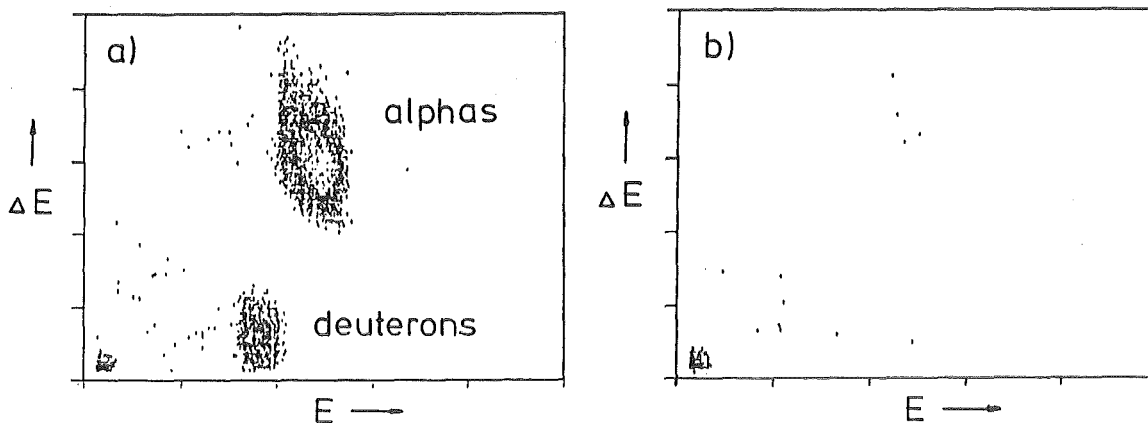
Fig. 2 Energy loss versus energy of alphas and deuterons from the reaction
156 MeV ^{6}Li + ^{12}C at Θ_{Lab} = 0°
a) with target (4.3 mg/cm² thickness)   b) without target

Typical ΔE-E spectra measured at Θ_{Lab} = 0° with and without a ^{12}C target
are shown in Fig. 2. The observed deuteron and α particles clearly resulting from

nuclear reactions in the target can easily be separated from the ^{6}Li background which is mainly due to edge and grazing forward scattering at the Faraday cup and the neutron absorber.

(1)   D.H. Youngblood et al., Phys. Rev. Lett. 39 (1977) 1188
(2)   D.K. Srivastava, H. Rebel. This report, Contr. 1.3.3
(3)   H.J. Gils, KfK-Report 2972 (1980)

+   Physikalisches Institut der Universität Erlangen-Nürnberg

1.3.12 NEUTRON DECAY OF THE GIANT RESONANCE REGION IN ^{90}Zr STUDIED IN A (^{6}Li, ^{6}Li'n) COINCIDENCE EXPERIMENT

B. Mühldorfer[+], W. Eyrich[+], G. Gottschalk[+], A. Hofmann[+], H. Rebel, H. Schlösser[+] and H. Wirth[+]

In the preceding annual report we presented first results from our (^{6}Li,^{6}Li'n) coincidence experiment concerning the decay of the giant resonance region in ^{90}Zr, using the 156 MeV Li beam of the Karlsruhe Isochronous Cyclotron. Meanwhile these measurements have been completed. In this contributions, we discuss briefly the latest data from the decay of the giant quadrupole resonance (GQR) region.

The measurements were performed with a detector arrangement similar to that used in former (α,α'n) experiments. To detect the scattered ^{6}Li particles, four Si(Li) telescopes were mounted rotatable around the beam axis. The coincident neutrons were measured, using the time-of-flight method, with four plastic scintillators. In this way, the angular correlation function could be sufficiently averaged for all multipolarities by measuring at 16 special ^{6}Li-n-angular combinations.

The aim of the experiment is to extract model-indepent branching ratios of the n-decay of the giant resonance region into the individual low lying states. The spins of these states allow the separation of strenghts with higher multipolarities L $\geq$ 4 from E2- and E0-strength. This spin-filter method is described in more detail in refs. (1) and (2). At excitation energies above E_x = 13 MeV, the E2-strength predominantly decays into the low spin states 1/2$^-$ and 3/2$^-$, whereas higher multipolarities mainly feed the 9/2$^+$ high spin state.

A typical decay spectrum of the GQR region in ^{90}Zr is shown in the upper part of Fig. 1. The strongly populated 9/2$^+$ ground state indicates additional strength with higher multipolarities L $\geq$ 4. The comparison with data from our (α,α'n) experiment (2), shown in the lower part of Fig. 1 in which the background contributions are strongly different indicates that the L $\geq$ 4 strength is mainly of resonant type.
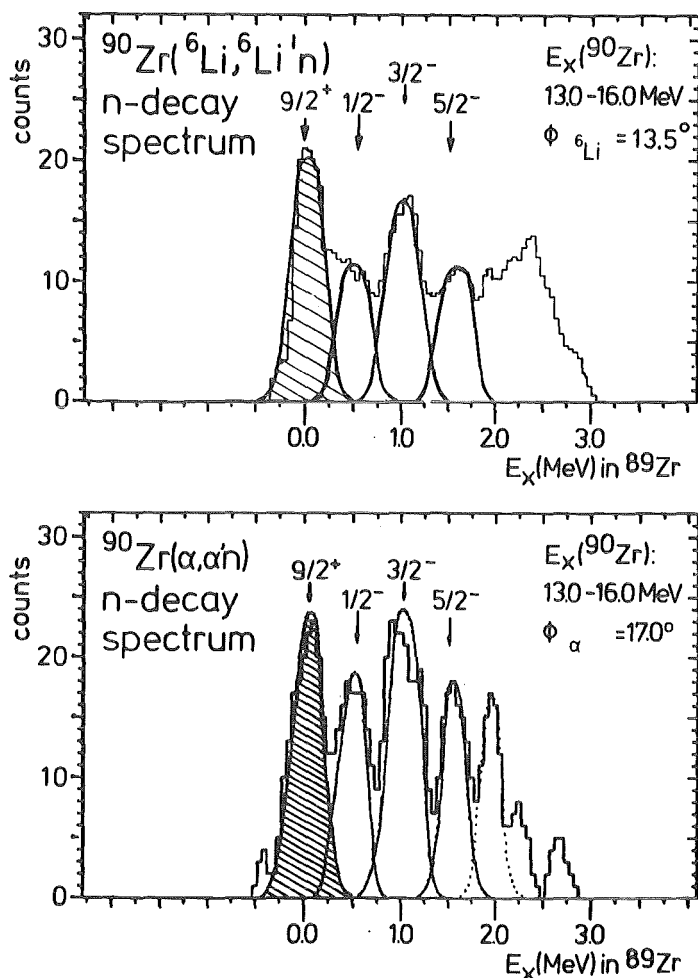
Fig. 1

n-decay spectra of the giant quadrupole resonance region in ^{90}Zr from ^{90}Zr(^{6}Li,^{6}Li'n) (upper part) and ^{90}Zr(α,α'n) measurements (lower part).

(1)   H. Steuer, W. Eyrich, A. Hofman, H. Ortner, U. Scheib, R. Stamminger, D. Steuer, H. Rebel, Phys. Rev. Lett. 47 (1981) 1702
(2)   K. Fuchs, W. Eyrich, A. Hofman, B. Mühldorfer, U. Scheib, H. Schlösser, H. Rebel, Phys. Rev. C32 (1985)
+   Physikalisches Institut der Universität Erlangen-Nürnberg

1.3.13 INVESTIGATIONS OF THE ISOSCALAR GIANT RESONANCES IN THE Sn-ISOTOPES USING ^{6}Li-SCATTERING

H. Schlösser[+], W. Eyrich[+], H.J. Gils, G. Gottschalk[+], A. Hofmann[+], B. Mühldorfer[+], H. Rebel, H. Wirth[+], and S. Zagromski

An important quantity accessible by measurements of giant resonances is the nuclear compressibility K_A, which is directly related to the excitation energy of the EO isoscalar mode (GMR). The compressibility depends on surface, Coulomb-, and asymmetry-effects:

$$K_A = K_{vol} + K_{surf} \cdot A^{-1/3} + K_{sym} \cdot \left[\frac{N-Z}{A} \right]^2 + K_{Coul}$$

The Sn-isotopes are good candidates for studies of the asymmetry term $K_{sym} \cdot \left[\dfrac{N-Z}{A}\right]^2$ because all members of the Sn-series between A = 112 and 124 are known to be spherical. Up to now systematic studies of the GMR in the Sn-isotopes were performed only by α-particle scattering (1).

We started a systematic investigation of the isoscalar GR's of the isotopes 112, 116, 120, and 124 using 156 MeV ^{6}Li scattering at the Karlsruhe Cyclotron. The advantage of ^{6}Li-scattering is mainly the different and lower background especially in the GMR-region due to the break up of the ^{6}Li-particles. We started our measurements at scattering angles between 9 and 15 degrees using two Si-telescopes. In Fig. 1a a typical spectrum is shown, taken from ^{124}Sn at θ = 9.5°.
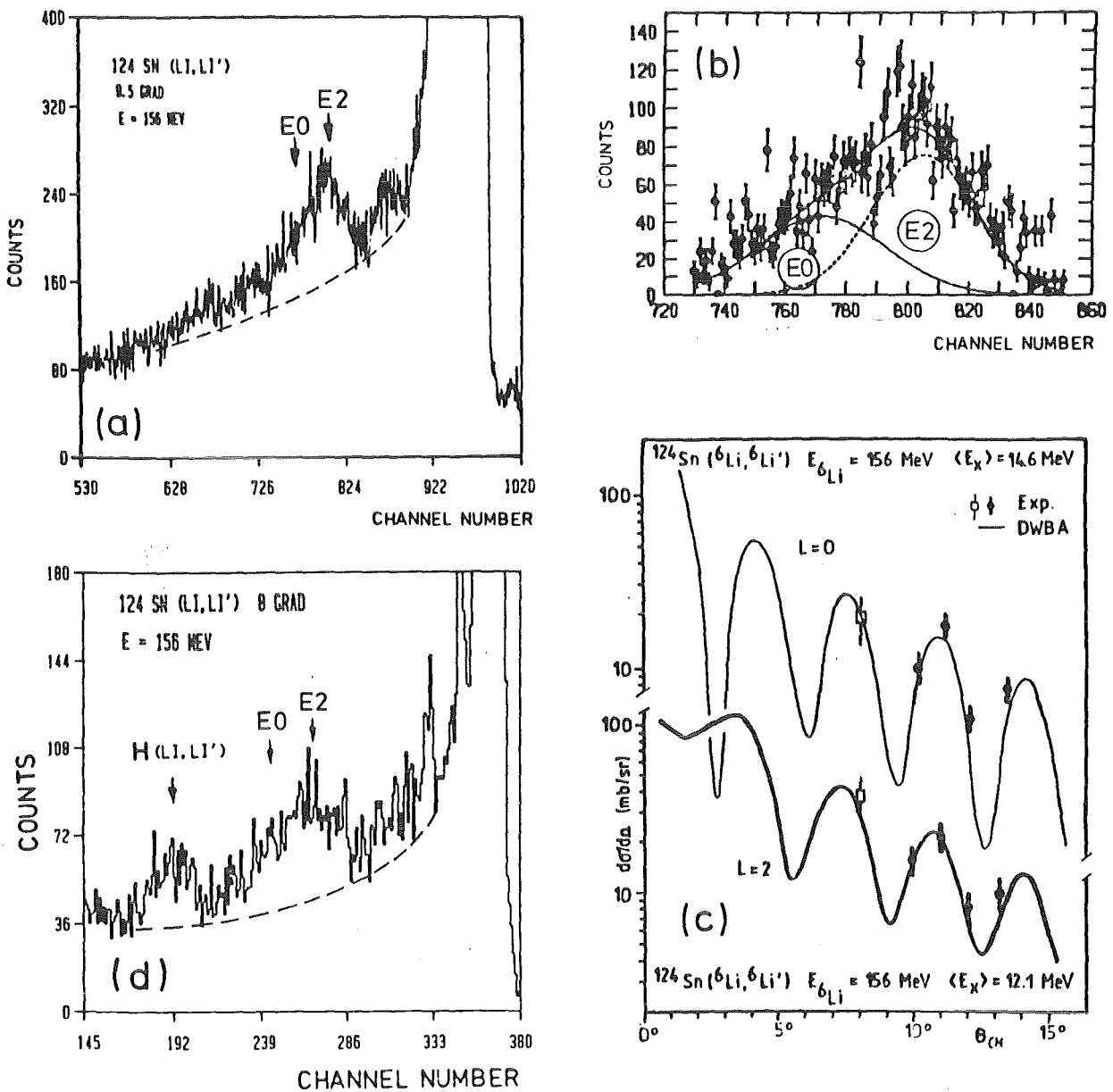
Fig. 1 Spectra and angular distributions of the isoscalar giant resonances in ^{124}Sn from ^{6}Li, ^{6}Li' scattering

The dashed line shows the chosen background which is subtracted in Fig. 1b. The two Gaussians are fits to the GMR and the GQR from which excitation energies of (14.6+1.0) MeV for the GMR and of (12.1 + 0.8) MeV for the GQR were extracted, in good agreement with the α-particle scattering results (1).

In Fig. 1c a DWBA calculation is shown as compared with the experimental ^{6}Li-data of the GMR and GQR in ^{124}Sn. The extracted sum rule values of (60+15) % E2 EWSR and (80+20)% EO EWSR differ from the α-scattering values especially for the GMR ((186+60)%). To reach the angular region between 0° and 5° where the EO-distribution has the known characteristic behaviour allowing a more precise extraction of excitation energy and strength, we started measurements using the new Karlsruhe magnet spectrograph "Little John". Fig. 1d shows a (^{6}Li,^{6}Li') spectrum taken with the spectrograph for ^{124}Sn at 8°. Measurements down to 0° are in progress.

(1)   Y.-W. Lui, P. Bogucki, J.D. Bronson, D.H. Youngblood, U. Gary, Phys. Rev. C30 (1984) 51

+   Physikalisches Institut der Universität Erlangen-Nürnberg

1.3.14 NEUTRON DECAY OF THE ISOSCALAR GIANT RESONANCE REGION IN ^{90}Zr

K. Fuchs[+], W. Eyrich[+], A. Hofmann[+], B. Mühldorfer[+], U. Scheib[+], H. Schlösser[+], H. Rebel

The neutron decay of the giant resonance region between 13.0 and 18.0 MeV in ^{90}Zr has been studied in an (α,α'n) coincidence experiment at E_α = 104 MeV. In the region of the giant quadrupole resonance between 13 and 16 MeV, additional strength with multipolarity L ≥ 4 was identified. For the resonant strength in the region of the giant monopole resonance, a direct decay component of about 12% can be estimated. In addition, evidence for a preequilibrium decay was found.

(1)   ditto, Phys. Rev. C32 (1984)

+   Physikalisches Institut der Universität Erlangen-Nürnberg

1.3.15 INVESTIGATIONS OF THE RADIAL DISTRIBUTIONS OF NUCLEONS IN $1f_{7/2}$-SHELL NUCLEI BY ELASTIC ALPHA PARTICLE SCATTERING

H.J. Gils (1)

The radial size and shape of the distribution of nucleons - i.e. the sum of protons and neutrons - in atomic nuclei of the $1f_{7/2}$ shell was investigated. The experimental basis of the studies are differential cross sections of elastic α-particle scattering by ^{40,42,43,44,48}Ca, ^{50}Ti, ^{51}V, ^{52}Cr precisely measured

over a wide angular range at the 104 MeV α-particle beam from the Karlsruhe Isochronous Cyclotron. The experimental cross sections are analyzed using so-called "model independent" optical potentials by which the data are reproduced very well. The error bands of these potentials are determined in a well-defined form from the analyses. The high sensitivity of the data to the radial form of the real optical potential justifies, in principle, that the experiments are a suitable tool for investigating nuclear density distributions. Some pre-informations on this questions are obtained from the optical potential analyses.

For a more direct access to the nuclear matter distributions - in particular to differences between neighbouring nuclei - a semimicroscopic reaction model is presented which on the one hand is based on a fully microscopic many body approach. On the other hand all quantities being of no particular interest for the results are treated in a phenomenological way. Thereby, it is possible to reproduce the experimental cross sections as well as by the "model independent" potentials and to obtain full consistency between the two approaches. This has not been achieved by any other microscopic reaction model.

As main result of the analyses differences of nuclear matter distributions between the investigated nuclei of the $1f_{7/2}$ shell are obtained which show an interesting behaviour. In the isotope chain of the even mass number nuclei the additional neutrons are obviously distributed over a wide radial region in particular in the case of ^{48}Ca. However, when adding protons in the isotone chain a sharper localization of the $1f_{7/2}$ shell is observed and also occupation of other shells is indicated.

The nuclear matter radii of the odd mass number nuclei show an unexpected behaviour as compared to the corresponding charge radii. Whereas the latter are smaller than those of the neighbouring even mass number nuclei one observes larger radii for the nuclear matter distribution of the odd nuclei. This behaviour is not understood theoretically neither in the framework of the shell model nor in Hartree-Fock calculations.

(1)   ditto, KfK-Report 3765 (Dezember 1984)

1.3.16 COMBINED ANALYSIS OF PIONIC ATOMS AND ELASTIC SCATTERING OF ALPHA PARTICLES

H.J. Gils and E. Friedman[+] (1)

A combined analysis of strong-interaction level shifts and widths in pionic atoms and of elastic scattering of alpha particles has been performed for the isotopes ^{40,42,44,48}Ca in terms of neutron density distributions. Although the nature of the two types of data is widely different, a reasonable coupling between the two problems is observed with the former providing constraints on the latter leading to a reduction of errors in the neutron density distribution and its various integral moments.

(1)   ditto, J. Phys. G: Nucl. Phys. 11 (1985) 85

+   The Racah Institute of Physics, The Hebrew University of Jerusalem, Jerusalem, Israel

1.4   NUCLEAR FISSION

1.4.1   MASS AND ENERGY DISTRIBUTION OF FISSION FRAGMENTS IN $^{249}Cf(n_{th},f)$

E. AKER[+], R. BRISSOT[++], D. ENGELHARDT[+], P. GELTENBORT[++],

J. GINDLER[+++], F. GÖNNENWEIN[++], A. OED[++], B. WILKINS[+++], (1)

The measurement of the mass and energy distribution of the fission fragments in the reaction $^{249}Cf(n_{th},f)$ was performed at the new time-of-flight spectrometer Cosi fan tutte at the High Flux Reactor of the Institut Laue - Langevin at Grenoble. The masses of the fission fragments after prompt neutron evaporation are obtained by combining their velocities and kinetic energies (2).

The performance of this instrument was tested by a $^{235}U(n_{th},f)$ run. The comparision of these data with literature proved the reliability of the spectrometer. The experimental setup consisted of a time-of-flight system of one meter length with a time resolution of about 100 ps followed by an axial ionization chamber with an energy resolution of roughly 400 keV. With this geometry the resulting mass resolution was better than $m/\delta m = 170$. So the single masses at least in the light fragment group are clearly separated. The detectors were calibrated by a $^{233}U(n_{th},f)$ run. Using a 8.6 µg ^{249}Cf-target and a thermal neutron flux of nearly $10^{10}n/cm^2s$ we obtained a counting rate of 1 event per second. Altogether about 1.4 million fission fragments were detected.

In Fig. 1 the two-dimensional matrix data of TOF and energy of the ^{249}Cf fission fragments for the light and heavy fragment group are depicted as a contour plot. This figure shows the raw data without any corrections. In the light group the events corresponding to a given mass are accumulated on separated lines. These mass lines allow the determination of the mass - energy distribution.

The total mass yield of the final fission fragments is plotted in Fig. 2. The mean mass in the light group is (106.0 ± 0.1) amu, in the heavy one (140.0 ± 0.6) amu. Asuming a similar charge density in the compound nucleus and in both fragments these masses correspond to nuclei in the region of ^{106}Nb and ^{140}Cs. 97.2% of the total mass yield in the light group belongs to masses in the range from 85 to 123 amu, the most probable mass is m = 108 amu. The average number of prompt neutrons per fission is 4.0. These results are in good agreement with radiochemical data (3).

In the light group the highest observed kinetic energies are about 125 MeV. In this energy range the fragments have a vanishing probability for emitting neutrons due to their low excitation energy. Therefore these secondary masses are equal to the primary ones. Furthermore the mass distribution is influenced by
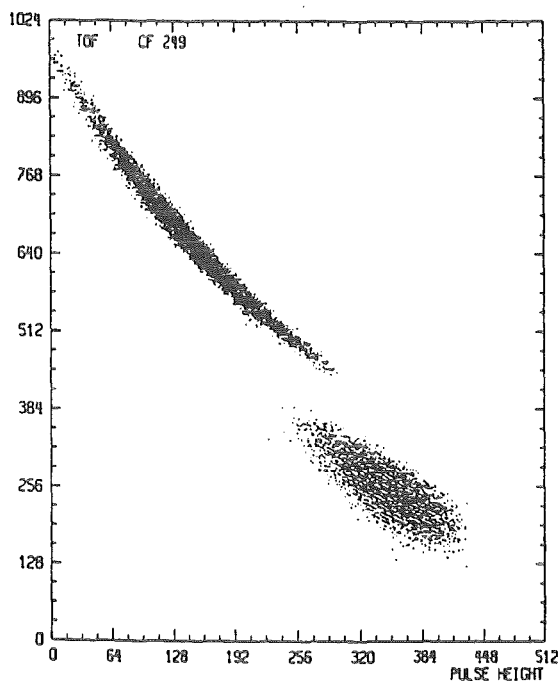
Contour plot of correlated TOF and energy data from ^{249}Cf(n,f) for thermal neutrons. Target thickness 8.6 μg/cm^2

TOTAL MASS YIELD
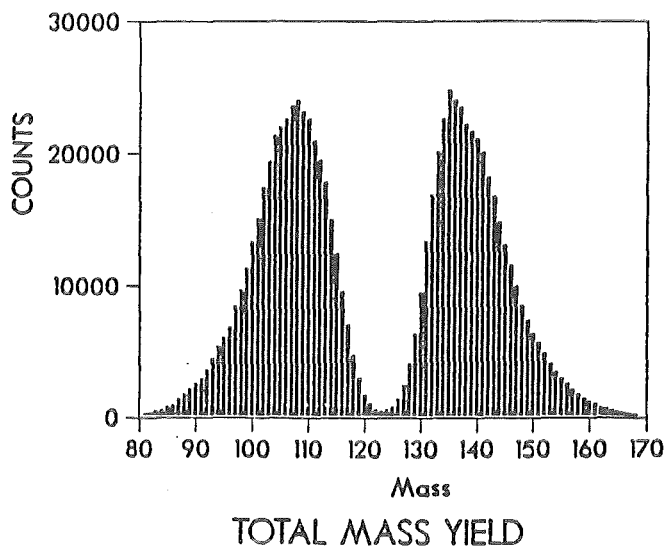
Fig. 2

Mass distribution of the fission fragments of ^{249}Cf after neutron evaporation

shell effects. For energies higher than 123 MeV the mass distribution of the ^{249}Cf fission fragments shows a weak structure. Mainly the mass 116 is dominating. The correlated heavy mass is 134. This mass is also prefered in the cold fragmentation of ^{235}U.

The mean kinetic energy of the fragments ranges from about (105 ± 1) MeV for m = 91 to (100 ± 1) MeV for m = 119 and drops down to (90 ± 1) MeV near the symmetric mass m = 123 amu.

The kinetic energy distribution for a given secondary mass is not purely Gaussian shaped, but shows a clear asymetric broadening towards lower energies.

(1)   E. Aker, R. Brissot, D. Engelhardt, P.Geltenbort, J. Gindler,
      F. Gönnenwein, A. Oed and B. Wilkins, Int. Conf. on Nucl. Data
      for Basic and Appl. Science, May 13-17, Santa Fe (1985)
(2)   A. Oed, P. Geltenbort, R. Brissot, F. Gönnenwein, P. Perrin,
      E. Aker and D. Engelhardt, Nucl. Inst. Meth. 219(1984)569-574
(3)   J. Gindler, J. Glendenin and B. Wilkins
      J. Inorg. Nucl. Chem. 43(1981)1743-1749

+   Inst. für Exp. Kernphysik, Universität Karlsruhe
++   Institut Max von Laue - Paul Langevin, Grenoble
+++   Argonne National Lab.

1.4.2 MASS AND KINETIC ENERGY DISTRIBUTION OF FISSION FRAGMENTS IN ^{239}Pu(n_{th},f)

C.Schmitt[+], A. Guessous[++], J.P. Boquet[++], H.-G. Clerc[+], R. Brissot[++],

D. Engelhardt[+++], H.R. Faust[++++], F. Gönnenwein[++++], M. Mutterer[+],

H. Nifenecker[++], J. Pannicke[+], Ch. Ristori[++], J.P. Theobald[+], (1)

A series of experiments (1) was performed at the 'LOHENGRIN' recoil spectrometer of the Institut Laue-Langevin in Grenoble in a collaboration with groups from Darmstadt and 'Centre d'Etudes Nucléaires de Grenoble', in order to measure the yields of the light fission products from the thermal-neutron-induced fission of ^{239}Pu as a function of atomic mass number A, nuclear charge Z, kinetic energy E and the ionic charge states q. A complete set of data as can be obtained at the 'LOHENGRIN' spectrometer was not available before this experiment was performed. As at the 'LOHENGRIN' spectrometer each atomic mass A has different ionic charge states q one has to measure all these contributions to the total mass yield and sum them up. Thus the nuclear charge and mass distributions summed over all ionic charge states were determined for the light fission product kinetic energies between 93 and 112 MeV. The proton odd-even effect causes considerable fine structure in the fission yields. It was measured to be (11.6 $\pm$ 0.6)%, whereas the neutron odd-even effect is (6.5 $\pm$ o.7)%. The average kinetic energy of even-Z elements in the light fission product group is larger than for odd-Z elements by 0.3 $\pm$ 0.1 MeV.

These data were compared to previously published data (2) for the reaction ^{235}U(n_{th},f). This comparision shows a correlation between the proton odd-even effect in the yield and in the kinetic energy of the elements investigated in both experiments. The dependency of the proton odd-even effect on the fragmentation is rather similar for both target nuclei ^{235}U and ^{239}Pu when it is considered as a function of the nuclear charge of the heavy fission products. The isobaric variances σ_z^2 for thermal-neutron induced fission of ^{235}U and ^{239}Pu coincide at all kinetic energies if the influence of the proton odd-even effect is averaged out. This supports the hypothesis that the magnitude of σ_z^2 is determined only by quantum-mechanical zero-point fluctuations.

The influence of the spherical shells Z = 50 and N = 82 on the fragmentation is observed in the data and is discussed in detail in (1).

(1)   dito, Nucl. Phys. A430(1984)21-60
(2)   W. Lang, H.-G. Clerc, H. Wolfahrt, H. Schrader, and K.-H. Schmidt, Nucl. Phys. A354(1980)34

+   Technische Hochschule (TH) Darmstadt,
++   Centre d'Etudes Nucléaire de Grenoble
+++   Universität Karlsruhe
++++   Institut Laue-Langevin, Grenoble

1.5 THEORY

1.5.1 QUANTIFICATION OF THE CLUSTERING PROPERTIES OF NUCLEAR STATES

R. Beck, F. Dickmann and R.G. Lovas[+] (1)

The term nuclear clustering is used in various senses, which are defined only in broad qualitative terms. We quantify its definition by adopting the viewpoint of the microscopic cluster models, which describe the nuclear states as antisymmetrized products of cluster intrinsic and relative wave functions. We define clustering as the property, of nuclear states, that they overlap with such cluster-model states. As a quantitative measure of a particular type of clustering, we use the norm square of the projection of the wave function onto the particular cluster-model subspace, and we call this quantity the amount of clustering. This quantity differs from the familiar spectroscopic factor in that the spectroscopic factor involves a projection onto a non-antisymmetrized cluster subspace.

We have pointed out that the amount of clustering is analogous but not identical to a quantum mechanical probability, and that the probability of finding two clusters locally cannot be defined. The cluster-model component of the wave function is proved to have a variational property, which facilitates the computation of the amount of clustering.

The model dependence of the amount of clustering S and its relationship to the corresponding spectroscopic factor s is illustrated by calculations for the $\alpha+d$, ^5He+p and $t+\tau$ clustering in the ground state (g.s.) and first excited 1^+, 2^+, 3^+ triplet of ^6Li. One of the models considered is a pure $\alpha+d$, and the other is a mixed $\{\alpha+d, {}^5He+p\}$ cluster model. The table below gives sample results.

State	Model	$\alpha+d$ clustering		^5He+p clustering		$t+\tau$ clustering	
		S	s	S	s	S	s
g.s.	$\alpha+d$	1	1.073	0.534	0.631	0.539	0.485
	mixed	0.969	1.041	0.612	0.708	0.535	0.482
$1^+,2^+,3^+$	$\alpha+d$	1	1.069	0.495	0.597	0.513	0.461
	mixed	0.942	1.013	0.631	0.736	0.537	0.482

It is concluded that the spectroscopic factor is also characteristic, though only in a relative sense, of the clustering contents of different states or models of the same nucleus, but it cannot be used for comparisons between different nuclei or clusterings.

(1)   ditto, submitted to Ann. Phys. (N.Y.)

+   Institute of Nuclear Research, Debrecen, Hungary

1.5.2 DECOMPOSITION OF ^{6}Li INTO α+d

R. Beck and F. Dickmann, A.T. Kruppa[+] and R.G. Lovas[+] (1)

We report on the calculation of the α+d fragmentation properties of ^{6}Li (2). This is a generator-coordinate version of the cluster models with dynamical distortions. The investigation shows that there is a marked change caused by the inclusion of the compressional vibration of the clusters. That this change is in fact an improvement is guaranteed by the underlying variational principle. The improved value of the spectroscopic factor is about $\sim$0.7 - 0.85.

(1)   ditto, Proc. 10th European Symp. on Dynamics of Few-Body Systems,Balaton-füred, June 3-7, 1985; ed. P. Doleschall (KFKI, Budapest 1985, p. 13

(2)   R. Beck, F. Dickmann, A.T. Kruppa, Phys. Rev. $\underline{C30}$ (1984) 1044

+   Institute of Nuclear Research, Debrecen, Hungary

1.5.3 APPRAISAL OF MACROSCOPIC CLUSTER MODELS

R. Beck, F. Dickmann and R. G. Lovas[+] (1)

Light nuclei are often described macroscopically as compositions of two or three structureless clusters that interact via (local or separable) cluster-cluster potentials. The nuclear properties are then calculated from the relative wave function (and some assumed intrinsic properties) of the clusters. This level of approximation seems as yet indispensable if the three-body dynamics is to be treated properly. The quality of such a description may be tested with microscopic calculations or with direct cluster rearrangement reactions. The aim of this contribution is to clarify how these tests are to be made and to formulate quantitative criteria in microscopic terms for the applicability of macroscopic cluster models. The considerations largely rely upon the familar notions of the rasonating group method. Although all our explicit considerations concern two-cluster systems, it is straightforward to generalize them to three-cluster systems as well.

(1)   ditto, Proc. 10th European Symp. on Dynamics of Few-Body Systems, Balatonfüred, June 3-7, 1985; ed. P. Doleschall (KFKI, Budapest 1985, p. 16

+   Institute of Nuclear Research, Debrecen, Hungary

1.5.4 QUASIELASTIC CLUSTER KNOCK-OUT REACTIONS AND THE MICROSCOPIC CLUSTER MODEL

R. Beck, F. Dickmann and R.G. Lovas[+] (1)

The spectroscopic information contained in quasielastic cluster knock-out reactions is examined with a microscopic approach to the impulse approximation. It is shown that, because of the Pauli principle, the extracted spectroscopic factor is distinct from the probability (or amount) of clustering. A formalism is elaborated for the calculation of these quantities in a generator-coordinate model for a superposition of different clusterizations. This formalism is used to study the $\alpha + d$ clustering properties of ^{6}Li described as a superposition of the $\alpha + d$ and ^{5}He$+p$ systems. The model predicts the spectroscopic factor (amount of clustering) to be 1.04 (0.97) and 1.01 (0.94) for the ground and first excited state, respectively. The calculated spectroscopic amplitude, as a function of the $\alpha + d$ relative momentum, is in good agreement with those extracted from high-energy ^{6}Li(p,pd)α and ^{6}Li(α,2α) experiments.

(1)   ditto, Nucl. Phys. (in press)

+   Institute of Nuclear Research, Debrecen, Hungary

1.5.5 EFFECTS OF THE PAULI PRINCIPLE IN QUASIELASTIC CLUSTER KNOCKOUT REACTIONS

R. Beck, F. Dickmann and R.G. Lovas[+]

In the conventional model (1) of quasielastic cluster knockout reactions $A(a,a'A_1)B_1$ (e.g. ^{6}Li(p,p'd)^{4}He) the treatment of the antisymmetrization between the reaction partners is unsatisfactory. It leads to an expression for the transition amplitude which involves the amplitude

$$g(\vec{k} I \nu JM) = \langle \vec{k} I \nu | \psi(JM) \rangle .$$ (1)

Here $|\vec{k}I\nu\rangle$ is an antisymmetrized product of two intrinsic wave functions of clusters A_1 and B_1 coupled to the channel spin I_ν and a plane wave with momentum $\vec{k}$ for their relative motion:

$$|\vec{k} I \nu\rangle = \mathcal{A}[(\phi_{A_1}\phi_{B_1})_{I\nu} \exp(i\vec{k}\cdot\vec{r}_{A_1 B_1})]$$ (2)

while $\psi(JM)$ is a normalized A-particle $(A=A_1+B_1)$ wave function with angular momentum JM. It has been pointed out by Feshbach (2) that $g(\vec{k}I\nu JM)$ cannot be interpreted as the probability amplitude of finding in $\psi(JM)$ the clusters ϕ_{A_1} and ϕ_{B_1} moving relative to each other with momentum $\vec{k}$.

We have found that a consistent treatment of the Pauli principle (within the spectator approximation) also involves the conventional amplitude $g(\vec{k}I\nu JM)$. As this function is usually (erroneously) interpreted as a probability amplitude,

we investigate its probability content.

We use microscopic wave functions of ^{6}Li, assuming (3) that this nucleus may be described by a superposition of the α+d and ^{5}He+p clusterization and compare the spectroscopic factor

$$S_{\alpha d}(IJ) = \sum_{M\nu} (2J+1)^{-1} \int d^3k \, | g(\vec{k}I\nu JM)|^2 \qquad (3)$$

and the probability (amount of α+d clustering)

$$P_{\alpha d}(IJ) = \sum_{M\nu} (2J+1)^{-1} \int d^3k \, d^3k' \, g^*(\vec{k}I\nu JM)$$
$$\times \langle \vec{k}I\nu | \vec{k}'I\nu \rangle^{-1} g(\vec{k}'I\nu JM). \qquad (4)$$

The results are summarized in Table I.

Table I Spectroscopic factor $S_{\alpha d}(IJ)$ and amount of clustering $P_{\alpha d}(IJ)$ for the ground ($J=1^+$) and first excited state ($J=3^+$, E* = 2.18 MeV) in ^{6}Li. The effective nucleon-nucleon interactions V1, V2 and B are the forces 1 and 2 of Volkov (4) and the force of Brink (5), respectively. The channel spin of the α+d system is I = 1.

Effective Interaction	Ground state			First excited state		
	V1	V2	B	V1	V2	B
$S_{\alpha d}$	1.038	1.041	1.033	1.010	1.013	1.006
$P_{\alpha d}$	0.967	0.969	0.972	0.940	0.942	0.952

All spectroscopic factors $S_{\alpha d}$ are larger than 1, showing that they are not probabilities. The corresponding probabilities $P_{\alpha d}$ are some 5-7% smaller. Despite the smallness of this discrepancy here, it is important to keep in mind that there seems to be no experimental method by which the true probabilities can be determined.

(1)   N.S. Chant and P.G. Roos, Phys. Rev. C15 (1977) 57
(2)   H. Feshbach, Annals of Physics 19 (1962) 287
(3)   R. Krivec and M.V. Mihailović, J. Phys. G: Nucl. Phys. 8 (1982) 821
(4)   A.B. Volkov, Nucl. Phys. 74 (1965) 33
(5)   D.M. Brink, Proceedings of the International School of Physics Enrico Fermi, XXXVI (1966) 247.

+   Institute of Nuclear Research, Debrecen, Hungary

1.5.6 ON FLIESSBACH'S APPROACHES TO DIRECT REACTIONS

R.G. Lovas[+]

The conventional models of direct cluster reactions treat the nuclear wave-function overlaps or reduced-width amplitudes as single-particle wave functions, which is contrary to the Pauli principle. The motivation of Fliessbach's two approaches reviewed in this paper is to improve on these models by a proper treatment of antisymmetrization. Fliessbach's approaches involve refined reduced-width amplitudes, which can be regarded as single-particle wave functions. We show, however, that in the approach specialized to transfer reactions the antisymmetrization is in fact treated incorrectly, and the more general approach seems applicable only to processes that involve just two nuclear fragments, like α-decay or radiative capture. We outline how single-particle wave functions can be used correctly in approximating reduced-width amplitudes. We show that our approach helps to bring the phenomenological spectroscopic factors into agreement with the nuclear structure models.

+ Permanent address: Magyar Tudományos Akadémia Atommagkutató Intézete, Debrecen, Hungary

2. LASERSPECTROSCOPY

2.1 NUCLEAR MOMENTS AND THE ISOTOPIC VARIATION OF MEAN SQUARE CHARGE RADII OF STRONTIUM NUCLIDES BY ATOMIC BEAM LASER SPECTROSCOPY

M. Anselment, S. Chongkum, S. Göring, A. Hanser, G. Meisel, H. Rebel and G. Schatz

The recent interest in studies of nuclear moments and of the isotopic variation of the mean square charge radii in neutron deficient Sr nuclei arises from theoretical predictions (1) and gamma ray spectroscopic results (2) indicating a peculiar transition to strongly deformed shapes, when removing neutrons from the closed shell (N = 50). We measured the hyperfine splittings and the isotope shifts of the atomic ($5s^2$ ^1S_o–5s6p $^1P_1$, λ= 293 nm) transition in SrI for a series of stable and radioactive Sr nuclides (A = 82 - 90) and evaluated the observed
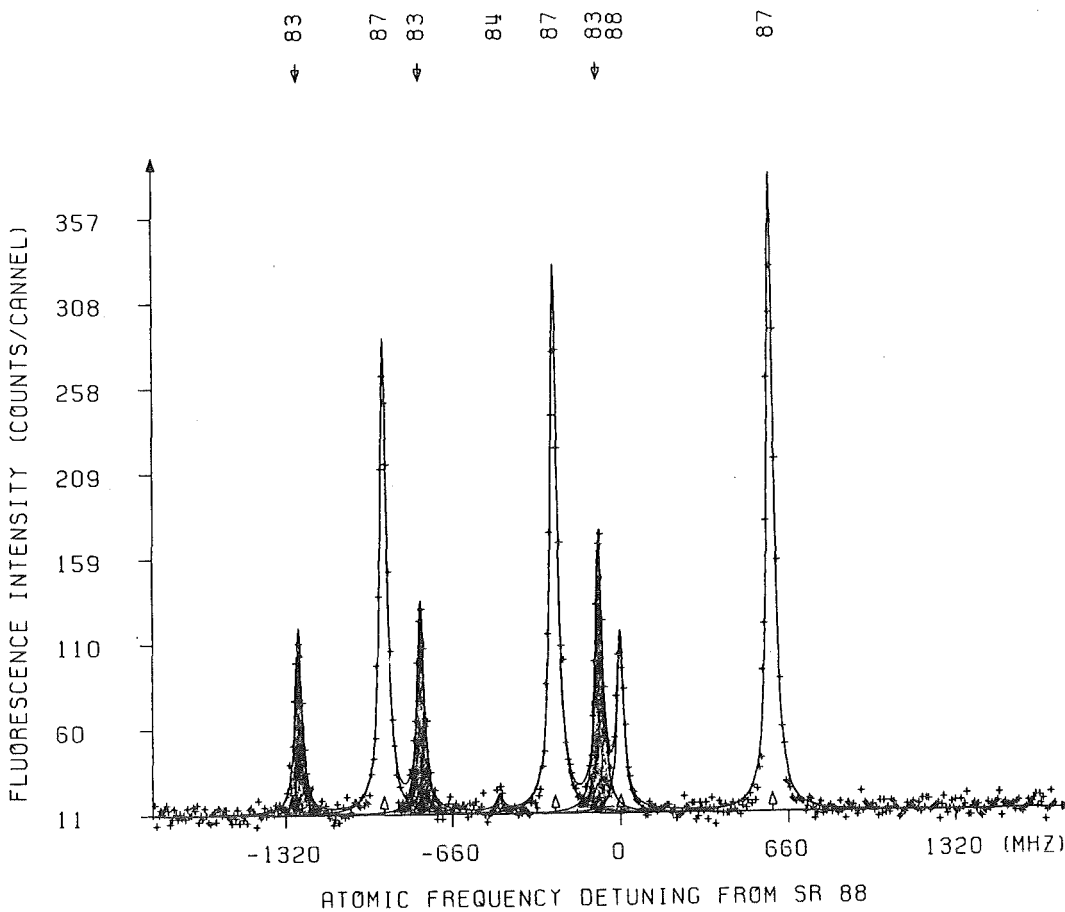
Fig. 1 Record for the ^{83}Sr component search. ^{87}Sr was added as reference; ^{88}Sr was present as impurity.

Mass number A	A [MHz]	μ [n.m.]	B [MHz]	Q [b]
83	149.017(90)	-0.82976(53)	31.6(1.4)	0.816(62)
85	139.723(28)	-1.00029(28)	12.35(24)	0.319(21)
87	152.756(28)	-1.093602(1)*	12.95(24)	0.335(20)*
89	290(5)	-1.155(20)	-2(19)	-0.06(50)

Table 2 Magnetic dipole (A) and electric quadrupole (B) interaction constants resulting from the hyperfine splittings of Table 1 for odd Sr isotopes together with the dipole (μ) and quadrupole (Q) moments as derived thereof. The values marked * for ^{87}Sr are taken from reference (5) and used to find the moments for the other isotopes by scaling.
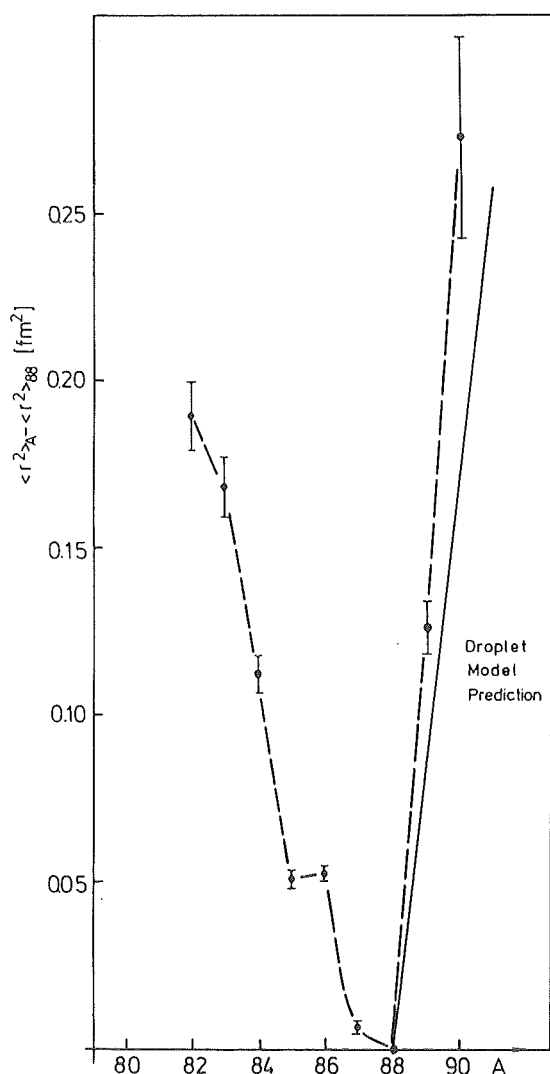
Fig. 2

Changes of the mean square charge radii for Sr isotopes.

(1)   K. Heyde, J. Moreau and M. Waroquier, Phys. Rev. C 29 (1984) 1859
(2)   C.J. Lister, B.J. Varley, H.G. Price and J.W. Olness, Phys. Rev. Lett. 49 (1982) 308
       B. Burghardt, W. Jitschin and G. Meisel, Appl. Phys. 20 (1979) 141
(4)   M. Anselment, S. Chongkum. H. Hoeffgen and G. Meisel, KfK-Report 3621 (1983) 65.
(5)   C.M. Lederer und V.S. Shirley (Hrsg.), Table of Isotopes, 7. Auflage, J. Wiley, New York (1978)

results in terms of electromagnetic moments and changes $\delta\langle r^2\rangle$ of the nuclear charge radii.

The method applied was cw dye laser induced fluorescence of free atoms in an atomic beam. The dye laser beam intersected the atomic beam perpendicularly, and the excitation was signalled by measuring the fluorescence intensity of a re-emission transition ($5s6p\ ^1P_1 - 5s4d\ ^1D_2$, λ = 717 nm).

The 293 nm light was generated by frequency doubling the output of a cw dye laser in a temperature tuned ADA crystal. For accurate measurements a special rf technique was used to tune the dye laser repetitively over the atomic reso-nance of interest and to give it the long term stability required for reference to stable isotopes (3,4).

The radioactive Sr isotopes were produced either by neutron capture of stable Sr or by (α,xn) reactions with a Kr gas target. The samples were purified by an electromagnetic mass separator and their sizes were of the order of 100 pg. Fig. 1 displays an excitation spectrum of ^{83}Sr($t_{1/2}$ = 32.4 h) and Tables 1 and 2 compile the results. The strong increase of the nuclear charge radii for neutron deficient isotopes (Fig. 2) is in agreement with the variation of the mean square deformation extracted from measured B(E2) values).

A	I	F	Position [MHz]	Isotope Shift [MHz]	$\delta\langle r^2\rangle = \langle r^2\rangle^A - \langle r^2\rangle^{88}$ [fm²]	Staggering Parameter γ
82			-728.3(1.5)	-728.3(1.5)	0.190(10)	-
		5/2	-1264.59(30)			
83	7/2	7/2	-782.4(1.5)	-610.92(54)	0.169(10)	0.64(36)
		9/2	-81.47(50)			
84			-474.05(30)	-474.05(20)	0.1236(70)	-
		7/2	-1077.55(20)			
85	9/2	9/2	-462.69(20)	-314.73(12)	0.0513(30)	2.05(12)
		11/2	317.11(20)			
86			-224.82(30)	-224.82(30)	0.0530(30)	-
		7/2	-927.89(20)			
87	9/2	9/2	-255.06(20)	-93.67(12)	0.0070(14)	1.74(5)
		11/2	596.98(20)			
88			0.0	0.0	0.0	-
		3/2	-1050(20)			
89	5/2	5/2	-320(20)	-32(12)	0.1267(80)	0.43(7)
		7/2	693(20)	.		
90			-79.72(50)	-79.72(50)	0.273(30)	-

Table 1 Measured hyperfine component positions, isotope shifts, changes of the mean square charge radii and staggering parameters for Sr isotopes.

2.2 PRECISE DESCRIPTION OF THE ODD PARITY ENERGY LEVELS IN THE SPECTRUM Ge I

J. Dembczyński[+] (1)

A fine structure analysis for the system $4s^2 4pn's(n' = 5$ to $14) + 4s^2 4pn''d$ ($n = 4$ to $14) + 4s4p^3$ is performed on the basis of available experimental data. The Slater integrals and spin-orbit parameters are determined. The configuration $4s4p^3$ is shown to influence the odd level system of Ge I strongly. On the basis of the theoretical results precise spectroscopic assignments of 154 odd parity electronic energy levels are given. The quantum numbers n' and l' for excited electron states fail to be good quantum numbers in many cases.

(1)   Physica C (in press)

+   permanent address: Politechnika Poznańska, Instytut Fizyki, Poznan, Poland

2.3 THE ODD-EVEN STAGGERING OF THE NUCLEAR CHARGE RADII OF THE Pb ISOTOPES

M. Anselment, W. Faubel[+], S. Göring, A. Hanser, G. Meisel, H. Rebel and G. Schatz

A conspicuous feature generally observed with the isotopic variation of nuclear charge radii, is a distinctive odd-even staggering. The nuclear mean-square charge radii $<r^2>$ of the odd-neutron isotopes appear to be slightly smaller (usually of the order of 10^{-2} fm²) than the averages of their even-neutron neighbours. In contrast to the remarkly long history of the experimental observation, a convincing and consistent theoretical explanation, which quantitatively reproduces the data by a microscopic nuclear structure description, is missing, although several kinds of effects have been discussed as the origin of the phenomenon. In addition, empirical systematic features of the normal odd-even staggering, which could guide the theoretical investigation, are not very pronounced and not well worked out, since most often other influences on isotopic changes of the ms radii, i.e. fluctuations of the mean square deformation and shell effects, do obscure the trend of the relatively tiny odd-even staggering.

However, the nuclei in the neighbourhood of the doubly-closed shell nucleus ^{208}Pb may provide a more favourable situation, due to the distinct and clear microscopic nuclear structure and due to the reduced importance of deformation effects. With this aspect we have extended our previous laserspectroscopic measurements (1,2) of isotope shifts (IS) and hyperfine splittings of the ($6p^2$ ^3P_o - $6p7s$ $^3P_1^0$) PbI resonance line by using essentially the same experimental arrangement and procedures as described in Ref. (1). Most recently, we succeeded in preparing an atomic beam of ^{211}Pb ($T_{1/2} = 36.1$ m) by extracting a 10 pg sample as daughter product from a freshly prepared emanating ^{227}Ac source. The success-

ful measurements on ^{211}Pb complete the results of a series from ^{196}Pb to ^{214}Pb
(except for the inaccessible ^{213}Pb). The staggering is characterized by the staggering parameter

$$\gamma_{A+1} = \frac{2(<r^2>_{A+1} - <r^2>_A)}{<r^2>_{A+2} - <r^2>_A} \qquad (A = \text{even})$$

which equals to 1, when no staggering is present. This quantity can be evaluated with the measured data without explicitly introducing the electronic factor F calibrating the field shifts in terms of $<r^2>$.

$$\gamma_{A+1} = \frac{2(\delta\nu_{A+1} - \delta\nu_A - \frac{M}{A(A+1)})}{\delta\nu_{A+2} - \delta\nu_A - \frac{2M}{A(A+1)}} \qquad (A = \text{even})$$

^{211}Pb:

Isotope shift:

5625.4(3.0) MHz

A = -2326.4(7) MHz

B = -16(6) MHz

$\delta<r^2>$ = 0.2994(25) fm^2
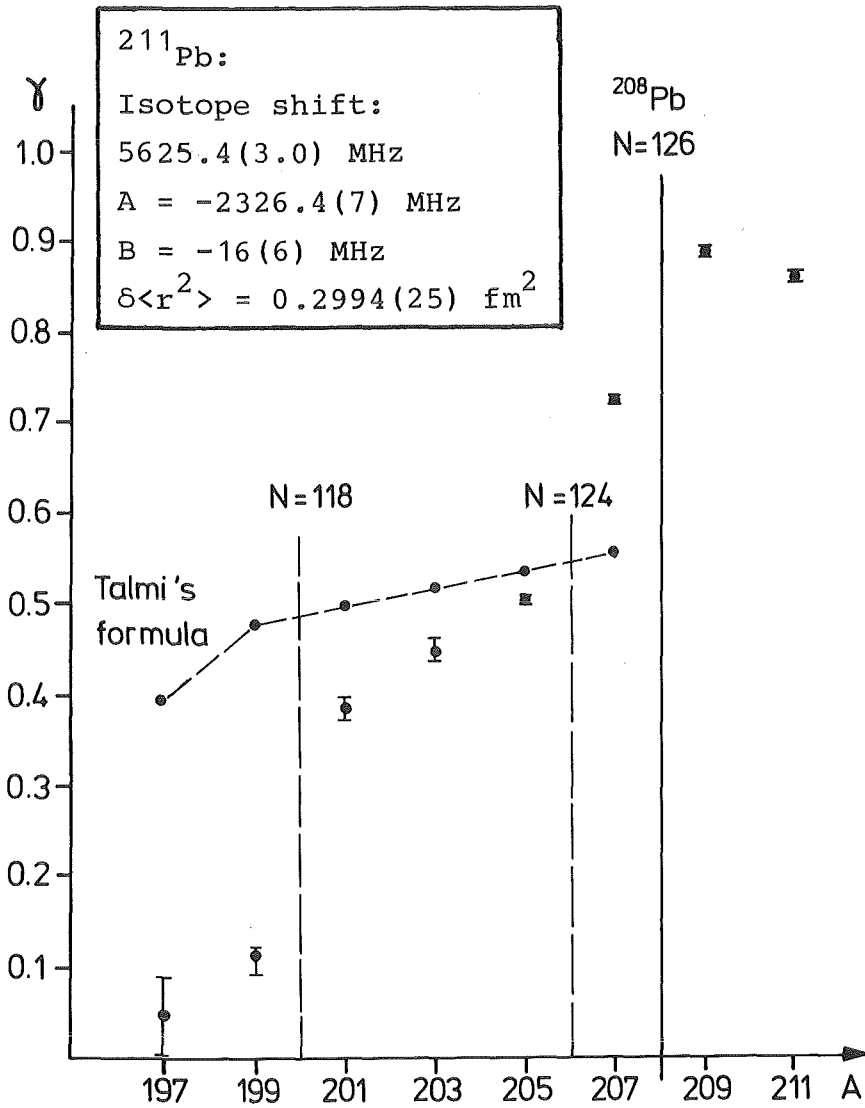
Fig. 1
The variation of the staggering parameter γ of the Pb charge radii. The inset gives the new data of ^{211}Pb (relative to ^{208}Pb)

M is the mass shift factor which has been determined in Ref. (1) by muonic X-ray results to be M = (1 $\pm$ 10) times the normal mass shift factor (NMS). A recent theoretical estimate (3) reduces the uncertainty of this factor considerably M = (0.19 $\pm$ 0.75)$\ast$NMS. Using this value the variation of γ is displayed in Fig.1, revealing a systematic development of the staggering on the neutron deficient side, while the staggering for Pb nuclei beyond ^{208}Pb appears to be less pronounced.

(1)   R.C. Thompson, M. Anselment, K. Bekk, S. Göring, A. Hanser, G. Meisel, H. Rebel, G. Schatz, B.A. Brown, J. Phys. G: Nucl. Phys. <u>9</u> (1983) 993
(2)   M. Anselment, S. Göring, A. Hanser, J. Hoeffgen, G. Meisel, H. Rebel, G. Schatz, W. Faubel, KfK-Report 3671 (1983) p. 63
(3)   W.M. King and H. Wilson, J. Phys. G: Nucl. Phys. <u>11</u> (1985) L 43

+   Institut für Radiochemie, Kernforschungszentrum Karlsruhe

2.4   OPTOGALVANIC SPECTROSCOPY OF EUROPIUM

W. Kälber (1)

An optogalvanic laserspectrometer was set up; its main part is a hollow cathode discharge cooled with liquid nitrogen. It was tested with stable europium isotopes. Selected optical transitions in the red to yellow spectral range, among them in particular the ground state transition EuI 6018 $\overset{o}{A}$, were investigated. The hyperfine splittings and isotope shift data obtained are compared with recent results. Of special interest was to find the operating conditions which lead to a high detection sensitivity to allow considerable reduction of the europium quantity required to take a spectrum. It was found that 300 ng (or 1.2 x 10^{15} atoms) of europium are sufficient to record the EuI 6018 $\overset{o}{A}$ transition in the Doppler limited mode with a 14 : 1 signal-to-noise ratio using an averaging time constant of 1 sec. In the intermodulated operating mode a reduction of the Doppler width by a factor of only 2 is obtained whereas the signal height drops by a factor of 10 to 20 for the 6018 $\overset{o}{A}$ line.

(1)   ditto, KfK-Report 3945 (1985)

2.5   ISOTOPE SHIFTS AND HYPERFINE STRUCTURE OF AmI SPECTRAL LINES BY OPTOGALVANIC LASERSPECTROSCOPY

W. Liewehr, K. Bekk, W. Kälber, G. Meisel and H. Rebel

In addition to the information on size and shape of the nuclear charge distributions, studies of the isotope shifts and hyperfine structure (hfs) splitting provide the basis for a detailed analysis and understanding of complex atomic

spectra. In the course of our current investigations of the variation of the nuclear charge radii and of the electromagnetic moments of Am nuclei, we measured several atomic transitions in AmI, resolving the hyperfine structure, in order to check some assignments in the atomic level scheme and to clarify open questions of the atomic structure.

Our measurements used the method of optogalvanic laserspectroscopy (1), (2), well suited for experimental studies of α-emitters, because the samples are hermetically sealed off in a hollow cathode.

In optogalvanic spectroscopy optical transitions are induced in atoms which participate in a glow discharge. The changes in atomic level population can be detected as current or voltage variation of the discharge. For separating the large dc-signal from the optogalvanic signal with lock-in technique, the incoming laser light is chopped with an electrooptical modulator. Using a chopping frequency of about 50 kHz a considerable reduction of the discharge noise is obtained. The experiments were done with aluminum foils that were inserted into a hollow cathode. About 1 to 5 μg Am was vacuum deposited onto each foil.

The accurate determination of the frequency of the laser light was done with a wavemeter (3) consisting of a grating spectrograph and three Fabry-Perot-interferometers.
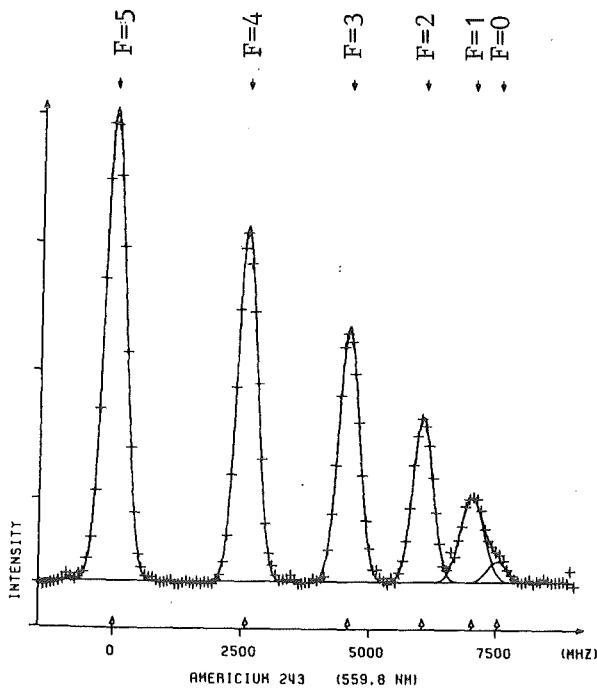
Fig. 1
Spectrum of the $\lambda = 5598.1$ Å transition of ^{243}Am. The splitting is due to the upper state hyperfine interaction.

We measured five transitions for ^{243}Am and ^{241}Am starting from the ground state $5f^7 7s^2 (^8S_{7/2})$ in the region from 5400 Å to 6405 Å. Fig. 1 shows the mea-

sured spectrum of the 5598.13 Å transition in ^{243}Am. For all these transitions
the isotope shifts for ^{243,241}Am and the A- and B-factors of the upper state
could be determined. The accuracy of these hfs-measurements allowed also to as-
sign unambiguously the J-values of these states. The results are summarized in
Tables 1 and 2. Some of them were already given by Fred and Tomkins (4) though
with much larger uncertainties and missing components; as far as they are com-
parable with our findings the results agree fairly well. The designation of the
terms is somewhat arbitrary because Am terms are rather far off Russell-Saunders
coupling and also configuration mixing occurs.

Table 1 Electronic Angular Momentum (J) and Isotopic Shifts for Am I transitions

Wave-length (nm)	Configuration	Term	J	Isotopic Shift ^{243}Am $-$ ^{241}Am (MHz)
540 2	$5f^7\,7s7p$	$^8P_{7/2}$	7/2	-5126(80)
542.4	$5f^7\,7s7p$	$^8P_{5/2}$	5/2	
559.8	$5f^6\,6d\,7s^2$	?	5/2	+4755(60)
605.4	$5f^7\,7s7p$	$^{10}P_{9/2}$	7/2	-6439(30)
640.5	$5f^7\,7s7p$	$^{10}P_{7/2}$	5/2	

Table 2 Hyperfine splittings coefficients for Am I - transitions

Wave-length (nm)	^{241}Am A (MHz)	B (MHz)	^{243}Am A (MHz)	B (MHz)
540.2	- 942.5 (3.0)	+ 696(66)	- 936.45(0.26)	+ 753.7(5.3)
542.4	-1248.74(0.25)	- 142(10)		
559.8	- 537.7 (1.1)	- 90(22)	- 533.40(41)	- 111.2(5.6)
605.4	+1732.22(0.41)	-3424(19)	+1719.36(0.43)	-3439 (21)
640.5	+1429.39(0.34)	+1056(7)		

(1)   H.O. Behrens, G.H. Guthörlein, J. de Phys. 44 (1983) C7
(2)   W. Kälber, KfK-Report 3945 (1985)
(3)   A. Steiger, KfK-Report 3820 (1984)
(4)   M. Fred, F.S. Tomkins, J. Opt. Soc. Am. 47 (1957) 1076

2.6 HOW ACCURATE ARE LASER SPECTROSCOPIC MEASUREMENTS OF ATOMIC HYPERFINE STRUCTURE?

M. Anselment, S. Chongkum, G. Meisel

In a series of experiments aiming at the determination of the hyperfine structure of radioactive Sn and Sr isotopes (1,2), the corresponding measurements were also done for the natural stable isotopes of these elements. The method applied was laser induced fluorescence using a collimated atomic beam. The measurements for the stable isotopes had been done before with basically the same methods (3,4) but the results differed somewhat from ours. Therefore we found it worthwhile to investigate this problem in more detail. For this purpose the Sn and Sr measurements were repeated with widely varying experimental conditions to find out to what extent they influence the result and thus to establish resonable limits of error not only with respect to the statistical fluctuations but concerning the even more important systematic errors, too. In addition, we have done similar measurements on the element Co, since its hyperfine structure had been determined by atomic-beam magnetic-resonance (ABMR) (5), which gives values that are beyond doubt in view of the precision accessible by present laser methods. The experimental methods applied are described elsewhere (6) so we do not give details here.

Among the parameters that were varied to test their influence on the frequency difference between hyperfine components are: Irradiated light intensity, direction of the atomic and light beam, atomic beam collimation, oven temperature changes and laser frequency control and tuning characteristics, choice of the rf and of the sideband used. The results showed that the Sn results are dependable to $\pm$ 150 kHz. The uncertainty for Sr was $\pm$ 50 kHz. As to Co, the ABMR results were reproduced to within $\pm$ 100 kHz.

Altogether, it is found that the main feature that limits the accuracy of the result is the observed line width of the resonances. Roughly, the precision is a fixed portion of the linewidth, about 1 % of the experimental FWHM. This has been observed in a series of corresponding investigations of Doppler-free two-photon resonances in Na and Li (7,8,9). The linewidths were between 3.5 and 12 MHz. This series has now been extended to collimated atomic beam type experiments and to broadened lines (see table 1). For wider resonances the ultimate uncertainty does not increase to the same extent as the linewidth, i.e. they can be localized to a somewhat smaller portion of the FWHM, e.g. down to 0.3 % of the FWHM.

Table 1: Accuracy of different laser experiments

Element	induced transition	Laser Wave-length [nm]	Type of experi-ment	Line width FWHM [MHz]	absolute accurary [kHz]	internal reproduci-bility [kHz]	in % of FWHM	Ref.
^{23}Na	$3s\ ^2S_{1/2} \to 4d\ ^2D_{3/2,5/2}$	578.7	Doppler-free two-photon.	3.5	-	30	0.8	[7]
^{23}Na	$3s\ ^2S_{1/2} \to 3d\ ^2D_{3/2,5/2}$	685.6	Uncolli-mated atomic beam	8.6	-	80	0.9	[8]
^{7}Li	$2s\ ^2S_{1/2} \to 3d\ ^2D_{3/2,5/2}$	639.2		12	-	80	0.7	[9]
$^{112-124}$Sn	$5p^2\ ^3P_0 \to 5p6s\ ^3P_1$	286.3	Single photon.	40	-	150	0.3	[1]
$^{84-88}$Sr	$5s^2\ ^1S_0 \to 5s6p\ ^1P_1$	293.2	Colli-mated atomic beam	5	-	50	1	[2]
^{59}Co	$3d^74s^2\ ^4F_{7/2} \to 3d^84p\ ^2F_{7/2}$	288.6		35	100	100	0.3	this work

(1)   M. Anselment, A. Hanser, J. Hoeffgen, S. Göring, G. Meisel, H. Rebel, KfK-Report 3815 (1984) 59

(2)   This Report, Contr. 2.1

(3)   Baird, P.E.G., Blundell, S.A., Burrows, G., Foot, C.J., Meisel, G., Stacey, D.N. and Woodgate, G.K., J. Phys. B: At. Mol. Phys. 16 (1983) 2485

(4)   E.R. Eliel, W. Hogervorst, T. Olsson, L.R. Pendrill: Z. Phys. A311 (1983) 1

(5)   W.J. Childs, L.S. Goodman: Phys. Rev. 170 (1968) 50

(6)   M. Anselment, S. Chongkum, J. Hoeffgen, G. Meisel: KfK-Report 3621 (1983) 65

(7)   B. Burghardt, M. Dubke, W. Jitschin, G. Meisel: Phys. Lett. 69A (1978) 93

(8)   B. Hoffmann: Diplomarbeit, Bonn 1982

(9)   B. Burghardt: Dissertation, Bonn, 1982

2.7   AN INSTRUMENT FOR RAPID AND PRECISE DETERMINATION OF WAVE-LENGTHS FOR VISIBLE LASER LIGHT

A. Steiger (1)

A wavemeter was built up that allows one to determine the wavelength of an incoming laser beam, having a wavelength in the range of 400 to 700 nm. The resolution is better than 10^{-7}, or correspondingly less than 50 MHz. An average laser power of about 1 mW across a beam diameter of 0.5 mm is sufficient. The instrument consists of a combination of three plane parallel Fabry-Perot interferometers with graded thicknesses and a small grating spectrograph. For the measurement of the wavelength the interference patterns produced by these are continuously recorded by four linear photodiode arrays and fed into a small on-line computer which analyses them. The program provides a new wavelength output approximately every second. The design and operation of the instrument as well as the calibration procedure are described in detail.

(1)   ditto, KfK-Report 3820 (Okt. 1984)

2.8 PRECISION FREQUENCY METROLOGY FOR LASERS IN THE VISIBLE AND APPLICATION TO ATOMIC HYDROGEN

B. Burghardt[+], H. Hoeffgen[+], G. Meisel, W. Reinert[++], B. Vohwinkel[++] (1)

A multi-step method is discussed that permits the determination of frequency differences between lasers in the visible in cases where the beat frequency is too large for direct detection. A step width of 80 GHz is used; the beat signal is picked up with millimeter-wave GaAs photodiodes. The resulting beat signals can be measured without further smoothing using a frequency counter. We report on experiments with atomic hydrogen, applying the method to measure transition frequencies aiming to determine the Rydberg frequency and the electron/proton mass ratio with increased precision.

3. NEUTRINO PHYSICS

Karlsruhe Rutherford Medium Energy Neutrino Experiment KARMEN

G. Drexlin, H. Gemmeke, G. Giorginis, W. Grandegger, A. Grimm,
R. Gumbsheimer, J. Hesselbarth, H. Hucker, L. Husson, S. Kiontke,
J. Kleinfeller, D. Mann, R. Maschuw, M. Momayezi, K.H. Ottmann,
P. Plischke, F. Raupp, M. Reuscher, F.K. Schmidt, G. Spohrer,
P. Wild, J. Wochele, B. Zeitnitz

Kernforschungszentrum Karlsruhe, IK I and University of Karlsruhe

E. Finckh, W. Kretschmer, K. Stauber, D. Vötisch, J. Böttcher

University of Erlangen

N.E. Booth

Oxford University

J.A. Edgington, G. Marinos

Queen Mary College, London

KARMEN denotes a programme of neutrino physics to be performed at the pulsed Spallation Neutron Source SNS at the Rutherford Appleton Laboratories RAL (1,2). The main purpose is to contribute to the questions of neutrino oscillations, neutrino nuclear physics, and neutrino electron scattering.

Two detectors will be employed, the 60 to liquid scintillator detector KARMEN 1 being under construction. Results of prototype measurements and Monte Carlo simulations for KARMEN 1 are reported below. The second detector dedicated to ν-e scattering below 50 MeV will have much finer granularity. The techniques to be used are still under discussion. At KfK, prototype tests are in progress for a liquid Argon wide gap drift chamber approach.

(1)   R. Maschuw, B. Zeitnitz, KfK 3362 (Juni 1982)
(2)   B. Zeitnitz, Progress in Particle and Nuclear Physics 13 (1985) 445

3.1 STATUS OF THE PROJECT

3.1.1 THE NEUTRINO FACILITY

The KARMEN experimental area consists of the neutrino blockhouse located within the SNS experimental hall, and an extension to this hall which is needed for assembling and servicing the detector and for housing the electronics. The blockhouse is made from iron slabs with walls and roof of 2.2 and 3.0 m thickness respectively. The inner dimensions are 10x4x7 m^3, the

overall weight is about 6000 to. Fig.1 shows the blockhouse seen from the hall extension, the manually movable sliding door of 600 to of iron being partly open.

All of the blockhouse has been completed except the upper layers of the roof. The floor has a flatness of ± 3 mm within 3 m distance adequate for the use of airpads for moving the 300 to detector. An 80 000 1 storage tank for the liquid scintillator has been installed at RAL together with the supply pipes into the experimental area. The scintillator supply system (pumps, valves, pipes etc.) is now ready to be used with the Protoype III detector at KfK and will be shipped to RAL to run the main detector when ready for operation in 1986.

Fig. 1 Neutrino blockhouse

3.1.2   KARMEN 1 DETECTOR

KARMEN 1 is a 60 to liquid scintillator detector suited for the detection of neutrino interactions with ^{1}H and ^{12}C. The liquid is contained in a single vessel which is optically segmented by a totally reflecting lucite structure. The detector vessel is under construction and will be delivered until November 1985. It will be surrounded by an inner passive iron shield of 18 cm thickness which has already been delivered.

The optical segmentation consists of totally reflecting double lucite sheets with Gadolinium coated paper inserted into the air gap between the two layers. The Gadolinium serves for the detection of neutrons from the reaction $\bar{\nu}_e$ + p → e$^+$ + n. The detector is divided into 512 (16w x 32h) modules with cross section 178x174 mm^2 and 3500 mm length. In addition, 96 half-width modules at the outer sides serve as inner anticounters. The op-

tical segmentation is currently manufactured at KfK.

Each detector module will be viewed by two 3" Photomultiplier tubes (PM) of type XP 3462. Of the final quantity of 2500 PM, 1200 have been delivered. Each tube is tested at the RAL PM test facility which has been optimized for our needs. The 600 tubes tested up to now generally show better values than the specified ones for risetime (3 nsec), resolution (10% for ^{57}Co, 3" x 3" NaJ), and linearity (2% up to 100 mA). The nominal gain of the 8-stage tube with integrated bleeder is 10^6 at 1500 V.

The XP 3462 tube, a μ-metal magnetic shielding and a PVC support sleeve are glued together thus forming one single PM unit (fig.2). The unit is provided with an optical fibre to be coupled to the laser calibration system and with electrical leads for signal and HV supply. The PM units will be mounted in aluminium sleeves with 5 mm glass windows looking into the scintillator tank. Fabrication of the PM units is scheduled to start in September 1985 at RAL.
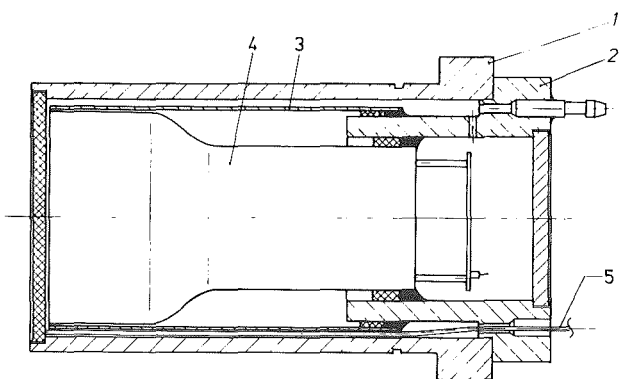
Fig. 2 PM unit

1 - Aluminium sleeve

2 - PVC sleeve

3 - μ-metal

4 - XP 3462 tube

5 - optical fibre

3.1.3 THE LIQUID SCINTILLATOR FOR KARMEN 1

Investigations on scintillator cocktails for the KARMEN 1 neutrino detector have been completed. Finally they were concentrated on a cocktail consisting of the one component fluor PMP* solved in a mixture of mineral oil and pseudocumene. Light output and attenuation length have been measured as function of the PMP concentration and the solvents mixing ratio. A figure of merit has been deduced given as light output times the light transmission for half the detector length, i.e. 175 cm. A model describing the various transfer and relaxation processes leading to scintillation has been developed. It not only allowed the interpretation of the experimental results but also predicts the scintillator properties for any composition.

*PMP = 1 phenyl-3 mesityl-2 pyrazoline

Thus a composition best suited for our purposes has been deduced. This cocktail which we call PPP consists of 2g/l PMP solved in a mixture of 75 Vol% liquid paraffine (mineral oil) and 25 Vol% pseudocumene (1,2,4 trime-thylbenzene). The resulting figure of merit was $g = 0.308$ which exceeds the value $g = 0.282$ measured for the best commercial liquid scintillator NE 235 H. The superior properties have been confirmed by energy loss measurements of minimum ionizing particles in our 200 l test detector (3500x150x150 mm). These results together with price considerations led to the decision to apply this scintillator cocktail for our 60 000 l KARMEN 1 detector. In the meantime the supplier MERCK, Darmstadt, succeeded in producing both the scintillation fluor PMP and the solvents to meet our quality requirements.

3.1.4   ELECTRONICS AND DATA HANDLING

For each out of 512 modules of the KARMEN 1 detector the electronic system analyses the anode signals of the phototubes at each end of a module accor-ding to pulse height and time information. The physical quantities derived are the energy deposit in the module, the event location along the module and the event time relative to the SNS pulse.

An improved version of the front-end electronics (ASTERIX board) is being tested. A test system already exists for checking the 190 ASTERIX boards scheduled to be produced at the end of this year. A private bus sy-stem has been developed to link the ASTERIX-boards to the ADC- and read out CAMAC modules. At the end of 1985 a readout system for 12 detector modules will be available.

The digitized data will be collected and formatted by a very fast CAMAC processor (CES 2180). Programming of this unit has been started. Com-plete tests of the full CAMAC electronics are now possible. In parallel, the control software of the 1280 channel high voltage system was developed and successfully tested.

Hard- and software development is supported by the Hauptabteilung Datenverarbeitung und Instrumentierung - HDI -.

3.1.5   THE LASER BASED CALIBRATION AND MONITORING SYSTEM

The laser based monitoring system for the KARMEN 1 detector will be able to report the status of the detector modules (PM failure, light guide defect) as well as to monitor slowly varying parameters, e.g. the PM gain.

The system consists of a nitrogen laser which is the primary light source for the whole system. The laser light is being sent through a diffu-

sor to achieve more spatial uniformity. The light is then coupled into nine optical quartz fibres. The laser intensity at the location of the fibre ends can be varied by changing the distance between diffusor and fibres. Each quartz fibre is lead into the geometric center of a light distribution box. These boxes are filled with liquid scintillator which shifts the laser light to scintillation wavelengths and gives a good optical coupling to the lucite fibres located in the side wall. Integrated in the distribution box there is a vacuum photo diode to monitor the laser intensity. The lucite fibres will lead to the ends of the detector modules (fig.2).

Tests on a prototype distributor with 25 lucite fibres yielded a variation in the light output from fibre to fibre of 3% r.m.s..

By varying the laser intensity the energy resolution of a realistic prototype configuration was measured covering the whole energy range of 1 MeV to 50 MeV. The laser hereby simulates the light emitted by a cosmic muon passing through the middle of the prototype module. Over the whole range the resolution is described very well by $\sigma = 14.2\%/\sqrt{E}(\text{MeV})$ for a single PM pair. For the sum of the signals out of the two opposite PM pairs belonging to one module the energy resolution drops to $\sigma = 10.5\%/\sqrt{E}(\text{MeV})$. This was measured with four PM's whose gains were matched to within 5% but we found the resolution to remain unchanged if the gains were mismatched by 25%.

3.1.6 PROTOTYPE III TEST DETECTOR

The prototype III detector vessel has been installed at KfK. It is essentially a five modules wide and seven modules high cut of the KARMEN 1 detector surrounded by 24 half wide inner veto modules, all having the same dimensions and design features as KARMEN 1 modules. This allows a full test of all detector components like optical segmentation, phototube mounting, electronics, and laser calibration system. 10 000 l of PMP-based liquid scintillator will be delivered in August 1985. A storage tank has been installed. The scintillator supply system for KARMEN 1 will be tested with the prototype III detector.

Measurements with cosmic muons triggered by wire chambers are planned in a similar fashion as the prototype II ones. Thus the position dependent light output as well as consequences of the detailed structure of the optical segmentation will be studied using the actual detector geometry. These measurements will start in autum 1985.

3.2 RELATED ACTIVITIES

3.2.1 NEUTRON EFFICIENCY FOR $\bar{\nu}_e$+p DETECTION

The appearance of $\bar{\nu}_e$ at SNS would be strong evidence for the oscillation $\bar{\nu}_\mu \rightarrow \bar{\nu}_e$ because there are no $\bar{\nu}_e$ in the primary beam.

The selective reaction is the inverse β-decay

$$\bar{\nu}_e + p \rightarrow e^+ + n \quad .$$
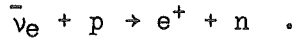
The neutron will be detected after thermalization by γ-rays with a total energy of about 8 MeV via the $Gd(n, \gamma)$-reaction. The thermal neutron cross section of Gadolinium is the highest of any element ($\sigma_{therm} = 49000b$). Therefore Gd_2O_3-painted paper is used between the lucite double layer of the KARMEN 1 liquid scintillation detector.

A mock-up experiment has been carried out to measure the time distribution of the n-capture in Gd, the (n, γ) efficiency, and the energy and spatial distribution of the absorbed γ's from the $Gd(n, \gamma)$ process in our prototype II detector. Fig. 1 shows the experimental setup.

1. Am-Be source (100 mCi)
2. Neutron flight path
3. Gd_2O_3 between the lucite sheets
   177 g Gd/m^2 = $6.9 \cdot 10^{19}$ atoms/cm^2
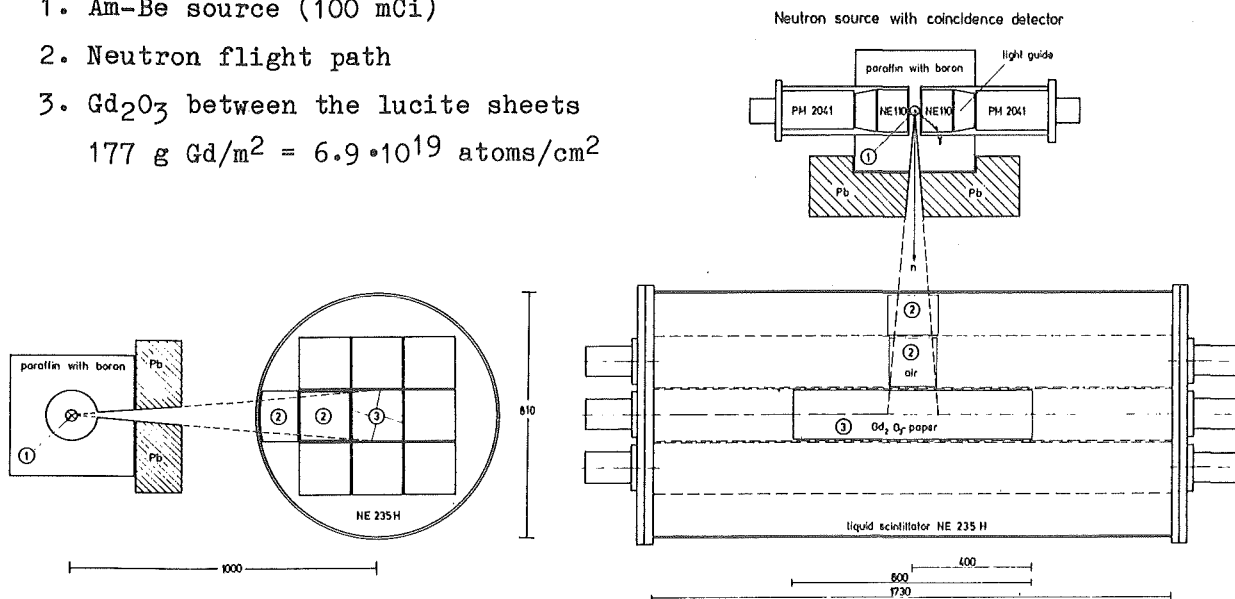
Fig. 1   Front and top schematic view of the experimental setup

Only the center module was partly coated with Gd_2O_3 paint. Tagged neutrons from an Am-Be source (4.4 MeV γ's from $\alpha + ^9Be \rightarrow ^{12}C^* + n \rightarrow ^{12}C + \gamma + n$ are associated with 2 - 6 MeV neutrons) are detected by n-p scattering in the center module with $E_p > 2$ MeV. A neutron in the center module is then defined by the fast coincidence between this p-recoil and the γ-tag in a pla-

stic scintillator (NE 110) near the source. The neutron energy is determined within $\Delta E \sim 1$ MeV by time of flight methods. To measure the time until the neutron is captured, the tagged neutron starts a TDC and any event with absorbed energy greater than 2.5 MeV in all modules stops it. From this measurement the experimental n-detection efficiency by the $Gd(n, \gamma)$ process was determined to be $\varepsilon = 0.25$.

The time distribution of neutron capture was calculated by a MC simulation using the transport code MORSE. The result is in excellent agreement with the experimental data (see fig.2). This provides good confidence for similar calculations applied to the KARMEN 1 detector.
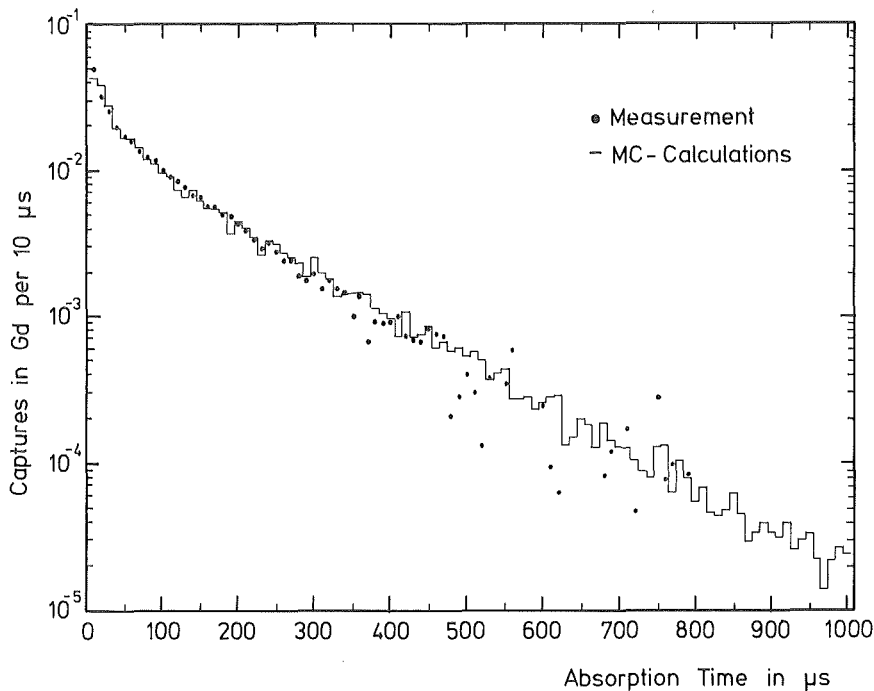
Fig. 2
Time distribution of neutrons captured in Gd.

3.2.2 MONTE-CARLO SIMULATION OF MUON BACKGROUND IN KARMEN 1

A Monte-Carlo simulation program has been written to determine the number of cosmic muons which pass through or stop in the KARMEN 1 detector. The calculations take into account the specific shielding of the massive ν-blockhouse (2 m iron walls and a 3 m iron roof) and the inner passive shield (18 cm iron slabs) as well as the energy and angular distribution of cosmic muons.

The calculated number of muons reaching the detector was normalized to the flux of cosmic muons $J_\mu = 1.01 \times 10^{-2}/cm^2$ s ($E_\mu > 1$ GeV) at sea level. The results of the calculations are:

- muons which pass through the detector: ~ 1050/sec
- muons which are stopped in the detector: ~ 150/sec

Furthermore one has to reckon on about 80 muons/sec which are stopped in the inner passive shield.
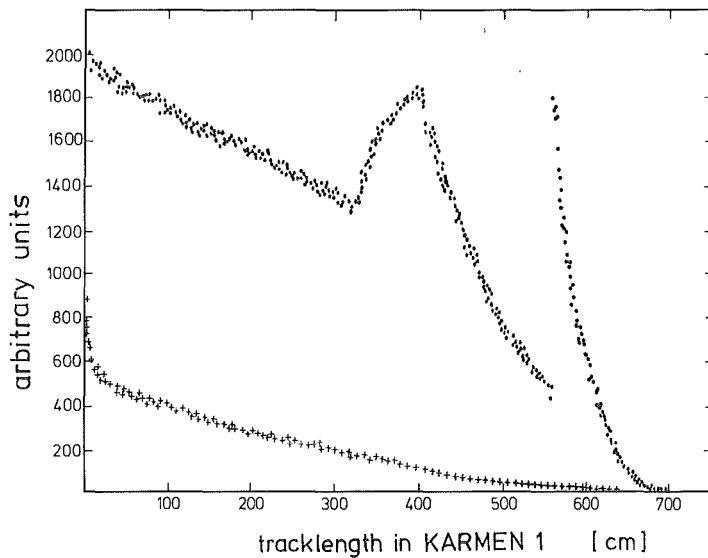
Fig. 1
Tracklength distri-
bution of muons in
the KARMEN 1 detec-
tor.
(•) muons which pass
through the detec-
tor. (+) muons which
are stopped in the
detector.

Fig.1 shows the tracklength distribution of the muons which pass through the detector compared to the one of the stopped muons. Both distributions are used to calculate the multiplicity distribution of cosmic muons in order to set up an effective muon suppression at KARMEN 1.

3.2.3 PROTOTYPE RESULTS

Measurements with the prototype I test detector (1 module, 3500x150x150 mm) were carried out using the PPP-scintillator and the phototube arrangement to be applied to the KARMEN 1 detector (2x3" XP 3462 on each side of each module). From energy loss measurements of minimum ionizing particles an energy resolution of $\Delta E/E = 14\%/ \sqrt{E}(MeV)$ was deduced, UV-laser calibration experiments yielded an even better value of $\Delta E/E = 10\%/ \sqrt{E}(MeV)$. Thus for 10 MeV electrons typically to be measured in the KARMEN detector an energy resolution of $\Delta E/E = 10\%$ FWHM can be achieved.

The experiments also confirmed the design value for the spatial resolution of $\Delta x = 10$ cm from time difference measurements between both ends of the detector modules.

Prototype II (see issue 1982/83 and 1983/84) has been designed to investigate the position dependent energy, time and spatial resolution of a segmented liquid scintillation detector as well as module correlations. It consists of 3x3 modules and is triggered by multiwire proportional chambers on top and bottom of the scintillator tank. The chambers serve to determine the intersecting points of passing minimum ionizing muons. The energy loss of the particles is described by the Landau distribution (see fig.4).

Fig. 1 shows the position dependent light output for particles that pass completely through one segment as viewed by one 2" photomultiplier. The pulse height has been calibrated to photoelectrons by an independent

LED measurement. The detector resolution is found from the primary energy loss spectrum by unfolding the Landau distribution. This resolution vs. the pulse height calibrated to photoelectrons agrees with the resolution found by the LED measurement (Fig. 2).
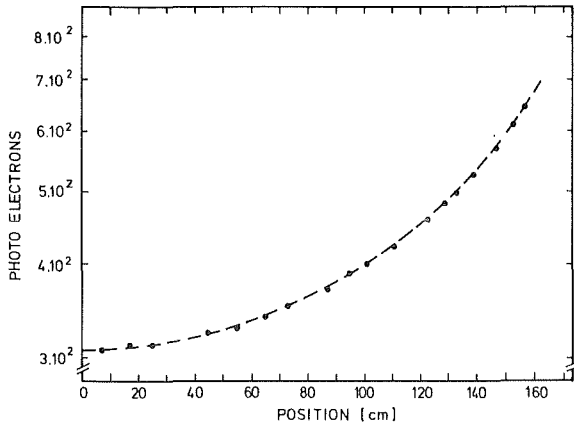
Fig. 1 Position dependent light output as viewed by one phototube located at position d=175 cm.
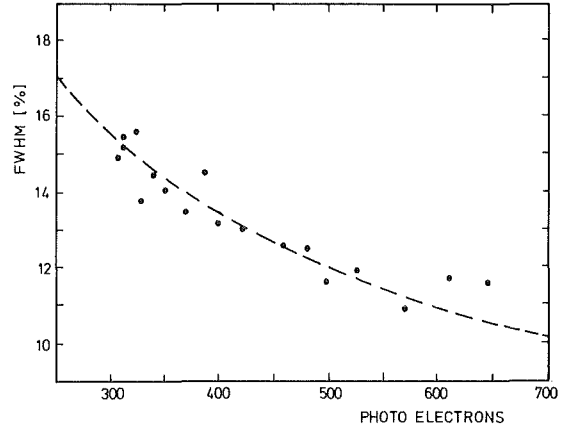
Fig. 2 Detector resolution from unfolding procedure vs photoelectrons. Solid line: resolution found from independent LED measurement.

The track length of the passing particles can be reconstructed. Thus it is possible to investigate the energy resolution in the range from 10 to 37 MeV. Two types of tracks are possible: some muons intersect only with horizontal walls and thus deposit energy amounts equal to or greater than 28 MeV (type 1), others leave the segment through a vertical wall and thus have tracks shorter than the height of one module (ΔE < 28 MeV; type 2). Fig. 1 and 2 have been determined for type 1 particles.

Fig. 3 shows the pulse height spectrum for type 2 particles. The spectrum displays the typical Landau distribution. But due to uncertainties in determining position and angle for this kind of tracks (they are close to vertical walls) the spectrum is very broad and extends to small pulse heights. The pulse height spectrum for the sum of type 2 tracks in adjacent units (as shown in the insertion of Fig. 4) has a FWHM which is nearly as good as for equivalent tracks for type 1 particles. Nevertheless the effects of the module boundaries on the light output have to be carefully taken into account in a detector Monte Carlo.
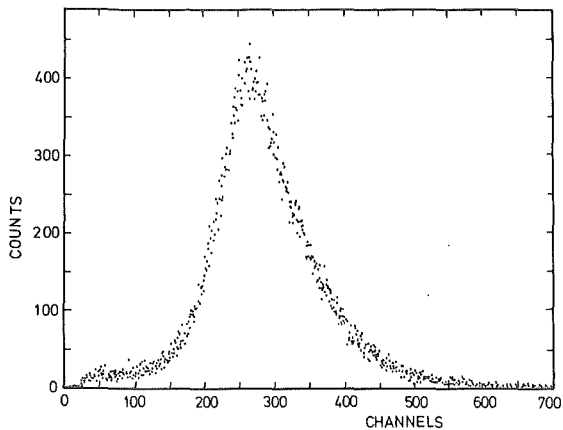
Fig. 3 Pulse height spectrum of
minimum ionizing muons
of type 2 (see text).
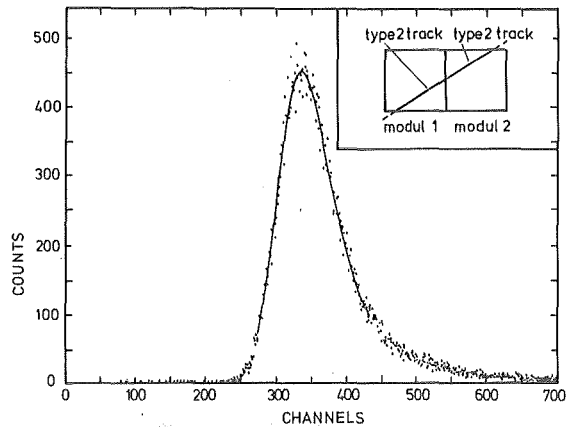
Fig. 4 Pulse height spectrum for
particles of type 2 in two
adjacent units. Solid line:
χ^2-minimum fit for Landau
distribution and Gaussian
resolution curve.

3.2.4 A LIQUID ARGON TEST DETECTOR

For the measurement of neutrino electron scattering at energies ≤ 50 MeV
the use of a 50 ton liquid gas time projection chamber (TPC) is under in-
vestigation.

So far liquid Argon (LAr) and liquid methane (LCH_4) have been con-
sidered. LAr is well known from various LAr-calorimeters whereas LCH_4 would
have advantages with respect to the ν-physics, i.e. simultaneous observa-
tion of ν-e^-, ν-^{12}C and ν-p scattering.

Long distance electron drift in both LAr and LCH_4 is limited by the
loss of ionization electrons due to electronegative impurities. This effect
was measured in a 20 l LAr-ionization chamber shown in Fig. 1.

Conversion electrons from a ^{207}Bi-source located at the cathode
were stopped in LAr within about 1 mm. The ionization electrons were then
collected at the anode after passing a Frisch grid just in front of it.
Fig. 2 shows a typical ^{207}Bi spectrum. The energy resolution of about 17%
FWHM for 1 MeV electrons was sufficient to separate the 1 MeV conversion
line of ^{207}Bi from the associated Compton continuum. The pulse height va-
riation of the 1 MeV line as function of the drift distance at constant
drift field is well exponential, as illustrated in Fig. 3 for a typical
measurement.
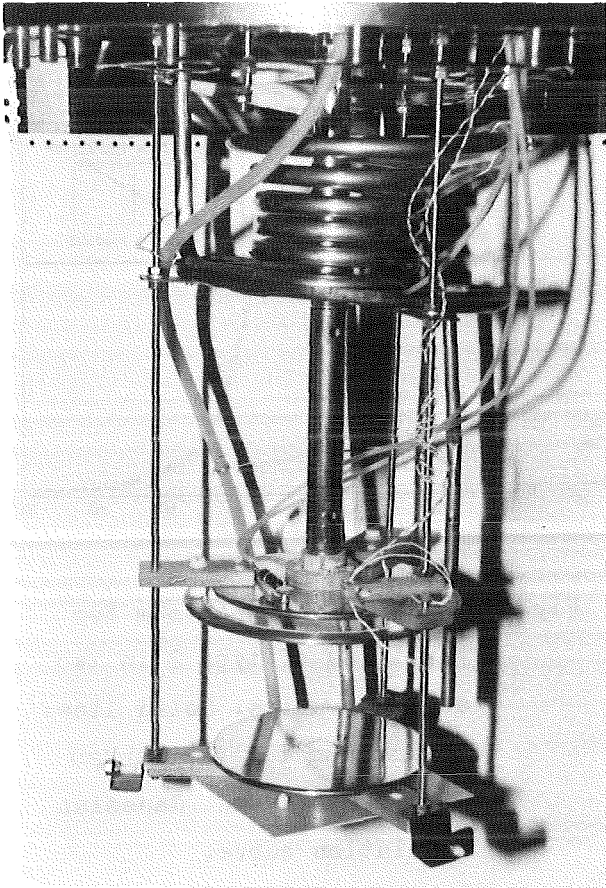
A drift distance of 8 cm and attenuation lengths for ionization electrons of about 100 cm have been achieved.

Further developments concentrate on a continuously operating purification system as well as the application of a structured X-Y anode for TPC operation of the test detector.

Fig. 1 Inner structure of the 20 ℓ LAr test detector.
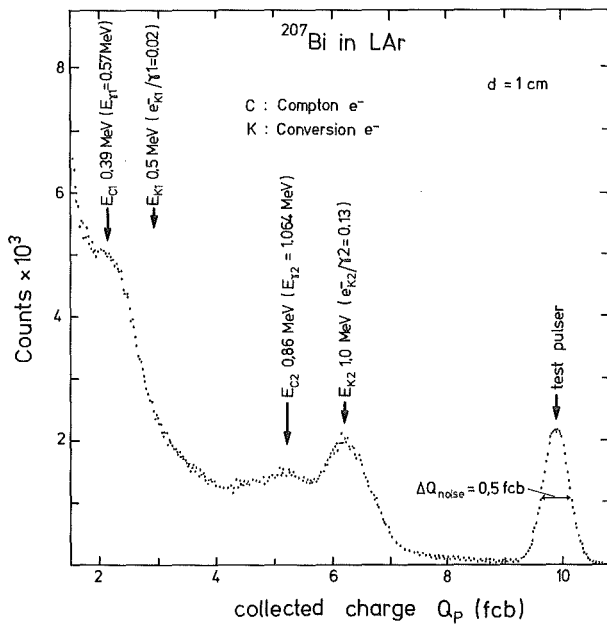
Fig. 2   Typical [207]Bi-spectrum measured with the LAr test detector.
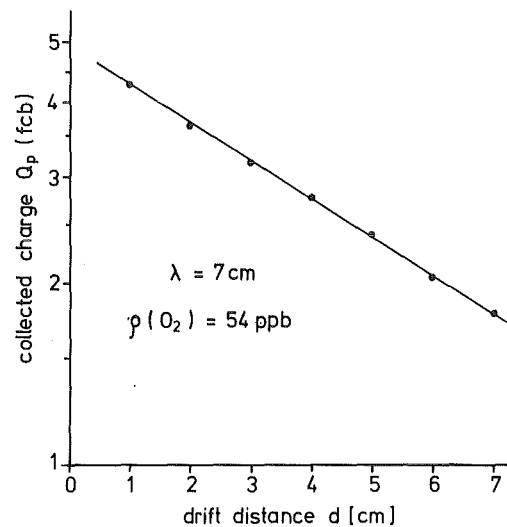
Fig. 3 Collected charge versus drift distance.

4. INTERMEDIATE ENERGY PHYSICS

4.1 PION-NUCLEUS INTERACTIONS

4.1.1 LARGE ANGLE πd SCATTERING IN THE REGION OF THE (3,3) RESONANCE

C.R. Ottermann, E.T. Boschitz, W. Gyles, W. List, R. Tacik,

R.R. Johnson[+], G.R. Smith[+], and E.L. Mathie[++]

The interaction of pions with deuterons has been of interest for many years
because of its fundamental importance for the understanding of pion interactions

Fig. 1

Comparison of the πp data from this
experiment (full squares) with the
results from ref. 2 (open circles)
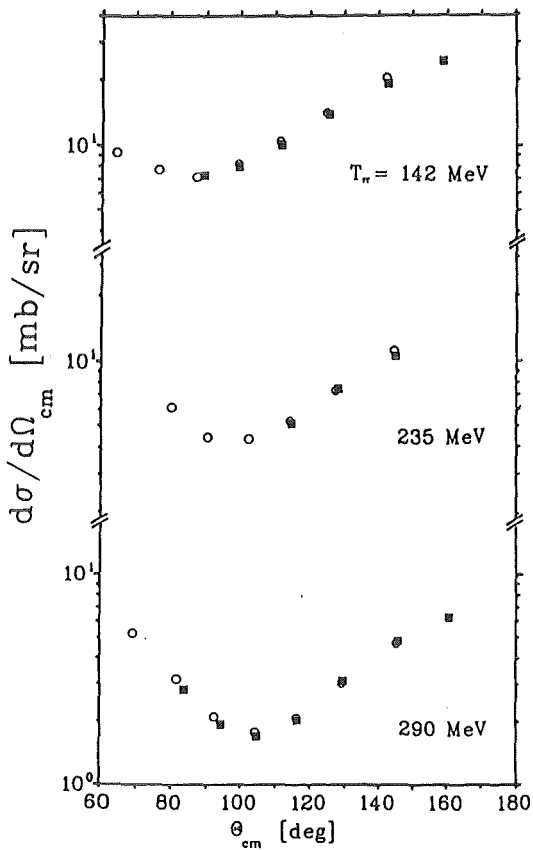
Fig. 2

The differential cross section for
πd elastic scattering in the region
of the (3,3) resonance. The data
are from Gabathuler et al. [1]
(open cirlces) and the present
experiment (solid squares). The
dashed curves are predictions
by Garcilazo.
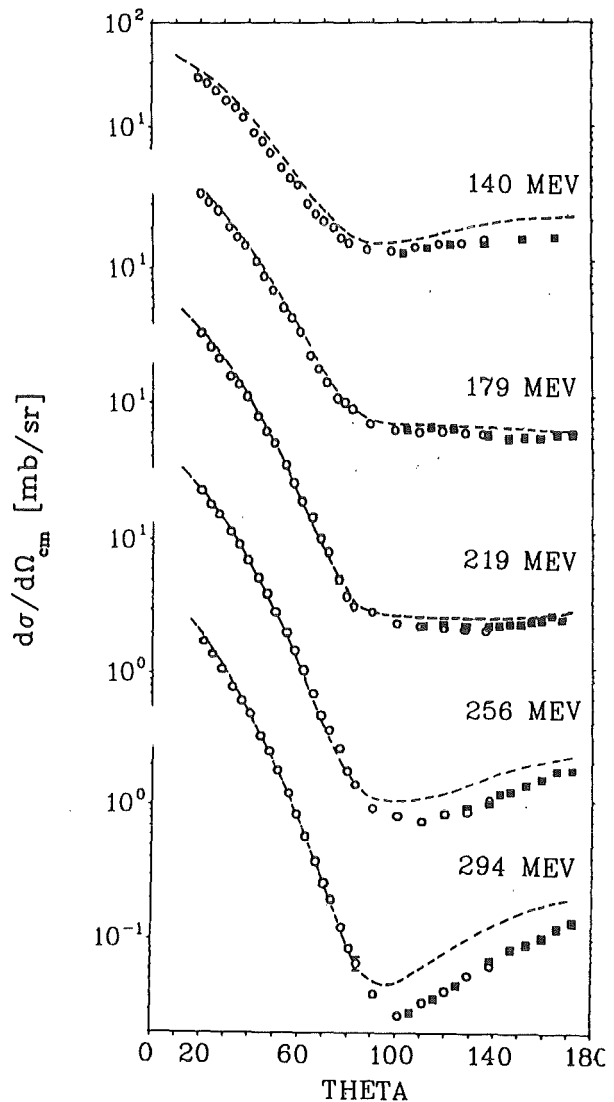
with complex nuclei. Among all possible reactions the πd elastic channel is by far the best studied case theoretically.

In comparison to the wealth of theoretical calculations the body of experimental data in πd elastic scattering is still rather limited. Precise data on the differential cross section for example exist only up to 130° in the region of the (3,3) resonance (1). For this reason we have measured the differential cross sections between 73° and 172° at 11 energies between 124 and 324 MeV. The data were obtained by measuring the pions and recoil deuterons in the elastic scattering reaction in coincidence with a multi-counter time-of-flight arrangement. πp differential cross sections were also measured at several energies with the same experimental apparatus and compared with the most reliable πp data in literature (2). This provided a check of the reliability and absolute normalization of the πd data. The πp data are shown in Fig. 1. The open circles are the results obtained by Bussey et al. (2), the solid squares are our results. The excellent agreement demonstrates that the various corrections (multiple scattering, solid angle, pion decay etc.) which had to be applied in the data reduction were properly done. In Fig. 2 we show a small sample of our large angle πd data (solid squares) together with the earlier data from Gabathuler et al. (1). Again very good agreement is observed in the region of angular overlap. As an example of one of the sohpisticated theoretical calculations the predictions of Garcilazo are shown (dashed lines). Very good agreement between theory and experiment exists near the (3.3) resonance. At lower and higher energies there are discrepancies in the large angle region the nature of which is not yet understood.

(1)   K. Gabathuler et al., Nucl. Phys. A350(1980)253
(2)   P.B. Bussey et al., Nucl. Phys. B58(1973)363

+   TRIUMF, University of British Columbia, Vancouver, B.C., Canada
++   University of Regina, Regina, Saskatchewan, Canada

4.1.2   INVESTIGATION OF THE π^+d $\rightarrow$ π^+pn REACTION AS A TEST OF RELATIVISTIC
        FADDEEV THEORIES: THE DIFFERENTIAL CROSS SECTION
        W. Gyles, E.T. Boschitz, H. Garcilazo[+], W. List, E.L. Mathie,
        C.R. Ottermann, G.R. Smith, R. Tacik, and R.R. Johnson

The systematic experimental investigation of the πNN system is of foremost importance because it is a 3-body system where one can hope to obtain reliable theoretical predictions. In this system the following reaction channels are coupled together:

$$NN \rightarrow NN \longleftrightarrow \pi d \longleftrightarrow \pi d$$
$$\qquad \downarrow_{\pi NN} \uparrow$$
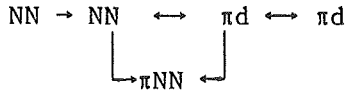
There is rather little experimental information on the reaction channels leading to the three body final state πNN. After having measured differential cross section and vector analyzing power for the $\pi d \rightarrow \pi d$ and the $\pi d \rightarrow 2p$ reaction we have started an experimental program to investigate the behaviour of these observables for the πd breakup reaction.

Utilizing the same experimental set-up as described in the last Annual Report (1) we have detected pions and protons, and measured in a kinematically complete experiment the three fold differential cross section $d^3\sigma/d\Omega_\pi \, d\Omega_p \, dP_p$ for 36 angle pairs at 225 MeV and 294 MeV incident pion energy. The data are
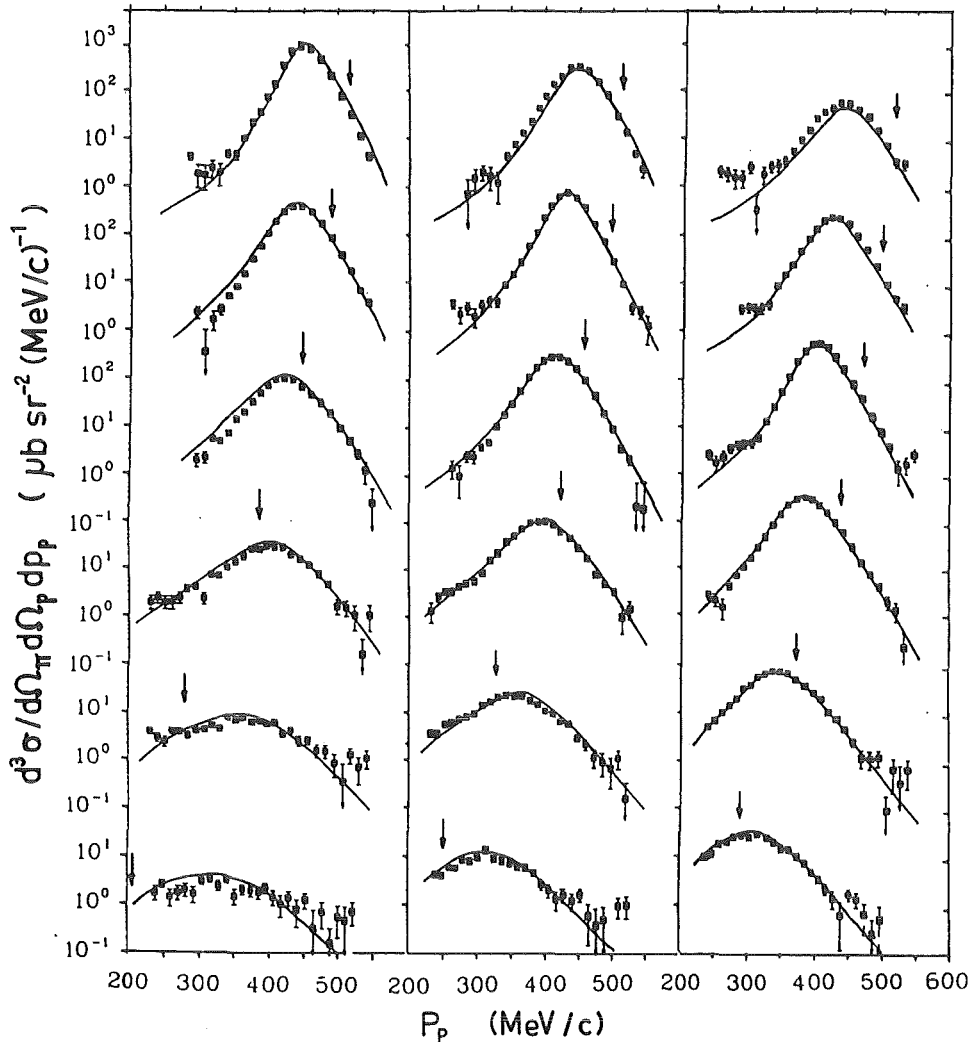
Fig. 1 Comparison of the present data at T_π = 228 MeV with the calculations described in the text. The pion angles are, from top to bottom, 106.5, 95,5, 85,0, 75.0, 61.6 and 50.0 degrees. The proton angles are from left to right - 27.9, -32.8 and -37.8 degrees. The positions where the πp invariant mass is equal to the Δ^{++} mass are indicated by arrows.

compared with predictions from a relativistic Faddeev calculations (2). Excellent agreement is found over most of the phase space, the magnitude of the cross section varying by almost four orders of magnitude. From this good agreement between theory and experiment there appears to be no need for the inclusion of non-conventional dynamics, such as the excitation of dibaryon resonances. In Fig. 1 about one quarter of the data are displayed.

(1)   Kfk 3815(1984)87
(2)   H. Garcilazo, Phys. Rev. Lett. 48(1982)577

+   On leave from the Escuela Superior de Física, Matemáticas, Instituto Politecnico Nacional, México 14, D.F., Mexico
++   TRIUMF/University of British Columbia, Vancouver, B.C., Canada

4.1.3   INVESTIGATION OF THE $\pi^+d \rightarrow \pi^+pn$ REACTION AS A TEST OF RELATIVISTIC FADDEEV THEORIES: THE VECTOR ANALYZING POWER

W. Gyles, E.T. Boschitz, H. Garcilazo, E.L. Mathie, C.R. Ottermann, G.R. Smith, S. Mango, J.A. Konter, and R.R. Johnson

In order to put the πd-break up reaction to a more stringent theoretical test we have measured for the first time the vector analyzing power iT_{11} for this reaction. In a kinematically complete experiment the threefold differential cross section $d^3\sigma/d\Omega_\pi \, d\Omega_p \, dP_p$ was measured for the two polarization states P^+ and P^- of a polarized deuteron target and iT_{11} was calculated from:

$$iT_{11} \quad \frac{1}{\sqrt{3}} \quad \frac{\sigma^+ - \sigma^-}{\sigma^+P^- + \sigma^-P^+ - \sigma^B(P^+ + P^-)}$$

where σ^+ and σ^- are the differential cross sections for the polarization P^+ and P^- in opposite directions (perpendicular to the scattering plane) and σ^B is the cross section measured with the background target. To simulate the background originating from the carbon and oxygen nuclei in the polarized C_4D_9OD target an appropriate sandwhich target made of dry ice (CO_2) and carbon was prepared. A particular problem in the data analysis arose from the fact that a 2,5 Tesla magnetic field surrounded the polarized target. This acted as a momentum analyser which distorts the pion and proton trajectories. For a particular counter, therefore, the scattering angle depends on the momentum of the detected particle. The trajectories and the time-of-flight of the particles were calculated with a ray tracing program.

In this experiment the momentum dependence of iT_{11} was obtained for 35 pion-proton angle pairs at pion bombarding energies of 180 MeV, 228 MeV and 294 MeV. The wealth of data is compared with predictions from a Faddeev
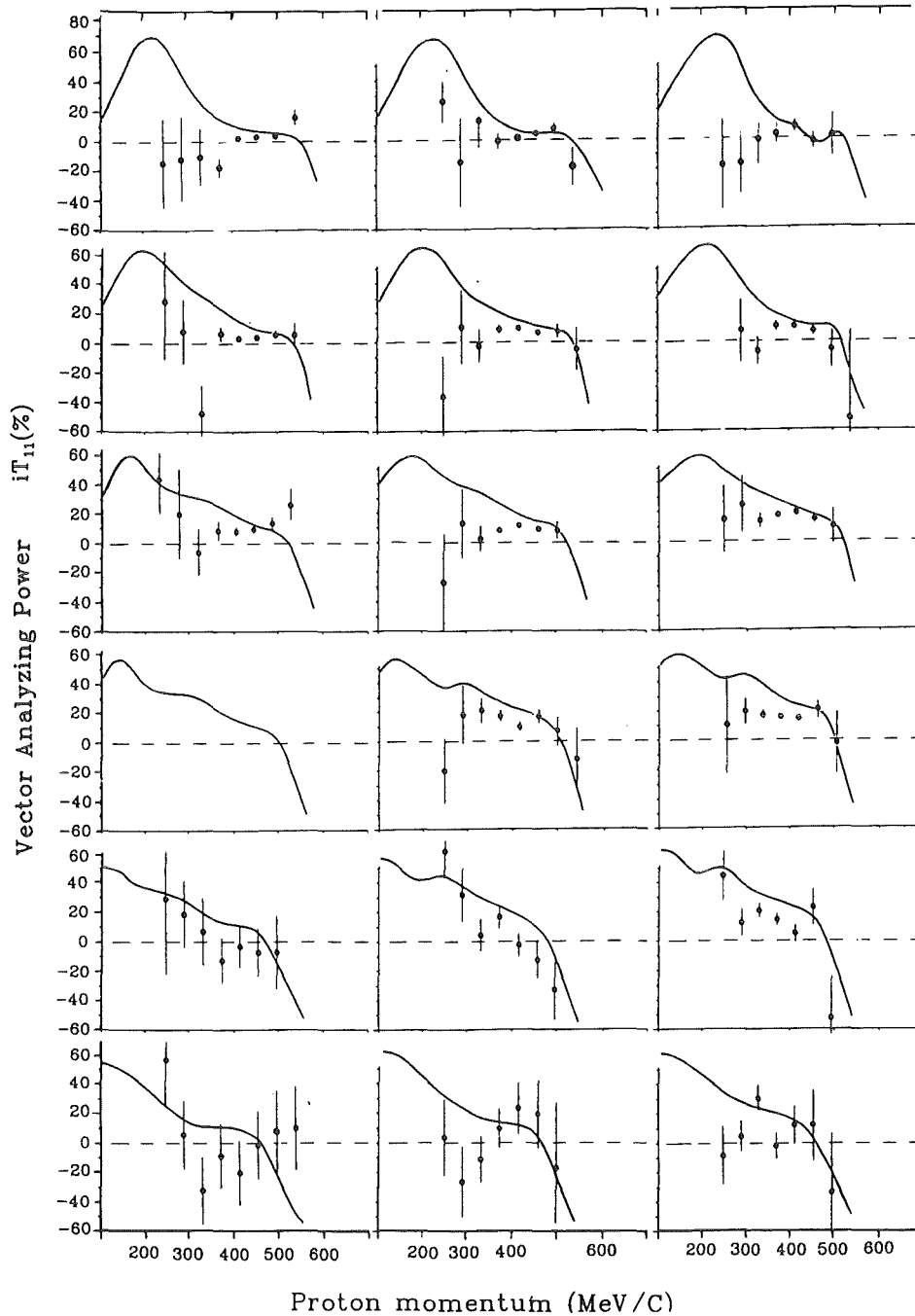
Fig. 1 Values of iT_{11} vs. proton momentum for vaious pion-proton angle pairs at incident pion energy of 228 MeV. The solid lines are the results of Faddeev calculations of reference (1). The pion scattering angles are (from top to bottom) 107, 96, 85, 74, 61 and 50 degrees. The proton scattering angles are (from left to right) -28, -33, and -38 degrees.

calculation of Garcilazo (1). The trend of the data is clearly reproduced, as can be seen in Fig. 1 where only one sixth of all data is displayed.

(1)   H. Garcilazo, Phys. Rev. Lett 48(1982)577

+   TRIUMF, University of British Colombia, Vancouver, Canada

4.1.4 EVIDENCE FOR A DIRECT THREE NUCLEON ABSORPTION PROCESS

S. Cierjacks, S. Ljungfelt, U. Mankin, H. Ullrich, G. Backenstoss[+],
M. Izycki[+], M. Steinacher[+], P. Weber[+], H.J. Weyer[+], M. Furić, and
T. Petković[++]

A new absorption mechanism has been observed in ^{3}He for positive as well as for negative pions of 220 MeV/c. The mechanism shows no structure throughout the available phase space and its measured density distributions follow the phase space factor. This behaviour is in contrast to the so far known mechanisms, the quasifree absorption on a nucleon pair and the absorption in the region of the classical final state interaction.

In the experiment pp- and pn-pairs were measured in a kinematically complete way, thus providing one constraint for the three-body final state. The main parts of the apparatus containing a liquid ^{3}He target, a large TOF-counter and a total absorbing plastic scintillator hodoscope preceded by two MWP-chambers has been described elsewhere (1). Most experimental information about the new process comes from phase space regions far away from the quasifree 2N-domain i.e. far away from the quasi-deuteron angle. Since there the differential cross sections are relatively small considerable effort was devoted to eliminate background events from the target support. The information from the chambers was used to trace back the events and perform target cuts. In addition the kinematical constraint was used for further background reduction as demonstrated in Fig. 1. The figure shows the mass distribution of the target nucleus as reconstructed event by event for a set-up far away from the quasi-deuteron angle. The expected peak at the ^{3}He mass is superimposed on a flat background which could - by empty target measurements - be mainly attributed to the aluminum windows of the target cell. Only the area of the Gaussian which fits the ^{3}He peak was taken to determine the number of good events.
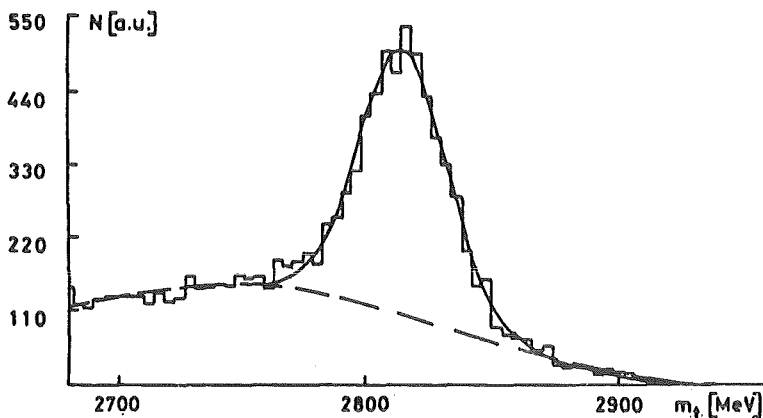
Fig. 1 Reconstructed mass distribution of the target nucleus for a measurement far outside the quasi-deuteron angle.
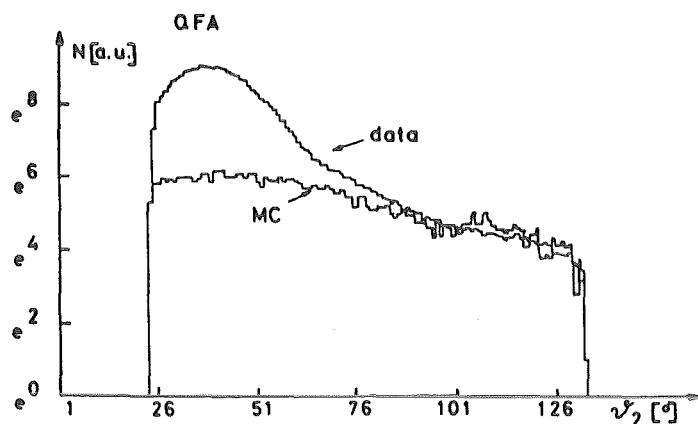
Fig. 2 Angular correlation of pp-pairs following $\pi^{\pm}$ absorption in ^{3}He. The upper curve shows the lab. angle distribution of proton 2 relative to the beam direction while the counter for proton 1 was kept at $117°$. The lower curve shows a Monte Carlo simulation of the 3N-phase space density normalized at large angles.

Fig. 2 shows an angular correlation of two detected nucleons. The pronounced peak at the quasi-deuteron angle originates from the quasifree 2N-absorption. Its shape can be well understood by the Feri motion of the absorbing pair. Accordingly the cross section for this process should vanish at angles far away from the maximum. Instead, the measured distribution levels off at a nearly constant value about two orders of magnitude below the peak value. Also shown in Fig. 2 is a Monte Carlo simulation of the 3N-process assuming a constant matrix element. At large angles the simulation fits well the shape of the measured distribution, assuming a certain value of the matrix element. Similar measurements were performed at various other counter positions covering a considerably part of the total phase space. Comparisons with complete Monte Carlo simulations lead to the conclusion that the matrix element is constant corresponding to an integrated cross section of (3.4 ± 0.5) mb and (2.8 ± 0.5) mb for positive and negative pions respectively.

Comparing this number with integrated cross sections for 2N-absorption we find that the 3N-cross section is about 20% of the 2N-cross section for isospin $I = 0$ pairs and about three times that for $I = 1$ pairs. Hence the new process forms an important part of the total cross section and cannot be neglected.

(1)   S. Ljungfelt, Dissertation, Universität Karlsruhe, 1984 and KfK report 3792 (1985)

+   Institut für Physik, Universität Basel
++   Faculty of Science, University of Zagreb

4.1.5 ANGULAR DISTRIBUTIONS OF NUCLEON PAIRS EMITTED AFTER PION ABSORPTION IN ^{3}He

S. Cierjacks, S. Ljungfelt, H. Ullrich, G. Backenstoss[++], M. Izycki[+],

P. Salvisberg[+], M. Steinacher[+], P. Weber[+], H.J. Weyer[+], M. Furić[++],

T. Petković[++], and N. Simicević[++]

The isospin dependence of the quasifree pion absorption on nucleon pairs (QFA) is still not yet well undestood. Best experimental information about this effect can be obtained with ^{3}He. There the suppression of the absorption on isospin I = 1 pairs has been observed in the ratio $r(\pi^-,nn)/r(\pi^-,pn)$ for stopped pions (1). For absorption in flight this suppression was found to be even stronger (2,3) but the measured ration $\sigma(\pi^+,pp)/\sigma(\pi^-,pn)$ showed indications to depend on the CM-emission angle of the nucleons relative to the beam direction (2,3). Such an angular dependence could be caused by asymmetries around 90° in angular distributions, which in turn would be the result of interference effects. For further investigations measurements on the angular distributions of both isospin channels seemed to be interesting.

The measurements were performed with positive and negative pions of 220 MeV/c momentum. NN-pairs were detected in coincidence with an already existing apparatus (3,4). Since the pairs were measured in a kinematically complete way the QFA events could be well separated from those with final state interactions. Due to the large counter dimensions only small corrections had to be applied in order to take into account limitations in the acceptance of the apparatus for the strongly correlated QFA events. Measured angular distributions together with Legendre fits are shown in Figs. 1 and 2. Indeed, the I = 1 channel has a slight asymmetry with $A_1 = -(60 \pm 12)$ μb/sr. Also the other coefficients for the polynomial are given in the figures. The integrated cross sections for the quasifree pair absorption are:

$$\sigma(I = 0) = (13 \pm 2.5) \text{ mb}$$
$$\sigma(I = 1) = (1.3 \pm 0.3) \text{ mb}$$
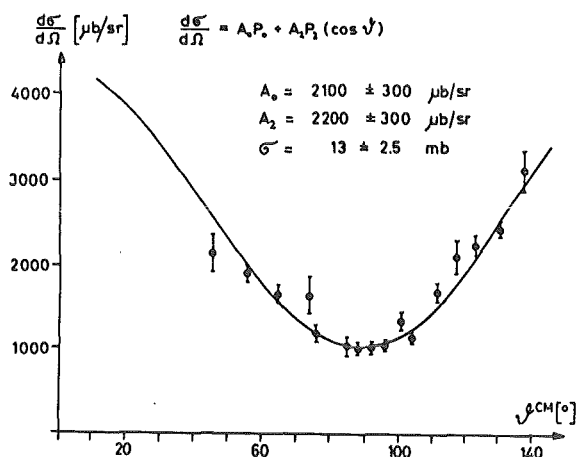
Fig. 1

Angular distribution of the reaction ^{3}He (π^+,pp) as function of the angle between one nucleon and the pion in the CM-system of the absorbing pair. The curve is a Lengendre fit with coefficients A_0 and A_2.

$\frac{d\sigma}{d\Omega} \left[\mu b/sr\right]$ $\frac{d\sigma}{d\Omega} = \sum_{i=0}^{2} A_i P_i (\cos \vartheta)$

$A_o = 100 \pm 20 \ \mu b/sr$
$A_1 = -60 \pm 15 \ \mu b/sr$
$A_2 = 145 \pm 30 \ \mu b/sr$
$\sigma = 1.3 \pm 0.3 \ mb$
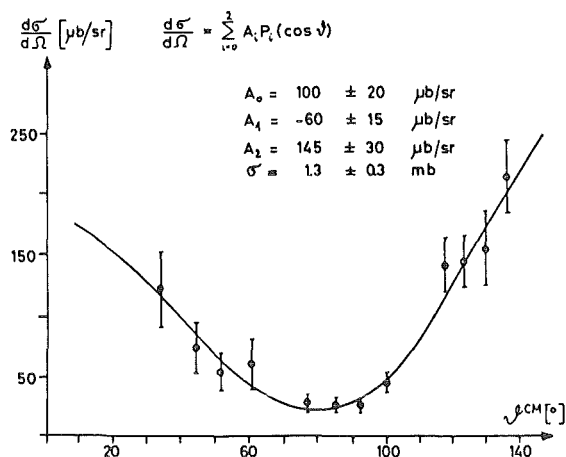
Fig. 2

Same as Fig. 1 for the reaction ^{3}He (π^-,pn). The Legendre fit has coefficients A_o, A_1, and A_2.

(1)   D. Gotta, M. Doerr, W. Fetscher, G. Schmidt, H. Ullrich, G. Backenstoss, W. Kowald, I. Schwanner, H.J. Weyer, Phys. Lett. 112B(1982)129

(2)   D. Ashery, R.J. Holt, H.E. Jackson, J.P. Schiffer, J.R. Specht, K.E. Stephenson, R.D. Mckeown, J. Ungar, R.E. Segel, P. Zupranski, Phys. Rev. Lett. 47(1981)895

(3)   G. Backenstoss, M. Izycki, M. Steinacher, P. Eber, H.J. Weyer, K.v. Weynmarn, S. Cierjacks, S. Ljungfelt, U. Mankin, T. Petković, G. Schmidt, H. Ullrich, M. Furić, Phys. Lett. 137B(1984)329

(4)   S. Ljungfelt, Dissertation, Universität Karlsruhe, 1984, and KfK report 3792(1985)

+   Institute of Physics, University of Basel
++   Faculty of Science, University of Zagreb

4.1.6   MEASUREMENT OF THREE PROTONS IN COINCIDENCE FOLLOWING ABSORPTION OF 228 MEV π^+ IN CARBON

T. Tacik, E.T. Boschitz, W. Gyles, W. List, and C.R. Ottermann

An important question which has been raised recently regarding pion absorption in nuclei is whether the main mechanism is that of absorption on a p-n pair with the quantum numbers of a deuteron present in the nucleus or whether more exotic processes such as absorption on heavier clusters or double-delta formation play
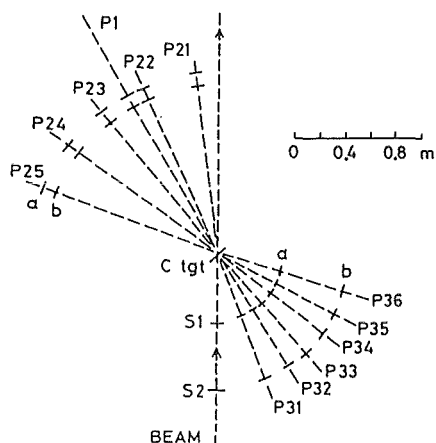
Fig. 1

Set up of the experimental apparatus

an important role. In view of the dabate on the number of nucleons involved in this process, we have measured for the first time in a counter experiment the energy and angular distributions of three protons following π^+ absorption on a nucleus. We chose ^{12}C and T_π = 228 MeV, an energy where theoretical calculations exist (1).

The experimental arrangement, as seen in Fig. 1 consisted of 12 plastic scintillator telescopes arranged in such a way that one could observe the two-

Fig. 2
Angular distribution of measured differential cross sections for fixed P1 and P3 angles. The arrows indicate the expected peak positions from the two step process. The solid curves are Gaussian fits to the data. The long-dashed and short-dashed curves represent phase space calculations assuming quasi-four-body and quasi-three-body absorption mechanisms respectively. Note that the phase space calculations do not include the effects of Fermi motion.

Fig. 3
Distribution of proton kinetic energies measured with the P3 counters. The solid and dashed curves represent phase space calculations assuming quasi-four-body and quasi-three-body absorption mechanisms respectively.
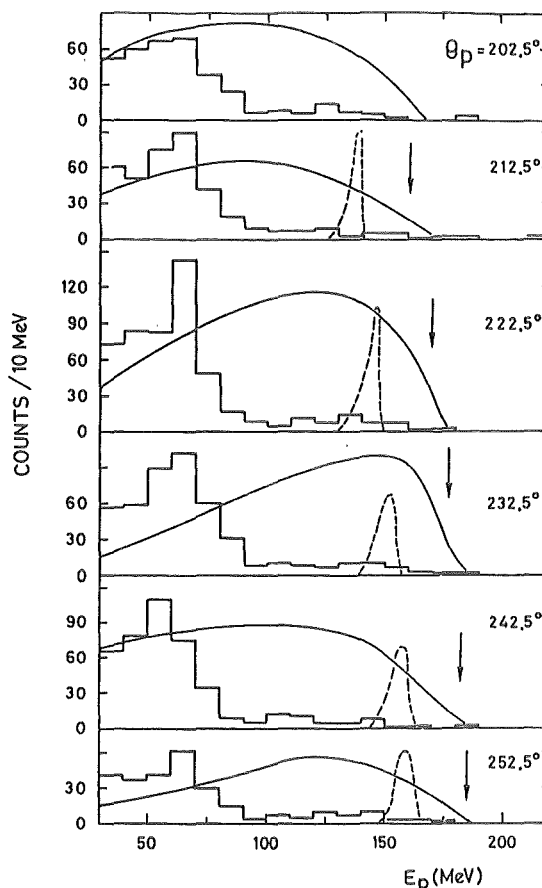
step process proposed recently (1): A positive pion impining on the nucleus knocks out a proton (P1) in the forward direction. The recoiling pion is then absorbed on a quasi-deuteron resulting in the emission of two more protons (P2 and P3). Pulse height and time of flight information were recorded for each counter, the latter being used to determine the proton energies.

From the large quantity of data obtained only one set of energy and one set of angular distributions are presented (Fig. 2 and 3). In order to interpret these data phase space calculations have been performed assuming several different models for the absorption process (quasi-three-body, quasi-four-body and quasi-many body absorption). Fermi motion has not been included in the calculation. This would broaden the distributions even more than shown in the figures.

Comparing the results from the phase space calculation with the data one can draw the following conclusions: In some cases the calculated quasi-four-body distribution are already too broad. Therefore the relatively narrow width of the measured angular distribution indicates that the absorption occurs on fewer than four nucleons. Regarding the energy distributions one notes that the distributions of the measured proton energies at backward angles are limited to smaller energies than chose predicted by any of the two step, quasi-three step or quasi-four body mechanisms. In fact, the measured energy distributions resumble most closely those from quasi-deuteron absorption on a forward going low energy ($\leq$ 40 MeV) pion. Thus the following mechanism suggest itself: The incoming pion scatters several ($\geq$ 2) times, losing its kinetic energy to several nucleons one of which we observe, before finally being absorbed on a quasi-deuteron, and producting the additional two observed protons.

(1)   K. Ohta, M. Thies, and T.-S.H. Lee, to be published in Ann. Phys.

4.1.7   COULOMB-NUCLEAR INTERFERENCE IN $\pi^{\pm}p$ SCATTERING AT 55 MeV

U. Wiedner, K. Göring, U. Klein, W. Kluge, H. Matthäy, M. Metzler, E. Pedroni[+], W. Fetscher[++], H.J. Gerber[++]

In summer 1984 angular distributions of the elastic scattering of pions on protons in the region of the Coulomb-nuclear interference have been measured (between θ_{lab} = 7.5° and 27.5°) at the πM3 channel of SIN set to 140 MeV/c (corresponding to about 55 MeV actual scattering energy in the laboratory system). During the rest of the year the data have been evaluated.

The goal of the measurement and the experimental set-up have been descri-bed in the last Report of this series (1) and in the SIN Annual Report 1984 (2). The evaluation of the data carried out so far includes a Monte-Carlo simulation of the actual solid angle of the pion detector, takes into account the Coulomb
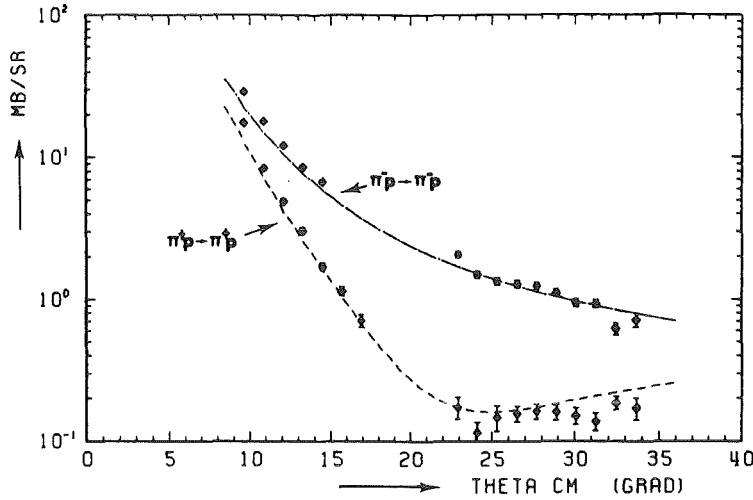
Fig. 1 Differential cross section $\frac{d\sigma}{d\Omega}$ of the elastic scattering of pions ($\pi^{\pm}$) on protons in the centre-of-mass system within the Coulomb-nuclear interference region. The lines represent calculations (predictions) using the Karlsruhe-Helsinki phases (3).

multiple scattering in the target and in the wire chambers and the pion decay in the entrance and exit channel. The still preliminary results are shown in Fig. 1, where the differential cross-sections of the elastic $\pi^{\pm}$p-scattering $\frac{d\sigma^{\pm}}{d\Omega}$ in the centre-of-mass system together with calculations using the Karlsruhe-Helsinki phases (3) are plotted. Significant deviations of the data from the Karlsruhe-Helsinki phases are observed only at the most forward angles. No data points are shown for angles between $\theta_{cm} = 17^{\circ}$ and 22° due to the heavy background of muons arising from pion decay within the Jacobian cone. In Fig. 2 the dimensionless expression [1 mb GeV^2 = 2.568]

$$ t \cdot [\frac{d\sigma^+}{d\Omega}(t) - \frac{d\sigma^-}{d\Omega}(t)] = \text{Re } D^+(t) \cdot \frac{2\alpha M^2 \omega}{\pi s} + d_1 t + d_2 t^2 + d_3 t^3 \qquad (1) $$

is displayed, which represents basically at $t = 0$ the real part of the isospin even πN amplitude Re D^+ (4). The coefficients d_1, d_2, d_3 of the polynomial in the four momentum transfer t can be expressed by bilinear combinations of the partial waves, while s is the squared total energy in the center-of-mass system, ω the pion laboratory energy, M the nucleon mass and α the fine structure constant. The amplitude D^+ at the unphysical Cheng-Dashen point $t = 2 \ m_{\pi}^2$, $\nu = \omega + \frac{t}{4M} = 0$ is closely connected with the $\sigma_{\pi N}$-term of πN scattering.

As can be seen in Fig. 2 the extrapolation of the data points $t = 0$ results in a value of about $11.0 \cdot 10^{-3}$, which is about 15% higher than the value obtained with the current Karlsruhe-Helsinki phases (given as solid curve in Fig. 2). Although the evaluation of the data has not yet been finished completely
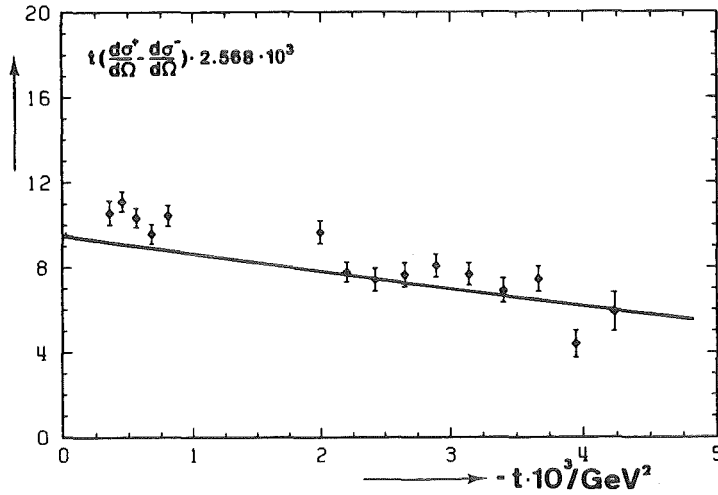
Fig. 2 The dimensionless expression $t \cdot [\frac{d\sigma^+}{d\Omega} - \frac{d\sigma^-}{d\Omega}]$ as a function of the four momentum transfer t, which represents basically at t = 0 the real part of the isospin even pion-nucleon amplitude Re D^+. The solid line has been calculated by means of the Karlsruhe-Helsinki phases (3).

it looks like that the value for the $\sigma_{\pi N}$-term tends towards the upper limit of the "experimental" value of Koch, who obtained $\sigma_{\pi N} = (60 \pm 8)$ MeV (4). Insofar the disagreement between the QCD-value of Gasser and Leutwyler of $\sigma_{\pi N} \approx 35 \pm 10$ (5) and Koch's value will increase.

(1)   U. Wiedner, K. Göring, U. Klein, W. Kluge, H. Matthäy, M. Metzler, E. Pedroni, W. Fetscher, H.J. Gerber, Annual Report on Nuclear Physics Activities edt. by. D.C. Fries, P. Matussek, Ch. Weddigen, KfK Report 3815, Oct. 1984, p. 77
(2)   W. Fetscher, H.J. Gerber, K. Göring, U. Klein, W. Kluge, H. Matthäy, M. Metzler, E. Pedroni, U. Wiedner, SIN Jahresbericht 1984, p. NL 25
(3)   R. Koch and E. Pietarinen, Nucl. Phys. A336(1980)331
(4)   R. Koch, Z. Physik C15(1982)161
(5)   J. Gasser and H. Leutwyler, Phys. Reports 87(1982)77

+   Schweizerisches Institut für Nuklearforschung
++   Institut für Mittelenergiephsik, ETH Zürich

4.2 INTERACTIONS OF ANTIPROTONS AND ANTINEUTRONS

4.2.1 ANTIPROTONIC X-RAYS IN $\bar{p}$H and $\bar{p}$D

R. Bacher, P. Blüm, D. Gotta, W. Kunold, D. Rohmann, M. Schneider, and L.M. Simons

Using the cyclotron trap (1) antiprotonic hydrogen and deuterium X-rays were measured at 60 mbar pressure. At this pressure it is expected from cascade calculations that the intensities of the radiative transitions are saturated (2).

The experiment was performed at the LEAR facility at CERN with a beam momentum of 202 MeV/c. The stray field of the supraconducting magnet was shielded by a 4,5 t iron yoke. The X-rays were measured with a 30/200 mm^2 Si(Li)-guard-ring and a 200/500 mm^2 Ge-guardring detector placed at the bore hole of the magnet. The absolute intensities of the X-ray transitions were determined by comparison to a $\bar{p}$ ^{4}He spectrum measured at 72 mbar using the results of a cascade calculation (3). From the intensities observed it was deduced that about 35% of the incoming $\bar{p}$ are stopped near the centre of the stopping chamber. One of the main problems when measuring low intensity transitions is the large background in the few keV region produced by the annihilation products. The spectrum observed in the Si(Li) guardring detector proves that the background mainly stems from the large flux of low energetic X-rays of the electro-magnetic shower produced in the vicinity of the detector. The background suppression therefore scales approximately with the geometric ratio of the inner to outer area of the detector (4). Due to the low compton cross-section in silicon for γ-rays in the 100-300 keV region compton induced events alone underestimate the background by a factor of 1000.

In fig. 1 the antiprotonic X-ray spectra of the hydrogen isotopes H/D are shown . The yields of the L-series are about 50% less than expected which means that the cascade is far from saturation even at 60 mbar (Table 1). Thus the K_α-transitions is suppressed accordingly. The measured yields can be explained by the fact that the stark mixing for the l-sublevels in the upper cascade had been underestimated by a factor 2.5. Cascade calculations based on the program of Borie and Leon (2) with a new set of stark-mixing parameters are able to explain such low yields. In this calculation the saturation of the K_α -transition is almost reached at 10 mbar gas pressure.

.In the second part of the $\bar{p}$D-measurement the 12 µm beryllium window of the Si(Li)-detector was replaced by an 8 µm polypropylen window. With this ultra-thin window the energy threshold is at about 550 eV which allows for the first
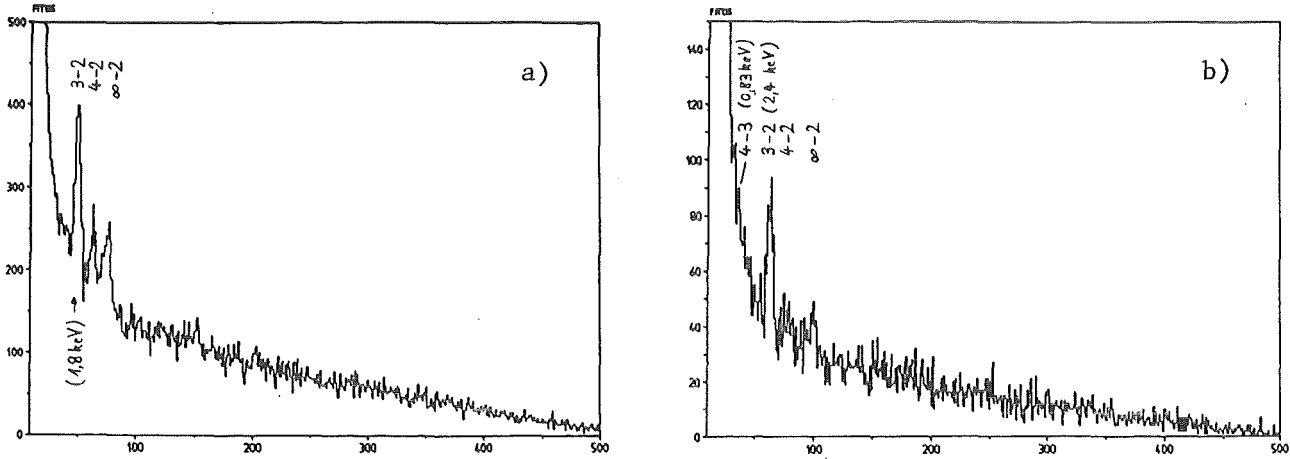
Fig. 1 Antiprotonic X-ray spectra of the hydrogen isotopes H/D at a pressure of 60 mbar measured with a Si(Li)-detector in guardring-configuration.

a)   X-ray spectrum of $\bar{p}H$ for $8.2 \cdot 10^9$ incoming $\bar{p}$. Detector window: 12 μm Beryllium

b)   X-ray spectrum of $\bar{p}D$ for $2.2 \cdot 10^9$ incoming $\bar{p}$. Detector window: 8 μm Polypropylen

time the observation of the $\bar{p}D$ 4-3 transition (Fig. 1b).

In the $\bar{p}H$ spectrum of the Ge-detector a line pattern could be identified, which corresponds to the 2 → 1, 6 → 1, 7 → 1 and ∞ → 1 transitions. The best fit gives 306 ± 142 events for the candidate of the K_α-transition. The shift of the electro-magnetic pattern is $\Delta E = -(700 \pm 150)eV$ and the width is consistent with 1 keV. Due to the poor statistics and the large background these results are regarded up to now as an upper limit (table 1). For this reason a measurement at 10 mbar gas pressure is planned using the 100 MeV/c beam at LEAR. The yields will then increase by a factor 2. No corresponding el-mag pattern could be found in the $\bar{p}D$-spectrum.

Table 1 Predicted and measured antiprotonic X-ray yields in $\bar{p}H$ and $\bar{p}D$
at 60 mbar pressure

	$\bar{p}H$		$\bar{p}D$	
	Prediction	Experiment	Prediction	Experiment
YL_α	0,43	0,180±0,023	0,48	0,177±0,022
YL_β	0,06	0,071±0,013	0,06	0,044±0,009
YL_{tot}	0,55	0,359±0,037	0,59	0,290±0,021
YK_α	$5,2 \times 10^{-3}$	$\leq(2,4\pm1,1)\cdot10^{-3}$	$1,5\cdot10^{-3}$	-
YK_{tot}	$10,6 \times 10^{-3}$	$\leq(7,0\pm1,7)\cdot10^{-3}$	$2,2\cdot10^{-3}$	-

(1)   P. Blüm, D. Gotta, R. Guigas, H. Koch, W. Kunold, M. Schneider, and
       L.M. Simons, CERN proposal PS175(1980)
(2)   E. Borie, M. Leon, Phys. Rev. A21(1980)1460
(3)   R. Landua, private communication
(4)   Annual Report on Nuclear Activities 1983/84, KfK 3815 (1984)148 and
       contribution 4.2.2 to this Annual Report

4.2.2   ANTIPROTONIC X-RAY IN $\bar{p}\,{}^3\mathrm{He}$ and $\bar{p}\,{}^4\mathrm{He}$

R. Bacher, P. Blüm, D. Gotta, W. Kunold, D. Rohmann, M. Schneider,

and L.M. Simons

The aim of our experimental work at the LEAR facility at CERN is to study strong interaction effects in antiprotonic atoms. Using the cyclotron trap (1-3) measurements in very low presssure gaseous targets become possible. Low pressure reduces the Stark effect, yielding higher intensities of the X-ray transitions. During the last experimental period in spring 1985 we stopped $\bar{p}$'s with 202 MeV/c momentum in helium gas of 72 mbar. The X-rays were detected with semiconductor detectors placed at the bore holes of the magnet. We used both a Ge- and a Si(Li)-detector (see Tab. 1) in guardring configuration, i.e. the inner part of the crystal is surrounded by an outer detector ring. Thus one achieved a better peak-to-background ratio by a good reduction of the background, which is mainly caused by the low-energy part of the electromagnetic shower produced from the annihilation products in the surrounding materials. Such a shower leads to an energy deposit not only in the inner part of the detector but also in the guardring, which allows to veto these signals.

The spectra aquired with the Si(Li)-guardring detector are shown in Fig. 1. The measuring time was 3 spills (about 3 h) with $15.44 \cdot 10^8$ incoming $\bar{p}$'s in $^3\mathrm{He}$ and 2 spills with $14.28 \cdot 10^8$ incoming $\bar{p}$'s in $^4\mathrm{He}$. Comparing these spectra with the first $\bar{p}\,{}^4\mathrm{He}$ measurement of our group in December 1983 (3) with a standard Si(Li)-

Table 1 Properties of the guardring-semiconductor detectors

detector	inner/outer area (mm^2)	thickness (mm)	resolution at 5.9 keV (eV)	Be-window thickness (μm)
Si(Li)	30/200	5	200	12
Ge	200/500	10	250	130
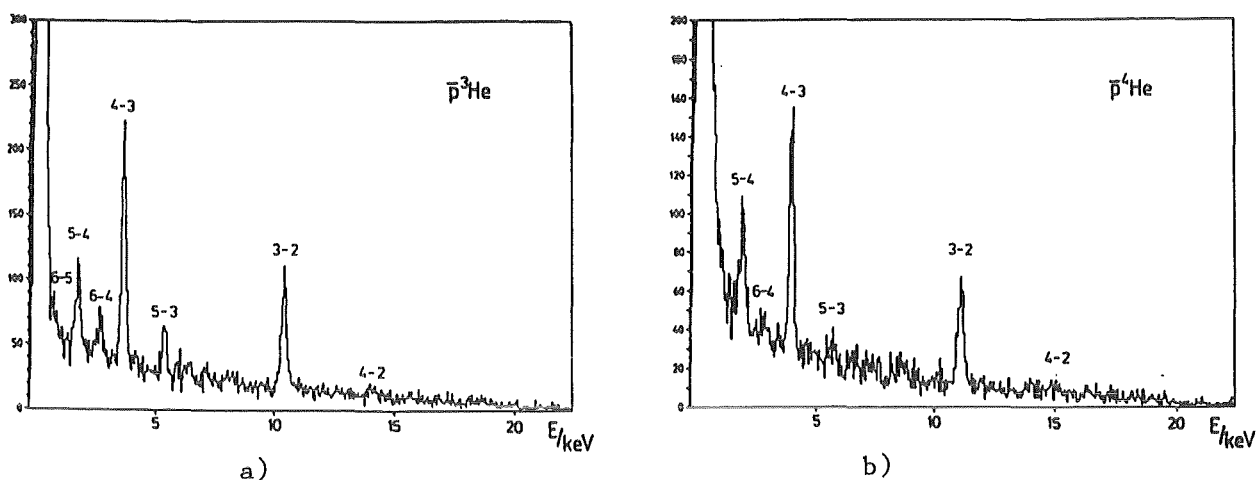
Fig. 1 Antiprotonic X-ray spectra of the helium isotopes ^{3}He/^{4}He at a pressure of 72 mbar

a) $\bar{p}$ ^{3}He for $1.5 \cdot 10^9$ incoming $\bar{p}$

b) $\bar{p}$ ^{4}He for $1.4 \cdot 10^9$ incoming $\bar{p}$

detector (effective area 20 mm^2, resolution 160 eV at 5.9 keV) the peak-to-background ratio is improved by a factor of about 5. In addition, there are no visible contamination lines. This indicates that no $\bar{p}$'s have stopped in the walls of the target chamber. Due to the low gas pressure and the 12 μm Be-window X-rays down to 1 keV could be measured.

From these spectra, the ratio of annihilation to X-ray emission from the 3d level was determined to be $\Gamma_{ann}/\Gamma_{rad} = 2.7 \pm 0.3$ for ^{4}He and 3.2 ± 0.6 for ^{3}He.

The inner transitions in ^{3}He are pronounced compared to ^{4}He: The ratio M_β/M_α is 0.29 ± 0.09 for ^{3}He and 0.14 ± 0.04 for ^{4}He. This may be expected from the lower mass of the $\bar{p}$ ^{3}He atom and the smaller binding energies both increasing the Stark effect.

(1) P. Blüm, D. Gotta, R. Guigas, H. Koch, W. Kunold, M. Schneider, L.M. Simons; Proposal PS175 CERN/PSCC/S27 (1980)
(2) Annual Report on Nuclear Activities 1982/83; KfK 3621(1983)165
(3) Annual Report on Nuclear Activities 1983/84; KfK 3815(1984)148

4.2.3 RESULTS FROM ANTIPROTONIC ATOM STUDIES AT LEAR

G. Büche, A.D. Hancock, H. Koch, Th. Köhler, A. Kreissl, H. Poth, U. Raich, D. Rohmann, Ch. Findeisen[+], L. Tauscher[+], A. Nilsson[++], S. Carius[++], M. Suffert[+++], S. Charalambus[++++], M. Chardalas[++++], S. Dedoussis[++++]

The study of antiprotonic atoms at LEAR was continued in 1984/85 and the evaluation of the previously accumulated data was persued. The Basel-Karlsruhe-Stockholm-Strabourg-Thessaloniki collaboration received further beam for

experiment PS176 in May 1985 after the success of the initial measurements in 1983 and 1984. As before the experiment was performed in close coopoeration with a group of the Technical University of Munich and a group of University, Missisippi, USA. The experimental set-up and related physics were described earlier (1) and the first results were presented in the previous annual report (2) and in Ref. 3 and Ref. 4.

The first measurements concerning strong interaction effects aimed mainly at the study of hadronic shifts and widths in light antiprotonic atoms around oxygen, to establish a universal $\bar{p}A$ potential followed by an investigation of details of the $\bar{p}A$ and $\bar{N}N$ force. These studies of particular aspects were mainly concentrated on the measurement of isotope effects caused by strong interaction (in the stable oxygen isotopes) and the search for spin-orbit dependences of the $\bar{N}N$ interaction (in Ba-138). Furthermore a high precision measurement of the antiproton magnetic moment and a feasibility study concerning the accurate determination of an X-ray energy for settling the question of long range QCD effects were performed. The first measurements were complimented by an invest-igation of the antiproton absorption through residual nuclei spectroscopy and a search for high energy gamma rays indicating a possible $\bar{p}A$ state bound essen-tially by the strong force. As a byproduct a lot of information concerning the antiproton atomic cascade was sampled.

The primary results from the first beam time - still in analyzing stage - can tentatively summarized as follows:

The hadronic widths and shifts in light nuclei were measured with an un-precedented precision in the range between nitrogen and sodium. For these nuclei the strong interaction in the 3d and 4f level shows up as an intensitiy reduction a broadening and an energy shift of the 4-3 transition. The increase of these effects with increasing nuclear mass is very well seen in Fig. 1. The 4-3 line is sandwiched between two transitions (8-4, 9-4) not affected by strong inter-action. This fortunate situation provides an excellent means of calibration and allows for precision measurement. The ordinate in Fig. 1 scaled for the targets in such a way that the positions of the unperturbed lines fall on top of each other. In this representation the strong interaction effects in the 4-3 line are clearly seen increasing from nitrogen to sodium. In nitrogen the shift is invisible. The relative intensities of the 8-4 and the 9-4 line may differ from target to target, depending on the atomic cascade.

Large isotope effects in the stable oxygen isotopes were observed. Their magnitude is surprising, they amount up to 50% in the average shift and 26% in the average width of the 3d level for the isotope pair O-16/18. The values for O-17 lies in between. They are being analyzed in terms of an optical model in order to extract information about the $\bar{p}n$ interaction and the ratio of the real
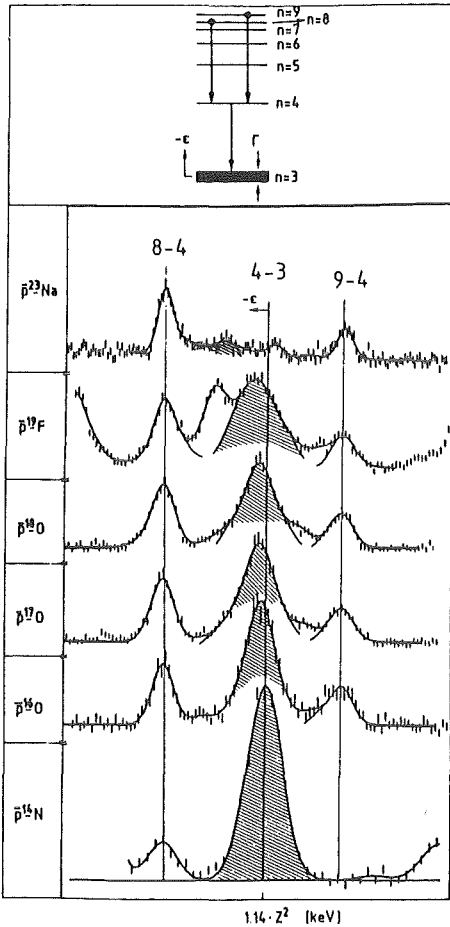
Fig. 1

Part of the X-ray spectrum of light antiprotonic atoms showing the unperturbed $8 \to 4$ and $9 \to 4$ lines and the $4 \to 3$ transition shifted in energy, broadened and attenuated. The ordinate is scaled for the different targets, so that the energy difference between the $8 \to 4$ and $9 \to 4$ is equal in all cases.

to imaginary part of the $\bar{p}n$ forward scattering amplitude at low energies.

A first search for spin-orbit dependences in the $\bar{p}A$ interaction was attempted in an experiment on $\bar{p}Ba$-138 through the measurement of hadronic shifts and widths in separated fine structure components. The fine struchture levels of the n = 8 level could just be resolved, however, the accumulated statistics were too low in order to establish a significant effect, although the analysis indicates slight differences.

The magnetic moment of the antiproton was remeasured by extracting the fine structure splitting in the 11-10 and the 10-9 transition (unaffected by strong interaction) in $\bar{p}Pb$-208. In Fig. 2 the relevant X-ray transitions are shown. One clearly observes the two most intensive components resolved, which are separated by 2.1 (1.2) keV for the 10-9 (11-10) transition. With the present statistics we will be able to determine the magnetic moment with a precision of the order of 3×10^{-3}, i.e. a factor of 2 better than the actual world average.

The feasibility study to measure the energy of a particular X-ray transition with very high accuracy by using the critical absorber technique was successfully performed. After a careful scan of calculated $\bar{p}$ X-ray energies and a comparison with absorption edge energies, we found a promising candidate in Ge-70 (9-8 transition) and the K_β edge of Hg. In our test measurement on Ge-70

PS176 AT LEAR   331 MIO ANTIPROTONS

X-ray spectrum from antiprotonic (^{208}Pb)
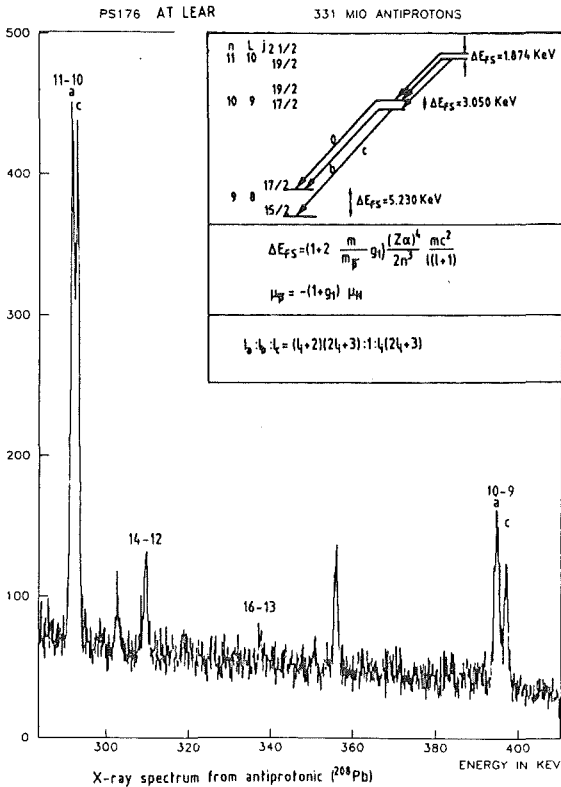
Part of the $\bar{p}$-Pb spectra showing the X-ray transition used to determine the magnetic moment of the antiproton.
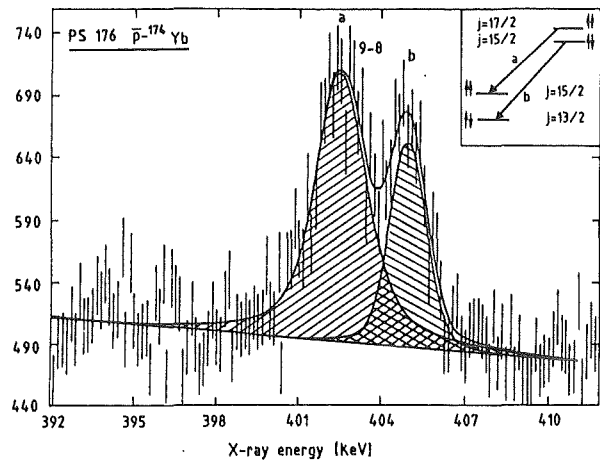
Fig 3 →

Part of the $\bar{p}$-Yb spectra showing the strong interaction effects in resolved fine-structure levels.

we verified this energy degeneracy and observed a very clear effect. With this method we hope to arrive at an absolute energy determination with an error below 1 eV. The purpose of this measurement is manifold. On the one hand it could serve as an energy standard for determining the $\bar{p}$ mass with high precision; on the other hand, other effects which could alter the $\bar{p}$ X-ray energies, such as nuclear and $\bar{p}$ polarizibility or long range contributions of the $\bar{N}N$-force, could be traced out.

Antiproton absorption was studied in three different ways. Firstly a spectroscopy of gammas emitted from excited residual nuclei left over after $\bar{p}$ absorption was performed; secondly; the spectrum of the emitted neutrons was measured; and thirdly, high-energy gammas in the range between a few tens of MeV and 1 GeV were detected. Already at the present stage of evaluation one can state the observed $\bar{p}$ annihilation in light nuclei on a single nucleon with an intact residual nucleus left over in an excited state is unexpectedly frequent. The measured neutron spectra in the range between 1 MeV and 100 MeV showed essen-tially three regions: evaporation neutrons corresponding to a temperature of about 7 MeV; faster neutrons with temperatures around 45 MeV; and a few very fast neutrons. The high-energy gamma spectrum shows no obvious evidence for

possible $\bar{p}$-nucleon or $\bar{p}$-nucleus bound states.

In the continuation of the experimental programme of PS176 during 1985 another series of measurement were performed mainly aiming at further study of isotope effects (in Yb-174) and the achievement of an even higher accuracy for the determination of the antiproton magnetic moment (Th-232). In lithium and nickel a pronounced isotope effect was again seen and for the first time a significant difference in the strong interaction quantities in different fine structure levels of the n = 8 states of Yb-174 were observed (Fig. 3) indicating a L-S dependence of the $\bar{N}N$-force.

(1)   H. Poth, Physics of antiprotonic atoms, Proc. 2nd LEAR Workshop on Physics with Low-Energy Cooled Antiprotons, Erice, 1982, eds. U. Gastaldi and R. Klapisch (Plenum Press, Inc., New York, 1981) p. 567
(2)   Annual report 1983/84, p. 93
(3)   H. Koch et al., Proc. VII. Eur. Symp. Antiproton Interactions, Durham 1984 Inst. Phys. Conf. Ser. 73: Section 3
(4)   H. Poth et al., Proc. 3rd LEAR Workshop on Physics in the ACOL Era with Low-Energy Cooled Antiprotons, Tignes, 1985

+   Institute for Physics, University of Basel, Klingelbergstr. 84, Basel, Switzerland
++   Research Institut for Physics, Stockholm, Sweden
+++   Centre de Recherches Nucléaires and Université Louis Pasteur, Strasbourg, France
++++   Department of Nuclear Physics, University of Thessaloniki, Greece

4.2.4 CRITICAL ABSORPTION OF ANTIPROTONIC X-RAYS

B. Jödicke, G. Zach, G. Büche, H. Koch

Aiming at a precise energy determination the spectroscopy of antiprotonic X-rays can profit from an application of the method of critical absorption. Therefore we continued to study the cases where the energy of an antiprotonic X-ray transition coincides with the energy of an atomic K-edge. The use of an improved computer programme for calculations of electromagnetic transition energies and the discussion of the shape of atomic K-edges enabled us to work out a final list of candidates. Atoms covering the whole series of stable nuclear isotopes were scanned. The most promising candidates were discussed in detail in Ref. 1. With respect to a measurement cases were taken into account where (i) the pure electromagnetic transition energies taken from a calculation can be tested against the experimental value, (ii) properties of nuclear matter like nuclear polarisability or the existence of strong interaction potentials with long range could be tested; and (iii), with progressing experience, the existence of a non-vanishing mass-difference $m_{\bar{p}} - m_p$ and its consequence for the CPT-theorem could be checked.
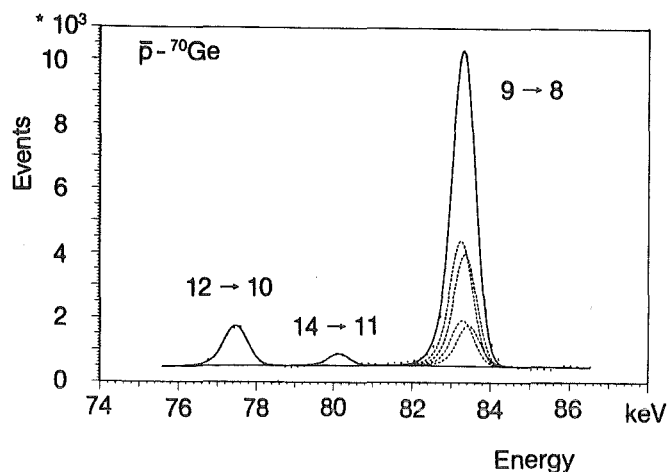
Fig. 1

Part of the antiprotonic ^{70}Ge X-ray spectrum

Presently the X-ray transition $n_i = 9 \rightarrow n_f = 8$ of the $\bar{p}^{70}$Ge atom is being investigated experimentally using the K-edge of natural Hg. Fig. 1 shows part of the photon spectrum that was measured from $6,5 \cdot 10^7$ antiprotons received from the LEAR facility. Three separated lines appear on a flat background. The prominent line can be interpreted in terms of a sum of at least four line structure transitions, e.g. $n_i = 9$; $j_i = 17/2 \rightarrow n_f = 8$; $j_f = 15/2$ at 83.068 keV etc. Two more lines correspond to the multiplets of the antiprotonic transitions $12 \rightarrow 10$ and $14 \rightarrow 11$. Fig. 2 shows the same spectrum filtered by 0.35 g $\cdot$cm^{-2} Hg. The intensity reduction of the $9 \rightarrow 8$ transition by the action of the critical absorber is clearly revealed from a comparison to the intensity of the $12 \rightarrow 10$ line whose energy is well below the K-edge. Contributions from the electronic X-ray transitions $K_{\beta 1}$, $K_{\beta 2}$, and $K_{\beta 3}$ modify the intensities and shapes of the 2 lines on the upper half of the energy scale. The shape of the background is at least partly governed from the energy dependent action of the critical absorber. The further evaluation of the $9 \rightarrow 8$ line with respect to a precise energy determination of the fine structure components depends essentially from an exact knowledge of the absorption coefficient $\mu(E)$ in function of the photon energy. A precision measurement of μ over the energy region of the components is presently being prepared which uses the synchrotron radiation from DESY at Hamburg in connection with a monochromator.
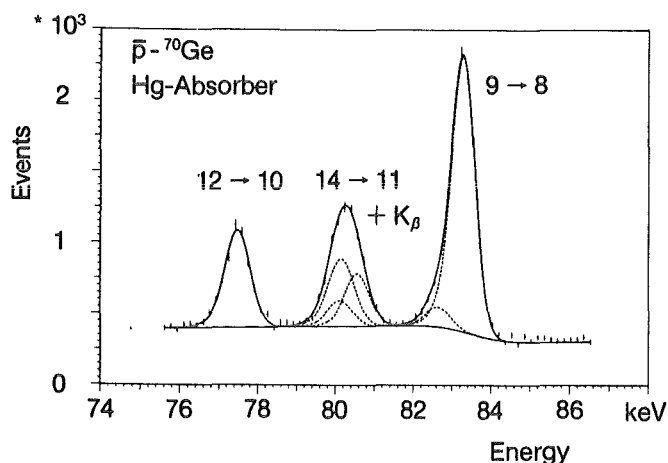
Fig. 2

The antiprotonic ^{70}Ge X-ray spectrum filtered by a critical Hg-absorber

(1)   B. Jödicke, Über die Bestimmung von Röntgenenergien antiprotonischer
        Atome durch kritische Absorption an Kanten und die theoretische Deutung
        von Ergebnissen, KfK-Report 3933 (June 1985)

4.2.5   HIGH SENSITIVITY SEARCH FOR NEUTRAL DECAYS OF THE $\bar{p}p$ BOUND STATES

A. Angelopoulos[+], A. Apostolakis[+], T. Armstrong[++], G. Büche, L. Bürcker,
M. Fero[++], M. Gee[+++], N. Graf[+++], H. Koch, R.A. Lewis[++], M. Mandelkern[+++],
S.M. Playfer[++], W. Rohrbach, G.A. Smith[++], T. Usher[++], D. Walther, and
K. Willuhn[++]

At the beginning of the year 1985 a group from our institute joined the collabora-
tion PS183 working at the LEAR facility of CERN. It is our aim to measure
the spectrum of photons immediately emitted from bound states of the $\bar{p}p$-system
or from a few of the vaious neutral decay channels, e.g. $\pi^0\omega$, $\pi^0\eta$, $\pi^0\eta$, $\pi^0\gamma$,
and $\pi^0\pi^0$. Photon energies are measured using a magnetic $180°$ e^+e^- pair spectro-
meter. The set up which has been used in the May 1985 run is shown in Fig. 1.
A beam of 330 MeV/c antiprotons is stopped in a target of liquid hydrogen. Two
sets of drift chambers surround the target which were formerly used to
reconstruct tracks of charged annihilation products. The photons interact with
the lead converter and cause three main groups of photon events to be observed.
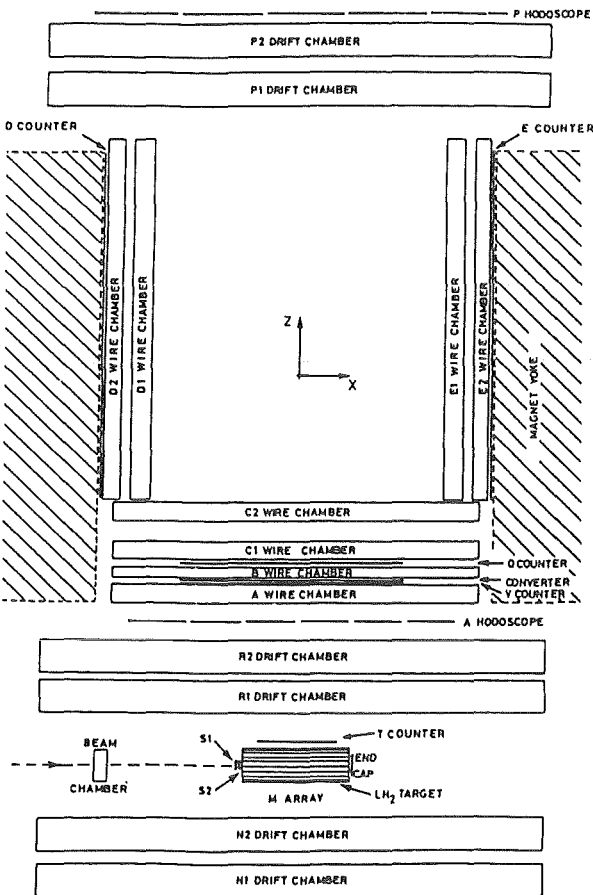
Fig. 1

The pair spectrometer
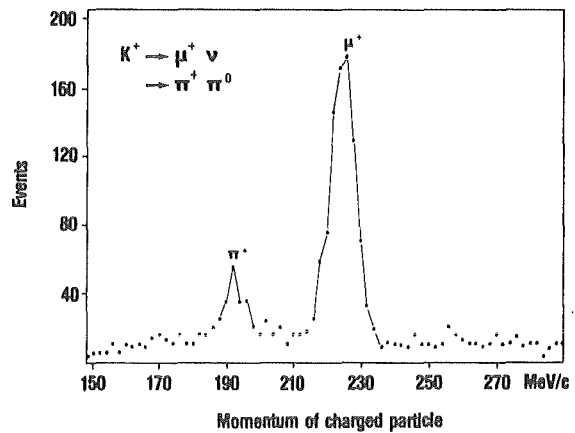
Fig. 2

The spectrum of delayed charged

events

Depending of their initial directions and their momenta e^+e^- tracks are back bended within the C1/C2 multiwire chambers, go aside into the D or E chambers or penetrate the whole magnetic field space and are detected in the P chambers and hodoscope. A photon event is defined by a coincidence of signals from the scintillators $S_1S_2\bar{V}Q$ <u>and</u> from two of the scintillators A, D, E or P. If this occurs the system reads out the chamber and scaler data and write them to magnetic tape.

The analysis of the photon events taken during the May 1985 run is in progress. The raw photon spectrum without the application of cuts during a detailed analysis of the event structure shows a more or less unstructured shape in function of the reconstructed photon momentum. In order to test appropriate cuts two gauge lines are available (see Fig. 2): Positively charged muons and pions generated in the decay processes of $K^+ \rightarrow \mu^+\nu$ (63,5%) and $K^+ \rightarrow \pi^+\pi^0$ (21,2%). These particles are monochromatic, since a certain amount of kaons have the chance to stop within the hydrogen target. These muons and pions are emitted with delay, i.e. according to the lifetime of the kaon. They could be easily discriminated against the overwhelming number of charged particles which leave the target immediately after the annihilation of the $\bar{p}p$ system and which are vetoed by the action of the detector V. The study of the μ^+ and π^+ tracks and of the conditions which determine the momentum resolution will guide us to evaluate the expected structures in the photon spectrum.

+   Nuclear Phyiscs Laboratory, University of Athens, Athens, Greece
++   Dept. of Physics, Universit of California, Irvine, California, USA
+++   Dept. of Physics, Pennsylvania State University, Pennsylvania, USA

4.2.6   STUDY OF LOW ENERGY ANTINEUTRON INTERACTION

D.I. Lowenstein[a], M. Furic[f], E. Hungerford[b], T. Kishimoto[b], B. Mays[b], L. Pinsky[b], L. Tang[b], Y. Xue[b], S. Cierjacks, H. Poth, B. Bassalleck[g], T.A. Armstrong[d], R.A. Lewis[d], W. Lochstedt[d], B.Y. Oh[d], S.M. Playfer[a], G. Mutschler[c], M. Moss[e], W. von Witsch[e]

An experiment was set-up at the low energy separated beam LESB II of the AGS at Brookhaven National Lab, to study the low energy antineutron interaction. The primary aim was to measure $\beta \cdot \sigma_a(\bar{n}p)$ (antineutron velocity χ annihilation cross section) for antineutron-proton annihilation at energies extremely close to the $N\bar{N}$ threshold. This quantity is proportional to the imaginary part of the $I = 1$ $\bar{N}N$ s-wave scattering length. Such a measurement may reveal dramatic departures from the classical $\beta \cdot \sigma$ = constant dependence, which would be suggestive of the existence of bound and resonant $\bar{N}N$ states. The energy region in question

(T < 1MeV) has never been explored, and was studied with practical upgrades of an existing apparatus which measured $\bar{n}p$ annihilation cross section at higher energies (1).

The experimental arrangement was as follows. Antiprotons of 400 MeV/c are impinging on a large liquid hydrogen target (50 cm length, 40 cm diameter) and most of them stop around the target center. A fraction of the antiprotons will undergo the charge exchange reaction

$$\bar{p} + p \rightarrow \bar{n} + n$$
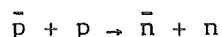
which represents the antineutron source. About 6% of the total cross section is due to the charge exchange reaction. Antineutrons originating from this process will be produced mostly along the beam direction and traverse the remaining hydrogen. Their lifetime τ in the liquid hydrogen target is related to the annihilation cross section through:

$$\tau \ [\,ns\,] \ = \ \frac{790 \ mb}{\beta\sigma_a}$$

It was one of the main goals of the experiment to determine this lifetime and to deduce in this way the low energy behaviour of $\beta\sigma_a$.

The incoming antiprotons were detected in MWPC and scintillation counters in order to determine the $\bar{p}$-trajectory and the time zero. The target was surrounded by a scintillation counter hodoscope of cylindrical shape and eight large drift chambers. These detectors were used to deduce the annihilation time and to reconstruct the antineutron annihilation vertex. Downstream of the target a large neutron counter was installed to tag the neutrons coming from the charge exchange reaction.

In the first half of 1985 beam time was received at the LESB II beam line at BNL and about 3×10^9 antiprotons were stopped. The experiment was completed in June 1985 and the data are presently being evaluated.

(1)   D. Lowenstein et al., Proc. 3rd Workshop on Physics with cooled low
        energy antiprotons, Tignes (1985), to be published

a   Brookhaven National Lab., Upton, New York
b   University of Houston, Houston, Texas
c   Rice University, Houston, Texas
d   Penn. State University, University Park, Pennsylvania
e   University of Bonn, Bonn
f   University of Zagreb, Zagreb
g   University of New Mexico, Albuquerque, New Mexico

4.3 MUONIC ATOMS

4.3.1 MUONIC ATOMS WITH VACANT ELECTRON SHELLS

R. Bacher, P. Bluem, D. Gotta, W. Kunold, J. Missimer[+], M. Schneider, and L.M. Simons

The muonic atom completely ionized of atomic electrons is a quantum mechanical system as simple as the hydrogen atom. The production of muonic atoms in this ideal state would facilitate the study of weak neutral current effects in a atomic system, for which the muonic 2s - 1s M1 transition must be observed (1). However, this has been hindered by the fact, that an even incompletely ionized muonic atoms is very attractive to electrons and consequently any vacancies in its electron shell refill.

We have pointed out (2), that it is possible to prepare completely ionized light muonic atoms in gases and that they remain isolated during the lifetime of the muonic 2s-state. At low pressures the electron refilling from the surrounding gas atoms can be neglected. After the forming of the muonic atom the muonic transitions are accompanied by rearrangement processes in the electron shell due to vacancy cascades. This means, that totally up to 3 electrons are ejected by electronic Auger and Coster-Kronig transitions from the shell at each muonic cascade step. To clarify the question whether the 2s - 1s M1 transition can be observed and the main mechanism for the depletion of the 2s-state via Auger effect can be avoided, it is necessary to know the remaining average number of the electrons in the shell during the lifetime of the muonic 2s-state.

To this purpose radiation transitions between the principal quantum numbers 6, 5, 4 and 3 in muonic neon and argon were observed, because a detailed numerical analysis (3) of the cascade process showed that the intensity ratios $I(6 \rightarrow 5)/I(5 \rightarrow 4)$ and $I(5 \rightarrow 4)/I(4 \rightarrow 3)$ of the transitions $6 \rightarrow 5$, $5 \rightarrow 4$, and $4 \rightarrow 3$ are extremely sensitive to the number of electrons in the shell. In the presence of electrons the radiative $5 \rightarrow 4$ transition is strongly suppressed. Figure 1 shows the remaining average number of electrons (N_e) on the shell as a function of the intensity ratio $I(5 \rightarrow 4)/I(4 \rightarrow 3)$ in muonic neon.

The experiment was done at the $\pi E1$-channel of the SIN using our cyclotron trap, a device to produce the worldwide highest stop densities at low pressure (4). The entering pions decayed in the target chamber and up to 10^5 μ^-/sec from the π-decay could be stopped in 20 mg of neon. Pressures below 1000 mbar and the use of thin windows allowed the observation of these low energy transitions for the first time.

For muonic neon our measurements give $I(5 \rightarrow 4)/I(4 \rightarrow 3) = 0.873 \pm 0.086$.

N_e

1.00

0.40

0.5   4.0
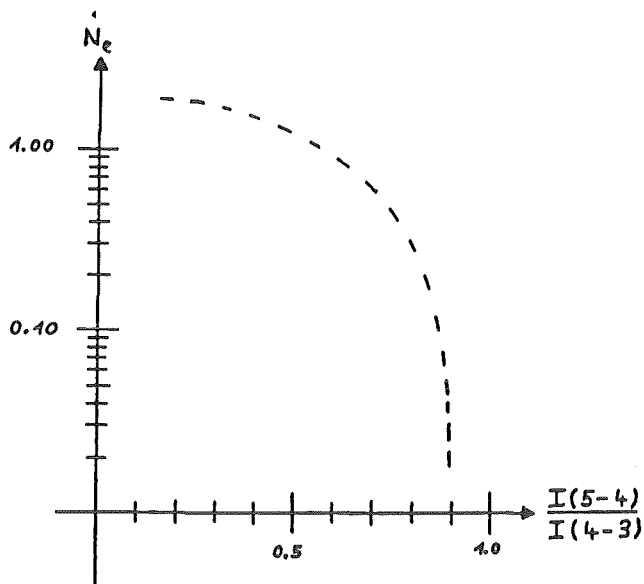
$\dfrac{I(5-4)}{I(4-3)}$

Fig. 1

Average number of electrons in the electron shell (N_e) versus the intensity ratio $I(5 \rightarrow 4)/I(4 \rightarrow 3)$ of the radiative transitions $5 \rightarrow 4$ and $4 \rightarrow 3$ in muonic neon (cascade calculations)

This means that in neon the upper limit of the probability to find an electron in the shell is 35%, if the muon stays in the 2s-level.

In muonic argon we measured the intensity ratios $I(6 \rightarrow 5)/I(5 \rightarrow 4) = 0.600 \pm 0.162$ and $I(5 \rightarrow 4)/I(4 \rightarrow 3) = 0.498 \pm 0.088$, which correspond to an average number of electrons $N_e < 1.5$ during the lower part of the muonic cascade.

(1)   J. Missimer and L.M. Simons, Phys. Rep. 118, No 4,(1985)180
(2)   R. Bacher, D. Gotta, J. Missimer, N.C. Mukhopadyay, and L.M. Simons, Phys. Rev. Letters 54, No 19,(1985)2087
(3)   V.R. Akylas and P. Vogel, Comp. Phys. Com. 15(1978)291
(4)   Annual report on nuclear physics activities, KfK 3815(1983/84)148

+   Schweizerisches Institut für Nuklearforschung

4.4   THEORY

4.4.1   SEPARABLE POTENTIALS FOR RELATIVISTIC THREE-BODY CALCULATIONS OF THE NNN, NNπ, Nππ, AND πππ SYSTEMS

H. Garcilazo and L. Mathelitsch[+]

The relativistic generalization of the Faddeev equations has been considered by many authors within the context of the three-body Bethe-Salpeter equation applying the methods developed by Blankenbecler and Sugar. These methods result in integral equations with the same general structure as those of the non-relativistic three-body problem but satisfying relativistic three-body unitarity and Lorentz invariance. Although these equations have been very successful in the treatment of the various reactions of the pion-deuteron system, it has been found recently (1) that they are completely inadequate for calculations in the bound-state region, since they contain spurious bound-state solutions and lead to a singular behaviour as the invariant mass squared tends to zero. Moreover, in the case of two-body interactions with a very long range in momentum space, this pathological behaviour can appear also in the scattering domain. Thus, it has become necessary to modify these equations in order to avoid such problems. The modified equations that we have proposed (1) are well behaved as a function of the invariant mass of the three body system $\sqrt{S}$ throughout the bound-state region. The main difference between our approach and the standard one is that the two-body amplitudes now are constructed by solving the two-body integral equation proposed by Kadyshevski (2) rather than by the solution of the two-body Blankenbecler-Sugar equation.

We have constructed a set of separable potentials for the nucleon-nucleon, pion-nucleon, and pion-pion subsystem for all partial waves with angular momentum $L \lesssim 2$ within the frame-work of the relativistic two-body Kadyshevki equation. These interactions can serve as input for relativistic calculations of three body systems composed of nucleons and pions.

Among the possible applications of these interactions are the systems composed of i) three nucleons, ii) two nucleons and one pion, iii) one nucleon and two pions, iv) three pions. As an example of our formalism and the use of these separable interactions, we have studied recently (3) the possible existence of bound states or resonances of a pion and two nucleons in the three-body channels with isospin 0 and 2. Another obvious application of this theory would be the calculations of πNN resonances with isospin 1 which correspond to the so-called dibaryon resonances.

Similarly, these interactions can be used to study the scattering and bound-state problems of three nucleons. In addition, one has now a reliable framework in which to study the possible existence of three-pion resonances as well as those of a nucleon and two pions.

(1)   H. Garcilazo and L. Mathelitsch, Phys. Rev. C28(1983)1272
(2)   V.G. Kadyshevki, Nucl. Phys. B6(1968)125
(3)   H. Garcilazo and L. Mathelitsch, to be published

+   Institut für Theoretische Physik, Universität Graz, A-8010 Graz, Austria

4.4.2   ANGULAR MOMENTUM EFFECTS IN THE $\pi^- nn$ BOUND-STATE PROBLEM

H. Garcilazo

We discussed in a previous paper (1) the possibility that a negative pion and two neutrons may form a stable bound state, by solving the relativistic Faddeev equations at threshold using the pion-nucleon P_{33} channel and the nucleon-nucleon $^1S_0$ channel as input by means of separable potentials. Since the pion is likely to be found mainly in a P-wave state with respect to the two neutrons and the neutron-neutron interaction is stronger in the $^1S_0$ channel, we assumed that the $\pi^- nn$ bound state would have the quantum numbers $J^P = 1^-$, where J is the total angular momentum and P is the parity of the system defined as $P = (-)^{\ell+\lambda}$, with ℓ the orbital angular momentum of a pair and λ the orbital angular momentum of the third particle with respect to the pair.

It turns out that the configuration $J^P = 1^-$ in which the pion is in a P-wave state and the two nucleons are in the $^1S_0$ channel is very disadvantageous for two reasons: First of all, since the two neutrons are in an S-wave state, their spins have to be antiparallel which has the consequence that if the magnetic projection of the P-wave pion is parallel to the spin of one of the neutrons such that they form the P_{33} resonance with full strength, the total magnetic projection of the pion with the second neutron is only 1/2, so that with this neutron the P_{33} resonance is formed with only one third of its strength. Seondly, since the two neutrons are in a state with $\ell = 0$, they can come very close to one another and therefore they feel the strong repulsion at short distances a large fraction of the time which has the effect of working against the bound state.

Let us now see what is the situation for the channels $J^P = 0^+$ and $J^P = 2^+$. First of all, if the pion is in a P-wave state with respect to the two neutrons, then the neutrons themselves must be in a relative P-wave state, so that in this case their spins are parallel and therefore the pion can form the P_{33} resonance with full strength with both neutrons. Secondly, since the neutrons are in a

	J = 0	J = 1	J = 2
parity +	0.026	3.71	-0.058
parity -	1.35	0.85	1.61

Table I

Values of the Fredholm
determimant at threshold

relative P-wave state they can not come very close to one another and therefore they do not feel very much the strong repulsion at short distances, both of which effects help towards the formation of the bound state. Of course, if the pion is in a state with $\lambda = 0$, the repulsion of the ^1S_o channel can contribute in the $J^P = 0^+$ state; however, it still will not contribute in the $J^P = 2^+$ state, since for this it is necessary that the pion be in a state with $\lambda = 2$. Thus, one expects that the $J^P = 2^+$ state will have the most favourable conditions to form the bound state.

In order to see numerically the results of these considerations, we have solved the relativistic Faddeev equations at threshold using as input all the pion-nucleon S and P-wave channels and all the nucleon-nucleon S, P and D-wave channels.

We present in Table I our results for the six three-body channels corresponding to $J \leq 2$ and positive and negative parity. As we see, only the $J^P = 2^+$ channel gives rise to a bound state which is in good agreement with our previous considerations. As a matter of fact, the nucleon-nucleon interaction has only a minor effect on the $J^P = 2^+$ channel, which is due as we mentioned before, to the fact that the dominant neutron-neutron interaction which is the ^1S_o wave, has total angular momentum $j = 0$ and therefore it couples very weakly to the system in the $J^P = 2^+$ channel.

To conclude, we have shown that the most favourable configuration to form a bound state of two neutrons and a negative pion, is that with angular momentum $J = 2$ and positive parity, since in this channel the pion can produce the P_{33} resonance with full strength with both neutrons while at the same time the neutron-neutron short-range repulsion is strongly suppressed.

(1)   H. Garcilazo, Phys. Rev. C26(1982)2685

4.4.3 RELATIVISTIC EFFECTS IN THE NEUTRON-DEUTERON SCATTERING LENGTHS

H. Garcilazo, L. Mathelitsch[+] and H. Zankel[+]

Relativistic corrections in the three-nucleon problem have been restricted mainly to the calculation of these effects in the binding energy of the triton. The results of these calculations indicate that relativistic effects are small

amounting to approximately 3%, since they increase the binding energy by about 0.25 MeV.

In order to calculate the relativistic corrections to the neutron-deuteron scattering lengths, we will solve simultaneously the Faddeev equations and their relativistic generalization (1), (2), for several local potentials that act only in S-waves. As far as we know, this is the first attempt to calculate the relativistic corrections to the three-nucleon continuum problem.

We give in Table I our results for the quartet scattering length, where we see that for the four models considered the relativistic effects increase the scattering length by about 0.2 fm, and the results of the two relativistic versions of the Faddeev equations differ from each other by only 0.01 fm. The relativistic effects represent a correction of approximately 3% which is similar to that found in the bound-state problem.

In Table I we give also the results for the doublet scattering length, where we see the opposite effect of the relativistic corrections, since in this case they decrease the scattering length.

The changes in the scattering length due to the relativistic effects are, as in the quartet case, about 0.2 fm for the two realistic models and for the Yamaguchi model, with the results of the two Blankenbecler-Sugar reductions differing among themselves by about 0.02 fm. The Malfliet-Tjon II-IV model, gives both a larger effect for the relativistic corrections and a larger difference between the two Blankenbecler-Sugar reductions. This model, however,

		UNCOUPLED REID	MALFLIET-TJON I-III	MALFLIET-TJON II-IV	YAMAGUCHI
	N R	6.37	6.44	6.53	6.29
QUARTET	A A Y	6.55	6.61	6.71	6.46
	A T	6.56	6.62	6.72	6.46
	N R	0.63	0.70	-5.62	-0.92
DOUBLET	A A Y	0.43	0.55	-5.92	-1.14
	A T	0.41	0.54	-6.01	-1.16

Table I Quartet and doublet scattering lengths (in fm) calculated using four different models of the nucleon-nucleon interaction in a non-relativistic formalism (N R) and in the relativistic formalisms of Aaron, Amado and Young (A A Y) and Ahmadzadeh and Tjon (A T). The experimental value is $^4a = 6.35 \pm 0.02$ fm, $^2a = 0.65 \pm 0.04$ fm.

is completely unrealistic, so that if we disregard it we see that the relativistic effects are of the same size for the quartet and doublet channels. The changes in the doublet scattering length coming from the relativistic effects, represent a correction of more than 20%.

To conclude, we have found that the relativistic effects increase the quartet scattering length by about 0.2 fm and decrease the doublet scattering length by a similar amount. This represents a correction of approximately 3% for the quartet case and of more than 20% for the doublet case. The relativistic effect seems to be nearly independent of the underlying nucleon-nucleon interaction and of our choice of relativistic reductions.

(1)   R. Aaron, R.D. Amado, and J.E. Young, Phys. Rev. 174(1968)2022
(2)   A. Ahmadzadeh and Tjon, Phys. Rev. 147(1966)1111

+   Institut für Theoretische Physik, Universität Graz, A-8010 Graz, Austria

4.4.4   MOMENTUM SPACE CALCULATION OF ^{3}He BOUND STATE ENERGIES

H. Garcilazo, G.H. Berthold[+], H. Zankel[+] and L. Mathelitsch[+]

We have solved momentum space Faddeev equations that include the Coulomb potential in one N-N subsystem in order to find ^{3}He binding energies. The nuclear interaction models we have used were rank one separable potentials of Yamaguchi type with varying level of sophistication.

To faciliate momentum space ^{3}He binding energy calculations with N-N tensor force we have introduced an approximation by truncating the orbital angular momentum of the spectator, i.e. λ was set equal to zero. For purely attractive potentials this approximation turned out to be very close to the full calculation of the ^{3}He binding energy (it deteriorates with increasing deuteron D-state probability). ^{3}He binding energies were calculated with varying p_D and the known fact that E_c roughly scales with the three-nucleon binding energy was

P_D	$E_{^3He}$	$E_{^3He}$	E_c
%	MeV	MeV	MeV
2.15	-9.690	-8.835	0.855
4.00	-8.940	-8.121	0.819
5.50	-8.350	-7.585	0.765
7.00	-7.812	-7.087	0.725
8.98	-7.265	-6.583	0.682

Table I
Trinucleon binding energies with $^3S_1 - {}^3D_1$ potentials of varying D-state probability.

Potential	$E_{^3He}$ MeV	$E_{^3He}$ MeV	E_c MeV
PEST1-6-no tensor	-8.635	-7.924	0.711
MT I-III	-8.54	-7.87	0.666
PEST1-6-with tensor	-7.049	-6.434	0.615
Reid	-6.38	-5.77	0.608

Table II Trinucleon binding energies and E_c for the realistic PEST1-6 inter-action and comparison with the configuration space results using the Malfliet-Tjon (MT I-III) and the Reid potential.

confirmed. We show the result of these calculations in Table I.

With separable potentials that were either modeled on a pure S-wave Paris potential or on the coupled $^3S_1$-$^3D_1$ part of this allowed a comparison with configuration space results that were obtained with the S-wave Malfliet-Tjon potential and the Reid soft core potential respectively. Our momentum space result is in fair agreement with the configuration space result, both for the purely S-wave calculations and for the case of coupled channel calculations. These results are shown in Table II.

+   Institut für Theoretische Physik, Universität Graz, A-8010 Graz, Austria

4.5   THE CRYSTAL BARREL PROJECT AT LEAR

CBC-Collaboration

G. Büche, S. Cierjacks, D. Engelhardt, H. Koch, M. Kunze, W. Rohrbach,
W. Schott, D. Walther,

Kernforschungszentrum Karlsruhe, IK II and University of Karlsruhe

M. Gee, M. Mandelkern

University of California, Irvine

D. Bugg

Queen Mary College, London

E. Klempt, U. Straumann

Universität Mainz, Institut für Physik

C. Zupancic

Universität München, Sektion für Physik

T.A. Armstrong, R.A. Lewis, S.M. Playfer, G.A. Smith

Pennsylvania State University, Physics Department

M. Suffert

Centre de Recherche Nucléaires et Université Louis Pasteur, Strasbourg

A.S. Clough

University of Surrey, Physics Department, Guildford

C. Amsler, P. Truöl

Universität Zürich, Physikalisches Institut

The aim of the project is to construct and operate at Lear a detector for charged and neutral $\bar{N}N$-annihilation products. The apparatus (see Fig. 1) detects charged and neutral particles in a nearly 4π solid angle, measures the energies of the Gammas with good energy resolution in the full solid angle and the momenta of the charged particles in 60% of 4π.

The project is performed by an international collaboration consisting of 10 institutions with about 40 people, of whom 20 work full- or part-time already on the project. H. Koch was elected as the first spokesman of the collaboration. A letter of intent (1) was submitted in May 1985 to the CERN authorities (PSCC). The final proposal will be submitted at the end of 1985. The present cost estimate for the total project is 7.1 Mio sfr and is covered by the funds of the participating groups.

The CsI-barrel as the major part of the set up will be built and financed by the German groups (KfK, University of Karlsruhe, Mainz, Munich) with a leading role of KfK and the University of Karlsruhe.

The detector is designed to measure exclusively all annihilation Channels in the p̄-momentum region from 0 to 2 GeV. In contrast to the first round of experiments at LEAR it will be able to distinguish all annihilation channels (only

Cs I (Tl) Crystal Barrel
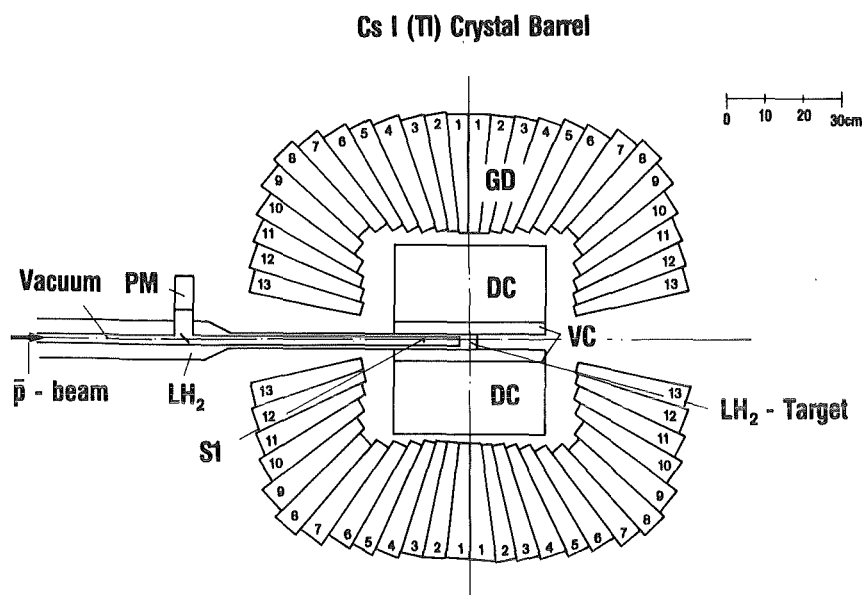
Fig.1 Crystal Barrel Detector

GD: Gamma Detector consisting of 1380 CsI-modules
VC: Cylindrical vertex chamber
DC: Cylindricyl drift chamber
S1: p̄-trigger scintillator
PM: Photomultiplier of S1

40% of all annihilation reactions were accessible for Asterix, e.g.) and thus has a very high sensitivity for all types of rare events which can be completely reconstructed via their decays. At a later time it could be inserted in the LEAR-ring to measure p̄p-collisions up to 4 GeV c. m. energy thus extending considerably the accessible mass range. E.g., higher mass hybrid states and the Ψ-system could be investigated then. The main emphasis at lower energies lies at

- Annihilation Dynamics

The first Lear results seem to show clearly that for the interpretation of the annihilation processes even at rest a quark-gluon-picture is indispensable (2,3). Unexpected selection rules, e.g. the I-dependence of the $\rho\pi$-channel, give first insights into the low energy quark behaviour the knowledge of which is urgently needed for all considerations on the confinement problem. The proposed detector will widely enlarge the range of accessible reactions (reactions with more than one π°, with η's,...). Furthermore, the powerful reconstruction of short living resonances will help to come one step closer to the primary products of the annihilation. Of particular interest for reactions above the threshold are 2-body processes, like $\pi^{\circ}\pi^{\circ}$,$\eta\eta$,..., which are extremely quantum number selective and promise clear comparisons with calculations, because only a small number of partial waves contributes.

- Meson Spectroscopy

Here is the question if all mesons are q̄q-states or if more exotic states

like $q^2\bar{q}^2$, or pure or mixed gluon states, like gg (Glue Balls) and $\bar{q}qg$ (Hybrids) exist. Experimentally, many hints for the existence of exotic states exist, but in none of the cases the interpretation in form of a (radially excited) $\bar{q}q$-state is excluded. More measurements are needed to pin down these questions and eventually find more candidates for exotic mesons. The $\bar{p}p$-annihilation reactions are promising candidates for such measurements, as many of the mesons have been firstly seen here.

For a further identification of the already known states and a final determination of their quark-contents more data on <u>decay modes</u> are necessary. Of particular importance are the <u>radiative</u> decays which are very sensitive against the quark-gluon-structure of the states. They can be excellently measured in a 4π γ-detector as proposed here.

Further measurements will search for yet undetected, rare exotic meson states in the $\bar{N}N$-system. Narrow states would even show up in inclusive γ, π^o, η - spectra. By the very effective π^o-reconstruction, the background in inclusive γ-spectra can be reduced so significantly that an improvement of the sensitivity for monoenergetic γ-events, e.g.,of 2-3 orders of magnitude compared to today's detectors seems feasible (4). Broad exotic states can be detected via reconstruction of their decay products. Recent theoretical work (5) suggests that the lowest mass hybrids preferentially decay to final states with one excited meson, e.g. B(1235)π, A_2(1320)π,..., which are difficult to reconstruct and have therefore escaped today's measurements. The CB-detector is optimally shaped for problems like these.

The discovery of states with exotic quantum numbers (0^{--}, 1^{-+}, 2^{+-},...) would unambiguously signal exotic mesons. These objects must be searched for in potentially exotic channels such as $\omega\pi^o$, $\eta\omega$, $\eta\pi^o$ and $\eta\eta'$, which are easily accessible to the CB-experiment.

- Radiative decays of mesons

Irrespective of their role in the identification of mesons, radiative decays, e.g.,$\rho \to \pi\gamma$,$K^* \to K\gamma$,$A_2 \to \pi\gamma$ are useful as test of quark magnetic moments. It should be possible to improve these measurements, and in addition to observe processes like $\rho \to \eta\gamma$, $\omega \to \eta\gamma$, $f \to \rho\gamma$, $\eta' \to \rho\gamma$, $\omega\gamma$. The radiative decays $\Phi \to \eta'\gamma$, $\eta\gamma$, $\omega\gamma$, $\rho\gamma$ are particularly interesting as a test of strange-quark components of light mesons.

- Rare decays of Mesons

The measurement of all final state particles allows any single particle to be tagged. This makes it possible to search for rare decays. Examples especially suited to this experiment would be $\pi^o \to 3\gamma$, $\eta \to \pi^o\pi^o$ and $K_s \to 2\gamma$. We are also considering the possibility of studying the CP violating channels $K_1 \to \pi^+\pi^-\pi^o$ and $\pi^o\pi^o\pi^o$.

(1)   Crystal Barrel Collaboration (CBC)
        Study of p̄p-Annihilation at LEAR with a 4π neutral detector
        CERN/PSCC/85-26
(2)   Asterix Collaboration
        Proceedings of the Third LEAR Workshop, Tignes, 1985
        To be published
(3)   C. Dover, H. Genz, Private communication
(4)   H. Koch, M. Kunze
        Monte Carlo Studies of Exotic p̄p Annihilations
        Contribution 4.5.2 to this Annual Report
(5)   N. Isgur, R. Kokoski, J. Paton
        Gluonic Excitations of Mesons: Why are they missing and where to find them
        P.R. L. 54(1985)869

4.5.1   THE CRYSTAL BARREL DETECTOR AT LEAR

CBC-Collboration

In the following a short survey is given on the results so far obtained in the studies of different technical working groups. More details can be found in the CBC internal notes.

1. The CsI-detector: CsI has been selected as material for the detector as it is best adapted to the use of Photodiodes which are indispensable because of the operation inside the strong magnetic field. An energy resolution (FWHM) proportional to $(E)^{-1/4}$ with 7% at 100 MeV is aimed for. The angular resolution will be better than $5°(\sigma)$, $5°$ being the average angle between neighbouring crystals.

        - Geometry of the CsI

        With a computer programm the individual shapes of the crystals making up the barrel as displayed in Fig. 1 (see above) have been calculated. To cover a solid angle of 98% x 4π, 1380 crystals of 13 shapes are necessary. Most of them are prismatic and tapered with a front face area of 10 cm² and a rear end area of 30 cm³ (typical values).

        - Electromagnetic shower

        The development of the γ-induced e.-m. cascade inside the crystals has been simulated by EGS4-calculations. Sixteen radiation lenghts were found to be sufficient for the measurements of γ-energies up to 1 GeV. At maximum, 2% of the shower energy leaks out at the rear end of the crystals. The effect of the magnetic field on the form of the shower is tolerable. Summation of the next eight neighbours of one hit module gives already a good energy resolution, which can be slightly improved by summation of the next 24 neighbours. An energy resolution (FWHM) of $4\%/\sqrt[4]{E[GeV]}$ seems feasible. Further calculations under even more realistic conditions are going on.

- Tests of crystals and Photodiodes

CsI-crystals of the size 5 x 5 x 30 cm³ , provided by different manufactures, have been tested with Photomultipliers and Photodiodes. Critical points for the achievement of a good energy resolution are the uniformity of the production and transport of the light along the length of the cystal and the noise of the Photodiodes. It was found that the uniformity of the light output should be better than 5%, and the electronics r.m.s. noise/module less than 300 keV, in order to reach the desired energy resolution. The measurements done so far indicate that the final goals can be reached.

- Calibration and stabilization of the crystals

The energy calibration of each individual module must be done with high accuracy ($\approx 1\%$), in order to reach the desired energy resolution for the total detector. It will be performed in an iterative procedure: A zero'st order calibration is done with radioactive sources and with higher energy Gammas originating from a proton induced nuclear reaction (van de Graaff of 400 keV). For the in situ calibration at higher energies annihilation reactions like $\bar{p}p \rightarrow \pi^+ \pi^- \pi^0$ ($\rightarrow \gamma\gamma$) can be used. If a calibration on an external $e^-(\gamma)$ beam is necessary is presently under investigation.

- Mechanics

The fixation of the CsI-crystals relative to each other and the holding of the total detector (4 t weight) within the magnet is studied. The amount of material between and in front of the crystals has to be minimized. Furthermore, the detector must be easily removable along the beam line to have quick access to the tracking chambers.

2. Charged particle tracking chambers: The detection system for charged particles will consist of an inner part - the Vertex Chamber - (Fig. 1 above) and an outer Drift Chamber (DC) for the momentum determination of the particles. The inner chamber will probably be a XDC-type chamber which was developed for Asterix. The vertex of a $\bar{p}p$-annihilation can be determined with a precision of about 1 mm, and the chamber has a good detection efficiency for K_s's which have an average flight path of 2,5 cm before decaying into $\pi^+\pi^-$. In addition, in combination with a gaseous target, the L-X-rays of the atomic systems can be detected and serve in at rest-experiments as trigger for the in ℓ-quantum number.

The outer drift chamber will have a spatial resolution of better than 150μ, corresponding to a relative momentum resolution (σ) of 4.3% • p [GeV/c]. In addition, it has a dE/dx-resolution of better than 30%, in order to discriminate between kaons and pions, at least for momenta lower than 600 MeV/c, and a spatial resolution in Z-(beam)-direction corresponding to about 1% of the wire length (40 cm). It will be realized as yet chamber consisting of 32 layers of sense wires (0.6cmdistance) forming 30 sectors. In total 960 sense wires

(20 μ $\emptyset$) and 2400 field wires will be used. The Z-information via charge division measurements will be done only in several of the 32 layers. Specific problems of the chamber (Large Lorentz-angle in the big magnetic field (1.5T)) are presently under investigation. The use of a slow gas is being considered.

3. Magnet: To produce the high magnetic field (1.5 T) which is neeeded for a high-resolution momentum measurement of the charged particles the Pluto-magnet will be lent from Desy. It will produce a mainly homogenous field with maximally 2% changes within the track-chamber volume. If the coil has to be slightly modified in order to reduce the cooling losses and if it can be used at CERN without He-refrigerator is under study.

4. Target: For the experiments both gaseous and liquid targets filled with H_2, D_2, ^3He, and ^4He will be used. The construction of a gasous target is no problem. The design of a liquid target minimizes the amount of material in the beam and the lateral dimensions in order to maximize the number of detectable K_s's. The trigger counter S1 should have a minimal distance to the target of 10 cm because in cases of pure neutral annihilations ($\pi^o \pi^o$, e.g.) the vertex determination can't be made better than that (result of MC-calculations)

5. Trigger: The number of events which can be registered on MAG-Tapes is limited to about 300/second. Therefore, to make optimal use of the available particles ($\geq 10^5$ $\bar{p}/s$) highly sophisticated triggers are needed. The present scheme aims at a multiplicity trigger for both charged and neutral particles, a fast trigger for K_s's and the total deposited energy. The trigger will have four levels working with different speeds. The fastest level (e.g. cluster counting in the CsI-barrel) will be done per hardware, while for the other levels CAB- and J-11-computers will be used. Thus, it is expected to have signals on the multiplicities and a K_s-vertex about 1 μses after the S1-counter has detected an incoming antiproton.

The work during the coming months concentrates on the preparation of the proposal and the set up of prototypes for the CsI-barrel and the charged particle detector. It is intended to perform both tests already with the electronics foreseen for the final set up. It is expected that the test with 27 modules of CsI can be finished in the first half of 1986, so that the order of the crystals can start then.

4.5.2 MONTE CARLO STUDIES OF EXOTIC $\bar{p}p$ ANNIHILATIONS

H. Koch, M. Kunze

One of the major aims of the measurements with the CsI-crystal-barrel detector is the investigation of exotic meson-like states like Glue-Balls (gg), Hybrids ($q\bar{q}g$) and multiquark states ($q^2\bar{q}^2$). They are supposed to show up in rare annihilation channels. The E-meson, e.g., which is a candidate for a glue-ball state, was seen in $\bar{p}p \rightarrow \pi^+\pi^-E^o$, $E^o \rightarrow \delta\pi^o$, $\delta \rightarrow \eta\pi^o$. To investigate the sensitivity of the proposed detector (see 4.5.1) for the detection of these and more hypothetical events a Monte Carlo program was set up which allows the creation of exotic events and to simulate their detection in the system. That was done in a manner as realistic as possible. Finite energy- and angular resolution (σ) for the Gammas ($\frac{\Delta E}{E} = 0.17/^4\sqrt{E\,[\,GeV\,]}$; $\Delta\theta = 5^o$ and for the charged particles ($\Delta p_\perp/P_\perp = 4.3\% \cdot p$ were assumed as well as low energy cuts, finite solid angles ($< 4\pi$) of the detectors and a target of realistic dimensions. These effects were taken into account by smearing the momenta of the kinematically corrects events according to the finite measuring accuracies and by truncating particles leaving the detector through its holes or having not enough energy to be detected. In addition to the interesting rare annihilation channels, most of the already known annihilation modes, like $\pi^+\pi^-\pi^o$, $2\pi^+2\pi^-\pi^o$, ..., also including resonant intermediate states were simulated according to their production rations at rest (1,2). In this way a realistic picture for the appearance of rare events and the unavoidable backgrounds (combinatorial and detector-dependent) was achieved.

Two examples of these calculations are discussed more in detail:

(i) $(\bar{p}p)_{Rest} \rightarrow \pi^+\pi^- E(1420)$, $E \rightarrow \delta^o\pi^o$, $\delta^o \rightarrow \eta\pi^o$

The interest in the E(1420) meson comes from its vicinity to the i(1440), a glueball candidate. While the former has been seen in $\bar{p}p$ annihilation at rest decaying into $K\bar{K}^*$ and $\delta\pi$, the latter is reported to decay only ino $\delta\pi$. The evidence for the $\delta\pi$ mode rests on $\delta \rightarrow K\bar{K}$ and must be firmly established by observing the decay $\delta \rightarrow \eta\pi$. A branching ratio of 2×10^{-3} for this channel was assumed. The main background contributions stem from $\pi^+\pi^-3\pi^o$ (23%) and $\pi^+\pi^-4\pi^o$ (3%). Exactly six photons are required, two pairs building a π^o, one pair building an η. In addition the $\eta\pi$-mass is required to be consistent with a δ(two possible combinations per event). Appropriate total momentum and total energy cuts are applied (kinematics fitting should even improve the situation substantially). The results are shown in Fig. 1. A total of 1400 events is seen in the (almost background free) E peak, corresponding to a simulated total of 3.2×10^6 annihilations. With a trigger requiring exactly 2 prongs and 6 γ and a writing speed of 200 events/s one would obtain this spectrum in 3 hours of LEAR beam time.

(ii) $(\bar{p}p)_{Rest} \rightarrow \gamma X \rightarrow \pi^+\pi^-\pi^o$
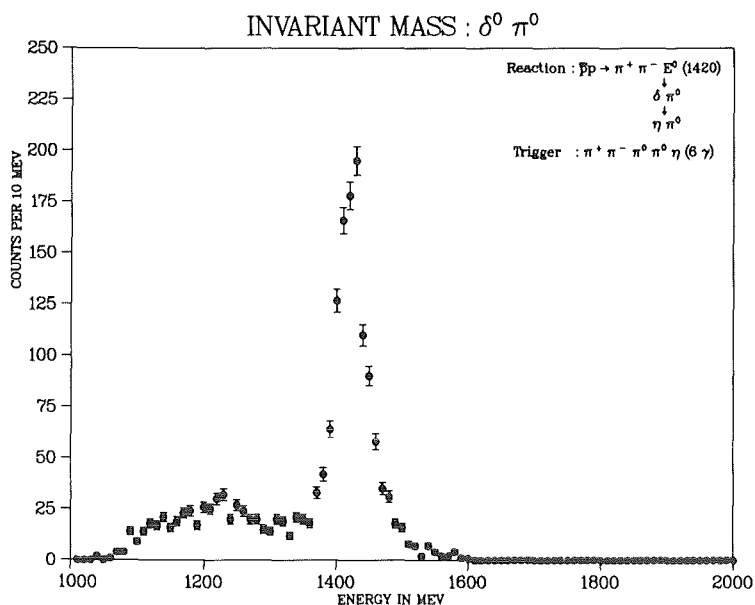
INVARIANT MASS : $\delta^0 \pi^0$

Fig. 1 Invariant mass of the $\delta^0 \pi^0$-system appearing in the $\bar{p}p$-annihilation channel $\pi^+ \pi^- \pi^0 \pi^0 \eta$ (6γ). Monte Carlo simulation of the expected Crystal-Barrel Detector results.

The yields for the narrow states X associated with monochromatic γ transitions are (3) 9 x 10^{-4} (1210 MeV), 10^{-3} (1383 MeV), 6 x 10^{-4} (1421 MeV), 3 x 10^{-3} (1638 MeV) and 1.6 x 10^{-3} (1694 MeV). Since the decay channels of these states are unkown we assume X $\rightarrow$ $\pi^+ \pi^- \pi^0$ (branching ratio 20%). The background is simulated by phase space distribution of the outgoing pions and the known charged and neutral pion multiplicities. The main background contribution comes from $\pi^+ \pi^- n\pi^0$ (n > 1) which only three photons detected. Again a total energy and momentum cut are applied. The result is shown in Fig. 2. With 100 hours of LEAR
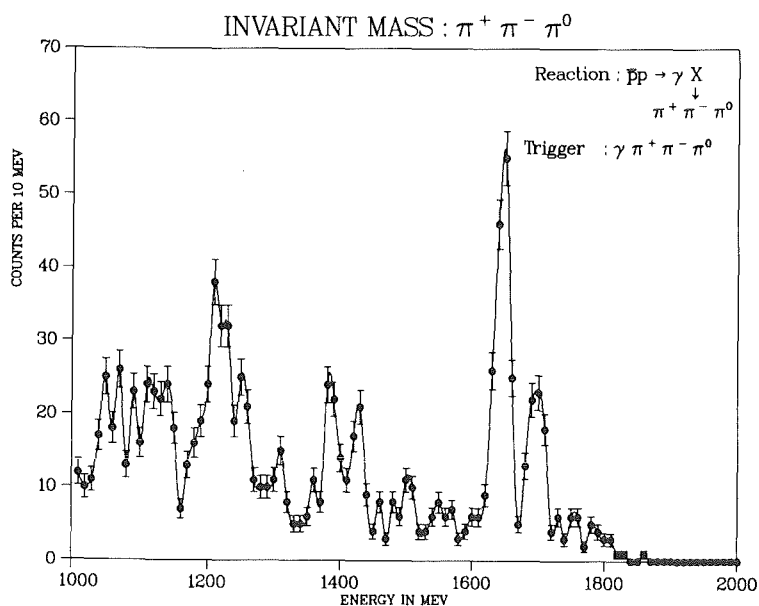
INVARIANT MASS : $\pi^+ \pi^- \pi^0$

Fig. 2 Invariant mass of the $\pi^+ \pi^- \pi^0$ - system potentially appearing in the $\bar{p}p$-annihilation channel $\pi^+ \pi^- \pi^0 \gamma$. Monte Carlo simulation of the expected Crystal-Barrel Detector results.

beamtime one could achieve sensitivities of the order 2×10^{-5} for $\bar{p}p \to \gamma X$, $X \to \pi^+\pi^-\pi^0$. The sensitivity does not depend strongly on the decay mode of the states, that is any decay mode could be observed with similar sensitivity owing to the nearly 100% solid angle for all particles.

(1)   Asterix-Proposal, CERN/PSCC/80-101
(2)   G. Backenstoss et al., Nucl. Phys. B228(1983)424
(3)   B. Richter et al., P.L. 126B(1983)284

5.   HIGH ENERGY PHYSICS

CELLO Collaboration

H.-J. Behrend, V. Blobel, J. Bürger, L. Criegee, H. Fenner, J.H. Field, G. Franke, J. Fuster, Y. Holler, J. Meyer, V. Schröder, H. Sindt, U. Timm, G.G. Winter, W. Zimmermann
Deutsches Elektronen-Synchrotron, DESY, Hamburg, Germany

P.J. Bussey, A.J. Campbell, J.B. Dainton, D. Hendry, G. McCurrach, J.M. Scarr, I.O. Skillicorn, K.M. Smith
University of Glasgow, United Kingdom

V. Blobel, M. Poppe, H. Spitzer,
II. Institut für Experimentalphysik, Universität Hamburg, Germany

W.-D. Apel, J. Engler, G. Flügge, D.C. Fries, W. Fues, K. Gamerdinger, P. Grosse-Wiesmann, J. Hansmeyer, Th. Henkes, G. Hopp, J. Jung, J. Knapp, M. Krüger, H. Küster, H. Müller, K.H. Ranitzsch, H. Schneider
Kernforschungszentrum Karlsruhe and Universität Karlsruhe, Germany

W. de Boer, G. Buschhorn, W. Christiansen, G. Grindhammer, B. Gunderson, Ch. Kiesling, R. Kotthaus, H. Kroha, D. Lüers, H. Oberlack, B. Sack, P. Schacht, B. Scharlemann, G. Shooshtari, W. Wiedenmann
Max-Planck-Institut für Physik und Astrophysik, München, Germany

A. Cordier, M. Davier, D. Fournier, M. Gaillard, J.F. Grivaz, J. Haissinski, V. Journé, F. Le Diberder, E. Ros, A. Spadafora, J.-J. Veillet
Laboratoire de l'Accélérateur Linéaire, Orsay, France

B. Fatah, R. George, M. Goldberg, O. Hamon, F. Kapusta, F. Kovacs, R. Pain, L. Poggioli, M. Rivoal
Laboratoire de Physique Nucléaire et Hautes Energies, Université de Paris, France

G. D'Agostini, M. Gaspero, B. Stella
University of Rome, Italy

R. Aleksan, G. Cozzika, Y. Ducros, P. Jarry, Y. Lavagne, F. Ould Saada, J. Pamela, F. Pierre, J. Jacek
Centre d'Etudes Nucléaires, Saclay, France

G. Alexander, G. Bella, Y. Gnat, J. Grunhaus
Tel Aviv University, Israel

During the last few years, the High Energy Physics group of the IK1 concentrated on e^+e^- physics with the CELLO detector at the e^+e^- storage ring PETRA at DESY in Hamburg. The CELLO detector is a large magnetic multipurpose spectrometer. It was initially built by three French (Orsay, Saclay, Paris) and three German groups (KfK and University of Karlsruhe, MPI München, DESY Hamburg). Meanwhile the detector has been improved several times, with a major upgrading in 1982. Also, five new groups from the former PLUTO collaboration have joined in. Another major improvement of the central detector - a new stereo wire chamber SWC - is being prepared. The SWC is ready and will be installed end of 1985.

The Karlsruhe group has several major responsibilities in the CELLO collaboration, including the spokesman (G. Flügge) until end 1984 and the analysis coordinator (W.-D. Apel). Since January 1985 J. Haissinski from Orsay took over the CELLO spokesmanship.

The main activities of the Karlsruhe group during the last year include

- Maintenance of the LAr system and installation of the new LAr-trigger.
- Participation at the construction of the SWC
- Processing and analysis of the CELLO data using the KfK computer center. The main physics topics were: test of QCD in hadronic final states, search for new particles and study of QED reactions.

5.1   HARDWARE ACTIVITIES
5.1.1   CELLO OPERATION AND UPGRADING

PETRA operates actually at a constant beam energy of 21.8 GeV. At this energy CELLO collected a luminosity of about 8 pb^{-1} since the start-up in 1984. The main improvement concerns triggering. A low trigger rate and good efficiency even for low energy events, e.g. single electromagnetic shower or two photon events, with a typical dead time of 10% have been achieved.

The CELLO detector was operational during all the beam periods of PETRA, except in May, when a failure of the helium compressor caused 10 days of data loss.

The upgrading of CELLO progresses due to schedule. For the new central detector, the stereo-wire-chamber, the wire stringing has been finished in may, and it is actually in a test-out phase. The institute participated with 1 man-year. Installation is foreseen during winter shut-down 85/86. The institute and its engineers have taken over the delivering and installation of low voltage power and its control for various   components

like amplifier, TDC and ADC, further the cabling, rack installation, etc.

5.1.2 CALORIMETER DEVELOPMENT

For a TMS-calorimeter R & D work continues. The Fe prototype modul has been finished and became operational in august. Also a track chamber using TMS has been built and is under test.

A TMS purification system has been set-up which is able to purify 50 ℓ/week, approximately. Other liquids are also under study. Successful tests have been made with TMT (tetramethyltin). This liquid is an interesting medium for future electromagnetic calorimeter due to its short radiation length and high density.

Design work for an uranium calorimeter is under way. Depleted uranium from the SNEAK stock has been taken over by the institute, to be used in the test calorimeter and for future applications. Uranium-TMS calorimeter promise to be an ideally compensated hadron calorimeter with optimal energy resolution.

5.2 ANALYSIS OF HADRONIC FINAL STATES
5.2.1 ENERGY DEPENDENCE OF JET-STRUCTURE AND DETERMINATION OF STRONG COUPLING CONSTANT α_s

We analysed multihadronic events obtained with the CELLO detector at the PETRA e^+e^- storage ring. The production of such events is described by a reaction in two steps:

$$e^+e^- \rightarrow q\bar{q}(g) \rightarrow hadrons.$$

Whereas the generation of partons (quarks and gluons) is explained by QCD, the fragmentation of those partons into observable particles can only be described by models. One of the main goals of this analysis is the comparison of different fragmentation models with data.

We first confirmed the predictions of the models for the energy dependence of jet-variables like sphericity and thrust and showed that for the higher energies (34 and 44 GeV CMS) the data contain a fraction of 3-jet and 4-jet events.

One of the most interesting problems in QCD is the determination of the strong coupling constant α_s. A former analysis showed that the different fragmentation models lead to different values for α_s. Other experiments claimed that this model dependence disappears in second order QCD. We

One of the most interesting problems in QCD is the determination of the strong coupling constant α_s. A former analysis showed that the different fragmentation models lead to different values for α_s. Other experiments claimed that this model dependence disappears in second order QCD. We therefore did a determination of α_s using different fragmentation models in second order. This was done by comparing the fraction of 3-jet events obtained in data with Monte Carlo predictions for different α_s values as shown in Fig. 1.

We find a strong model dependence and we see that the scheme for doing energy-momentum conservation has an influence on the results. Using the α_s values at the different energies we can determine the scaling parameter Λ:

TABLE I: Mean Λ for IF, IF1/IF0, SF

Model	Λ (34,44 GeV)	Error (34,44 GeV)
IF	70 MeV	+ 98 MeV - 60 MeV
IF0/IF1	127 MeV	+ 165 MeV - 105 MeV
SF	621 MeV	+ 620 MeV - 460 MeV
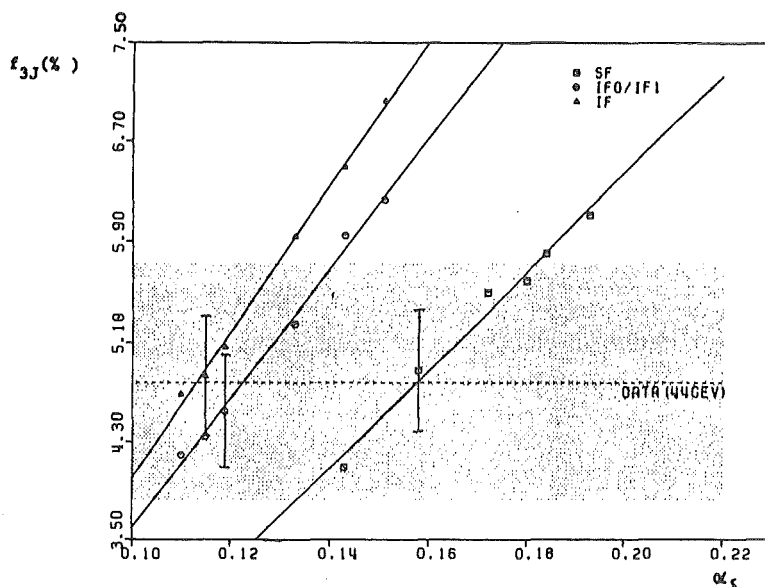
Fig. 1   Fraction of 3-jet events versus α_s for different models (44 GeV)

SF: String fragmentation

IF: Independent fragm. (energy-momentum conservation à la HOYER)

IF0: No energy-momentum conservation

IF1: Energy-momentum conservation à la ALI-ODORICO

In another analysis we studied the particle distribution in 3-jet events and found a light preference (2.0 S.D.) for the SF-model. The contradiction to the results of the α_s determination seems to be solved at the moment by corrections in the SF-model which would lead to smaller α_s values.

5.3   SEARCH FOR NEW PARTICLES

In this section we report on searches for supersymmetric particles, mono-jets and excited leptons. The CELLO detector is particularly well suited for such searches, since it has an almost hermetic coverage for charged and neutral particles and a good lepton identification over a large solid angle.

Most of the results are based on a data sample of 22 pb^{-1} at about 44 GeV, or more precisely:

11.5 pb^{-1} equally distributed between $\sqrt{s}$ = 40 and 46.78 GeV

9.4 pb^{-1} at $\sqrt{s}$ = 44 GeV

1.1 pb^{-1} at $\sqrt{s}$ = 46.3 GeV.

5.3.1   SEARCH FOR SCALAR ELECTRONS AND PHOTINOS IN e^+e^- INTERACTIONS

Here we report on a search for the supersymmetric (1) partner of the electron, the scalar electron $\tilde{e}$, in conjunction with the photino $\tilde{\gamma}$ being the spin 1/2 partner of the photon. Supersymmetry predicts the existence of two types of scalar electrons, namely the $\tilde{e}_L$ with the couplings of the left handed electron and the $\tilde{e}_R$ with the couplings of the right handed electron. These two types may have different masses due to different radiative corrections. In models with global supersymmetry breaking there appears a light spin 1/2 goldstino $\tilde{G}$ (2) and the photino, if massive, is expected to decay into a photon and a goldstino with a lifetime $\tau = (8 \ \pi d^2/m_{\tilde{\gamma}}^5)$ see ref. (3) where d characterizes the scale of supersymmetry breaking. In locally supersymmetric models, however, the goldstino is absorbed into a massive gravitino and the photino is expected to be stable as the lightest supersymmetric particle.

STABLE PHOTINOS

First we assume that the photino as the lightest supersymmetric particle is stable and escapes the detector unobserved. We have searched for the three supersymmetric reactions $e^+e^- \rightarrow \tilde{e}^+\tilde{e}^-$, $e^+e^- \rightarrow (e)\tilde{e}\tilde{\gamma}$, and $e^+e^- \rightarrow \gamma\tilde{\gamma}\tilde{\gamma}$.

A.   SCALAR ELECTRON PAIR PRODUCTION $e^+e^- \to \tilde{e}^+\tilde{e}^-$

If the mass of the scalar electron is below the beam energy it can be pair produced via one photon annihilation or via photino exchange in the t-channel (4) (see diagrams in Fig. 1a). The cross section for this process is given in Ref. (5) for arbitrary photino mass. The scalar electron is expected to decay into photino and electron with lifetime in the order of 10^{-23} sec. The signature for this process is a pair of electrons with missing energy and momentum carried away by the unobserved photinos.

No events were found satisfying the cuts. Fig. 2 shows the region of scalar electron and photino masses excluded at 95% C.L. by this analysis for the case $m_{\tilde{e},L} = m_{\tilde{e},R}$ (contour labelled A). For $m_\gamma = 2$ GeV and $m_{\tilde{e},L} \gg m_{\tilde{e},R}$ the range

$$3.8 \text{ GeV} < m_e < 21.9 \text{ GeV}$$

is excluded at 95% C.L.

B.   SINGLE SCALAR ELECTRON PRODUCTION $e^+e^- \to (e)\tilde{e}\tilde{\gamma}$

In e^+e^- collisions scalar electrons can be produced singly in association with a photino (6). This process, in contrast to pair production, is sensitive to $\tilde{e}$ masses above beam energy. Fig. 1b shows the dominant diagrams contributing to this process. The electron is scattered at very small angles and escapes unobserved down the beam pipe. The decay of the $\tilde{e}$ gives rise to an energetic electron distributed almost isotropically for high $\tilde{e}$ masses plus an unobserved photino. So the signature of this process is one energetic electron in the detector and nothing else.

The dominant background for this single electron signature is radiative Bhabha scattering either with both the other electron and photon at small angles or with one photon escaping through the acceptance gap between barrel and end cap calorimeter. After appropriate cuts we are left with no candidates.

The cross section for single scalar electron production has been computed first by M.K. Gaillard et al. (6) for massless photinos using the equivalent photon approximation (7) to compute the diagrams in Fig. 1b. Meanwhile, the cross section for $\gamma e \to \tilde{e}\tilde{\gamma}$ has been computed for arbitrary photino masses (8). The $\tilde{e}$ and $\tilde{\gamma}$ masses excluded by this experiment are indicated by contour B in Figs. 2a and b.

1A)

1B)

1c)

1D)
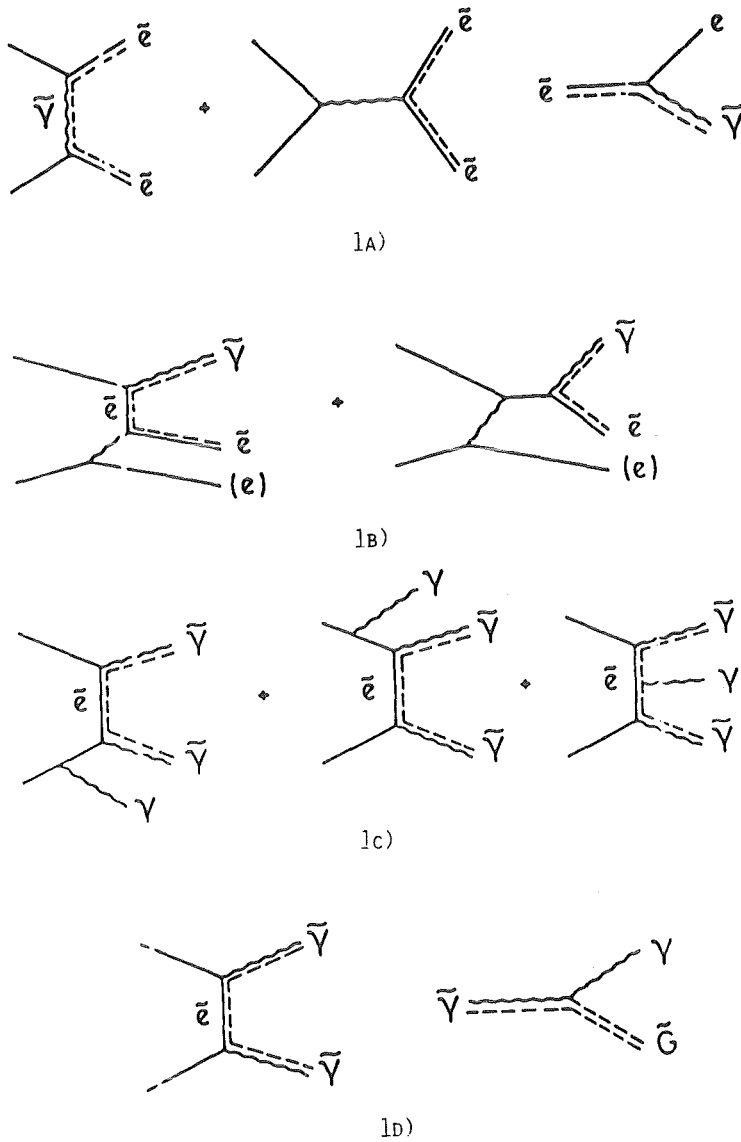
Fig. 1a Diagrams contributing to scalar electron pair production and decay

b Dominant graphs for single scalar electron production if final electron is not observed

c Diagrams for radiative photino pair production. The second diagram is suppressed for large ẽ masses to an additional ẽ propagator.

d Diagram for photino pair production and decay (if unstable)

C.   RADIATIVE PHOTINO PAIR PRODUCTION $e^+e^- \to \gamma\tilde{\gamma}\tilde{\gamma}$

The pair production of two stable (and hence invisible) photinos can be tagged by a Bremsstrahlung photon as suggested first by P. Fayet (9) (see diagrams in Fig. 1c). This process allows to access scalar electron masses above the center of mass energy provided the photino is not too heavy. The signature of this reaction is a single photon in the detector and nothing else. The photon cross section shows a typical Bremsstrahlung behaviour, i.e. the cross section drops rapidly with increasing photon energy and   is

A: $\mathcal{L} = 22.8\,pb^{-1}$, $\sqrt{s}_{max} = 46.8\,GeV$

B,C: $\mathcal{L} = 10.5\,pb^{-1}$, $\langle \sqrt{s} \rangle = 44.4\,GeV$

CELLO
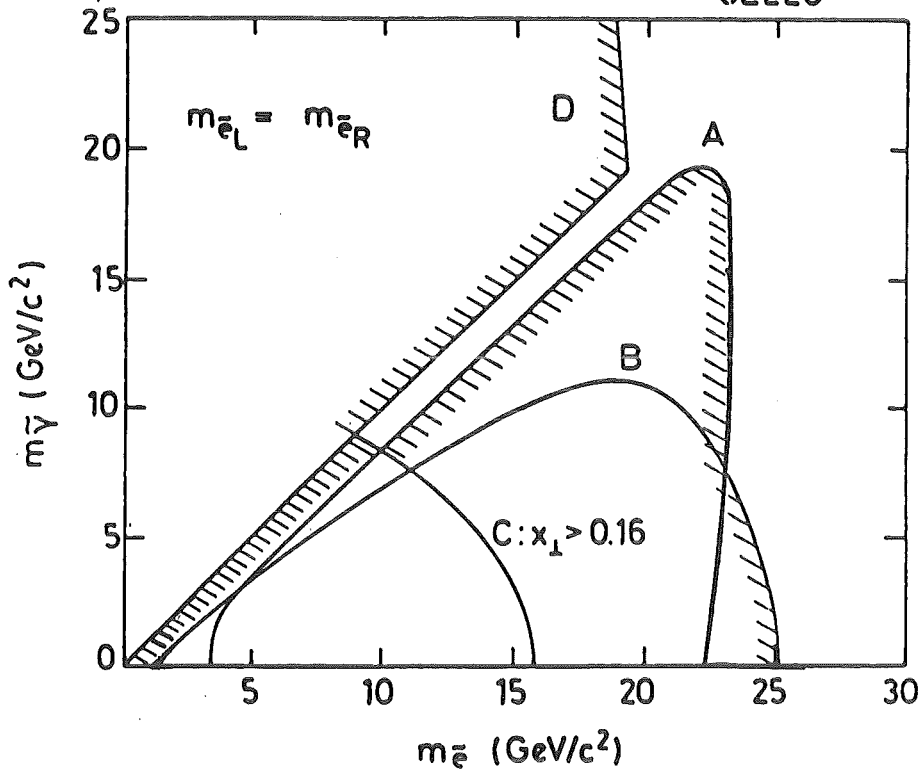
Fig. 2   Scalar electron and photino masses excluded at 95% C.L. by analysis.

A: $e^+e^- \to \tilde{e}+\tilde{e}$, $\tilde{e} \to \tilde{e}\tilde{\gamma}$,

B: $e^+e^- \to (e)\tilde{e}\tilde{\gamma}$,

C: $e^+e^- \to \gamma\tilde{\gamma}\tilde{\gamma}$, and

C: $e^+e^- \to \tilde{e}^+\tilde{e}^-$, $\tilde{e}$ stable

$\} \ m_{\tilde{e},L} = m_{\tilde{e},R}$

strongly peaked along the beam direction. Potential background for the single photon signature are cosmic showers in the calorimeter and the QED processes $e^+e^- \to \gamma ee$ or $\gamma\gamma\gamma$ where two electrons (photons) escape unobserved under small angle.

Applying appropriate cuts to our data sample we are left with 20 events of which 11 are obvious cosmic ray events (pattern of drift chamber hits). 7 events have unreconstructed showers or tracks and 2 events have showers without visible track but with a typical cosmic shower pattern. So after the scan we are left with no candidate.

The number of expected events was determined using the cross section of ref. (10). Contour C in Fig. 2 shows the limit on scalar electron and photino masses obtained from this analysis.

D.   PAIR PRODUCTION OF STABLE SCALAR ELECTRONS

If the scalar electron were the lightest supersymmetric particle it would be expected to be stable or long lived. Pair production of this particle (via the diagrams shown in Fig. 1a) would have a signature very similar to muon pair production leading to an apparent excess in the muon pair cross section. We have measured this quantity to be $R_{\mu\mu} = \sigma_{\mu\mu}/\sigma_{QED} = 1.00 \pm .08$ at $\langle\sqrt{s}\rangle = 44.0$ GeV (see section 5.). Fig. 2 shows the scalar electron and photino masses excluded at 95% C.L. by the absence of an excess in the μ pair cross section.

E.   PAIR PRODUCTION OF UNSTABLE PHOTINOS $e^+e^- \rightarrow \tilde{\gamma}\tilde{\gamma}$, $\tilde{\gamma} \rightarrow \gamma\tilde{G}$

If the photino decays into photon and goldstino the pair production of photinos via scalar electron exchange (9) (see Fig. 1d) would manifest itself in the signature of two photons and missing energy carried away by the goldstinos. Depending on the photino mass one expects two different types of event topologies: for a heavy photino ($>$ a few GeV) the $\tilde{\gamma}$ would decay nearly isotropically in the center of mass system giving rise to two acoplanar photons and missing energy. If the photino is light its decay products would be boosted in the original $\tilde{\gamma}$ direction producing two collinear photons and missing energy. In both cases the photino must be sufficiently

CELLO
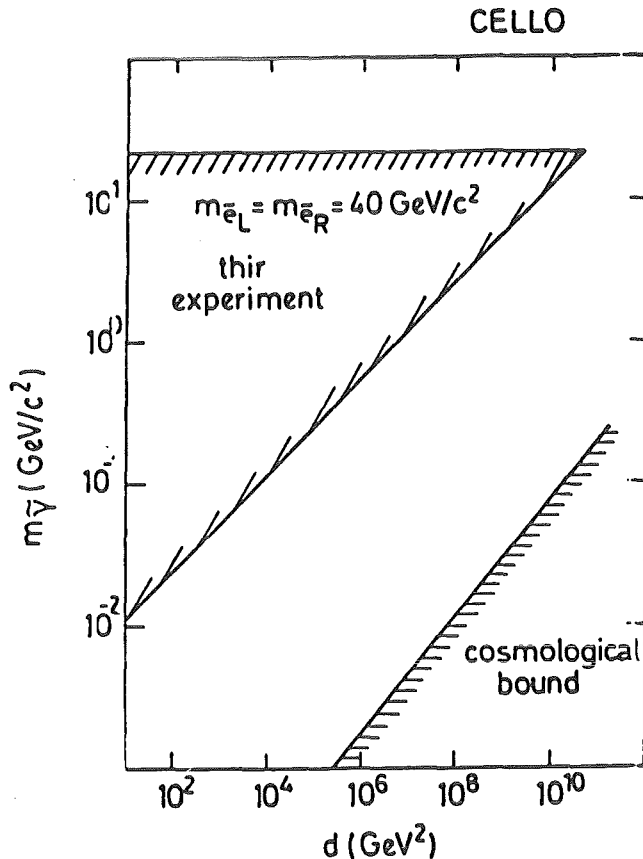
Fig. 3
Photino masses excluded for unstable photinos as a function of the scale breaking parameter d for $m_{\tilde{e},L} = m_{\tilde{e},R} = 40$ GeV. The cosmological bound is discussed in ref. (3).

short lived to decay inside the detector. No candidate events compatible with photino decay were found.

The region in the photino mass and scale breaking parameter d excluded by this analysis is shown in Fig. 3.

In conclusion we have searched for the scalar electron and photino assuming both stable and unstable photinos. Assuming stable photinos we investigated the processes $e^+e^- \rightarrow \tilde{e}^+\tilde{e}^-$, $e^+e^- \rightarrow (e)\tilde{e}\tilde{\gamma}$, and $e^+e^- \rightarrow \gamma\tilde{\gamma}\tilde{\gamma}$. We didn't observe any signal in any of these reactions. Limits were obtained on the scalar electron and photino mass. We can exclude scalar electron masses below 25.0 GeV for $m_{\tilde{e},L} = m_{\tilde{e},R}$ and below 21.2 GeV for $m_{\tilde{e},L} \gg m_{\tilde{e},R}$ assuming a photino mass of 2 GeV. Stable or long lived scalar electrons could be excluded over a wide range of scalar electron and photino masses. Unstable photinos could be excluded for scalar electron masses below $\simeq 100$ GeV and photino masses below $\simeq 20$ GeV assuming $m_{\tilde{e},L} = m_{\tilde{e},R}$ and d = 100 GeV) [2].

(1)   K.A. Gol'fan, E.P. Likhtman, JETP Lett. 13 (1971) 323
        J. Wess, B. Zumino, Nucl.Phys. B70 (1974) 39
        P. Fayet, S. Ferrara, Phys.Rep. 32C (1977) 249
(2)   P. Fayet in "Unification of the Fundamental Particle Interactions",
        Eds. S. Ferrara, J. Ellis, and P. Van Nieuwenhuizen (Plenum Press,
        N.Y., 1980), p. 587
(3)   N. Cabibbo, G.R. Farrar, and L. Maiani, Phys.Lett. 105B (1981) 155
(4)   G. Farrar, P. Fayet, Phys.Lett. 89B (1980) 191
(5)   M. Glück, E. Reya, Phys.Lett. 130B (1983) 423
(6)   M.K. Gaillard et al., Phys.Lett. 116B (1982) 279
(7)   C. Weizsäcker and E.T. Williams, Z. Phys. 88 (1934) 612
(8)   J.A. Grifols and R. Pascual, Phys.Lett. 135B (1984) 319
        M. Glück, Phys.Lett. 129B (1983) 255
(9)   P. Fayet, Phys.Lett. 117B (1982) 460
        J. Ellis and J.S. Hagelin, Phys.Lett. 122b (1983) 303
(10)   J.D. Ware and M.E. Machacek, Phys.Lett. 142B (1984) 301
        T. Kobayashi and M. Kuroda, Phys.Lett. 139B (1984) 208

5.3.2   SEARCH FOR GAUGINOS IN e^+e^- INTERACTIONS

We report on a search for the supersymmetric partner of the intermediate vector bosons (Z^0 and W), called the zino $\tilde{Z}$ and wino $\tilde{W}$.

In electron positron collisions zinos can be produced in association with the supersymmetric partner of the photon, the photino $\tilde{\gamma}$:

$$e^+e^- \rightarrow \tilde{\gamma}\tilde{Z} \tag{1}$$

via t-channel exchange of a scalar electron which is the spin 0 partner of the electron (1) (see Feynman diagram in Fig. 1). Unless otherwise noted, in this paper we take the usual assumption that the photino is the lightest
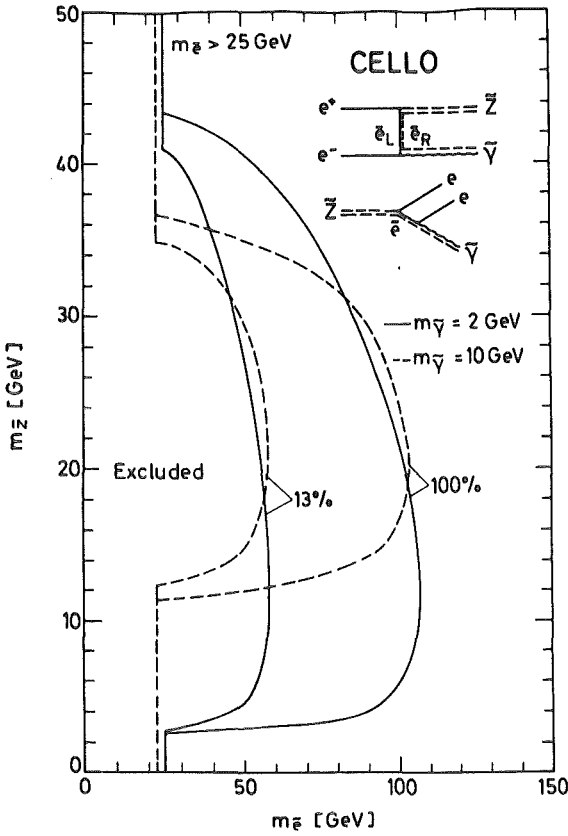
Fig. 1A
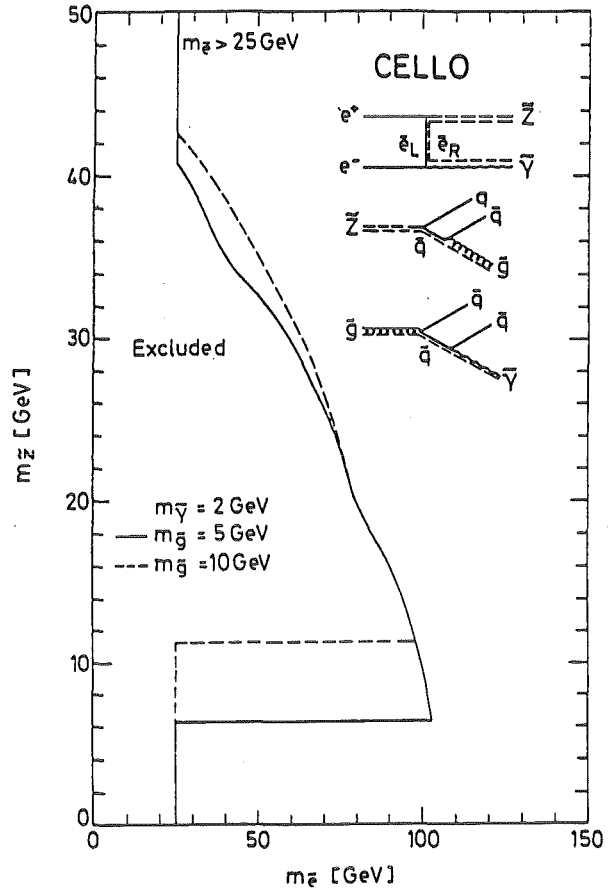
Fig. 1B

Fig. 1   Excluded zino masses (95% C.L.) as a function of the scalar elec-
tron mass. Scalar electron mases below 25 GeV (23 GeV) are excluded
for m_γ = 2 GeV (10 GeV) by our search for scalar electrons (3).

a)   for $\tilde{Z} \to ee\tilde{\gamma}$ with $m_{\tilde{\gamma}}$ = 2 GeV (full lines) and $m_{\tilde{\gamma}}$ = 10 GeV (dashed
lines) for two different branching ratios: BR($\tilde{Z} \to ee\gamma$ ~) = 100%
and 13%, respectively.

b)   For $\tilde{Z} \to q\bar{q}\tilde{g}$ with $m_{\tilde{g}}$ = 5 GeV (full line) and $m_{\tilde{g}}$ = 10 GeV (dashed
line) for a 100% branching ratio into $q\bar{q}\tilde{g}$.

supersymmetric particle and is thus stable and non-interacting in the de-
tector. Zinos are expected to decay (via scalar exchange) into a quark or
lepton pair and a photino (1,2) (see inset in Fig. 1a). However, if the su-
persymmetric partner of the gluon, the gluino $\tilde{g}$, is lighter than the zino,
the latter would decay predominantly into quark, antiquark, and gluino (see
Fig. 1b) due to the stronger hadronic $\tilde{g}\bar{q}q$ coupling. The gluino in turn can
decay into a quark pair and a photino (see Fig. 1b). Note that if the sca-
lar quark or lepton is lighter than the zino the two body decays $\tilde{Z} \to q\tilde{q}$ or
$\tilde{Z} \to l\tilde{l}$ will occur followed by the decay $\tilde{q} \to q\tilde{\gamma}$ or $\tilde{q} \to q\tilde{g}$ and $\tilde{l} \to l\tilde{\gamma}$.

The process $e^+e^- \to \tilde{\gamma}\tilde{Z}$ followed by the decay $\tilde{Z} \to e^+e^-\tilde{\gamma}$ leads to the
signature of an acoplanar electron pair with momentum and energy carried
away by the two unobserved photinos. In analogy, the decay $\tilde{Z} \to q\bar{q}\tilde{\gamma}$ gives

rise to a pair of acoplanar jets which for smaller zino masses are boosted into a single hemisphere giving rise to one handed 'zen' like event topologies. If the zino decays predominantly into $q\bar{q}\tilde{g}$ the average momentum of the decay photino is reduced but the general feature of missing energy and momentum, although less distinctive for high zino masses, is maintained.

Winos can be pair produced in electron positron annihilation

$$e^+e^- \rightarrow \tilde{W}^+\tilde{W}^- \tag{2}$$

via one photon annihilation and via t channel exchange of a scalar neutrino (see inset in Fig. 2). They can decay into $q\bar{q}\tilde{\gamma}$ or $l\nu\tilde{\gamma}$ final states either via W exchange or via scalar quark or lepton exchange (see Fig. 2a), the decay width being proportional to $1/m_w^4$ and $1/m_{scalar}^4$ respectively (3). However, if the scalar neutrino is the lightest supersymmetric particle as discussed for instance in Ref. (4) the wino would decay exclusively into lepton and an (invisible) scalar neutrino with a branching ratio of 1/3 for each lepton generation. In all three cases a clean signature for wino pair production is an acoplanar pair of leptons (not neccessarily of the same flavour) with missing energy and momentum either due to escaping photinos and neutrinos or due to two unobserved scalar neutrinos.

So the general signature of gaugino production and decay in e^+e^- collisions will be jets or lepton pairs with missing energy and momentum. Since the observed longitudinal momentum might be unbalanced due to unseen particles escaping along the beam pipe direction, we consider only missing momentum in the plane transverse to the beam direction and the acoplanarity of the final state particles. In case of two particles the acoplanarity is simply 180 - phi, where phi is the angle in degrees between the momenta of these particles projected on the transverse plane. If the transverse momentum is conserved, the acoplanarity is 0. In case of two jets, the acoplanarity is defined by the projection of the vectorial sum of the momenta of the particles in each jet.

After corresponding cuts no events with acoplanar lepton pairs or single jets survived. A few candidates remained with two acoplanar jets.

Fig. 3 shows an acoplanar jet event which was rejected due to an additional photon hitting the hole tagger. Without this photon the event would be a typical candidate for reaction (1). After the scan we are left with one candidate event recorded before installation of the hole tagger. A Monte Carlo study shows that in our data sample we expect ~ 1.2 events from multihadronic pair production.
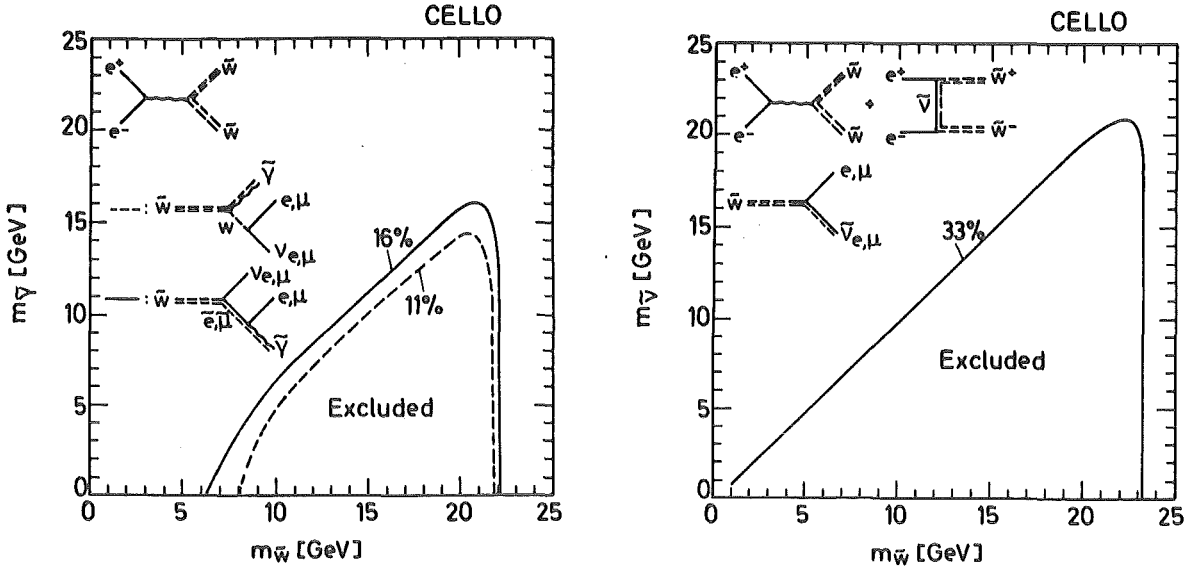
Fig. 2a Wino and photino masses excluded at 95% C.L. assuming a three body
wino decay and a leptonic branching ratio of 16% (full line) as ex-
pected for a wino decaying via scalar exchange and 11% (dashed li-
ne) as expected for a wino decaying via W exchange. The dashed con-
tour also holds for pair production of a charged higgsino decaying
into $l\nu\tilde{\gamma}$, the $\tilde{\gamma}$ being here the lowest lying neutralino mass eigen-
state.

2b Wino and scalar neutrino masses excluded assuming a 33% $\tilde{W} \to l\tilde{\nu}$
branching ratio as expected for $m_\nu < m_W$.

$e^+e^- \to \tilde{\gamma}\tilde{Z}, \tilde{Z} \to ee\tilde{\gamma}$:

For the Monte Carlo simulation of single zino production we used the diffe-
rential cross section given in Ref. (1). We assume that the scalar partners
of the left and right handed electron are degenerate in mass. Making the
assumption that all scalar partners of the quarks and leptons have equal
masses one can make predictions on the branching ratios of the zino into
quarks and leptons. For zino masses above $b\bar{b}$ threshold one would expect BR
$(\tilde{Z} \to ee\tilde{\gamma}) \sim 13\%$ if $m_e > m_z$ and $\sim 3.5\%$ if $m_e < m_z$. The difference is due to
the fact that in the first case the decay width is proportional to the pro-
duct of the $\tilde{Z}e\tilde{e}$ and $\tilde{\gamma}e\tilde{e}$ couplings whereas in the second case only the $\tilde{Z}e\tilde{e}$
coupling enters. Therefore, in the last case the decay channel $\tilde{Z} \to \nu\tilde{\nu}$ also
opens and the hadronic decays are enhanced. Fig. 1a shows the excluded zino
and scalar electron masses assuming 2 GeV and 10 GeV for the photino mass.
Contours are shown for a 100% and 13% zino branching ratio into electrons,
respectively. Scalar electron masses below 25 GeV (23 GeV) are excluded for
$m_\gamma = 2$ GeV (10 GeV) by our search for scalar electrons.
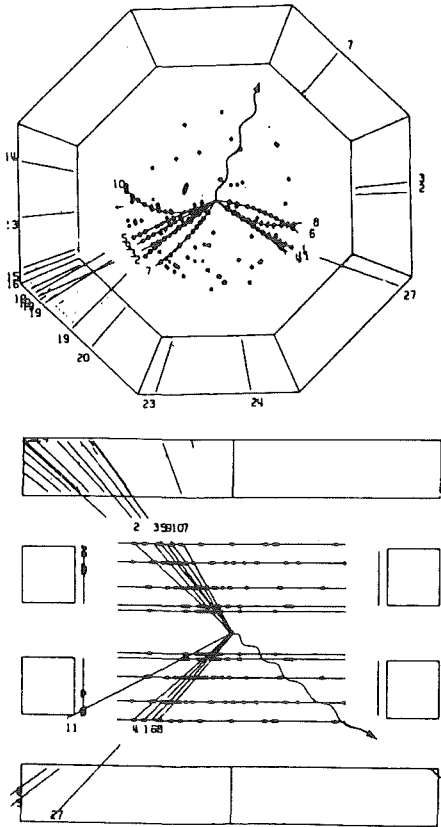
Fig. 3

An acoplanar jet candidate rejected due to a photon hitting the hole tagger counter (waggled line) indicating radiative quark pair production $e^+e^- \to q\bar{q}\gamma$. This event topology is expected for the hadronic decay of a relatively massive zino (m_Z > beam energy), provided the radiative photon is not there.

$e^+e^- \to \tilde{\gamma}Z, \ Z \to q\bar{q}\tilde{g}$:

This decay mode yields results similar to the ones in Fig. 1a.

$e^+e^- \to \tilde{W}^+\tilde{W}^-, \ \tilde{W} \to e\nu\tilde{\gamma} \ \text{or} \ \mu\nu\tilde{\gamma}$:

If the mass of the scalar neutrino is large the dominant amplitude contributing to wino pair production is the one photon annihilation. For an infinitive $\tilde{\nu}$ mass this process is identical to the production of a heavy lepton with a cross section $\sigma_{\tilde{W}\tilde{W}} = (3\beta-\beta^3)/2 \cdot \sigma_{\mu\mu}$. The cross section for wino pair production in e^+e^- collisions is given in Ref. 5. We considered both the wino decay via W exchange and via scalar lepton exchange assuming a scalar lepton mass of 100 GeV. If the wino decay proceeds dominantly via W exchange one expects a branching ratio of 11% into leptons. If the decay via scalar quark or lepton exchange is dominant one expects BR ($\tilde{W} \to l\nu\tilde{\gamma}$) ~ 16% in case all scalar masses are equal. Fig. 2a shows the wino masses excluded as a function of the photino mass for a leptonic branching ratio of 16% (full line) and 11% (dashed line). The limit is nearly independent on the scalar neutrino mass. Note that signature, cross section, and decay of heavy lepton pair production is identical to wino pair production and decay via W exchange. Therefore we can put a lower limit of 21.8 GeV on the mass of a new sequential lepton.

$e^+e^- \rightarrow \tilde{W}^+\tilde{W}^-$, $\tilde{W} \rightarrow e\tilde{\nu}$ or $\mu\tilde{\nu}$:

In case the scalar neutrino is light (4) the wino will decay into lepton and scalar neutrino. Moreover, the production cross section becomes large due to large $\tilde{\nu}$ exchange amplitude and the detection efficiency is generally larger than for three body wino decay due to a harder lepton spectrum. Therefore we can exclude essentially the whole kinematical allowed domain for wino masses below 23.2 GeV as indicated in Fig. 2b.

Until now we have assumed that we deal with a pure Z and $\tilde{W}$. In general, however, the neutral gauge bosons $\tilde{\gamma}$ and Z may mix with the two or more neutral higgsinos $\tilde{h}^0_1$ and $\tilde{h}^0_2$ (1) forming mass eigenstates, generally called neutralinos. Similarily, the $\tilde{W}$ and the charged higgsino $\tilde{h}^\pm$ may mix forming charginos (3).

Considering the general case of neutralino production $e^+e^- \rightarrow XX'$, X and X' being the two lowest lying neutralino mass eigenstates, followed by the decay $X' \rightarrow f\bar{f}X$ one finds that the production cross section is essentially proportional to the gaugino content in X and X', since the higgsino coupling (being proportional to the fermion mass) to electrons is small. As long as the gaugino component in X' is large enough for $e^+e^- \rightarrow XX'$ events to have an observable cross section, the X' decay is dominated by its gaugino component due to the small $\tilde{h}^0f\bar{f}$ coupling (1). Therefore, the $\tilde{\gamma}Z$ production cross section is lowered by a possible higgsino admixture, while the Z decay properties remain essentially unchanged.

If the wino in reaction (2) is replaced by a charged higgsino only the one photon annihilation amplitude contributes to production. Because of the small higgsino fermion coupling a higgsino is expected to decay exclusively via W exchange into the lowest lying neutralino (3) with a leptonic branching fraction of 11% independent of the supersymmetric particle mass spectrum. So the dashed contour in Fig. 2a holds for chargino pair production independent of the wino content of the lowest lying chargino mass eigenstate.

In conclusion we have searched for unusual lepton and quark pairs with missing energy and momentum. No signal has been found. This excludes copious production of SUSY type charginos or neutralinos within the PETRA energy range. The upper limits on the visible cross sections for acoplanar jets and acoplanar lepton pairs have been compared with specific models of wino - and zino production. Typical limits on the mass of the zino are 35 - 40 GeV assuming the scalar electron to be lighter than 50 GeV. Lower limits on the mass of the wino are between 21.8 GeV and 23.2 GeV depending on the wino decay mechanism. The lower mass limit of 21.8 GeV also holds for a charged higgsino and a new sequential heavy lepton. Similar limits have

been obtained by other PETRA experiments (6,7).

(1) E. Reya, Phys.Lett. 133B (1983) 245

(2) D.A. Dicus, S. Nandi, W.W. Repko, and X. Tata, Univ. of Texas at Austin, DOE-ER-03992-551 (1984)

(3) J.M. Frere and G.L. Kane, Nucl.Phys. B223 (1983) 331

(4) L.E. Ibanez and C. Lopez, Nucl.Phys. B233 (1984) 511
    J.S. Hagelin, G.L. Kane, and S. Raby, Nucl.Phys. B241 (1984) 638

(5) S. Dawson, E. Eichten, C. Quigg, FERMILAB-Pub-83/82-THY and LBL-16540, revised version October 1984

(6) Jade Coll., W. Bartel et al., Phys.Lett. 146B (1984) 126
    Jade Coll., W. Bartel et al., DESY Rep. 85-60 (1985)

(7) Mark J Coll., B. Adeva et al., Phys.Rev.Lett. 53 (1984) 1806

5.3.3 EXPERIMENTAL LIMIT ON MONOJET PRODUCTION IN e^+e^- ANNIHILATION

Recently the UA1 Collaboration (1) reported the observation of a novel type of events in $p\bar{p}$ collisions, containing a single narrow jet of particles ("monojet") associated with a large missing transverse energy. They found no conventional explanation for such events within the Standard Model.

Many speculations about the origin of these events have been put forward. They can be grouped into two categories: (i) the monojets originate from new types of particles (e.g. composite, coloured or supersymmetric particles), or (ii) the monojets arise from unusual decays of neutral vector bosons (Z^0). The latter hypothesis has been put forward by Glashow and Manohar (2), who pointed out that in such a case, the monojets should also be observable in e^+e^- annihilation. With a branching ratio of Z^0 into monojets of a few percent as suggested by the $p\bar{p}$ data, the monojet production cross section is in the order of 0.5 pb at a center of mass energy of 44 GeV. Around this energy we have an integrated luminosity of about 22 pb^{-1}. Therefore, such a clean signature as a monojet should be observable.

Monojets were defined as events having one hemisphere in the $r\phi$ projection without charged particles and with an electromagnetic energy below 0.5 GeV.

Since no genuine monojets were observed, we can obtain an upper limit on the monojet cross section.

Fig. 1 shows the 95% C.L. upper limit on the monojet cross section and the branching ratio of Z^0 into monojets. For masses m_{X_2} below 15 GeV the 95% confidence level upper limit is below the monojet cross section expected for a branching ratio of 3%, which is the order of magnitude for the monojets observed at the $p\bar{p}$ collider.

In terms of the specific model of ref. 2 the monojets arise from the decay of Z^0 into 2 neutral Higgs bosons, h_1 and h_2. Similar to Fig. 1 the experimental 95% C.L. upper limit on the cross section is below the
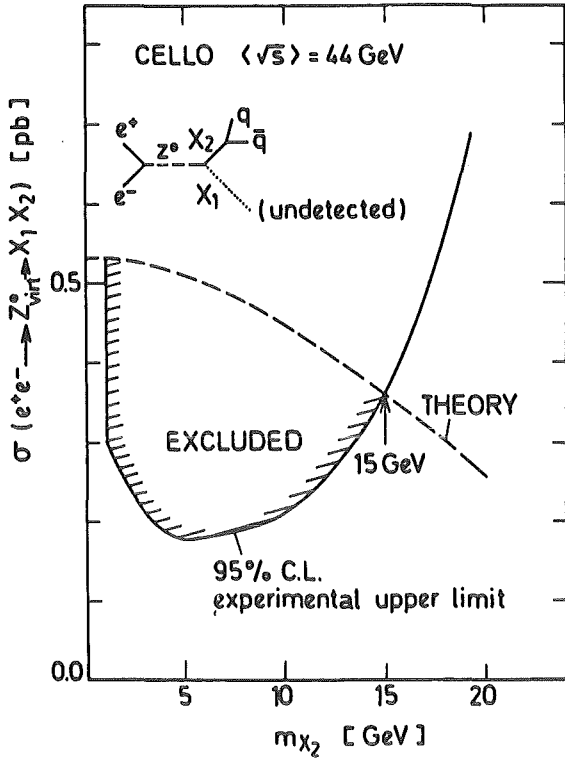
Fig. 1
The monojet cross section as a function of the mass of the heaviest of the two hypothetical particles X_1 and X_2. X_1 is assumed to be massless and escapes the detector without interactions and X_2 is assumed to fragment randomly into the kinematically allowed $q\bar{q}$ pairs. The dashed curve is calculated with BR $(Z^0 \to X_1 + X_2) = 3\%$.

theoretical cross section for masses between 1.2 and 13.6 GeV, thus excluding h_2 masses in this range. The Higgs masses well above $b\bar{b}$ threshold ($\sim$ 10 GeV) give an averaged charged multiplicity above 7. This seems too high to explain the UA1 monojets, for which the observed charged multiplicity is less than 5 and the charged particle invariant mass is also small (< 3.1 GeV).

A similar calculation can be performed if the neutral Higgs bosons are replaced by their supersymmetric counterparts, the Higgsinos, denoted by χ_1 and χ_2. The mass of χ_1 is assumed to be 0, so that it will be stable and escape the detector without interactions. χ_2 is assumed to decay into χ_1 plus a $q\bar{q}$ pair via virtual Z^0-exchange, for which we used the matrix element given in Ref. 3. The direct 2-body decay of χ_2 is forbidden, if we assume that the supersymmetric particles have their own conserved quantum number. In the limit of massless spin 1/2 Higgsinos and assuming no mixing with the supersymmetric partners of the photon and Z^0 but a maximum mixing between the Higgsions, the total cross section is four times bigger than the corresponding cross section for Higgs bosons production (3) and the differential cross section is proportional to $1 + \cos^2\theta$ instead of $\sin^2\theta$. The hadronic final states are determined by the coupling of quarks to the Z^0 and the available phase space, which leads to a hadronic branching ratio of 50-70% for χ_2 masses between 2 and 20 GeV. The theoretical Higgsino cross section is above the experimental 95% C.L. upper limit for χ_2 masses

CELLO $\langle\sqrt{s}\rangle = 44\,GeV$

$\sigma(e^+e^- \to Z^0_{virt} \to X_1 X_2)$ [pb]

2.0

THEORY

EXCLUDED / 19.5 GeV

95% C.L.
experimental upper limit

0.0

5   10   15   20

m_{X_2} [GeV]
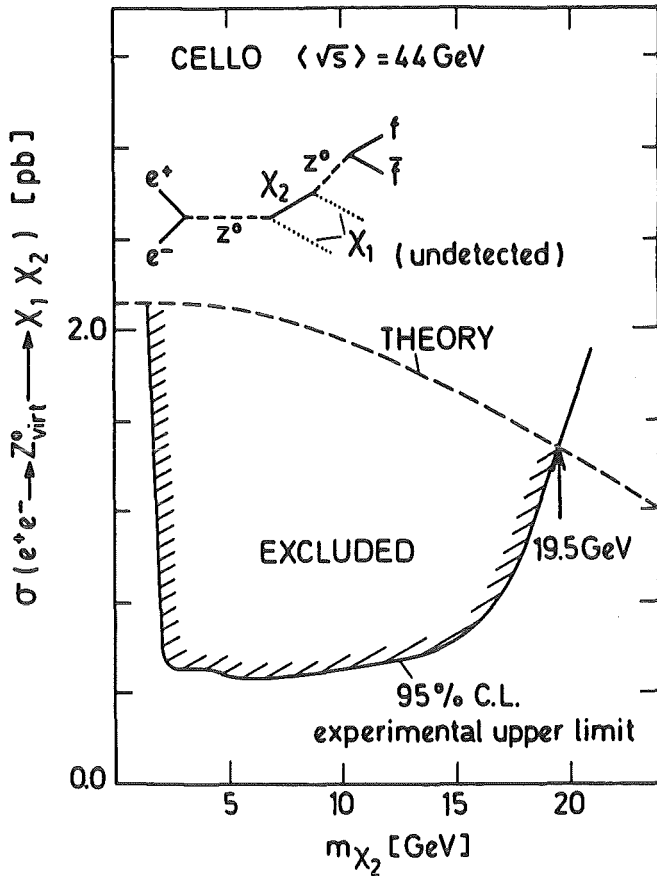
Fig. 2

As in Fig. 1 with X_1 and X_2 replaced by neutral Higgsinos. At values of m_{X_2} this cross section is four times larger than in Fig. 1 for the mixing conditions described in the text.

between 1.5 and 19.5 GeV (see Fig. 2), thus excluding X_2 masses in this range.

In conclusion, the non-observation of monojets in e^+e^- annihilation makes it unlikely that the monojets observed in $\bar{p}p$ collisions originate from unusual Z^0 decays. Similar conclusions have been reached by other collaborations (4).

(1)   UA1 Collaboration, G. Arnison et al., Phys.Lett. 139B (1984) 115
(2)   S.L. Glashow and A. Manohar, Phys.Rev.Lett. 54 (1985) 526
(3)   H. Baer, K. Hagiwara, and S. Komamiya, Phys.Lett. 156B (1985) 117
(4)   HRS Coll., C. Akerlof et al., Phys.Lett. 156B (1985) 271
        JADE Coll., W. Bartel et al., Phys.Lett. 155B (1985) 288
        MAC Coll., W.W. Ash et al., Phys.Rev.Lett. 54 (1985) 2477
        MARK II Coll., G. Feldman et al., Phys.Rev.Lett. 54 (1985) 2289

5.3.4   EXCITED LEPTON SEARCH

Excited lepton states are expected in models in which leptons are composite particles (1). In e^+e^- collisions such excited states could be produced either in pairs due to the normal gauge couplings, or singly due to a radiative transition between a normal and an excited lepton (2). Furthermore, the existence of an excited electron would modify the photon pair production cross section by introducing an additional propagator. The $l^*l\gamma$ coupling needed in the two latter cases is usually described by the following

TABLE I   Data sample for the various processes studied in l* search
           (* see text)

reaction	luminosity (pb^{-1})	$\sqrt{s}$ (GeV)	events	QED prediction
ee → eeγ	29.2	33.0 - 46.8	239	230
ee → eeγγ	29.2	33.0 - 46.8	2	*
ee → eγ(e)	14.0	44.0 - 46.8	410	420
ee → μμγ	32.6	33.0 - 46.8	26	25
ee → μμγγ	32.6	33.0 - 46.8	2	*
ee → ττγ	21.6	40.0 - 46.8	8	11
ee → ττγγ	21.6	40.0 - 46.8	1	*
ee → γγ	28.9	33.0 - 46.8	2533	*

gauge invariant effective Lagrangian

$$\mathcal{L}_{eff} = \lambda e/2m_{1*}\ \bar{1}^*\ \sigma_{\mu\nu}\ 1\ F^{\mu\nu} + h.c. \qquad [1]$$

where λ is a free parameter characterizing the strength of the l*1γ coupling.

In order to constrain the masses and the l*1γ coupling strength of excited leptons, we investigated the following three signatures:

1)   pair production of l*

        ee → 11γγ   1 = e, μ, τ

2)   single production of l*

        ee → 11γ   1 = e, μ, τ

3)   propagator effect in e*

        ee → γγ.

The center of mass energy varied from 33. to 46.8 GeV. The total integrated luminosity is about 30 pb^{-1}. Table I summarizes the data used for each analyzed reaction, together with the expectation from QED.

We observe 2 eeγγ and 2 μμγγ events. Excited leptons which could be pair-produced would show up as equal invariant mass lepton-photon pairs. None of the four events is compatible with this hypothesis.

For the reaction ee → γγ, two back-to-back photons with an acolinearity angle smaller than 15^0 are required. We observe 2533 events. The luminosity being taken from the measured large angle Bhabha scattering process, the measured cross sections are $\sigma_{exp}/\sigma_{QED}$ = 0.96 ± 0.04 at a center of mass energy of 34 GeV and 0.98 ± 0.05 in an energy scan between 40 and 46.8 GeV.

CELLO

CELLO
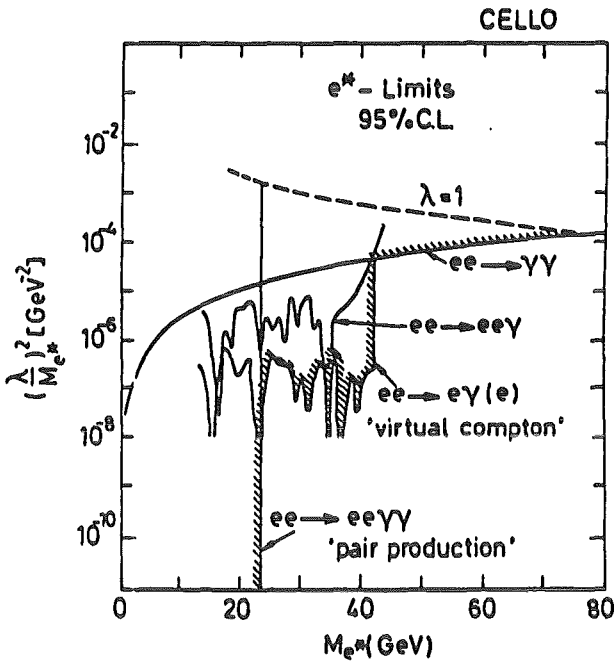
Fig. 1   Limits on the coupling
         strength λ and the mass
         of an excited electron e*
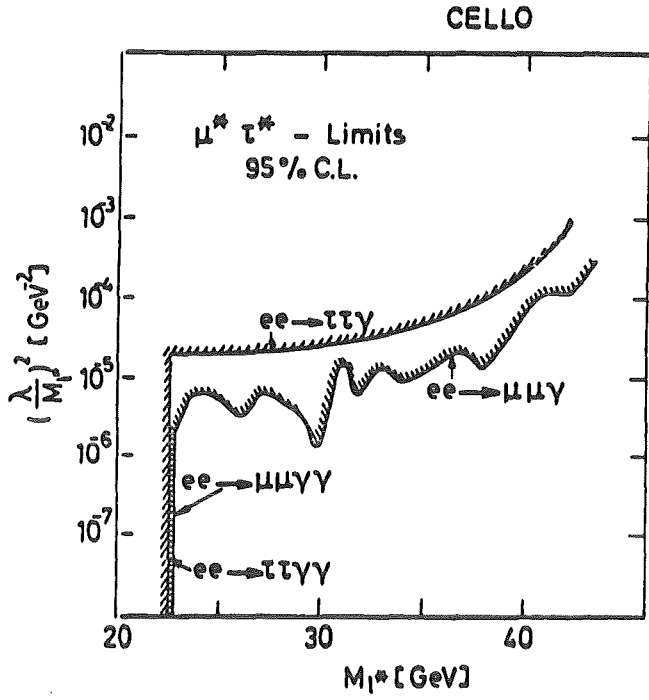
Fig. 2   Limits on the coupling
         strength λ and the mass of
         excited leptons μ* and τ*

In the pair production the β threshold factor allows to put limits on excited leptons close to highest beam energies, independent of the coupling strength λ. 95% C.L. lower limits for e*, μ* and τ* production of 23.0, 23.0 and 22.7 GeV are determined.

In order to set upper limits on the coupling strength of the effective Lagrangian (1) in case of single l* production the formulae of Ref. (1) - (3) are used. Concerning the reactions ee → eeγ and ee → μμγ we derive 95% C.L. upper limits for $(\lambda/m_{l*})^2$ from the invariant mass distribution after a bin-to-bin substraction of the known QED contributions. In the reaction ee → ττγ upper limits are determined from the total number of observed events only. In order to derive upper limits on $(\lambda/m_{e*})^2$ from the 'Virtual Compton' we use a maximum likelihood method considering only the shape of the invariant mass distributions.

Concerning the e* propagator effect in the reaction ee → γγ, we derived a 95% C.L. lower limit for the conventionally used Λ_+ cut off parameter of 76 GeV in a fit to the polar angle distribution, where Λ is related to λ in Lagrangian [1]

$$\lambda = m_{e*}^2/\Lambda_+^2 \ .$$

Figs. 1 and 2 summarize the limits derived from the various analyzed reactions.

In conclusion, we obtain good agreement with the expectation from known QED procecces. Up to the highest PETRA energies of 46.8 GeV no indication for an excited lepton, electron, muon or tau is observed. Lower limits of 23.0 GeV for the pair production of e^* and μ^* and 22.7 GeV of τ^* are derived. The coupling strength λ for the $l^*/l\gamma$-transition for a hypothetical e^*, μ^* and τ^* is restricted up to masses of about 43 GeV. A Λ-cut off parameter of 76 GeV at 95% C.L. is determined from the reaction ee $\rightarrow$ $\gamma\gamma$.

(1)   H. Terazawa et al., Phys.Lett. 112B (1982) 387
(2)   F.E. Low, Phys.Rev.Lett. 14 (1965) 238
        A. Litke, Thesis Harvard 1970, unpublished
(3)   A. Courau and P. Kessler, LAL/85-01 (1985)

5.4   STUDY OF ELECTROWEAK INTERACTION
5.4.1   MEASUREMENT OF THE MUON PAIR AND TAU PAIR ASYMMETRY IN
e$^+$e$^-$ ANNIHILATION AT 39.8 $\leqslant$ $\sqrt{s}$ $\leqslant$ 46.6 GeV

The reactions e$^+$e$^-$ $\rightarrow$ $\mu^+\mu^-$ and e$^+$e$^-$ $\rightarrow$ $\tau^+\tau^-$ have been studied at center of mass energies between 39.8 and 46.6 GeV with the CELLO detector at the PETRA e$^+$e$^-$ collider. We present here preliminary results on the charge asymmetry for muon pair and tau pair production.

The polar angular distribution was studied for the complete set of data at $\langle\sqrt{s}\rangle$ = 43.9 GeV. Because of the term due to the interference between γ and Z^0 exchange, this distribution is asymmetric and can be expressed as:

$$f(\cos\,\theta) = C(1 + \cos\,\theta^2 + b\,\cos\,\theta).$$

The parameter b gives a direct measurement of the total asymmetry over the whole cos θ range

$$\langle A_\ell\rangle = 3\,b\,/\,8.$$

The charge asymmetry is related to the axial coupling constant of the lepton ℓ (ℓ = μ, τ) to the neutral intermediate boson Z^0 in the following way:

$$\langle A_\ell\rangle = 3/2\,(\chi\,a_e\,a_\ell)$$

where
$$\chi = \frac{\rho \, G_F \, M_Z^2}{8 \sqrt{2} \, \pi \, \alpha} \cdot \frac{s}{s - m_Z^2}$$

G_F is the Fermi coupling constant and $\rho = M_Z^2/(M_Z^2 \cos^2 \theta_w)$.

In the G.S.W. model (1) ρ is equal to 1, and a_ℓ is equal to -1. Taking $M_Z = 93$ GeV/c^2, the value of the asymmetry at the Born level is -16.7% at $\sqrt{s} = 43.9$ GeV, and for $|\cos \theta| \leq 1.0$.

For the μ we get an asymmetry value after correcting for detector acceptance and after applying QED and electroweak radiative corrections of

$$\langle A_\mu \rangle_{corr} = (-18.3\% \pm 5.9)\% \text{ for } |\cos \theta| \leq 1.$$

Using this value and

$$a_e = 1.0 \pm .1 \quad \text{(ref. 2)}$$

for the electron axial coupling we obtain for a_μ

$$a_\mu = -1.09 \pm .35.$$

For the τ we obtain

$$\langle A_\tau \rangle_{corr} = (-15.4 \pm 5.2(\text{stat})^{+0}_{-1}.1(\text{syst}))\%$$

which is in good agreement with the prediction of the standard model. It agrees also very well with results from the other PETRA groups (3). That leads to an axial coupling constant of the τ of:

$$a_\tau = -.92 \pm .32.$$

After combining with our previous value $a_\tau = -1.1 \pm .56$ at 34 GeV (4) we get

$$a_\tau = -.96 \pm .28.$$

The axial coupling constants a_μ and a_τ are compatible with the hypothesis of lepton universality.

(1) S.L. Glashow, Nucl.Phys. 22 (1961) 579; Rev.Mod.Phys. 52 (1980) 539
    A. Salam, Phys.Rev. 127 (1962) 331; Rev.Mod.Phys. 52 (1980) 525
    S. Weinberg, Phys.Rev.Lett. 19 (1967) 1264; Rev.Mod.Phys. 52 (1980) 515
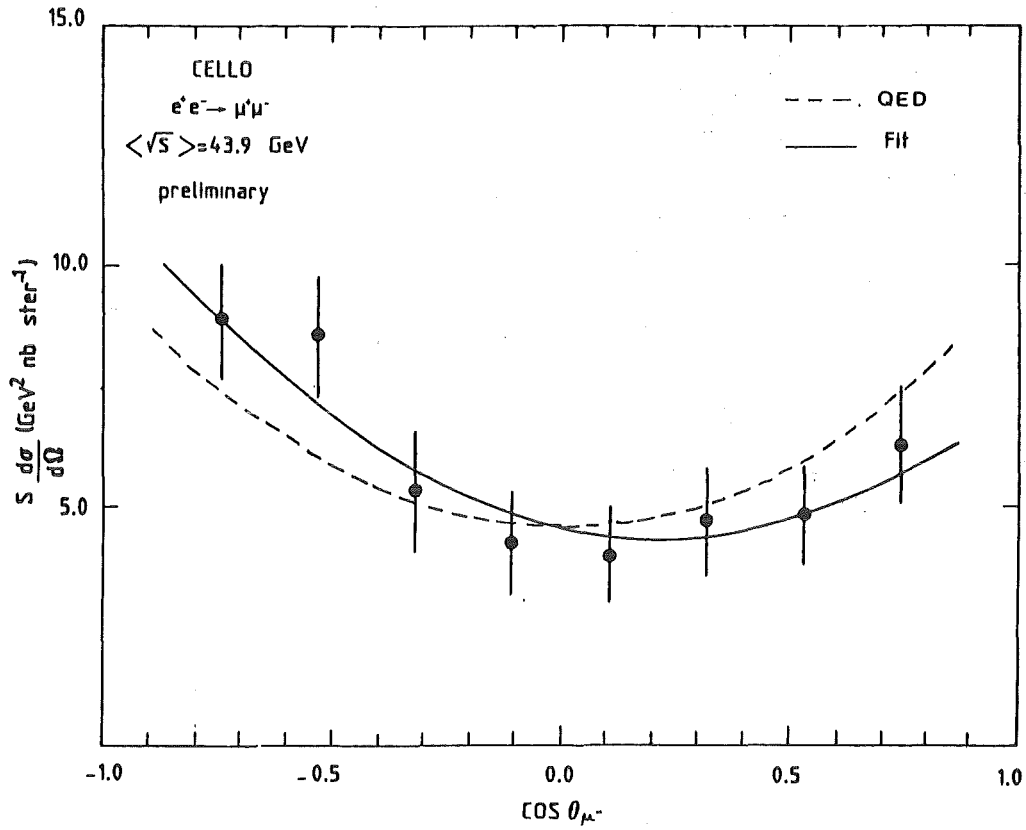
Fig. 1 $e^+e^- \rightarrow \mu^+\mu^-$ corrected angular distribution. Full line shows result of fit.
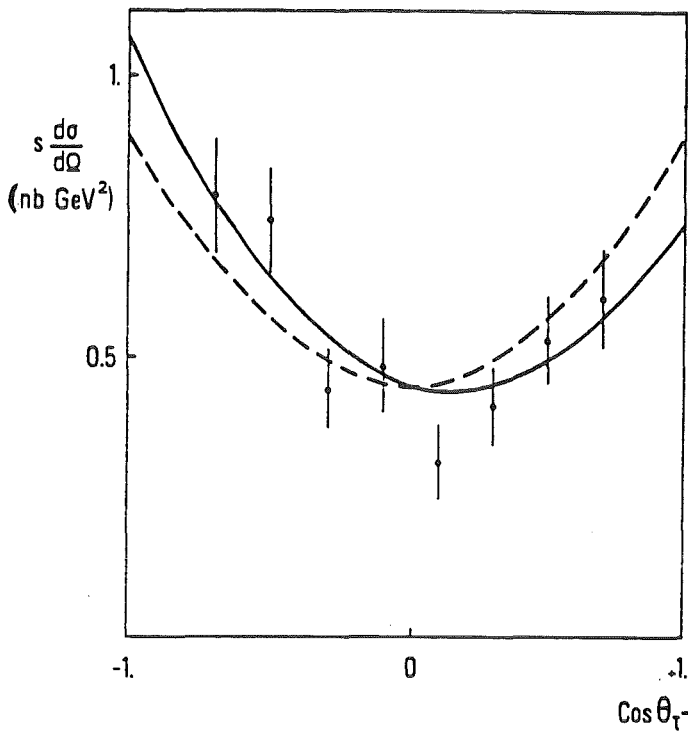
Fig. 2
$e^+e^- \rightarrow \tau^+\tau^-$ angular distribution. Full line shows result of fit.

(2) R.H. Hesterberger et al., Phys.Rev.Lett. 44 (1980) 635

(3) JADE Coll., Z.Phys. C Particles and Fields 26 (1985) 507-513
MARK J Coll., M.I.T. Technical Report 144 (1985), submitted to P.R.L.
TASSO Coll., private communication

(4) H.J. Behrend et al., CELLO Collaboration, Phys.Lett. 114B (1982) 282

5.4.2   AN INVESTIGATION OF THE PROCESSES $e^+e^- \to \mu^+\mu^-\gamma$ AND $e^+e^- \to e^+e^-\gamma$

The reactions

$$e^+e^- \to \mu^+\mu^-\gamma \qquad\qquad [1]$$

and

$$e^+e^- \to e^+e^-\gamma \qquad\qquad [2]$$

have been studied with the CELLO detector at the PETRA storage ring. These reactions should be well described by QED calculations (1,2) of order α^3. Data have been collected over a wide energy range, from $\sqrt{s}$ = 14 GeV to 46.8 GeV, the maximum center of mass energy reached by PETRA.

A complete description of processes [1] and [2] by QED to order α^3 is available (1) and widely used Monte Carlo generators exist. We have used such programs (3) and have also performed an independent Monte Carlo generation of events from reaction (2) which should be valid for hard radiation. We have included initial and final state radiative corrections to order α^4 following the prescription of Tsai (4), and estimate our knowledge of the absolute normalization to be $\pm 10\%$.

All information concerning the reaction ee $\to \ell\ell\gamma$ for unpolarised beams can be obtained from the Dalitz plot $(M^2_{\ell\ell}, (M^2_{\ell\gamma})_{low}, (M^2_{\ell\gamma})_{high})$, the orientation of the event plane with respect to the beam axis and the orientation of the event within this plane. We first consider the Dalitz plot population.

Since we are interested in the possibility of new phenomena, cuts are applied in order to eliminate the regions where the QED cross section is largest, namely $M^2_{\ell\ell}/s > .01$ and $M^2_{\ell\gamma}/s > .01$. These regions correspond to enhancements in the amplitudes for initial and final state radiation, respectively. Fig. 1 presents the experimental Dalitz plot distribution group the data in three energy domains and use dimensionless variables. Consequently the Dalitz plot population should be energy-independent up to an overall normalization factor. It should be emphasized that our kinematic knowledge of the events is such that the uncertainty on the Dalitz plot is very small $\Delta M^2_{\ell\gamma}/s < 0.01$. To compare with QED, 3 regions are defined and their respective polulation is compared to the corresponding QED   predic-
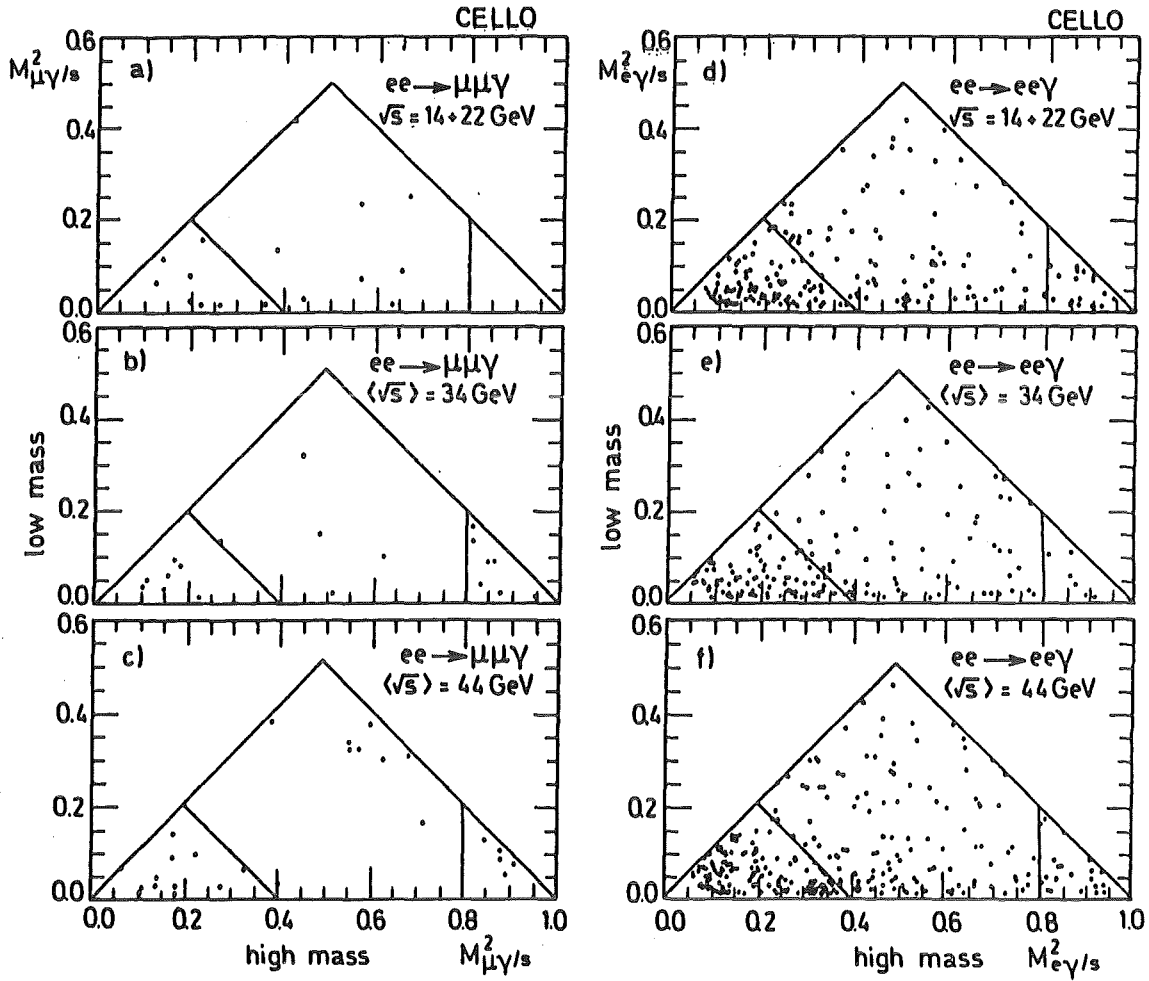
Fig. 1a,b,c,d,e,f:

The Dalitz plot population for the reactions $e^+e^- \to \mu^+\mu^-\gamma$ and $e^+e^- \to e^+e^-\gamma$ in the three different energy regions.

tions in Table I. Estimated background contributions are also included.

Good agreement with QED is observed in all regions except or reaction (1) in region III of Figs. 1b and 1c ($\sqrt{s} > 33$ GeV; $(M^2_{\mu\gamma})_{high}/s > 0.8$), where we observe 12 events and expect 3.9. In order to access the overall statistical significance of the observed enhancement independent of the boundary between regions II and III, we directly compared the experimental $\mu\gamma$ mass spectrum to the expected QED distribution in these regions. A Kolmogorov test gives a probability rise to 2%, when the uncertainty in the mass determination is stretched in the direction most favourable to QED.

The lepton-photon mass distributions from regions II and III are shown in Fig. 2: no significant structure is observed in either the $\mu\gamma$ or the $e\gamma$ mass distributions.

In conclusion, we have measured the properties of the radiative processes $ee \to \mu\mu\gamma$ and $ee\gamma$. We find that QED provides a proper description

TABLE I: Population of the Dalitz plot in 3 regions

Reaction	$\sqrt{s}$ (GeV)			Region I	Region II	Region III
ee → μμγ	14 + 22		data	8	9	0
			MC	7.0	7.4	1.4
			background	< 0.1	< 0.1	< 0.01
	33.1-36.7		data	7	5	7
			MC	8.1	8.7	1.6
			background	< 0.1	< 0.1	< 0.01
	40 -46.8		data	12	9	5
			MC	12.2	12.5	2.3
			background	< 0.1	< 0.1	< 0.01
ee → eeγ	14 + 22		data	80	76	17
			MC	90.1	71.4	9.7
			background	< 0.1	< 0.1	< 0.1
	33.0-36.7		data	98	85	8
			MC	99.4	77.9	10.1
			background	< 0.1	< 0.1	< 0.1
	40 -47.8		data	144	124	22
			MC	161.2	126.4	16.3
			background	< 0.1	< 0.1	< 0.1

region I	$.6 < M^2_{\ell\ell}/s < .9$
region II	$M^2_{\ell\ell}/s < .6$ and $M^2_{\mu\ell}/s < .8$
region III	$M^2_{\ell\gamma}/s > .8$
in addition	$M^2_{\mu\gamma}/s > .01$ and $M^2_{\mu\mu}/s > .01$

of our data, except for an excess of events for $\sqrt{s} > 33$ GeV and $M^2_{\mu\gamma}/s > 0.8$. The probability that this excess is due to a statistical fluctuation is at the 10^{-2} level.

(1) F. Berends, K. Gaemers, R. Gastmans, Nucl.Phys. B57 (1973) 381;
    Nucl.Phys. B63 (1973) 237
    F. Berends, R. Kleiss, Nucl.Phys. B177 (1981) 237
    F. Berends, R. Kleiss, S. Jadach, Nucl.Phys. B202 (1982) 63
(2) F. Berends, K. Gaemers, R. Gastmans, Nucl.Phys. B68 (1974) 541
    F. Berends, R. Kleiss, Nucl.Phys. B228 (1983) 537
(3) The Monte Carlo generators were based on the paper of
    F. Berends, R. Kleiss and S. Jadach, quoted in (1), and
    F. Berends and R. Kleiss, quoted in (2)
(4) Y.S. Tsai, SLAC-PUB 3129 (1983)
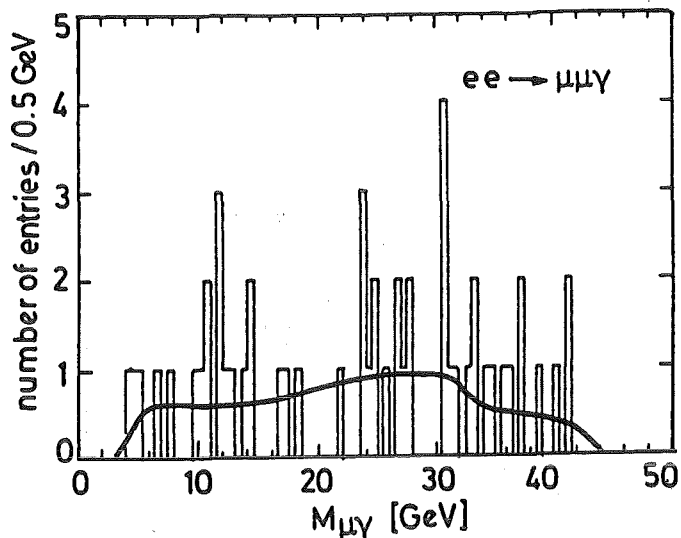
Fig. 2
The distribution of the lepton-photon invariant masses for $\sqrt{s} > 33$ GeV corresponding to regions II + III in Fig. 1. The curves are the prediction from the QED Monte Carlo calculations.
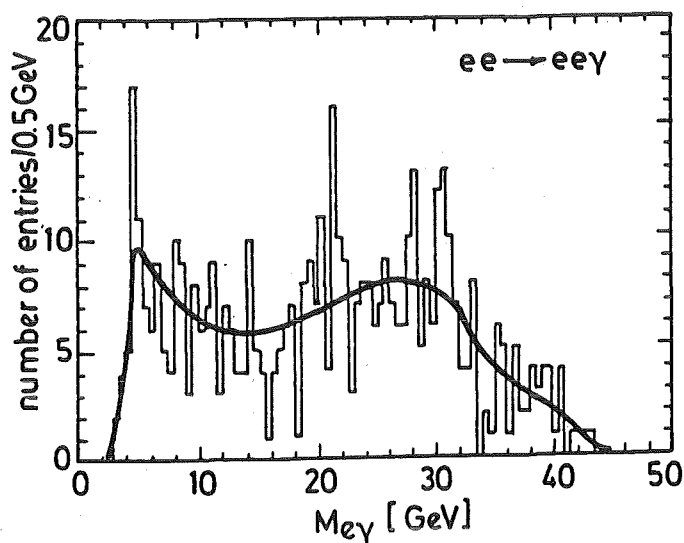
5.4.3 A STUDY OF FINAL STATES WITH FOUR CHARGED LEPTONS IN e^+e^- INTERACTIONS

Results of a search for 4 lepton events in the CELLO detector at the PETRA collider are presented.

The following reactions have been considered:

$$e^+e^- \rightarrow e^+e^- \, e^+e^- \tag{1}$$

$$e^+e^- \rightarrow e^+e^- \, \mu^+\mu^- \tag{2}$$

$$e^+e^- \rightarrow \mu^+\mu^- \, \mu^+\mu^- \tag{3}$$

$$e^+e^- \rightarrow e^+e^- \, \tau^+\tau^-. \tag{4}$$

Four lepton final states from e^+e^- interactions are examples of order α^4 QED processes (see graphs in Fig. 1).
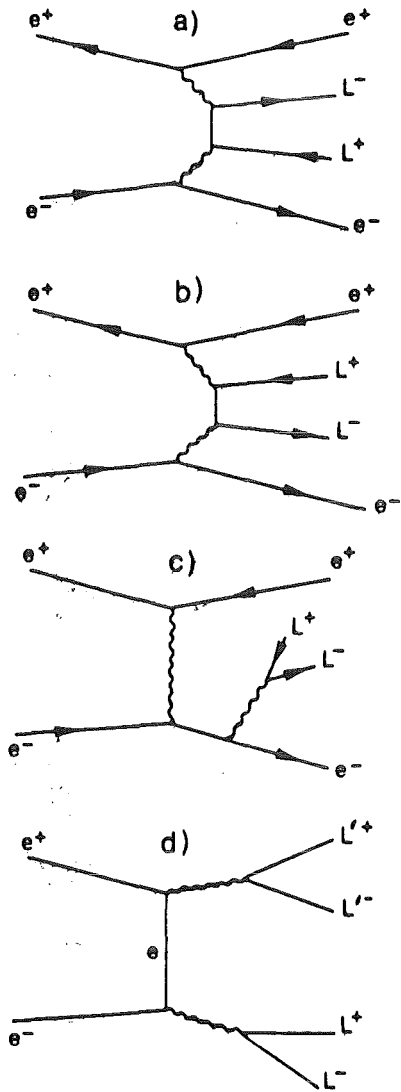
Fig. 1

a) and b) Multipherical diagrams;
c) an example of virtual brems-
strahlung diagram; d) diagram for
$e^+ e^-$ annihilation into two virtual
photons.
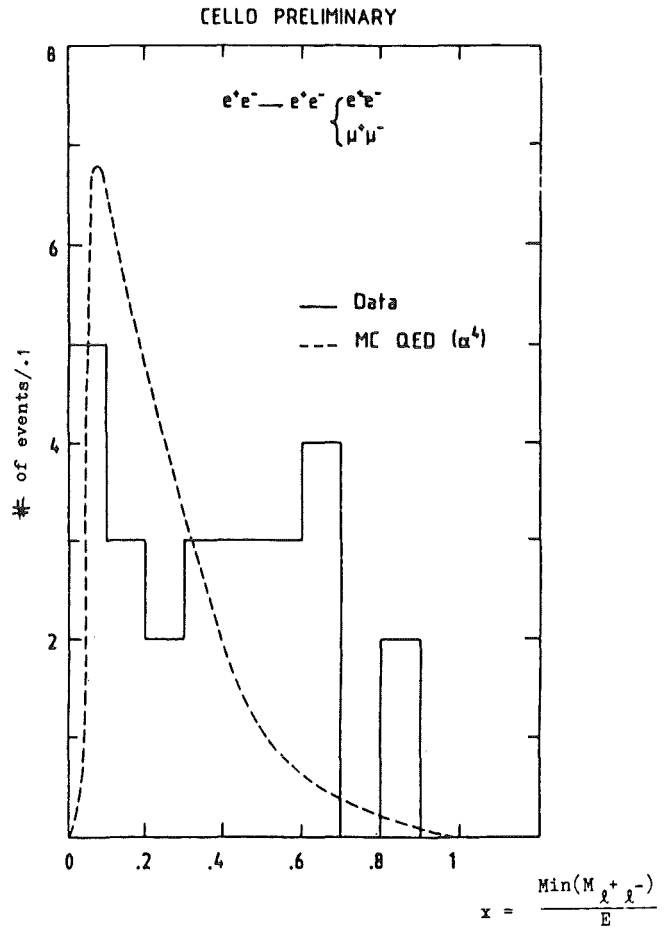
Fig. 2

Distribution of $X = M(\ell^+ \ell^-)/E_b$
for real events and QED predic-
tion.

We compare the results obtained with the QED prediction, with spe-
cial attention to the events with high invariant masses of lepton pairs
with zero leptonic charge.

For the number of events and the distribution of the minimal lepton
pair mass

$$X = \min \frac{M(\ell^+ \ell^-)}{E_{beam}}$$

we find good agreement with QED predictions (Fig. 2).

6. DEVELOPMENTS AND INSTRUMENTATION

6.1 DETECTORS

6.1.1 OPERATIONAL FEATURES OF MWPW's IN THE NEUTRON BEAM

P. Doll, R. Garrett, K. Hofmann, H. Krupp, K. Kärcher

During neutron-proton and neutron-deuteron scattering experiments at the neutron beam from POLKA, MWPC's were operated in a symmetric arrangement around the beam. One chamber (B) was put after a 50 mg/cm^2 polyethylene target in the beam and one chamber to the left (A) and one to the right (C), allowing the reconstruction of trajectories for charged reaction products from the target. The charged particles were identified by two ΔE-detectors (0.7 mm NE 102 A) before "B" to the left and to the right and two E-detectors (25 mm NE 102 A) backing A and C. Data aquisition was carried out through 7 charge sensitive camac ADC's and 16 TDC's. In an off-line analysis for all runs gain variations in the ΔE and E and the energy-loss spectrum in A, B, C were corrected and shifts for the total time-of-flight (TOF) to the E-detectors were checked.

The positions in the chambers are measured by delay lines. When a coincident ΔExE signal provided the common start signal for a multi-channel TDC, time difference with respect to the start amounts to the drift-time for the charges, produced by energy loss in a chamber to the anode wires, plus the propagation time through the delay line. Fig.1 shows a drift-time spectrum. The narrow spectrum ($\sim$ 5 nsec FWHM) is obtained after cutting off low pulse-height signals in chamber A. Fig.2 shows the correlation of x-position signals measured to both sides of the horizontal delay line of chamber A. Mainly the drift-time variation (see fig.1) causes the broad band, and after drift-time subtraction a narrow correlation is obtained. The background can be reduced, chosing a lower cut-off in the chamber energy-loss spectrum. For well correlated events the sum of the time measurements to both sides must be constant. There remain events below the correlation band which stem from shorter time sums due to fast coupling effects through the delay line. There remain events above the band, for which the ΔExE triggers had no corresponding "stops" from both or one side of delay line. An algorithem can be defined off-line to decide on the correct time measurement. Two different delay lines, one made out of cables and one made out of integrated LC chips, have been investigated and position resolutions of 4 mm and 2 mm respectively, have been observed with no cut on the energy loss spectrum of the chamber.
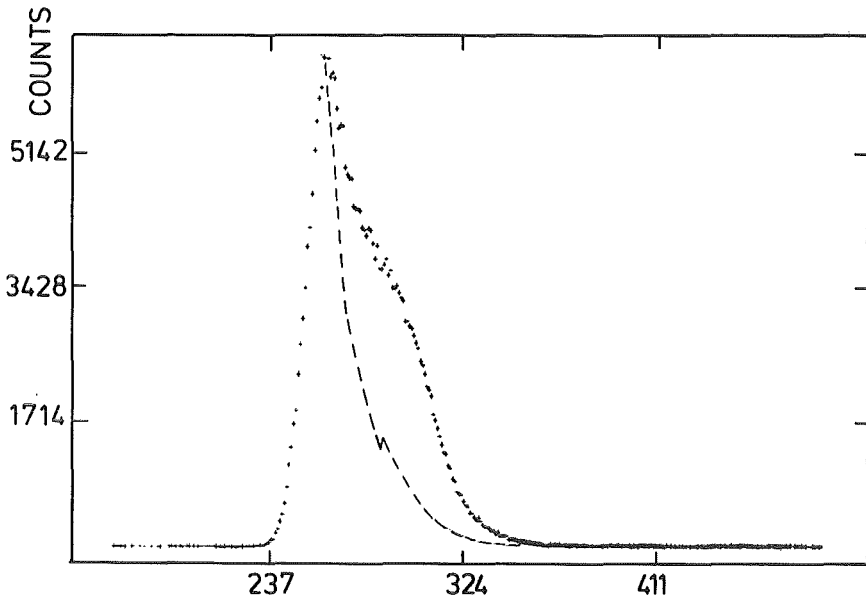
Fig. 1 Drift-time distribution
of chamber A
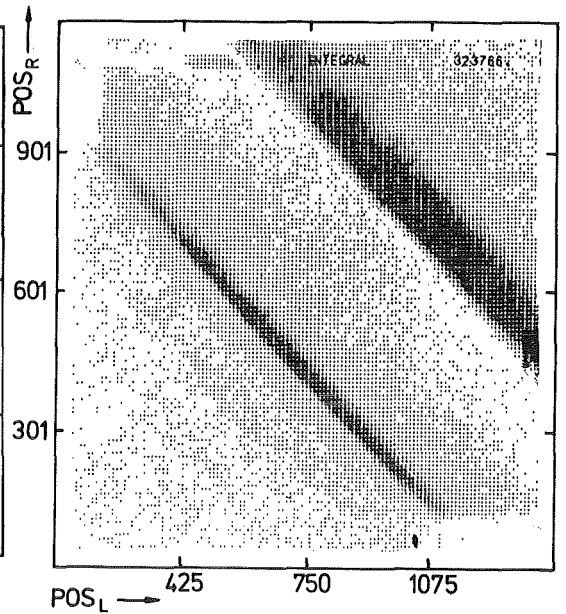
Fig. 2 Left-right position corre-
lation for the x-axis of
chamber A

Transforming the position spectra into real spatial coordinates is a difficult
task. Fig.3 shows a position spectrum of chamber B, triggered by particles which
are scattered into the right ΔE-E set up. The angle range assignement was done
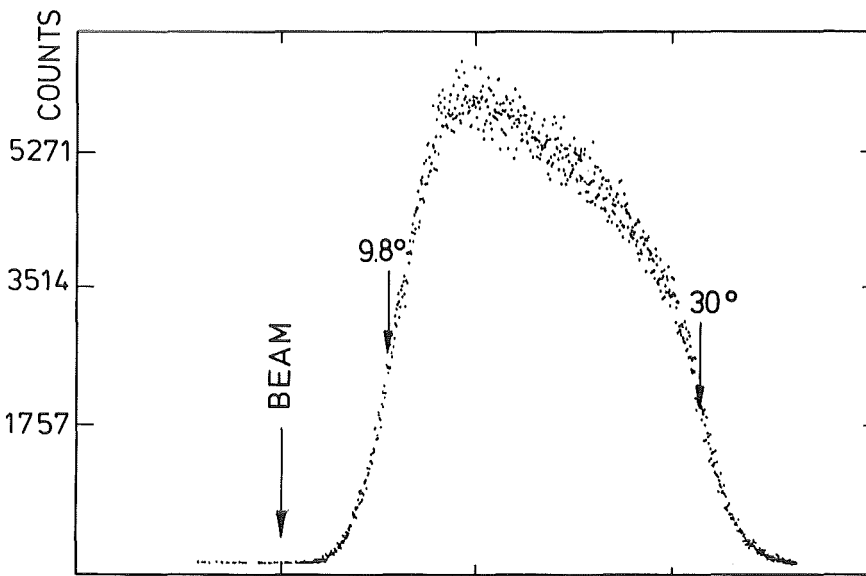
Fig. 3 Ungated position distri-
bution of chamber B opera-
ted in the beam
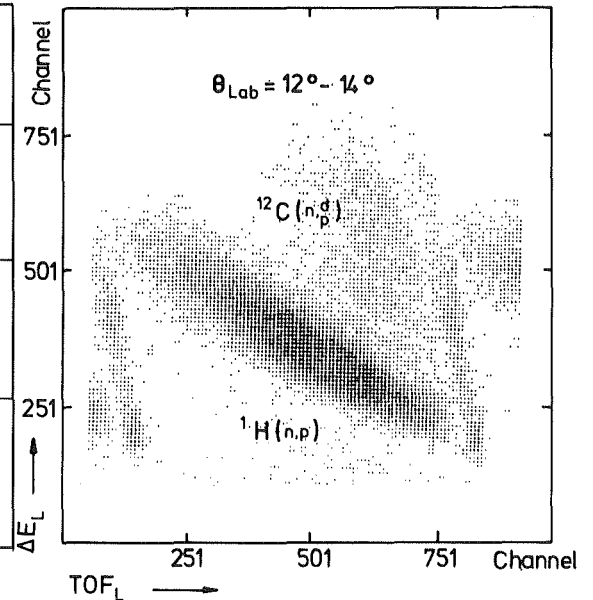
Fig. 4 Identification of reaction
products by ΔE and TOF to the
left side

by reconstructing trajectories based on a careful measurement of the chambers
geometrical positions. The real spatial coordinates are chosen to have their

origin in the left bottom corner of the left chamber A. Trajectories are calculated through B and A (left) or B and C (right) and their scattering angle is determined with an accuracy of about less than 0.8°.

When selecting an angle from 12° to 14°, a ΔE versus TOF spectrum is obtain as presented in fig.4, for one run. An intense ridge is visible from neutron-proton scattering events, distributed over all incident neutron energies. The further analysis uses the full statistics provided by all runs and will allow evaluation of neutron-proton scattering between 20 and 50 MeV and between 10 and 30 degrees.

The authors would like to thank H.Stelzer and H.Beeskow from GSI Darmstadt for valuable discussions.

6.1.2 NEUTRON-DETECTORS WITH GAIN-MONITORING BY LED's

V. Eberhard, H.O. Klages, G. Schmalz

For the measurement of the spin correlation coefficient A_{yy} for elastic n-p scattering at the Karlsruhe POLKA facility and the polarized p-target KRYPTA, neutron detectors with gain monitoring by"LEDS" were developed.

As a shielding against the magnetic field of KRYPTA, the detector-casing is build from an iron tube (11cm $\emptyset$ x 40cm). The volume for the liquid scintillator NE 213 is also made from an iron tube (10.6cm $\emptyset$ x 10cm), which is fixed to the casing through a fine thread. This leads to a total length of the outer shielding of about 48 cm, which gives a good shielding against penetrating end-fields. Against the through-fields, a Mu-metal cylinder (8cm $\emptyset$ x 27cm) is placed around the PMT.   This arrangement provides a shielding-factor S = B (extern)/B (intern) of about 5 x 10^4.

The front-side of the scintillation-volume is a 2 mm aluminum-plate, the rear is closed with a 5 mm quarz window. The inner walls are painted with NE 260 reflector paint. The scintillation light is transmitted to the XP 3462 PMT by a plexiglass-light-guide. The light guide is partially covered with reflector paint and aluminum-foil, to reduce the position dependence of the scintillation light (see fig.1).

To monitor the gain variation of the PMT through temperature, magnetic field and other influences, light-pulses well defined in amplitude and width are transmitted from a LED-light-source via fibre optic cables into the scintillation volume with a frequency of about 1 Hz (see fig.2).
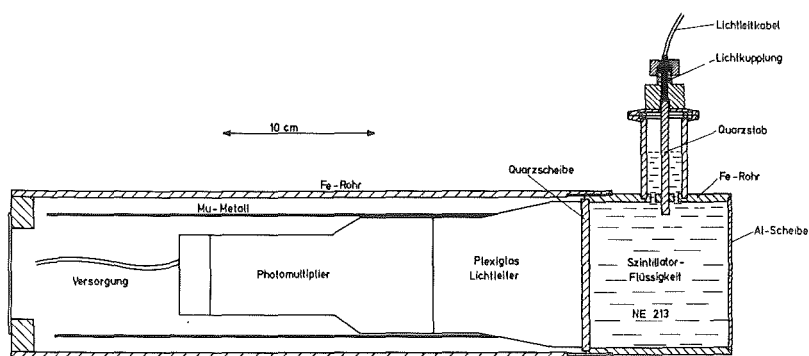
Fig. 1 Schematic view of the neu-
tron detector
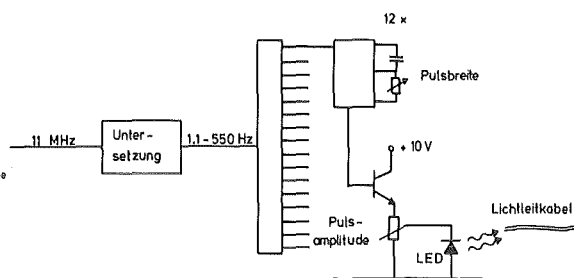
Fig. 2 Layout for pulse fre-
quency reduction and LED
powering for 16 detec-
tors

The fact that the light output of the LED's is temperature dependent (about 0.5%/
degr. cels.) made it necessary to stabilize the LED's against temperature chan-
ges. Therefore, the LED's are mounted in a 5 mm copper-plate, which can be coo-
led or heated by 4 Peltier-elements. The temperature of the copper plate is mea-
sured by a sensor. A controller regulates the current source (Fa. Cambion "Bi-
polar Temperatur Controller") of the Peltier-elements in such a way, that the
temperature of the copper plate with the LED's remains constant within 0.2 degr.
celsius.

The light-pulses are transmitted from the light source to the scintilla-
tion volume by Hewlett Packard light guide cables and a quarz-rod, which leads
through the expansion-volume into the scintillator (see fig.1). These light-pul-
ses are detected by the PMT. Changing the height and the width of the LED-pulses
enables bringing the "LED"-peak to a defined place in the spectrum. Depending on
the stability of the LED-light-pulses it is possible to determine the gain shifts
of the detector and to correct the measured spectra. the stability of the LED pul-
ses can be tested with γ-sources.

Ten neutron detectors have been used in the A_{yy} measurement for a period
of more than eight weeks. The energy resolution, the pulse shape properties, the
tuning and the stability of all detectors have been very satisfactory.

6.1.3 IMPROVED ENERGY RESOLUTION OF LARGE BARIUM FLUORIDE DETECTORS

K. Wisshak, N. Klay and H. Müller

The energy resolution of BaF_2 crystals has been improved significantly compared to previous results (1) by the use of a new reflector material and by changes in the photomultiplier base. The fast and slow component of the scintillation light in BaF_2 is emitted at wave length of 220 and 310 nm, respectively. Therefore, an optimum reflector in the far UV-region is required. According to literature (2) PTFE powder (poly-tetra-fluoro-ethylene) has a reflectivity of 0.96 at 200 nm, even better than that of widely used reflectance standards such as Eastman White ($BaSO_4$) or smoked MgO (3). PTFE foils were recommended for practical applications by Schutt et al. (4) as they are durable, easy to handle and not affected by atmospheric humidity. These features and the possibility to prepare thin reflectors favours the application of PTFE in the 4π BaF_2 detector. Very good energy resolution was obtained simply by a combination of three layers of commercially available PTFE tape (0.8 mm thick, normally used for tightening water pipes) and an outer layer of 0.1 mm thick polished aluminum. The results for gamma-ray energies between 0.6 and 6 MeV are shown in Fig. 1. (The isolated α-line in the background spectrum corresponds to a gamma energy of $\sim$3 MeV). The energy dependence of the resolution (given in the insert) can well be described by the relation

$$\frac{\Delta E}{E} \ [\%] = 7.9 \ E^{-0.45} [MeV] \quad .$$

The noise level of these spectra is below 20 keV as is demonstrated by the 32 keV X-ray line at the lower end of the ^{137}Cs spectrum.

Further improvement of the energy resolution is due to changes in the voltage divider chain of the EMI 9823 tubes. Such a design is always a compromise between energy resolution and gain linearity. The correlation between these quantities is shown in Fig. 2 as a function of the applied voltage. The energy resolution was measured with a ^{137}Cs source, and the energy scale was calibrated between 0.6 and 1.8 MeV using ^{137}Cs, ^{60}Co and ^{88}Y sources. This scale was linearily extrapolated and compared with the position of the 6.13 MeV γ-ray line from a ^{238}Pu - ^{13}C source. The observed position is lower than the linear extrapolation due to saturation effects in the PM tube, and this relative deviation in $\%$ is plotted in Fig. 2. As the detection of capture gamma-ray cascades is the ultimate purpose of the 4π BaF_2 detector and as these cascades are dominated by gamma-ray energies below 2 MeV our compromise was to choose an energy resolution of 9.6 $\%$ allowing for a moderate nonlinearity of $\leq$ 1.5 $\%$ at 2 MeV. At the selected voltage (2200 V) the current through the voltage divider chain was $\sim$ 2 mA.
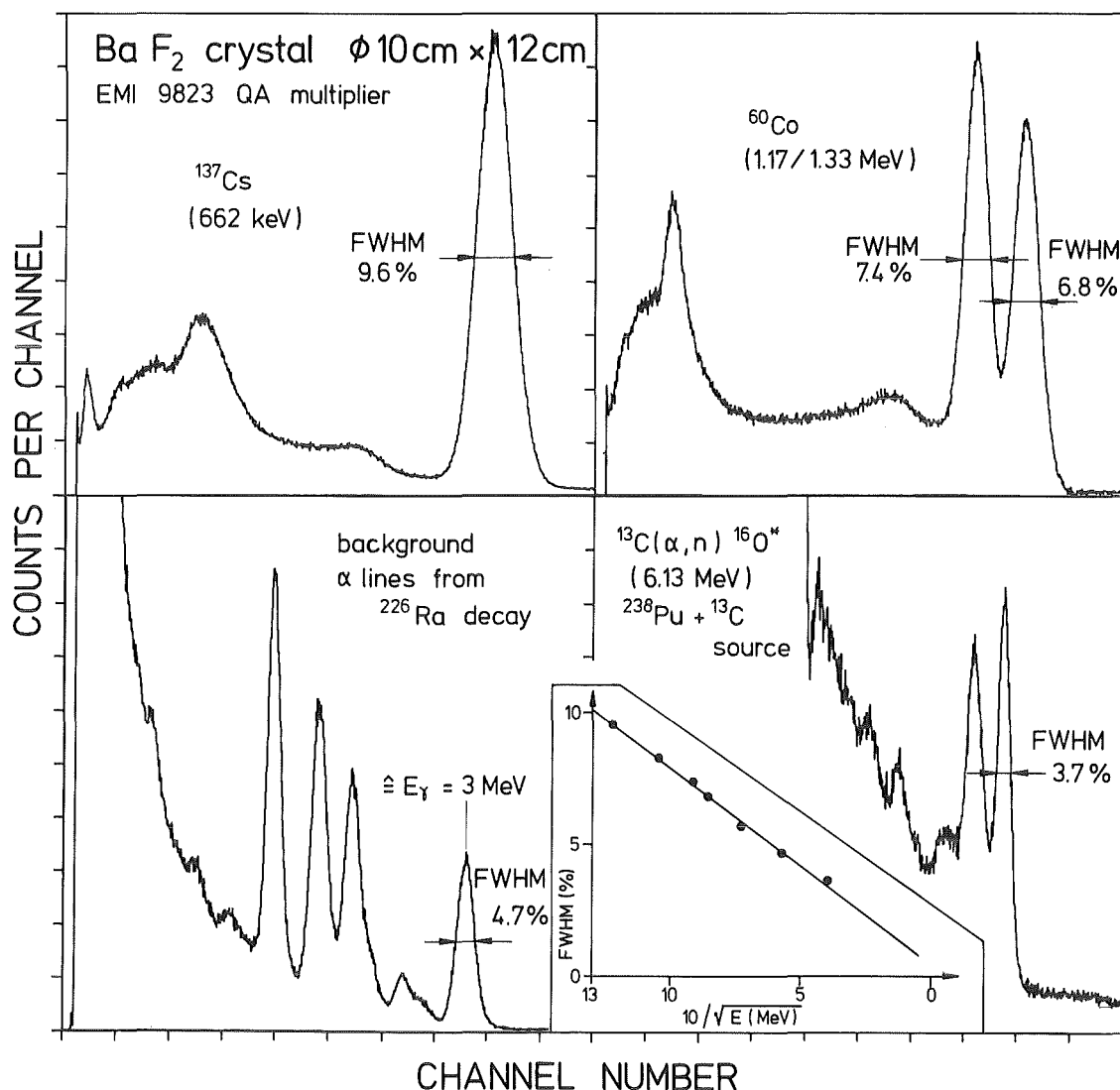
Fig. 1 Energy resolution of a large BaF$_2$ crystal measured with a PTFE reflector.

The energy resolution was measured at count rates of $\sim$ 5 kHz (0.7 kHz in the background spectrum) and proved to be stable up to $\sim$ 30 kHz. In addition, the peak efficiency of the test crystal (10 cm diameter, 12 cm thickness) was measured absolutely at 6.13 MeV. At a source distance of 13 cm a value of 37 % was obtained by summation of the full energy peak and the single- and double escape peaks. This result is in very good agreement with a calculation by Steven Wender

in Los Alamos (5) using the CYLTRAN code (35 %).

Fig. 2 Energy resolution at 0.662 MeV
and integral nonlinearity at
6.13 MeV as a function of de-
tector voltage.
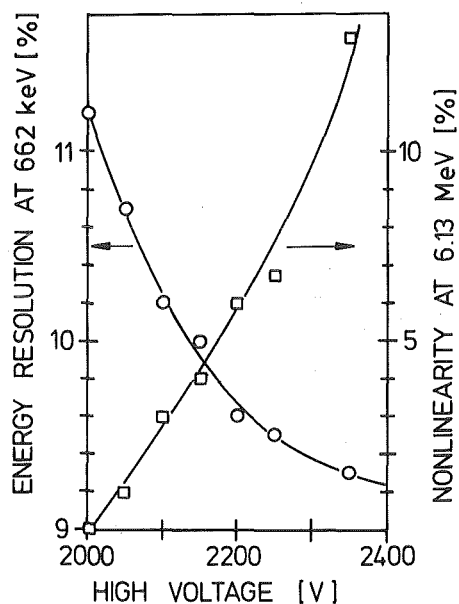
(1) K. Wisshak and F. Käppeler, Nucl. Instr. Methods 227 (1984) 91
(2) V.R. Weidner and J.J. Hsia, J. Opt. Soc. Am. 71 (1981) 856
(3) J.B. Schutt, J.F. Arens, C.M. Shai and E. Stromberg, Applied Optics 13 (1974) 2218
(4) J.B. Schutt, B.N. Holben, C.M. Shai, and J.H. Henninger, Applied Optics 20 (1981) 2033
(5) S. Wender, private communications 1985.

6.1.4 MECHANICAL DESIGN OF THE 4π BaF$_2$ DETECTOR

J. Krisch[+], G. Rupp, K. Wisshak and F. Käppeler

In the mechanical design of the 4π BaF$_2$ detector a high flexibility was aimed at to allow for future adjustments to different experimental conditions. The detector is mounted on a rectangular 2 by 3.5 m ground frame (Fig. 1). It is divided in two parts containing 16 and 26 detector elements, respectively. Each part can be moved independently on two rails in the direction of the neutron beam axis. In this way, the neutron flight path can be varied by 1.3 m, and the detector can be opened for inspection and mounting of samples. The 42 individual elements are held in place by a spherical honeycomb structure 86 cm in diameter which is fixed to octagonal frames by a selectable number of arms. The geometrical posi-
tion of these arms on the frames and in the honeycomb structure is quite flex-
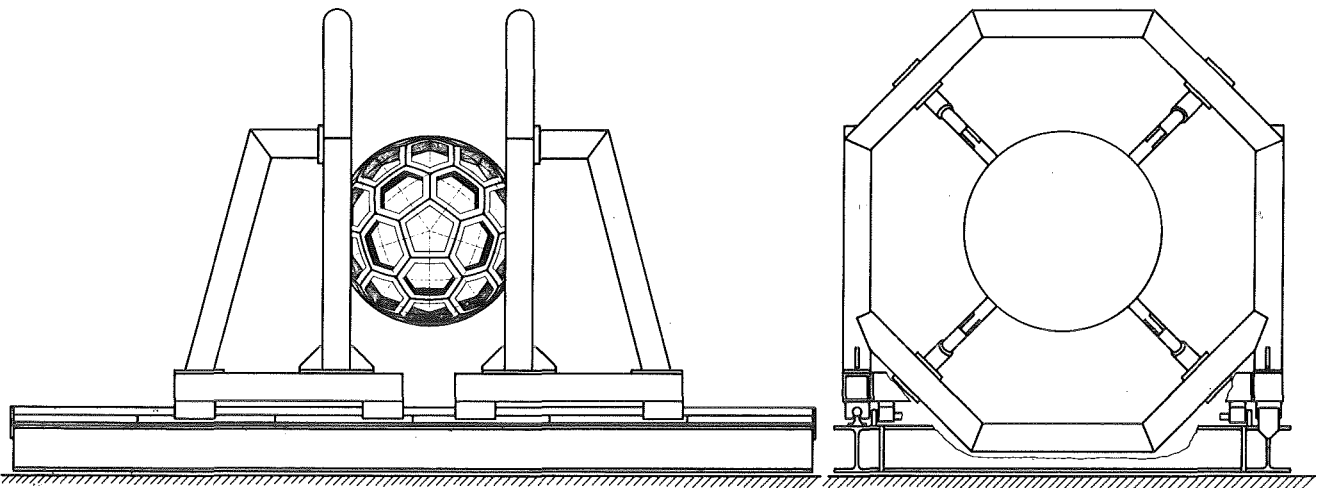
Fig. 1 Schematic view of the supporting structure for the 4π BaF$_2$ detector.

ible, thus allowing to remove part of the detector elements or even of the honey-comb structure. This might be of interest e.g. for measurements with a kinema-tically collimated neutron beam and very short flight paths.

The spherical honeycomb structure is composed of hexagonal and pentagonal parts made from aluminum casting. Machining of these parts is restricted to the spherical outer surface which facilitates mounting and adjustment of the entire structure and to narrow stripes on those surfaces which connect neighboring ele-ments. Fig. 2 illustrates schematically one of the honeycombs in the structure.
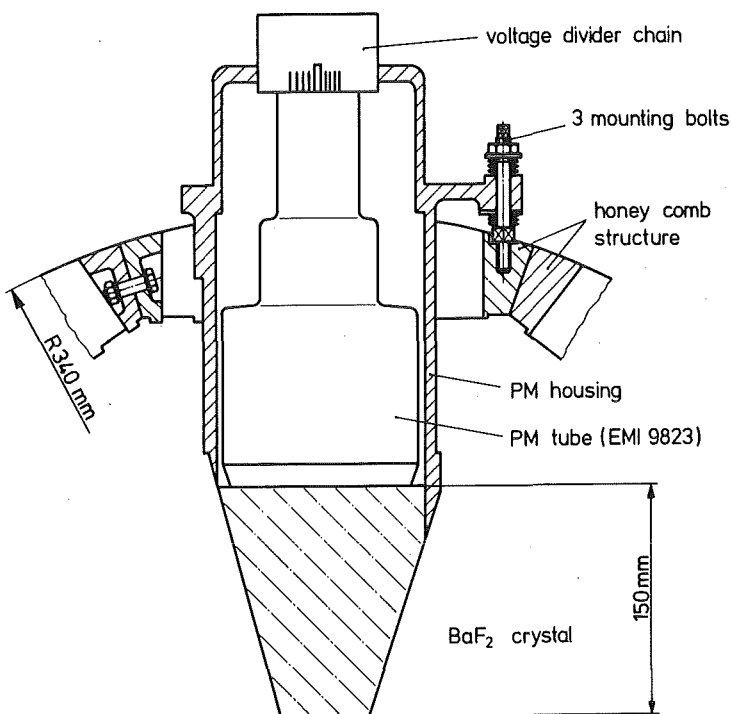
Fig. 2
Mounting of a detector element in the supporting honeycomb structure.

Each of these parts carries a detector element consisting of a BaF_2 crystal and a photomultiplier with housing and voltage divider chain. The detector elements can be adjusted in the structure via three mounting bolts. The design of the honeycomb structure followed closely example of the Heidelberg-Darmstadt crystal ball detector (1).

(1)   E. von Malwitz, "Crystalball-Trägerkugel Konstruktion und Fertigung" Report GSI 80 - 6 September 1980.

+   Kernforschungszentrum Karlsruhe, IT/M

6.1.5   CAD-STUDIES FOR THE 4π BaF_2 DETECTOR

H. Schäfer[+], J. Krisch[++] and K. Wisshak

Due to the complexity of the 4π BaF_2 detector it is difficult and time consuming to draw different sectional views by hand. The detector consists of 42 elements, 12 with pentagonal and 30 with hexagonal structure. This means that many equal parts have to be arranged at different positions in space - a problem for computer aided design (CAD). The second reason for CAD studies of the 4π detector was to check the geometry of the design for the spherical honeycomb structure and the crystal dimensions by an independent method.

The CAD studies were carried out with the BRAVO! code of Applicon running on a VAX 11-75 computer. The main task was to depict a three dimensional figure of the 42 BaF_2 crystals and the supporting honeycomb structure. In the first step the individual parts (hexagonal and pentagonal crystals, hexagonal and pentagonal honeycomb) were constructed on the computer and the respective coordinates of all edges are stored on disk as so called wire models. In the second step the coordinates of the relevant elements are provided as input. These first elements are then duplicated by rotation and reflection to obtain the complete spatial arrangement. As an example, Fig. 1 shows schematically one half of the 4π detector with the BaF_2 crystals in the center surrounded by the supporting honeycomb structure.

In the original wire model all edges of the individual parts are given. In general this representation is confusing and puzzling (see Fig. 1a). The readability is considerably improved by omitting all hidden edges in the wire model (see Fig. 1b). Further improvement is achieved in the so called facet-model. Different parts are shown in colour and the computer simulates a light source. As the position of the light source can be specified, light and shadow offer a very contrasting picture. Up to this point, curved surfaces are approximated by planes to a selectable degree of accuracy in order to save computer time. At last
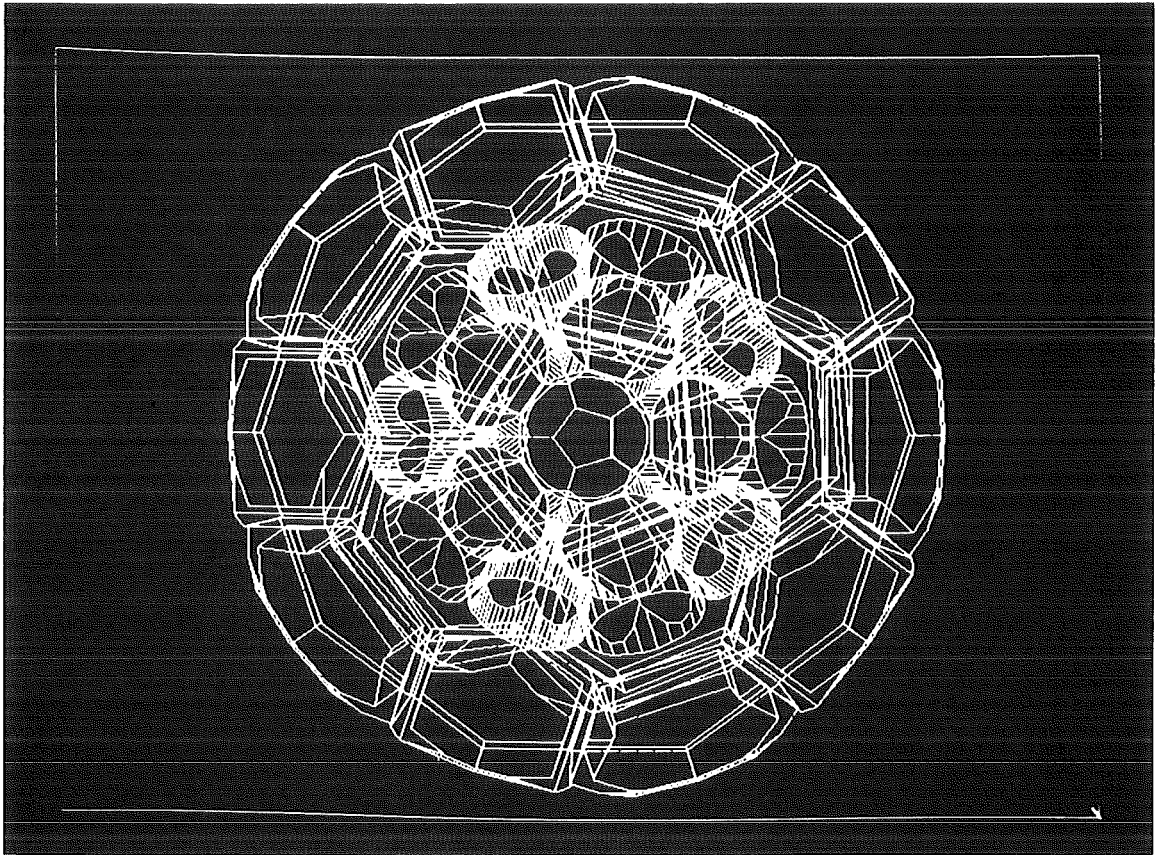
(a)
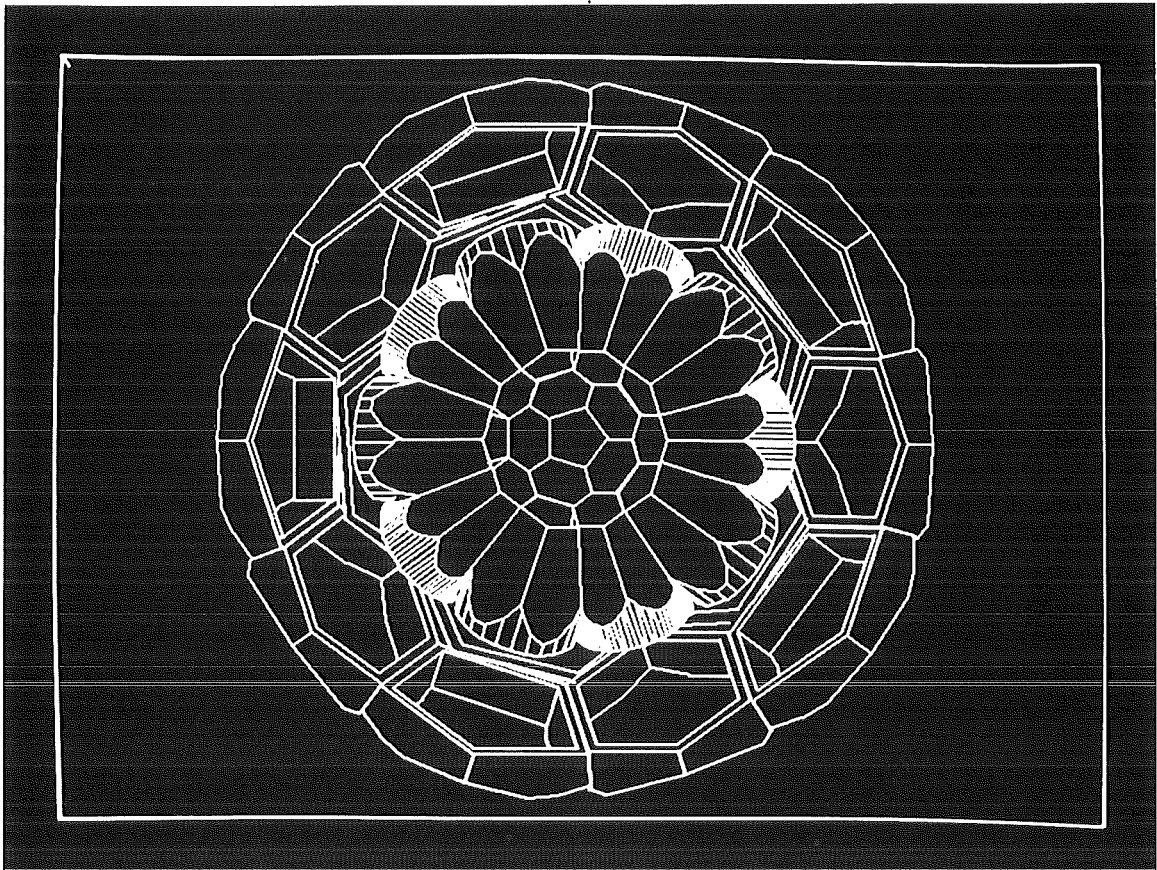
(b)
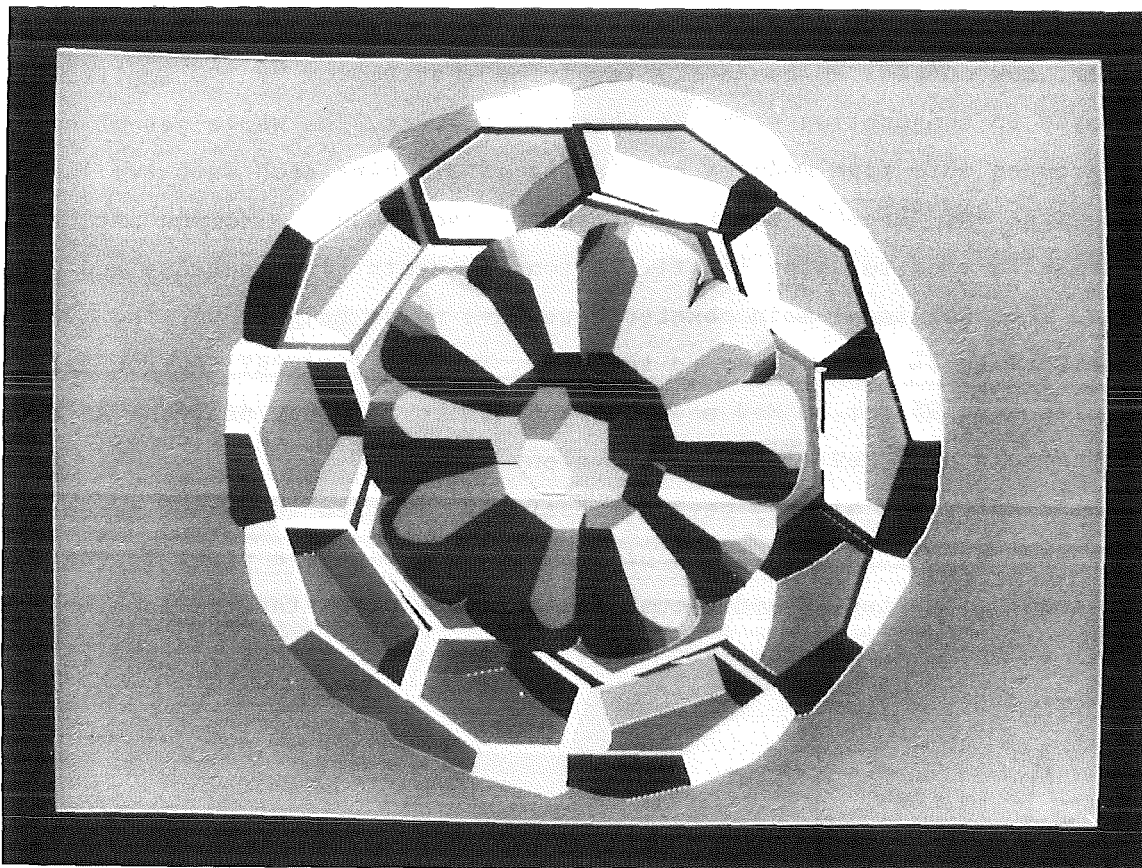
(c)

Fig. 1 Various steps in the CAD design of a hemisphere of the 4π BaF$_2$ detector:
wire model with all edges (a), with visible edges only (b) and facet
model (c).

a high precision run calculates all curved surfaces including the respective
light and shadow effects. However this step is very time consuming and therefore
it is often omitted.

+   Kernforschungszentrum Karlsruhe, PFT
++   Kernforschungszentrum Karlsruhe, IT/M

6.1.6 HIGH RESOLUTION STUDIES WITH A LARGE-AREA POSITION-SENSITIVE TIME-OF-
        FLIGHT COUNTER

S. Cierjacks, S. Ljungfelt, H. Ullrich, T. Petković[+], N. Simicević[+], and
H.J. Weyer[++]

The time and position resolution of a large TOF-counter developed for neutron and
charged particle detection in the range from 10 MeV to 300 MeV have been studied
(1). The counter consists of thirty bars plastic scintillator (NE 102 A) of
5 x 10 cm^2 cross section and 2 m length each, arranged in a suitable counter
matrix covering an overall effective detection area of 1 x 2 m^2. Each bar is

viewed from both ends by a XP 2230 or - in special cases - XP 2020 (Valvo) photo-multiplier. Low current PM-bases (2) involving fast LeCroy VV 100 amplifier chips are employed in conjunction with the photomultipliers. The whole set of counter bars is grouped into five modules consisting of six bars each with two layers of bars in height and three in depth. In front of each module a common anticounter 0.4 mm thick is used to allow identification of events from neutrons and charged particles. The individual main counter bars have pulse height response over the length uniform to 5% except close to the ends. Typical integral neutron detection efficiencies are 19% for 50 MeV neutrons and 13% for 170 MeV neutrons at a pulse height threshold of 5 MeV electron-equivalent energy.

The counter has already been successfully employed in recent measurements at SIN investigating the absorption of positive and negative pions in ^{3}He (3). For time resolution studies additional measurements with standard sources and cosmic ray muons were performed. Some results are shown in Figs. 1 and 2. The
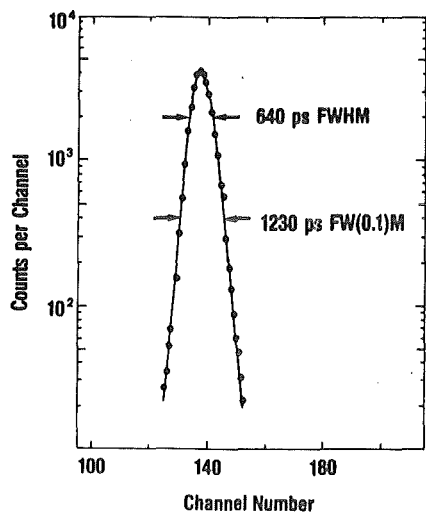
Fig. 1

Typical time resolution of main counter elements. The diagram shows the time dispersion of the coincidence peak for cosmic-ray muons tra-versing the 10 cm dimensions of two 200x10x5 cm³ NE 102A main counter bars. Position identification was used to eliminate events from the omnidirect-ional flux of muons with large zenith angles.
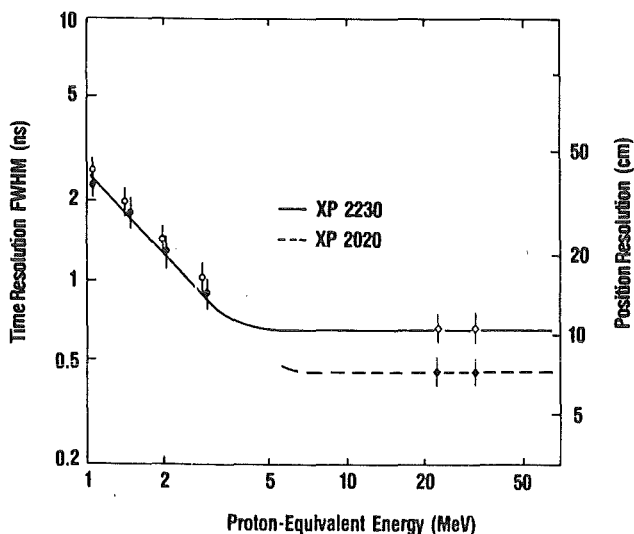
Fig. 2

Typical single-bar time and position resolutions versus proton-equiva-lent energies. Open and full circles correspond to measurements with a highly collimated ^{60}Co -source placed at the O and the -80 cm positions, respectively. Diamonds refer to two-rod cosmic-ray muon measurements employing XP 2230 (open symbols) and XP 2020 (full symbols) PM bases.

intrinsic time dispersion of the main counter bars has been determined to 450 ps (XP 2020). This results in a position resolution of almost 5 cm and a position independent energy resolution for neutrons with 4 m flight path of 3% and 8% for 10 MeV and 300 MeV neutron energy, respectively.

(1)   S. Cierjacks, T. Peković, H. Ullrich, D. Gotta, S. Ljungfelt, N. Šimičević, M. Izycki, P. Weber, H.J. Weyer, Nucl. Instr. and Meth. A238(1985)354

(2)   SIN Data Sheet for PM-Bases PMB-2230 (1979)

(3)   G. Backenstoss, M. Izycki, M. Steinacher, P. Weber, H.J. Weyer, K.v. Weymarn, S. Cierjacks, S. Ljungfelt, U. Mankin, T. Petković, G. Schmidt, H. Ullrich, M. Furić, Phys. Lett 137B(1984)329

+   Faculty of Science, University of Zagreb
++   Institute of Physics, University of Basel

6.1.7 NEUTRON COLLIMATION AND SHIELDING OF THE 4π BaF_2-Detector

F. Voss

The 4π BaF_2-detector described in chapter 6.1.4 requires shielding both against neutrons and against γ-rays from the neutron target and from neutron capture in the shielding. The basic considerations for the selection of appropriate materials remain the same as in previous experiments at the Karlsruhe VdG: a mixture of boron carbide and araldite for the bulk of the shielding and $^6LiCO_3$ for the collimator because of the γ-free neutron capture in ^6Li. But the desired flight path lengths of less than 100 cm in connection with constraints given by the geometry of the detector excluded simple estimates of the required dimensions on the basis of the most unfavorable assumption.

Monte Carlo simulation studies were carried out in order to investigate the shielding properties of cylinders of uniform as well as of non uniform composition, containing the elements H, C and B. Among others the following effects were studied: zones of pure paraffin to enhance the slowing down of neutrons and the use of boron enriched in ^{10}B to enhance neutron capture. The present results suggest that in the energy range of interest 20 cm of boron carbide/araldite would provide effective shielding of the detector against direct neutrons from the target.

The length and shape of the neutron collimator in the center of the shielding are determined by the size of the neutron target ($\emptyset$ = 6 mm), the size of the samples ($\emptyset$ = 20 mm) and the requirement to shield the forward detectors against neutrons directly from the target. For a flight path length of 65 cm approximately 40 cm of $^6LiCO_3$ are required immediately around the neutron beam, thus exceeding the thickness of the bulk of the shielding.

In order to determine the required thickness of the lead to shield against γ-rays from neutron capture in boron it was assumed that all neutrons are finally captured in ^{10}B producing 478 keV γ-rays. Taking into account solid angle considerations and the energy loss of Compton scattered γ-rays it was estimated that 7-8 cm of Pb would reduce the γ-ray flux by a factor of 10^6. If the space foreseen for the 180°-detector is used for a conical lead shielding between 7.5 and 25 cm of Pb can be placed between the BaF_2 crystals and the neutron shielding so that a sufficient attenuation of γ-rays is expected.

Based on the above considerations the design of the collimator and shielding is presently carried out.

6.2   INSTRUMENTATION

6.2.1   PERFORMANCE OF THE POLARIZED PROTON TARGET IN AN INTENSE NEUTRON BEAM
        W. Heeringa and Chr. Maier

In the polarized target facility KRYPTA (1) polarized protons are obtained by cooling a TiH_2 sample in the field of a 9 T superconducting split-pair magnet to a temperature of about 0.01 K by a ^3He - ^4He dilution refrigerator. Presently this target is employed for the measurement of the spin correlation parameter A_{yy} of n-p scattering. The polarized neutrons are produced in the facility POLKA (2) at the Karlsruhe cyclotron. They are obtained by bombarding a liquid D_2-target with polarized deuterons of 52 MeV. The neutrons have a semi-continuous energy distribution between 16 and 50 MeV, peaking around 27 MeV. For the A_{yy} experiment the neutrons are collimated to a diameter of 20 mm at a distance of 4800 mm from the source, corresponding to a small solid angle of $\Delta\Omega = 1.4 \times 10^{-5}$ sr. The neutron intensity in this beam has been upgraded recently by the installation of a new polarized deuteron source (atomic beam) at the cyclotron. With a deuteron current of 200 nA on the deuteron target the neutron intensity, integrated over the energy distribution, amounts to about 1.7×10^6 s^{-1}.
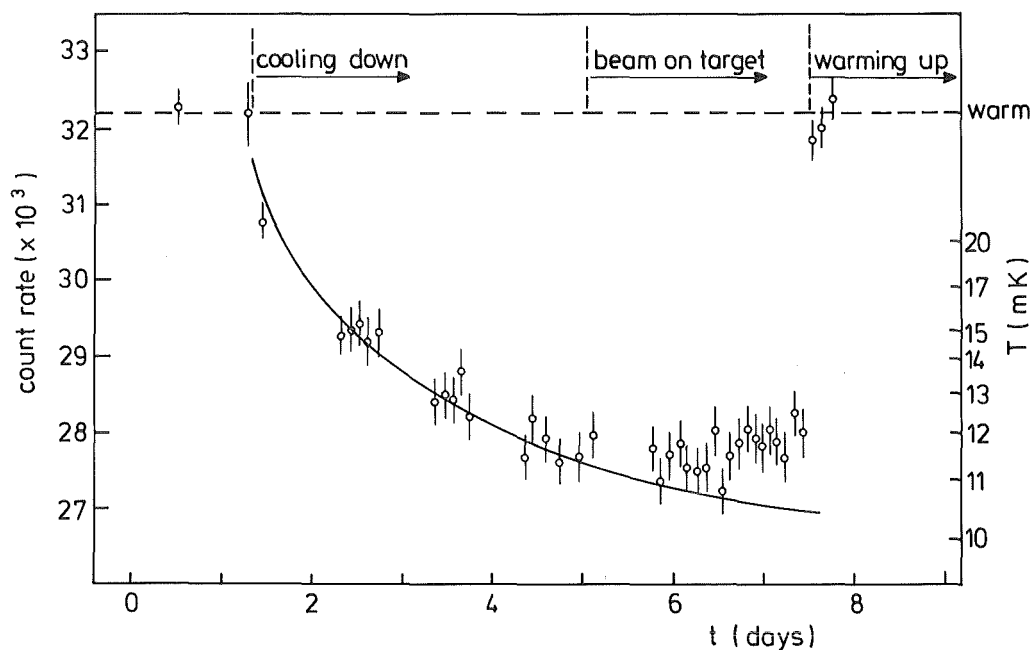
Fig. 1 Temperature of the TiH_2 target during cooling down and during bombardment with an intense beam of fast neutrons.

Fig.1 shows the temperature measured at the outside of the TiH_2 target during cooldown and subsequently with beam on target. The temperature is obtained from the γ-anisotropy of ^{60}Co. Previous experiments have shown, that this thermometer is coupled well to the protons, hence it gives a good indication of the proton temperature. The data in fig.1 show that with beam on target the temperature levels off at about 12 mK. The curve represents the temperature behaviour without beam. It ends at about 10 - 10.5 mK. The proton polarization at 12 mK (and 9 T) is still 65%, hence the neutron intensity after upgrading is still acceptable for the target.

(1)   R. Aures et al., Nucl. Instr. and Meth. 224 (1984) 347
(2)   H.O. Klages et al., Nucl. Instr. and Meth. 219 (1984) 269

6.2.2   EXCHANGE OF LOW-TEMPERATURE SAMPLES IN A STRONG MAGNETIC FIELD

W. Heeringa, Chr. Maier, H. Skacel

For the measurement of the scattering of polarized neutrons by the polarized protons in our brute-force polarized TiH_2-target, it is necessary to measure also the scattering of polarized neutrons by a Ti "dummy" target. The count rate of the neutrons scattered by protons is in principle determined by subtracting the count rate of the Ti-dummy from the count rate of the TiH_2-target.

The target nuclei are polarized by cooling them by a ^3He - ^4He dilution refrigerator to about 0.01 K in a magnetic field of 9 T produced by a superconducting split-pair magnet.

Up to recently the exchange of targets was carried out by warming up the cryostat and opening it. This procedure takes many days, which appears to be too long with regard to the stability of the neutron detectors, the electronics and the cyclotron beam properties. Therefore, we have built a construction, which enables to change the target without opening the cryostat.

The TiH_2- and Ti targets have been mounted above each other onto a copper rod to the mixing chamber of the dilution refrigerator. Their centres are 38 mm apart. A lifting mechanism (1) at the top of the cryostat enables to raise or lower the whole cryostat insert with respect to the helium dewar, the magnet and the neutron beam. The lifting has to be carried out slowly to avoid eddy current heating, which would destroy the polarization. In our set-up the 38 mm are covered in 67 min.

The target lifting mechanism has been employed recently in a neutron scattering experiment, which lasted about one week. Fig.1 shows the measured temperature as a function of time. It was obtained by measuring the γ-anisotropy of a ^{60}Co sample connected to the outside of the TiH_2 target. Also indicated are
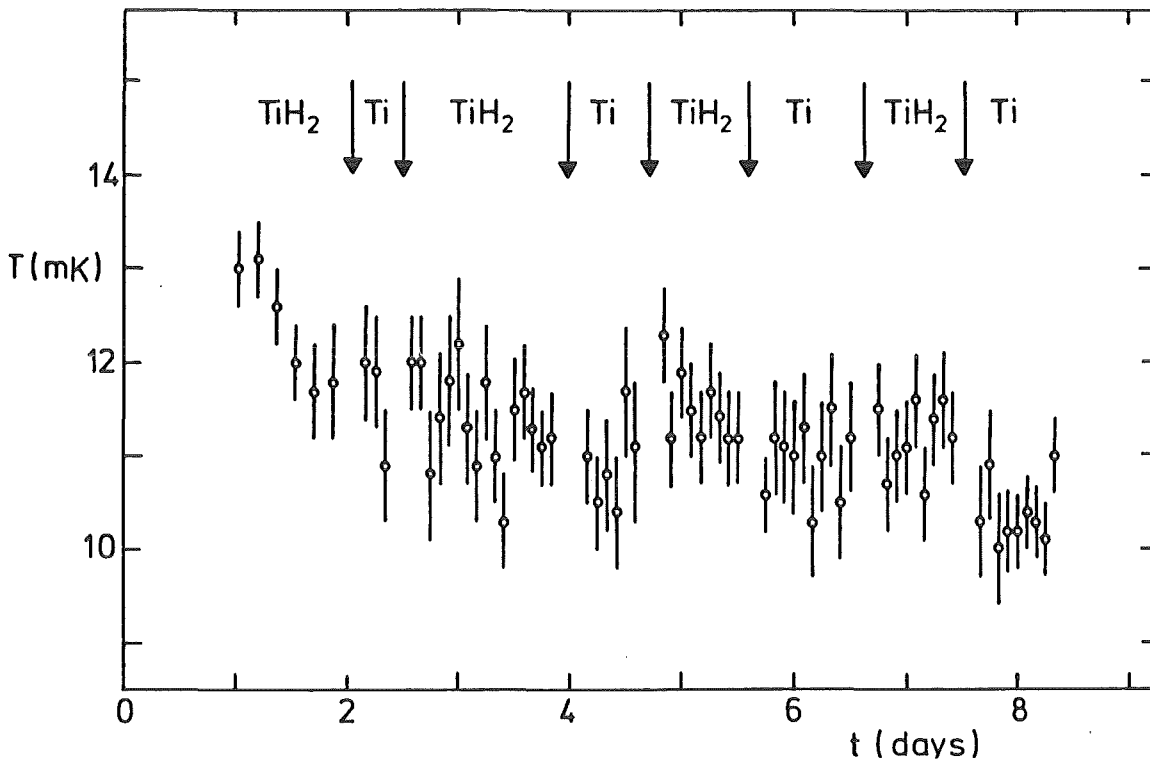
Fig. 1 Temperature measured at the outside of the TiH$_2$ target. The arrows indicate
when a target exchange has taken place.

the times when a target exchange was carried out and the specification of the tar-
get in the beam. About one target exchange was carried out per day. It can be
seen that the target replacement had little or no influence on the temperature.
Hence the lifting mechanism functions well. It is of great importance for the re-
duction of systematic errors in the measurements of polarized neutron scattering
by the polarized protons in TiH$_2$.

(1)   W. Heeringa, Chr. Maier and H. Skacel, to be published

6.2.3 SET UP FOR SPIN-SPIN CROSS SECTION MEASUREMENTS

W. Heeringa, H.O. Klages, H. Krupp, Chr. Maier, D. Reppenhagen

In the framework of the investigation of the nucleon-nucleon interaction the stu-
dy of the effective two-body interaction in systems with many nuclei is very im-
portant. The spin-dependence of this interaction has to be studied in experiments,
in which one or both of the reacting particles are polarized.

For such a experiment we made use of the polarized continuous energy neu-
tron beam (up to 50 MeV) from "POLKA" (1) in connection with the nuclear polari-
zation facility "KRYPTA" (2), which polarizes protons by a 9 T magnetic field at
a temperature of 0.01 K.

The first measurement of the spin-spin cross section was carried out simultaneously with the A_{yy} measurement of the elastic n - p-scattering. For this measurement highly stabilized flux monitors are necessary.

As the effects in the measurement of the spin-spin cross section are very small, it is necessary to get high count rates to improve the statistics. So it is usefull to adjust these detectors under zero degree in the polarized neutron beam. The flux was measured as well before as behind the polarized proton target.
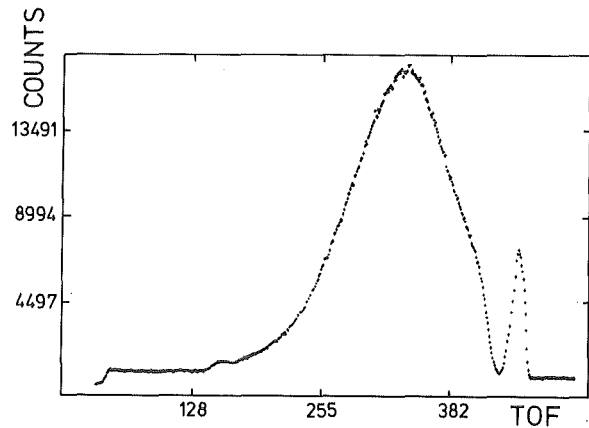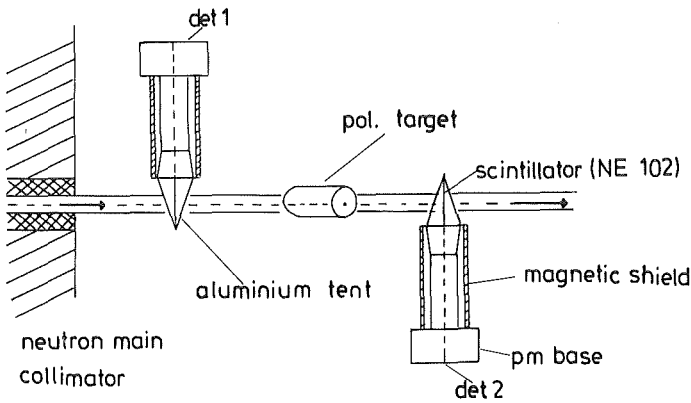
Fig. 1 Experimental set-up for the spin-spin cross section measurement.

Fig. 2 Time-of-flight spectrum measured by detector 1.

The neutrons were detected in a slice of 2 mm thickness of NE 102. This scintillator was shielded by a aluminum tent against light from outside (fig.1). Through a light guide the scintillating light reaches a XP 2020 photomultiplier tube. The photomultipliers are shielded against the stray field of the polarizing magnet by iron- and Mu metal tubes.

In the experiment the flux of the neutrons before and behind the polarized target was measured under 0 degree. To analyse these data in different energy bins in the range from 16 MeV to 50 MeV time-of-flight spectra for the four possible spin states were measured. A signal derived from the cyclotron r.f. (5.5 MHz) served as a time reference. Figure 2 shows a typical time-of-flight spectrum of one of these detectors.

(1)   H.O. Klages et al., Nucl. Instr. and Meth., 219 (1984) 269
(2)   R. Aures et al., Nucl. Instr. and Meth., 224 (1984) 347

6.2.4 PHASE SPACE BEHAVIOUR OF PARTICLE BEAMS IN MATTER

R. Bacher, P. Blüm, D. Gotta, W. Kunold, M. Schneider, and L.M. Simons

For a comprehensive theoretical description of the deceleration process inside the cyclotron trap (1) it became necessary to treat first the deceleration of particle beams in matter in absence of a magnetic field.

In the presence of dissipative forces Q_i acting on a beam of noninteracting particles with conjugate coordinates q_i, p_i the behaviour of the phase space volume

$$\Delta^6 V = \prod_i dp_i \, dq_i$$

in time is given by (2)

$$\frac{d\Delta^6 V}{dt} = \sum_i \frac{\delta Q_i}{\delta p_i} \quad .$$

Defining the average beam direction to be the z-axis of a cartesian coordinate system, we observe the phase space development at fixed steps Δz for all particles. This leads to a reduction of the dimension of the phase by one. Parametrizing the energy loss by $Q = const \cdot p^\alpha$ for small energy losses one obtains

$$\Delta^5 V_f / \Delta^5 V_i = (p_f/p_i)^{2+\alpha} \beta_i / \beta_f$$

for the ratio of the phase space volumes for beams with inital average momentum p_i and final average momentum p_f having transversed a thin slab of matter. $\beta = P/E$; E is the average total energy of the beam.

For a beam with all trajectories parallel to the z axis one obtains (3)

$$\Delta p_f / \Delta p_i = (p_f/p_i)^\alpha \, \beta_i / \beta_f$$

for the ratio of the momentum uncertainties Δp for the final to the initial beam. Knowing $\Delta p_f / \Delta p_i$ for a particle beam, the phase space behaviour is obtained by

$$\Delta^5 V_f / \Delta^5 V_i = p_f^2 / p_i^2 \, \Delta p_f / \Delta p_i \quad .$$

Relations for Δp have been derived not only for parallel beams but also for beams with finite emittances. In a second and a third step straggling processes and Coulomb scattering have been included. For the special case of pions decelerating in beryllium, a comparison of the theoretical expressions has been performed with a computer simulation. The results are shown in Fig. 1.

(1)   Annual report on nuclear physics activities, KfK 3815(1983/84)148
(2)   A.J. Lichtenberg, Phase space dynamics of particles, J. Wiley, New York, 1969
(3)   H. Daniel, N.I.M. 147(1977)297
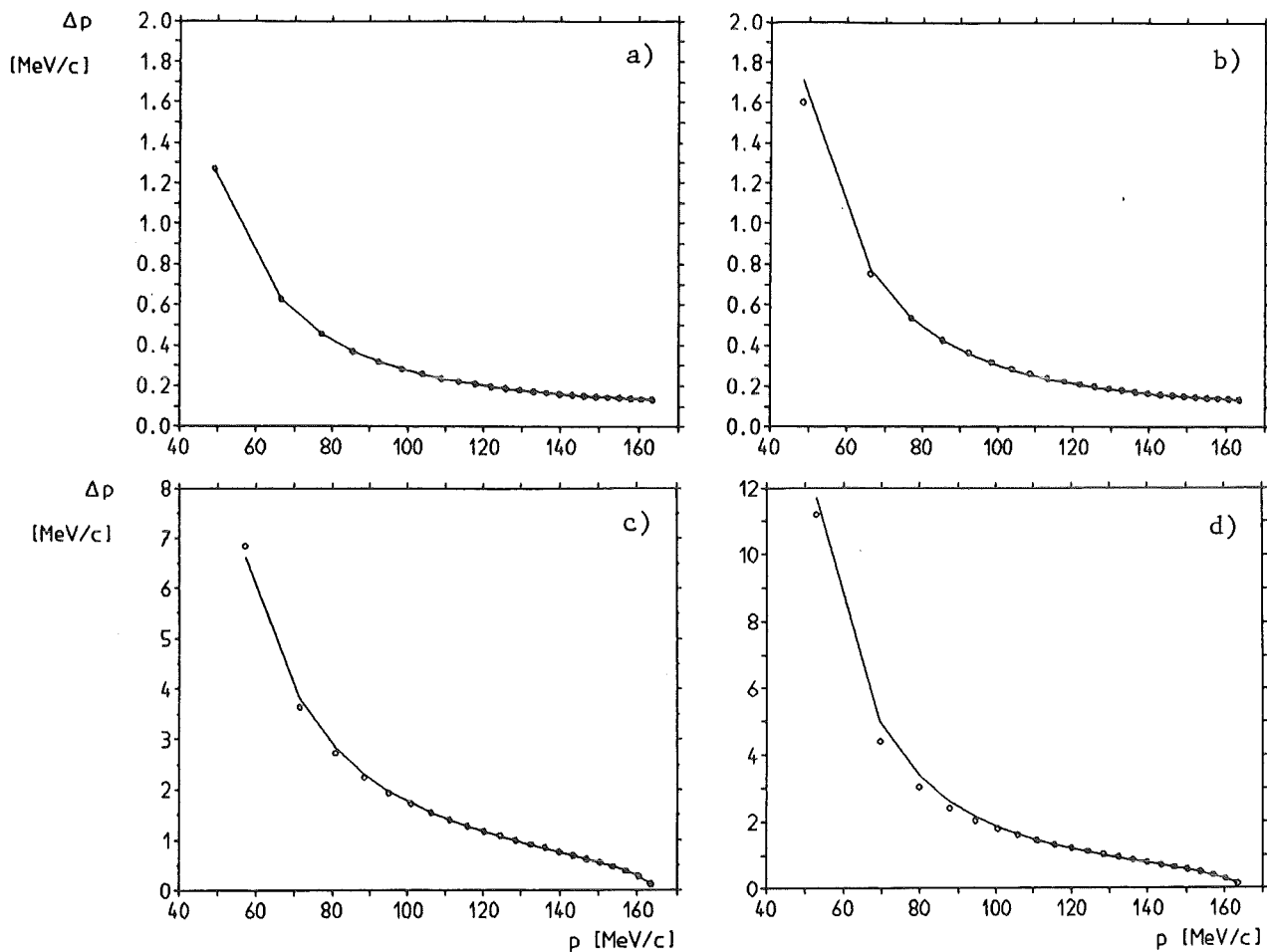
Fig. 1 Development of momentum uncertainties Δp for a pion beam decelerating in beryllium versus the average momentum of the beam. The straight lines interconnect theoretical points; the dots are from computer simulations:
a) all trajectories parallel to the z-axis (zero emittance), no straggling, no Coulomb scattering,
b) beam with finite emittance, no straggling, no Coulomb scattering,
c) beam with finite emittance, with straggling, no Coulomb scattering,
d) beam with finite emittance, with straggling, with Coulomb scattering.

In contrast to the IFD in the focal plane a vertical drift chamber (VDC) with an active area of 1000 x 180 mm^2 will be used. As its principle of operation and the basic characteristics have already been discussed elsewhere (3) only the main reason for the choice of this detector shall here be given again, i.e. the ability of the VDC to measure the coordinate x and the angle of incidence x' simultaneously using one readout plane only with an inherent spatial and angular resolution of $\Delta x \approx \pm 50$ µm and $\Delta x' \approx \pm 5$ mrad, respectively.

It is exactly the angular correlation between the angles x' as measured in the IFD-center plane and the focal plane that reduces drastically the background originating from π-decay in the spectrometer, which is one of the most serious problems for low energy pion spectrometry.

The accuracy of any predictions based on raytrace calculations is mainly limited by the accuracy of the input data in reproducing the magnetic fields of the different elements. As the original RAYTRACE-code (4) is based on a parametrization of the fields only we decided to modify this code in such a way that it makes direct use of field maps measured in the median plane of the spectrometer, the field off the median plane being calculated by a Taylor expansion to 4th order (5). The accuracy of this expansion was checked for the splitpole by a comparison with field maps measured off the median plane and for the quadrupoles by comparing the field map calculated in the center plane vertical to the median plane with the original field map. A set of 2000 rays covering almost the whole accepted phase space but with the momentum band being reduced to $\Delta p/p_o = \pm 10\%$ was generated and transported through the spectrometer. From these data using a linear regression method, a 5th order polynomial could be derived that describes the momentum in terms of the "measured" coordinates and angles.

From results of these calculations one can conclude that at least at the maximum center momentum setting of 200 MeV/c where the blurring due to multiple scattering is small a momentum resolution very close to the first order value $\Delta p/p_o = 5 \cdot 10^{-4}$ is achievable for the full phase space. A first set-up run for LEPS is scheduled for November 1985.

(1)   SIN Jahresbericht 1984 (SIN 1984) JB25, Annual Report on Nuclear Physics Activities 1983/84, Technical Report KfK 3815(1984)164
(2)   K. Göring, Diploma thesis, Universität Karlsruhe (1985)
(3)   Annual Report on Nuclear Physics Activities 1982/83, Technical Report KfK 3621 (1983)149, SIN Newsletter No. 15 (SIN 1983) NL 37
(4)   E. Enge, S. Kowalski, Code RAYTRACE internal MIT Report (1968)
(5)   M. Metzler, Diploma thesis, Universität Karlsruhe (1985)

6.2.5 THE NEW DATA ACQUISITION SYSTEM FOR CHARGED PARTICLE EXPERIMENTS AT THE CYCLOTRON

H.J. Gils, J. Bialy, H. Schlösser[+], S. Zagromski

A multi-parameter data acquisition system for the magnetic spectrograph "Little John" and other charged particle experiments is being installed at the cyclotron laboratory. The final set-up is schematically shown in Fig. 1.

The ADC-system consists of sixteen NIM-ADC's (Laben 8115 and 8215) eight of which are equipped with 8-fold router units. The ADC's are connected via special versions (1) of ADC-control units (Laben 8232) to the master control unit (Laben 8233). This configuration enables the definition of single-ADC experiments and/or independent coincidence groups (up to 16-fold) between any of the ADC's. The 32 bit conversion- and control-bit data words coming from the master control unit are split in a dual port data transfer unit (DPDT, Laben 8171) to be independently transmitted to two CAMAC-ADC interfaces (Laben 5911) connected to different CAMAC-systems. The conversion words may either be buffered (64 words) in the master control unit and sent to the interfaces blockwise or may be transfered word by word.

The splitting of the data by the DPDT unit allows to perform data acquisition and storage on tape on the one hand and on-line data evaluation on the other on two independent computer systems (ER 1 and ER 2) in a most efficient way. Each of these computer systems consists of a host computer (ER 1: LSI 11/73; ER 2: LSI 11/23) and a front-end computer which is a fast J-11 "starburst" processor (CPU 11/73) integrated in an auxiliary crate controller unit and equipped with a 256 k word memory. Due to space limitations and insufficient air conditioning in the electronic room (Vorhalle) the host computers and their respective periphery are placed around 100 m (cable length) away from the ADC- and CAMAC-systems. The connection along this distance is given via two independent "Ethernets" between the host and front-end computers.

The "starburst"-processors will mainly serve as intermediate buffers of the data coming from the CAMAC-interfaces 5911. In addition some presorting will be performed. The host computer ER 1 (11/73) will control the experiment (Start/ Stop/Reset of buffers, scalers etc.), aquire the data, and store it on magnetic tape. In addition also the computer control of several components of the magnetic spectrograph (acceptance slits, target position and angle, magnetic field, etc.) at present running on another computer (2) will be implemented on ER 1.

The second host-computer (ER 2) will exclusively be used for on-line data evaluation. The corresponding programs have already been developed. (3).
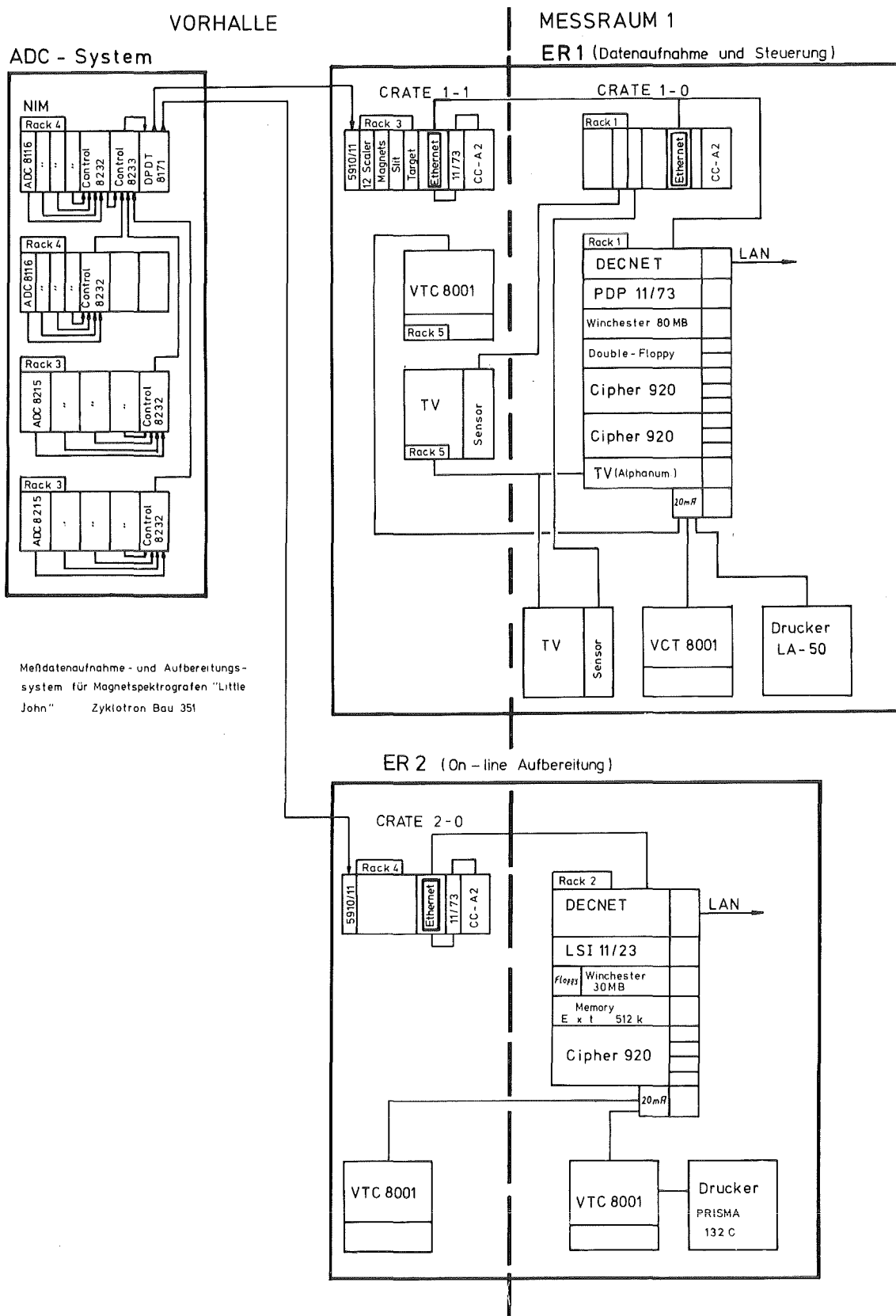
Fig. 1   Data acquisition system at the cyclotron

(1)   H.J. Gils; Specification for the ADC-system (unpublished)
(2)   D. Manger, H.J. Gils, J. Buschmann; to be published
(3)   H. Schlösser, H.J. Gils; KfK-Report 3815, Contr. 6.2.8
+   Physikalisches Institut der Universität Erlangen

6.2.6 A MODIFICATION OF THE FOCAL-PLANE DETECTOR OF THE MAGNETIC SPECTROGRAPH FOR ZERO DEGREE MEASUREMENTS

S. Zagromski, H.J. Gils, W. Eyrich[+]

The magnetic spectrograph "Little John" is to be used for measurements of inelastic scattering (1) and ^{6}Li break up reactions (2) at a reaction angle of zero degree. In both cases the reaction products have the same magnetic rigidity as the beam particles and, therefore, the primary beam may hit the focal plane (FP)-detector. In order to avoid this one may either stop the (focussed) beam just in front of the detector (3) or guide it through a pipe very close to the detector and stop the beam behind it. In the second case, shielding of the detector against particles coming from the Faraday cup can be performed more efficiently.

Therefore, a modification of the focal plane detector has been built up in which the primary beam is guided inside a vacuum pipe through the elements of the FP-detector on the high-energy side of the entrance-window and is stopped behind the detector as far as possible from it (Fig. 1). The horizontal angle of the vacuum pipe through the FP-detector is variable by means of an elastically sealed mounting and by a movable back-wall of the detector-box. This is necessary because of different angles of incident particles at different focal plane positions (different dispersion).

A thin scintillator with a hole mounted in front of the entrance of the vacuum pipe is used to center the beam inside the pipe and to work as an active slit rejecting all halo-particles. A ZnS-screen in the position of the Faraday cup is used to adjust the angle of the vacuum pipe.

The scintillator for the measurement of the residual energy of each particle in the FP-detector is cut on one side in this modified version. Only one photomultiplier is used and a special energy-to lightoutput calibration is taken.

A rather quick change between the modified components of the detector and the original ones is possible for measurements at angles different from zero degrees.
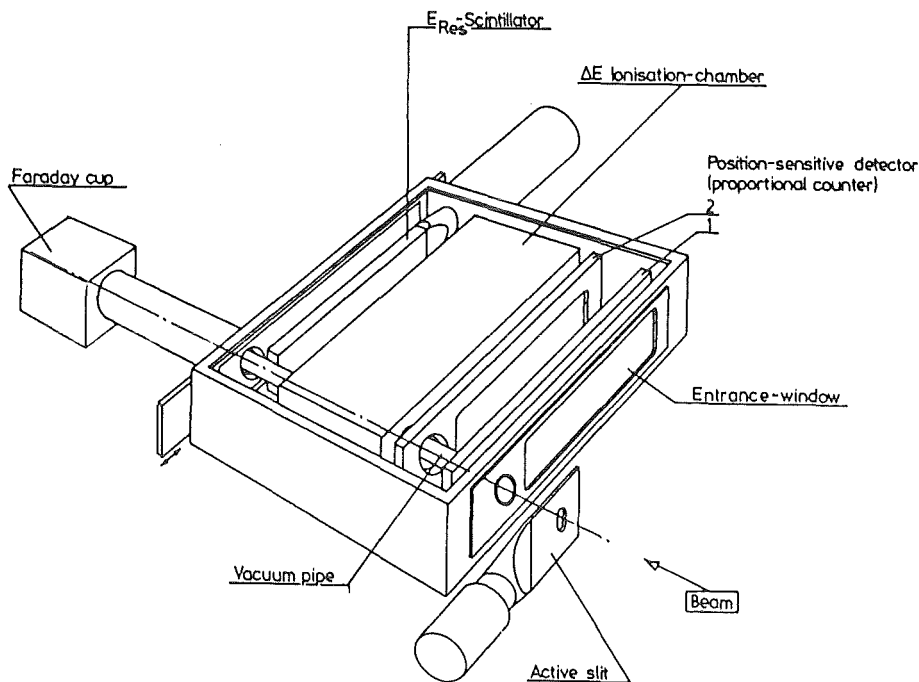
Fig. 1 View of the focal-plane detector showing the vacuum pipe for the primary beam through the detector housing

(1)   Schlösser, Eyrich et al., this report, Contr. 1.3.13
(2)   Jelitto et al., this report, Contr. 1.3.2
(3)   Gils et al., this report, Contr. 1.3.11

+   Physikalisches Institut der Universität Erlangen

6.2.7   THE COMPUTER CONTROL OF THE MAGNETIC SPECTROGRAPH "LITTLE JOHN"

D. Manger, J. Buschmann, H.J. Gils

The computer control of the magnetic spectrograph is characterized by the following special features (1):

  - several control hardware and a CAMAC system connected to a DG NOVA 2 computer

  - the Real-Time-Disk-Operating-System (RDOS) which allows multitasking, chaining, swapping and overlay-structuring.

These abilities provide to segment a voluminous program into smaller units which are loaded from disk on demand; although the program region of the NOVA 2 main memory includes only 36 k bytes, an extensive program system can be run on this small computer.

In this way a complex Real-Time program could be implemented (Fig. 1). The program system consists of 5 main tasks. Among these you will find LJ1 which

Fig. 1 Structure of the Control Program System for the magnetic spectrograph "Little John"

Main Task LJ1

CALL CHAIN
CALL CHAIN

Main Task MALJ2

Task	MAVB1
Task	MAVM1
Task	MAVO1
Task	UHR1
Subr.	MAVL1
Subr.	MAVBS1
Subr.	MAVBS2
Subr.	MAVBS3
Subr.	MAVU1
Subr.	MAREWR
Subr.	VFM1
Subr.	MAVP1
Subr.	MAEX1

CALL CHAIN

Main Task LJ2

Task	VB1
Task	VM1
Task	VO1
Task	UHR1
Task	TT1
Subr.	VFM1
Subr.	VL1
Subr.	LO1
Overlay	Area # 0
Overlay	Area # 1

Main Task VA1

CALL BACK
CALL FSWAP

CALL FSWAP

Disk File 'LJ2.OL'

Subr.	TTS1
Subr.	VBS1
Subr.	VBS2
Subr.	VBS3
Subr.	VST1

Subr.	VP1
Subr.	VU1
Subr.	REWR
Subr.	EX1

Main Task LJ3

Task	SELECT
Task	VM3
Task	VO3
Subr.	VFM1
Subr.	VL3
Subr.	JANEIN
Subr.	TRANS
Subr.	LO3
Overlay	Area # 0
Overlay	Area # 1

CALL BACK

Disk File 'LJ3.OL'

Subr.	TAPO
Subr.	DETA
Subr.	SLIT
Subr.	TANG
Subr.	MAG

Subr.	VP3
Subr.	VU3
Subr.	REWR3
Subr.	INF3
Subr.	EX3

initializes and stores on disk some global parameters (some of them describing the periphery to be controlled, others being parameters for interprogram communication). MALJ2 performs an automatic starting procedure of the vacuum system while main intention of LJ2 is to ensure the reliability of operation of the vacuum system by detecting unallowed states or actions which may occur (2). VA1 helps to do this by doing an initial check up. LJ3 performs the setting of stepping motors (3) (acceptance slits, target position and angle and detector support) and the setting and control of the magnetic fields. The settings of the stepping motors are similar: The desired positions will be given by the computer via CAMAC. The actual positions will be read by 36 turns absolute angular digitizers with 100 digits per turn. When the difference between the preselected and the actual position values are not zero, the stepping motors are engaged in the required sense, otherwise they are stopped.

The magnetic fields can be set in two ways: either by "set", which means that one out of four magnets can be selected and set or by "shift", which means that the value of the dipol magnet can be changed while all other magnets are varied at the same way (percentage modification). On demand, the selected values can be stored on disk for later use.

While LJ3 is active, no push-button commands for the vacuum system are accepted but all changes of state of the vacuum system are surveyed. In case of harmfull changes of state LJ3 initiates the same shutoff-procedure as LJ2 in order to put the whole vacuum system in a safe, predefined standard condition.

As soon as the new data acquisition computer system will be completed (4) the stepping motors and magnets will be controlled by this computer because the actual states of these units are important experimental quantities to be written on the data tape before and after each experimental run.

(1)   D. Manger, KfK-Report 3702B (1984)
(2)   J. Buschmann, H.J. Gils, H. Jelitto, J. Krisch, G. Ludwig, D. Manger, H. Rebel, W. Seith, S. Zagromski, KfK-Report 3681B (1985)
(3)   D. Manger, unpublished results, Kernforschungszentrum Karlsruhe (1985)
(4)   H.J. Gils, J. Bialy, H. Schlösser , S. Zagromski, unpublished report

6.2.8   STATUS OF THE LOW ENERGY PION SPECTROMETER PROJECT (LEPS)

K. Göring, W. Gyles, A. Höhne, K. Kärcher, W. Kluge, H. Matthäy,

M. Metzler, R. Tacik, and U. Wiedner

During the period of report, the activities within the LEPS-project (1) focused mainly on the final design and the assembly of the detector system. In addition a versatile Monte-Carlo-Programme has been developed. It allows a computer simulation of the particle transport through the spectrometer taking into account multiple scattering in the detectors as well as their operational characteristics (spatial and angular resolution and local efficiency).

LEPS is designed to analyse the momentum of the scattered pions and to
measure their primary momentum before scattering simultaneously. In particular,
the momentum of the pions impinging on the target is determined by reimageing
the target spot of the dispersed beam by a quadrupole triplet unto an intermediate
focus detector (IFD) in front of a splitpole. The momentum of the scattered pions
is determined from a measurement of their trajectories point and angles of inter-
section with IFD-center plane and a coordinate measurement in the focal plane of
the splitpole.

Consequently, the design of the IFD was primarily dictated by the following
requirements:

- Due to the large phase space acceptance of LEPS (solid angle $\Delta\Omega \approx 20$ msr,
source size $\Delta x \cdot \Delta y = 10 \cdot 5$ cm^2 , momentum range $-15\% \leq \Delta p/ p_o \leq 20\%$) the contribu-
tion of the higher order aberrations up to fifth order, despite of being minimized
by the ion optical design, is not at all negligible. For an efficient software
correction, a spatial resolution of $\Delta x = \Delta y = \pm 0,5$ mm and an angular resolution
ranging between ± 5 and ± 10 mrad turns out to be sufficient.

- The high pion flux to be expected with the rebuilt πE3-channel at SIN
requires stable operation without loss of efficiency even at high counting rates.

- In order to minimize the loss of resolving power caused by multiple
scattering in the IFD its effective mass/cm^2 should be as low as possible.

The most promising design for a detector that meets all these requirements
was found to be a stack of three MWPC's each with single wire read out for x- and
y-direction. Each read out plane consists of 128 wires, 10 µm in diameter with
a 1 mm pitch. The gapwidth was chosen to be 5 mm and the distance between
correspondent planes to be 50 mm. As an example of the results obtained from first
measurements with the prototype fig. 1 depicts the efficiency of one plane as
a function of the applied high voltage with an Ar-Isobutane mixture (60%/40%) at
different pressures (2). It demonstrates clearly that even at a pressure of 500
mbar the chamber can be operated reliably. Under these conditions of operation
the effective mass of the detector including the entrance and exit windows
separating it from the vacuum is reduced to 35 mg/cm^2 .
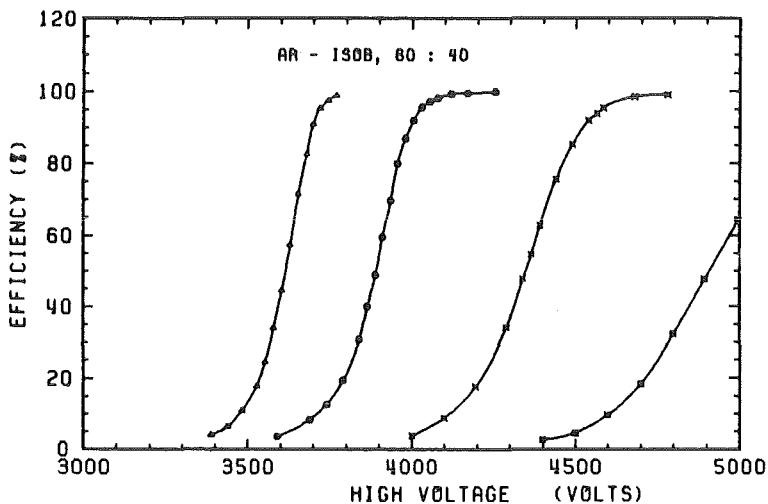
Fig. 1

Efficiency of one IFD-plane
as a function of high voltage
measured with a ^{90}Sr source
at different pressures (400,
500, 700, 984 mbar from the
left to the right)

6.3 ACCELERATORS

6.3.1 OPERATION OF THE ISOCHRONOUS CYCLOTRON (KIZ)

F. Schulz, H. Schweickert

During the period of report the machine has been in full operation (see Table I, II). The demand for beam time especially for nuclear physics experiments with Li-ions and polarized deuterons has increased by 20 %. The reason for this might be that there is no other machine in this area delivering these beams in the energy range of 26 MeV/nucleon where, in addition, experimental facilities such as the magnet spectrometer "Little John" and the unique polarized neutron facility POLKA are available. Therefore the main areas of improvement have been at the axial injection system and at the external ion sources:

- The special ERC-type ion source for Li^{3+}-ions (LISKA) is now operating very smoothly. The intensity of the 156 MeV extracted Li^{3+}-ions is routinely in the range of 100-150 nA and maximum currents up to 600 nA have been achieved (see Fig. 1);

- The new atomic beam source PASKA (see Fig. 1) for polarized deuterons, manufactured by SENTEC, Geneva, arrived in Karlsruhe at the end of 1985, with a delay of 6 months. Nevertheless since the end of June the source has been delivering up to 150 nA polarized deuterons (vector-polarization 0.5 - 0.55) on the POLKA target for nuclear physics experiments.

- During a short shut-down period in early 1985 the central region (puller, slit system) was readjusted and experimentally optimized for the injected beams. The injection efficiency is now 10 % without bunching.

- The new RF-amplifier is in routine operation at the cyclotron. A considerable improvement in stability (amplitude and frequency), compared to the odd selfexcited system has also led to an improvement in the external beam quality (especially energy resolution).
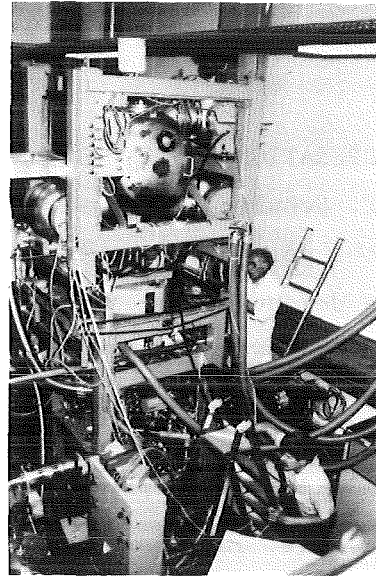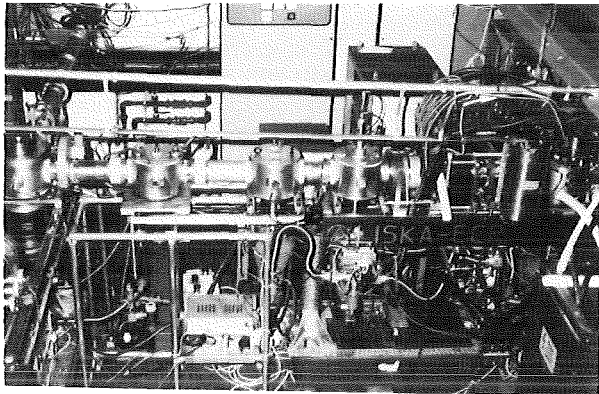
Fig. 1 The new ion sources LISKA (left side)
and PASKA (right side) inside the
ion source building

Cyclotron Operational	Internal Ion Sources		External Ion Sources		Total	
For Experiments	3165 h	37.3%	2672 h	31.5%	5837 h	68.9%
Beam Developments Testing new Components, Developments for Isotope Production	1178 h	13.9%	87 h	1.0%	1266 h	14.9%
Total Time of Operation with the Beam on Targets	4344 h	51.2%	2759 h*	32.5%	7103 h	83.8%
Scheduled shut-down for Maintenance, Repair and Installation	682 h	8.1%	45 h	0.5%	726 h	8.6%
Unscheduled shut-down	311 h	3.6%	337 h	4.0%	648 h	7.6%
Total Shift Time	5336 h	62.9%	3141 h	37.1%	8477 h	100.0%

*Lithium-6 (156 MeV) 2643 h, Polarized Deuteron 116 h

The real time of 8760 h is achieved by adding a total 11 days shut down 22.12.84 - 2.1.85

Table I Statistics of the cyclotron from July 84 to June 1985

Engineering	2.3%	
Neutron Physics	18.1%	
Solid State Physics	19.9%	

Nuclear Spectroscopy	1.9%	
Others	2.4%	
Nuclear Reactions	55.4%	
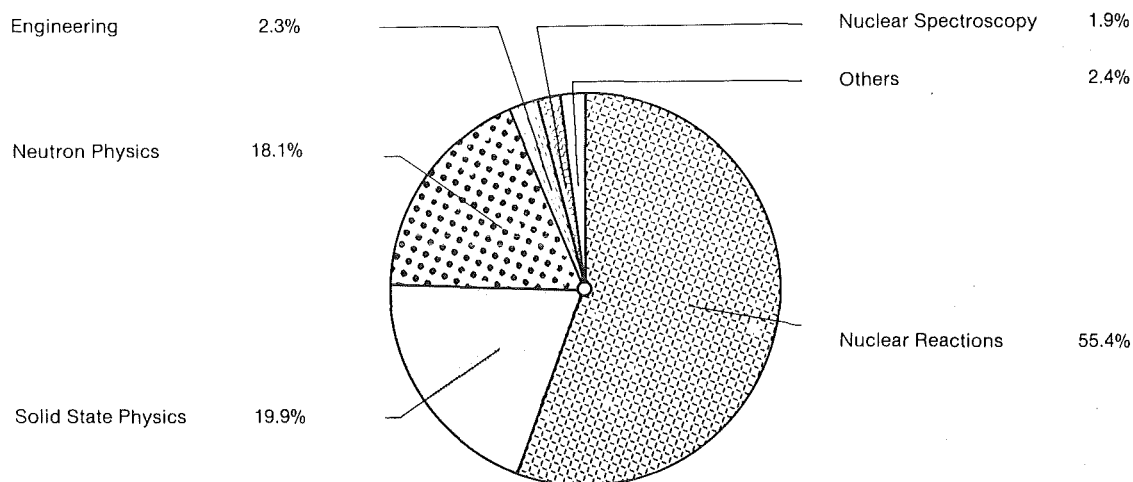
Internal Users

Institut für Kernphysik III	1679.17 h	28.76%
Institut für Kernphysik I	1063.42 h	18.22%
Institut für Radiochemie	55.50 h	0.95%
Laboratorium für Isotopentechnik	9.83 h	0.17%
Hauptabteilung Sicherheit/Dosimetrie	4.33 h	0.07%
Institut für Heiße Chemie	3.33 h	0.06%
	2815.58 h	48.23%

External Users

Universität Erlangen	947.75 h	16.24%
Freie Universität Berlin	652.83 h	11.18%
Technische Universität München	438.75 h	7.52%
Max-Planck-Institut Heidelberg	420.42 h	7.20%
Universität Tübingen	176.75 h	3.03%
Technische Hochschule Darmstadt	55.92 h	0.96%
Universität Münster	42.75 h	0.73%
Universität Mainz	42.33 h	0.72%
Universität Ulm	39.83 h	0.68%
Universität Konstanz	30.67 h	0.53%
Universität Bonn	25.58 h	0.44%
Universität Hamburg	19.50 h	0.33%
Universität Saarland	13.42 h	0.23%
Krebsforschungszentrum Heidelberg	4.75 h	0.08%
	2911.25 h	49.87%

Irradiation of Machine Parts	110.58 h	1.90%
Total	5837.41 h	100.00%

Table II   Statistics of the cyclotron from Juli 1984 to June 1985

6.3.2 OPERATION OF THE KARLSRUHE COMPACT H$^-$-CYCLOTRON (KAZ)

J. Möllenbeck, H. Schweickert

The present running mode of the cyclotron consists of four 24h-operation days, starting on late Sunday afternoon and ending on Thursday afternoon, for isotope production and irradiation of machine parts. Friday is used for maintenance, repairs and improvements. The period from Friday afternoon to Sunday afternoon will soon (late 1985) be used for materials research within the fusion project at Karlsruhe (see Fig. 1).

The reliability during the period of report was rather good, with only one isotope production failure because of problems with the D-side extraction foil mechanism. Besides the improvements of a number of electronic support equipment, the following weak parts at the machine have been upgraded:

- The radial reproducability of the extraction foil mechanism (for the irradiation of machine parts) was improved. In the energy range of 15-30 MeV the energy can now be reproduced to $\pm$ 50 keV.
- Much thinner extraction foils ($\sim$3 μg/cm^2) are now used on the isotope production side, for the energy range between 25-40 MeV, resulting in a longer life time of the foils (factor of 3-4) and also surprisingly in a better homogeneity of the beam.
- First experiments to extract simultaneously into both energy variable beam lines using a radially movable thin carbon wire ($\sim$1/10mm) were very successful.
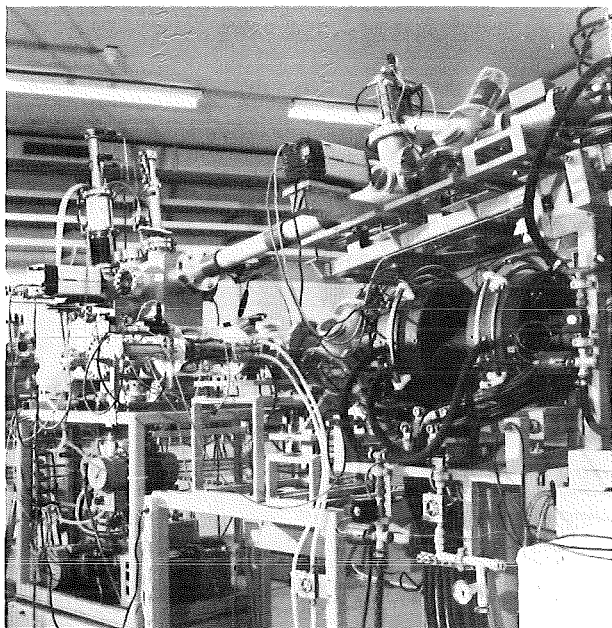
Fig. 1
Beam guiding system for the so called "Duàl-Beam-Installation". The upper beam (α-particles from KIZ) and the lower beam (protons from KAZ) are concentrated onto one target. First irradiations of fusion wall materials are planned for late 1985.

6.3.3 THE NEW COMPUTER-CONTROL FOR THE KARLSRUHE CYCLOTRON

J. Bialy, H. Heinzmann, W.-R. Kappel, B. Koegel, T.J. Thouw

The new computer control system for the Karlsruhe Cyclotron is a - three level - distributed computer system. At the first level, Data General NOVA-3 and PDP/J11 "STARBURST" computers will be used. The NOVA-3 will be used for the control-consol management, whereas the PDP's are front end process-control-computers. The PDP's are one board computers, incorporated in CAMAC. These computers of the first level will communicate with each other through CAMAC by sending and receiving defined codes. In the near future these "first level" computers will be directly connected to each other by the ethernet LAN, which is planned for 1986. In the second level "Free Programmable" Siemens Symatic-Computers will control the security system, interlock conditions and other crucial processes. These second level computers can either directly communicate with each other (through the Siemens own Symatic Communication System) or supervised by the first level computers. The third level microprocessors will be used for automated processes such as robots of power supply control, etc. These micro computers will both be connected to level two computers and/or level three computers. The communication between the three different computer levels will be based on several serial RS 232 (V-24) interconnections.

In accordance with the distributed hardware installation, a distributed control software, including distributed databases, is being developed. The software is written in FORTRAN and to a small part in ASSEMBLER. All programs are table driven to ensure flexibility for further expansion of the control system. Tables, pointers, databases, blockdiagrams etc. are generated by dialog and mask oriented off-line-programs. The results of these off-line-programs are compressed and prepared (pointers are defined and set etc.) as input data for the on-line control program.

The man-computer communication in the control system is done mainly through CAMAC touchpanels and potentiometer knobs, which are assigned through the touchpanels.

The first crude version of the control program, which controls the beamline elements, will be running by the end of 1985.

6.3.4 STATUS OF THE EXTERNAL ION SOURCES OF THE KARLSRUHE ISOCHRONOUS CYCLOTRON

H.-P. Ehret, R. Ernst, L. Friedrich, E. Huttel, J. Kaltenbaek, F. Schulz, P. Ziegler

LISKA, the ECR-source for Li^{+++} ions, has been satisfactorily operating for 2500 hours as a cyclotron injector. The intensity of the Li^{+++} beam extracted from the cyclotron is routinely about 100-150 nA during nuclear physics experiments and a maximum of 600 nA has been achieved. Since recharging of the Li-oven demands a stop of the Li-source for more than 12 hours until it is reconditioned, some efforts have been undertaken to reduce the Li consumption and to improve the charge state distribution. The best method seems to be to use a first stage ECR by which the Li vapor is ionized immediately after leaving the oven. For this purpose the field maximum of the longitudinal magnetic field has to be reduced to the 7 GHz resonance by a short iron ring. To adjust microwave power, Lithium vapor pressure and plasma flow in the first stage only by changing the dimensions of this iron ring in the small first stage plasma chamber is very time consuming, but first results are encouraging. This first stage enables a more stable operation of the source.

The ECR-source HISKA designed for fully stripped ions of gases (e.g. N^{7+}) is being reassembled. The superconducting coils have been reconstructed and the liquid He evaporation rate is now long enough (1.6 1/h) to allow detailed experiments to optimize the source.

The atomic beam source PASKA for polarized deuterons could not be installed in January as scheduled, because the guaranted intensity (60 µA) and emittance could not be achieved by the manufacturer. At the end of May the source delivered half of the specified intensity without prospects of further improvements within a reasonable time. Thus it was decided to install the source in Karlsruhe prior to achieving its specifications.

Since the end of June it has been operating at the cyclotron and has delivered polarized deuterons for nuclear physics experiments without any interruptions worth mentioning. The measured vector polarization was 0.5 - 0.55. In the analyzed beam after the horizontal deflection 12 µA of polarized deuterons were measured behind the ionizer and by shutting down the hexapoles an intensity of 23 µA of polarized deuterons in the vertical beam could be concluded. By this it is evident that the horizontal deflection has to be improved.

6.3.5 PRODUCTION OF ISOTOPES FOR MEDICAL APPLICATION

S. Augstein, K.H. Assmus, V. Bechtold, H. Dohrmann, D. Erbe, E. Foßhag, A. Hanser, R. Hüfner, N. Kernert, W. Maier, J.W. Peters, H. Ripp, U. Sahm, M. Seidler, H. Schweickert, S. Sheikh, S. Uhlemann

Radioactive isotopes for medical diagnostics are now routinely produced four times a week, starting Sunday night. Besides hospitals, the main customers are pharmaceutical companies in Germany. The status for the medical isotopes at the compact cyclotron is described in the following.

Ultra-pure I-123

Since August 1984 I-123, practically free of contamination, has been produced. The production process involved is:

$$^{124}Xe(p,2n)\,^{123}Cs \xrightarrow{\text{5.9 min}} \,^{123}Xe \xrightarrow{\text{2.08 h}} \,^{123}I$$
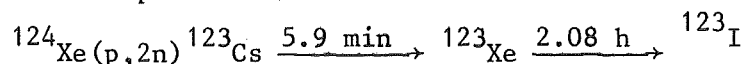
Fig. 1 shows the iodine production target.

The Xe-124 gas used is highly enriched ($\geq$ 99.8 %) which results in an ultra pure I-123 end product. According to measurements of the Physikalisch-technische Bundesanstalt in Braunschweig the impurity for I-125 is $1.5 \cdot 10^{-5}$ at EOB, whereas I-124 is not detectable. The production yields of I-123 with 30 MeV protons are 10 mCi/µAh. At present Karlsruhe is the only producer of this high quality I-123 in Germany. Since the ultra pure I-123 has been available the demand for it has grown by 30 % which has been met by a higher production rate. To increase the production capacity further a new target and a hot cell are under construction.

$^{81}Rb/^{81m}Kr$ Generator

Compared to last year 10 % more generators were delivered to hospitals for ventilation studies. Since early 85, a new cation exchange resin has been used in the routine production. It greatly simplifies the clinical use of the generator and enhances the elution reliability. In contrast to the resin used before it requires no humidification of the elution gas.

The installation of the new hot cell for ^{81}Rb distribution and quality control has been finished and extensively tested and is now used in routine production.

Since the demand for pure ^{81}Rb has increased over the last year, several generators per week are produced in addition for subsequent mass-separation (1).

^{201}Tl-Chloride

The irradiation facility for thallium has been built and tested. The isotope Tl-201 is produced via the reaction $^{203}Tl(p,3n)\,^{201}Pb \xrightarrow{\text{9.4 h}} \,^{201}Tl$. Due to this process a chemical separation must be performed after irradiation. The separation facility was completed in April 1985. The hot cell where the separation will be carried out has to be modified before the first test production can be started.
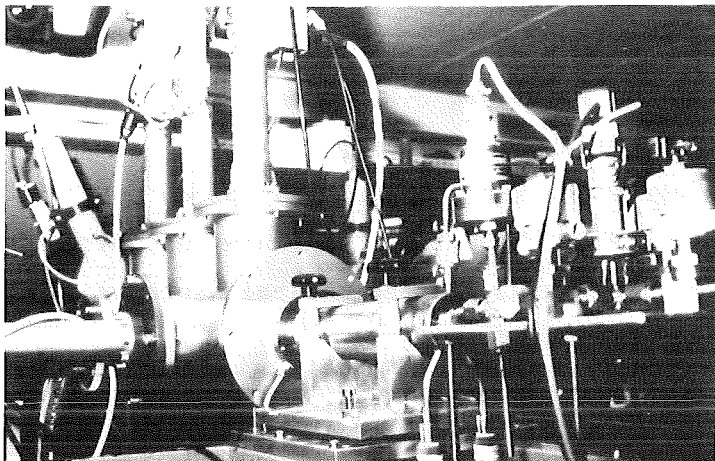
(1)   A. Hanser, this report Sect. 6.3.6

6.3.6 AN ISOTOPE SEPARATOR FOR ROUTINE SEPARATION OF ^{81}Rb

H. Dennerlein, B. Feurer, and A. Hanser

An electromagnetic isotope separator for routine production of isotopically pure ^{81}Rb for medical use has been constructed. High efficiency which is essential for such an application, is achieved by employing an ion source with surface-volume ionization (1,2); for convenient charging a special ion source set-up was developed. The acceleration voltage is 30 keV. The magnetic analyser has the following specifications: 50 cm mean radius, 90° deflection, 105 cm mass dispersion at the catcher position, edge focusing for the axial direction. An einzel lens between the ion source and the magnetic analyser is used for fine focusing. The catcher for the separated ^{81}Rb ions is a small removable stainless steel plate covered with a thin NaCl crust. This unusual catcher material is used because medical injection solutions can be easily prepared from it. The catcher is automatically masked if the position or the quality of the ^{81}Rb focus is not (near) optimum, or should another isotope be directed to it. Three 1200 l/s oil diffusion pumps with refrigerator-cooled baffles are used for vacuum pumping.

The radioactive rubidium is produced by irradiating natural krypton with 36 MeV protons using the existing facility for charging ^{81m}Kr generators (3). The isotopical composition i.e. the activity ratios one hour after EOB is ^{81}Rb: ^{82m}Rb: ^{83}Rb: ^{84}Rb = 1 : 1.3 : 0.02 : 0.02. This rubidium activity, fixed onto a small ion exchanger column, is transferred to the isotope separator and is washed from the resin with 1.5 ml 1nHNO$_3$. The solution is evaporated on a small tantalum plate, which can be conveniently introduced into the ion source using a vacuum interlock.

A series of test measurements carried out as random tests between the routine separations resulted in factors of $3-5 \cdot 10^4$, $1-2.5 \cdot 10^5$, and $2.5-10 \cdot 10^5$ for

the reduction of contamination by ^{82m}Rb, ^{83}Rb, and ^{84}Rb, respectively. The isotope separation process efficiency (corrected for radioactive decay) was measured to be (89 ± 9) %.

Since the beginning of routine production in November 1984, 57 batches with a total of 2.2 Ci have been prepared and delivered to clinics. During this time the isotope separator has been found to be reliable. The ion source which usually is the major wearing part of an electromagnetic isotope separator, did not require any repairs or maintenance.
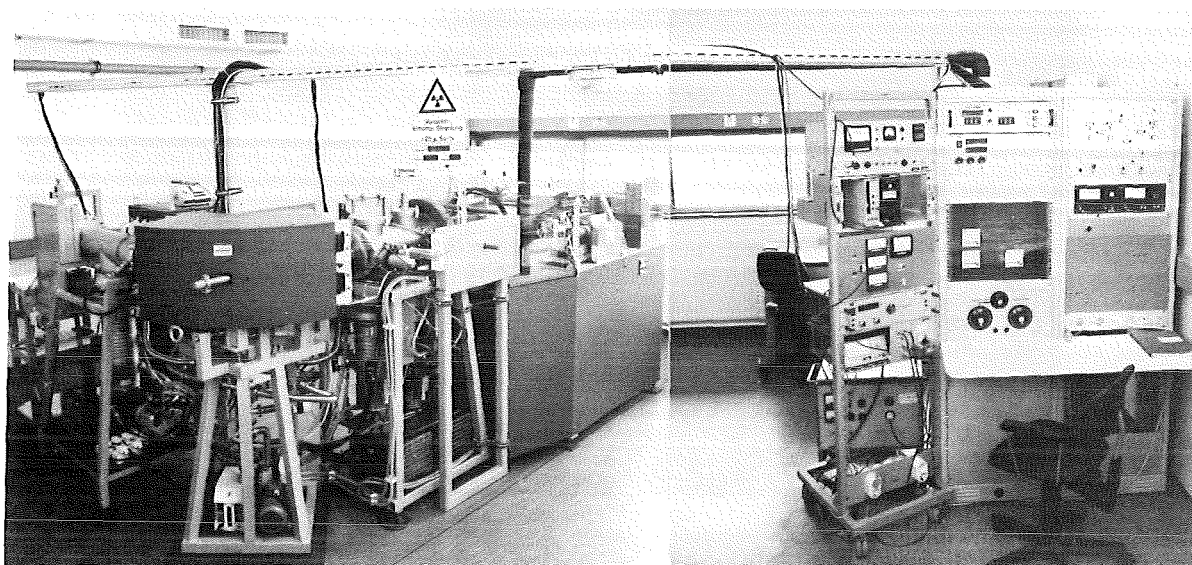
Fig. 1 View of the isotope separator in January 1985

(1)   G.J. Beyer et al., Nucl. Instr. Meth. 96 (1971) 439
(2)   P.G. Johnson et al., Nucl. Instr. Meth. 106 (1973) 83
(3)   this report, Sect. 6.3.5

6.3.7 ACTIVATION OF MACHINE PARTS FOR MECHANICAL ENGINEERING
       R. Blank, E. Bollmann, P. Fehsenfeld, A. Kleinrahm, B. Schüssler
The production of thin-layer-activated machine parts has been running without any difficulties. The new irradiation facility installed at the compact cyclotron has been working with the expected reliability for the service supplying activated components to industries and research institutes. Somewhat more interesting than this service may be the development of the activation and measuring technique for quantitative analysis of material displacements on stressed surfaces of wheel and rail tribosystems. This work has been performed in co-operation with the Bundesbahnversuchsanstalt Minden. The measuring method was put into test at the high-load wheels of a container crane (see Fig. 1 below).

The movement of the material was measured by autoradiogrammetric survey of thin layer activated spots on the wheel of the crane during operation. The material displacements of about 4 mm have been detected with an accuracy of 0.2 mm. The measurements have been performed in order to improve the service time of the crane wheels by a factor of six.
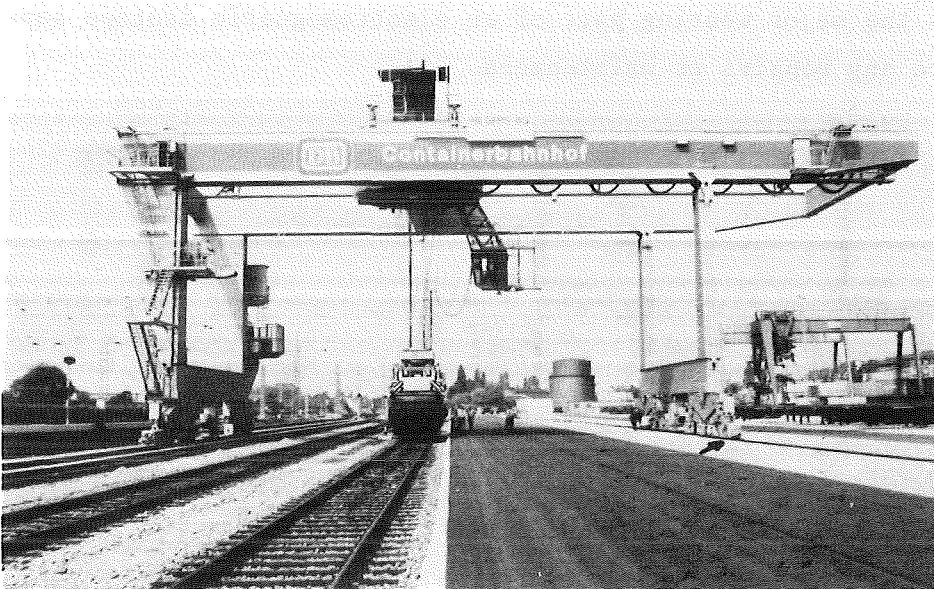
Fig. 1 Container crane of the Bundesbahn, weight 600 t, carrying capacity 35 t, spanwidth 40 m, speed (max.) 100 m/min. The tribological bahaviour of the high-load 24 crane wheels (26 t per wheel) has been analyzed by a new measuring procedure of radionuclide technique.

Fig. 2
Device for autoradiogrammetric survey on the wheel of the crane, recording quantitatively the material displacements in the tyre.

6.3.8 ELECTRON COOLING AT LEAR

H. Budig, M. Girardini[+], C. Habfast, H. Haseroth[+], C. Hill[+], L. Hütten, H. Poth, B. Seligmann, J.L. Vallet[+], and A. Wolf[++]

Complementary to stochastic cooling the installation of an electron cooling device in the Low Energy Antiproton Ring (LEAR) at CERN is planned for 1986. The major milestones for the electron cooler achieved between August 1984 and August 1985 were:

- assembling of the entire cooling device (Fig. 1),

- vacuum tightness,

- first electron beam in the unbaked vacuum system (17 kV, 1 A),

- successful in situ bakeout and achievement of the design vacuum limit for the cold system (5 x 10^{-12} Torr), and

- achievement of high pressure gradient with hot chathod.

As described in previous reports (1), the ICE (2) electron gun and collector with some modifications were successfully tested in a subassembly, while the vacuum system was completely rebuilt to meet the LEAR requirements (3). The entire electron cooler is designed for a maximum electron energy of 40 keV at about 4 A current.
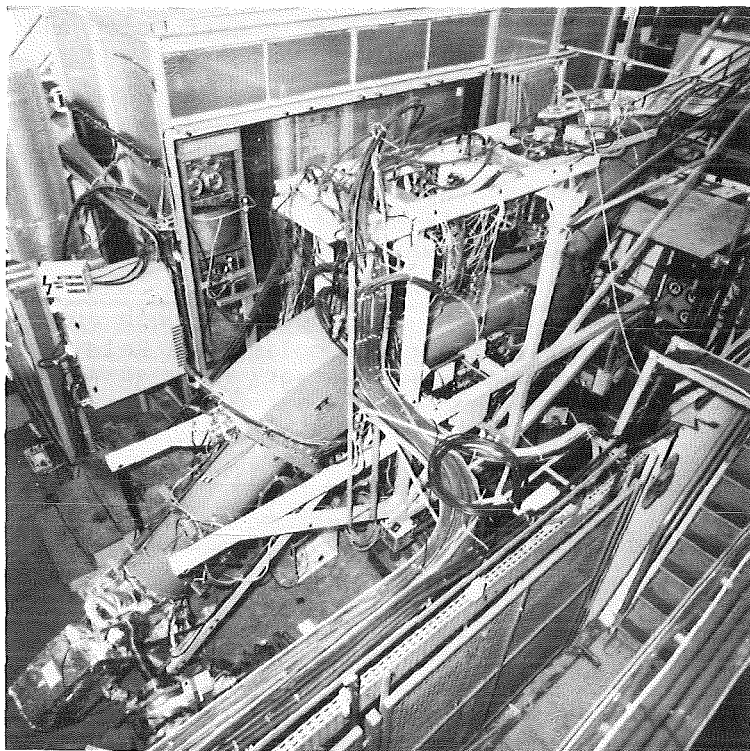
Fig. 1

The LEAR electron cooler

Contrary to their operation at ICE, gun and collector will work over a wide range of electron energies chosen to match the various $\bar{p}$ momenta. This energy ramping has been investigated. Useful invariant operating parameters of gun, col-

lector and magnets currents have been found. On the base of these results, the remote control software (4) has been extended.

Scanning the electron beam profile by measuring Thompson scattered and Doppler shifted photons was proposed in a previous report (5). An experimental set up in order to realize this method, known as laser diagnostics, has been designed and constructed. First measurements are scheduled before the end of 1985.

For determination of the transversal energy of the electron beam, antennas are distributed along the electron beam line in order to receive microwave radiation from electrons gyrating in the longitudinal magnet field. First signals were observed.

For the second stage of the electron cooler development at LEAR a new gun and collector are to be constructed in order to provide a high precision 100 keV electron beam of 4 A current. Extrapolation from measurements with the ICE collector led to the conclusion that it will not be possible to recuperate an electron beam of that power in a collector of this type. Therefore a new collector scheme was studied in computer simulations. A simple experimental set up to test different collector concepts is under construction.

Theoretical work has been done developing a computer code to simulate the cooling process for given storage ring and electron beam parameter (6). The program is producing data now for cooler rings planned or under construction all over the world.

(1)   C. Habfast, H. Haseroth, C.E. Hill, H. Poth, B. Seligmann, J.-L. Vallet and A. Wolf, Status and Perspectives of the Electron Cooling Device under Construction at CERN, contribution to the third LEAR Workshop, Tignes, 19-26 January 1985, CERN-EP/85-49 (1985); KfK-Report 3621 (1985) 187
(2)   M. Bell, J. Chaney, H. Ferr, F. Krienen, P. Møller-Petersen and G. Petrucci, Nucl. Instr. Methods 190 (1981) 237
(3)   M. Brouet, M. Girardi, C. Habfast, L. Hütten, A. Poncet, H. Poth and A. Wolf, contribution to the Workshop on Electron Cooling and Related Applications (ECOOL 84), Karlsruhe, 24-26 September 1984, KfK 3846 (1985)
(4)   Annual Report 1983/84, KfK 3815 (1984) 180
(5)   KfK-Primärbericht (1982)
(6)   A. Wolf, Realistic calculations concerning electron cooling in storage rings, CERN-EP/85-27 (1985) talk given at Workshop on Electron Cooling and Related Application (ECOOL 84) Karlsruhe, 24-26 September 1984, KfK-Report 3846 (1985)

6.3.9 STUDIES ON AN HIGH INTENSITY PROTON ACCELERATOR

P. Blühm, H. Koch, G. Schaffer (1)

A concept for an high intensity accelerator independent from SIN as injector was developed. The requirements caused by the design goals (30 Gev, 100 μA, slow and fast extraction, lowest possible beam losses) had direct impact to the design of the accelerator complex. The proposed scheme, as is shown in Fig. 1 and is characterized by the parameters indicated in Table 1 will be the starting approximation for the design of an European Hadron Facility - EHF - , which will be done by a larger community of european physicists in near future.

Table 1 Configuration of an high intensity accelerator complex operating at 25 Hz repetition frequency.

accelerator components	particle	particle energy [GeV]	radius [m]	circumference/length [m]	radiofrequency [MHz]	peak current $\hat{i}$ [ma]	average current I [ma]	$\frac{\Delta\omega}{\omega}$ [%]
linac	H⁻	0.001 → 0.6	--	300	⩾ 200	40	0.1	--
BO-SY booster synchrotron	p	0.6 → 5.0	∼ 215	1350	40 →50	880	0.1	25
SY synchrotron	p	5.0 → 30.0	∼ 215	1350	50 →50.5	880	0.1	1
stretcher	p	30.0	215	1350	--	--	0.1	--

Parallel to this technical details on an high intensity proton accelerator using the existing SIN cyclotron as an injector were discussed in close contact to the study group of SIN. Special attention was given to the problems of fast beam kickers (2000 Hz for Astor and 25 Hz for the synchrotron). Possible solutions were developed and proposed. On the field of secondary beams a high purity low momentum K-beam was investigated in context with a special extraction scheme from the primary target (2). In order to achieve a low π-contamination an intermediate focus was introduced in front of the separation stage, thus defining the channel acceptance properly. A 1.8 m long electrostatic separator will allow a good π/K separation at the mass slit over the whole momentum range from 400 MeV/c to 700 MeV/c. In a focus of 0.8 cm x 0.6 cm a K⁻ rate of 10^7 K⁻/sec at 700 MeV/c and 10^5 K⁻/sec at 400 MeV/c should be possible.

H⁻ source and RFQ preaccelerator

600 MeV linear accelerator
L ≈ 300 m
200 MHz, I_H^- ≈ 40 ma

BOOSTER-
synchrotron
0.6 - 5 GeV
40 - 50 MHz

SYNCHROTRON
5 - 30 GeV
50 - 50.5 MHz

foil

fast ejection
$\bar{I}$ = 100 µa

R≈215 m

slow ejection
$\bar{I}$ = 100 µa

STRETCHER 30 GeV

production
targets for
secondary beams
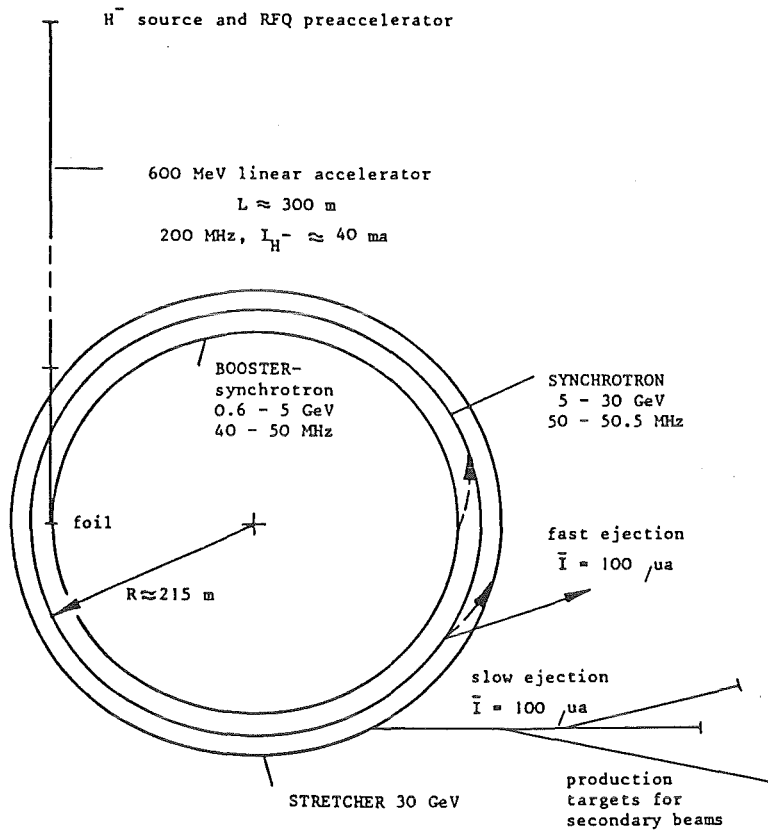
Fig. 1 Accelerator complex. The beam is accelerated to final energy in a rapid cycling synchrotron which receives it in a single turn from a rapid cycling booster synchrotron of about equal circumference. The booster is filled in several turns from an H⁻ linac by charge exchange (H⁻→H⁰→p)

(1)   ditto, Workshop on nuclear and particle physics at intermediate energies with hadrons, April 1985
(2)   Ch. Tschalär, internal report SIN TM 39-01

6.4   APPLICATIONS

6.4.1   THE KARLSRUHE ION MICROPROBE SETUP AND ITS APPLICATIONS

D. Heck, (1)

The ion microprobe setup is installed at the 3.75 MV Van de Graaff accelerator of the Karlsruhe nuclear research center. The generation of the tiny beam diameter with micrometer dimensions is achieved by narrow collimation with consecutive focussing of the projectiles. Details of the setup are described and the analytical capabilities are demonstrated. Proton induced X-rays are applied to the spatial resolved trace element analysis of human liver specimens. Nondestructive three-dimensional elemental analyses of light elements in specimens of solid state and material research are possible by energy discrimination of the charged particles emerging from nuclear reactions and scattering.

(1)   ditto, Atomkernenergie - Kerntechnik 46 (1985) 187

6.4.2   MATRIX CORRECTION FOR PIXE IN BIOMEDICAL SAMPLES

D. Heck and E. Rokita[+], (1)

This report describes the programs MATRIX2, STPPWRF2 and MUROFIT, which are used for the calculation of the matrix correction factors, which must be applied to concentrations determined by PIXE (Proton induced X-ray emission). The correction takes into account the slowing down of the protons along their path through the specimen, which causes a decreasing X-ray production along this path. Moreover these X-rays are attenuated penetrating the specimen towards to the X-ray detector. The matrix correction factors regard these effects in dependence on the proton impact energy, the specimen and detector geometry, the specimen composition and the energies of the interesting X-rays.

(1)   ditto, KfK-Report 3909 (1985)

+   Institute of Physics, Jagellonian University, Kraków, Poland

6.4.3   PROTON INDUCED X-RAY EMISSION FOR TRACE ELEMENT ANALYSIS IN HUMAN LIVER TISSUE

A. Ochs[+], D. Heck, C. Kratt[++], B. Schneider[++], K.P. Maier[+], (1)

The conventional procedures for trace element concentration analysis are affected with disadvantages: Special histological stainings permit only a grading by

estimation of the colour intensity. Wet chemical treatment, sputtering for atomic spectroscopy or neutron activation are very accurate, but a simultaneous determination of the trace element concentration and its correlation with the histological structure is not possible. The electron induced X-ray emission would permit a spatial correlation, but it is not sensitive enough for trace element analysis. This work examines, whether the method of proton induced X-ray emission with microfocussing enables a structure-correlated trace element analysis.

(1)   ditto, Verh. Deutsch. Ges. f. innere Medizin 90 (1984) 1531

+   Med. Klinik der Städt. Krankenanstalten, Esslingen
++   Patholog. Institut der Städt. Krankenanstalten, Esslingen

6.4.4   ELEMENTAL COMPOSITION OF THE HUMAN ATHEROSCLEROTIC ARTERY WALL

T. Cichocki[+], D. Heck, L. Jarczyk[++], E. Rokita[++], A. Strzalkowski[++], M. Sych[+], (1)

The elemental composition of human, atherosclerotic popliteal artery was examined by means of the proton induced X-ray emission (PIXE) method. Applications of the narrow proton beam (3×10 μm^2) enabled not only the determination of concentrations of following elements: Cl, K, Ca, Fe, Cu, Zn, Br and Pb, but also their localization in the different artery wall regions. The highest mean concentrations of Cl, K, Zn and Br were found in tunica media. The distributions of Ca and Fe varied in investigated sections, sometimes they prevailed in tunica intima, in other cases the highest concentrations were observed in tunica media or tunica adventitia. The concentration profiles of each element are characterized by many sharp narrow peaks. The highest concentrations of Ca and Fe showed so high levels that only one explanation is possible: presence of crystals. The correlation of Ca peaks with those of Zn and Fe is discussed.

The usefulness of the micropixe method for the investigation of biomedical materials is also considered.

(1)   ditto, Histochemistry (in print)

+   Academy of Medicine, Kopernika 7, Pl-31034 Kraków, Poland
++   Institute of Physics, Jagellonian University, Reymonta 4,
         Pl-30059 Kraków, Poland

6.4.5 THE EVALUATION OF TISSUE Ca BY PROTON INDUCED X-RAY EMISSION IN THE
ARTERIES OF SPONTANEOUSLY HYPERTENSIVE AND NORMOTENSIVE RATS

C. Spieker[+], D. Heck, W. Zidek[+], G. Kereny[++], H. Losse[+], H. Vetter[+], (1)

Numerous investigations have given evidence that Ca^{2+} plays a critical role in the pathogenesis of hypertension. The intracellular Ca^{2+} measurements were mainly carried out with Ca^{2+} selective electrodes. In the present study the particle induced X-ray emission (PIXE) was used for investigating the Ca distribution of arterial smooth muscle of spontaneously hypertensive and normotensive rats. PIXE yields a correlation of the Ca distribution with the morphological structure of the arterial muscle. The Ca content of the aortic wall of 6 spontaneously hypertensive and 4 normotensive rats was investigated. The results demonstrate that the tissue Ca found mainly in the smooth muscle containing tunica media of hypertensive rats are much higher (3105 $\pm$ 569 µg Ca/g tissue) than of normotensive rats (2031 $\pm$ 478 µg Ca / g tissue).

(1)   ditto, Klinische Wochenschrift 63 (1985) Suppl. III, p. 74-77

+   Medizinische Poliklinik, Universität Münster
++   Institut für Arterioskleroseforschung an der Universität Münster

6.4.6 SPATIALLY RESOLVED HYDROGEN ANALYSIS IN SURFACES WITH THE ION MICROPROBE

D. Heck

The importance of hydrogen concentration determination is rising with increasing interest in catalytic hydrogen burning for car drives and with the progress in fusion technology for energy generation. Of special interest is the metal corrosion by hydrogen embrittlement. In the ion microprobe the detection of hydrogen via ion induced X-rays is prohibited by their absorption in the entrance window of the detector. Hydrogen sensitive charged particle induced nuclear reactions are only possible with "exotic" ions which are not available with our RF ion source [e.g. for the reactions $^1H(^7Li,\alpha\gamma)$ or $^1H(^{11}B,\alpha\gamma)2\alpha$] or which need energies, which exceed the capabilities of our v.d. Graaff accelerator and cannot be focussed by the ion microprobe [e.g. for the reaction $^1H(^{19}F,\alpha\gamma)^{16}O$ with 16.3 MeV or $^1H(^{15}N,\alpha\gamma)^{12}C$ with 6.4 MeV]. For scattering experiments the projectiles must be different from protons to prevent an implantation of hydrogen in the sample, which cannot be distinguished from the original hydrogen distribution. For kinematic reasons, a backward scattering is impossible. But by a He-beam hydrogen may be knocked out by recoil in forward direction from a surface suitably inclined relative to the incoming beam (elastic recoil detection = ERD); it is detected in a surface barrier particle detector.
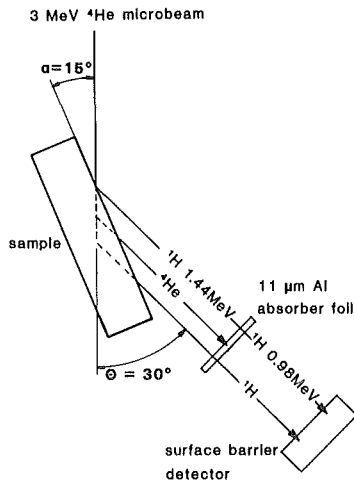
Fig. 1

Arrangement of sample and detector for ERD-analysis of hydrogen

First tests with a sapphire sample in the geometry of fig. 1 revealed an analysis within a depth of 1 μm. The depth resolution of 0.1 μm is caused by the kinematic broadening according to the detector acceptance angle ($29° \leq \theta \leq 31°$). In fig. 2 the hight of the peak at channel 210 corresponds to a hydrogen surface layer contamination of 2×10^{16} at/cm². The sensitivity is limited by the background which increases with lower channel numbers (increasing depth). This background is produced presumably by multiple scattering events. For spatially resolved analysis in the micrometer range further problems arise from the local sample modification. It limits the collection of a statistically relevant proton spectrum at the point of interest.
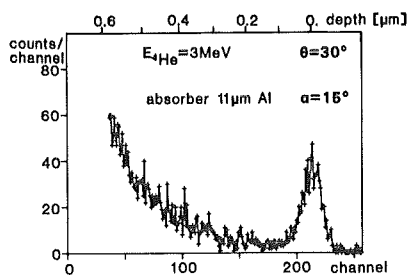
Fig. 2

ERD spectrum of Al_2O_3.
A total charge of 0.4 μC was collected in an area of 50 x 150 μm².

6.4.7 ACCURATE DETERMINATION OF THE ^{235}U ISOTOPE ABUNDANCE BY GAMMA SPECTRO-
METRY - A USER'S MANUAL FOR THE CERTIFIED REFERENCE MATERIAL EC-NRM-171 /
NBS-SRM-969

P. Matussek (1)

The purpose of the manual is to serve as guide in applications of the Certified
Reference Material EC-NRM-171/NBS-SRM-969 for accurate ^{235}U isotope abundance mea-
surements on bulk uranium samples by means of gamma spectrometry. The manual pro-
vides a thorough description of this non-destructive assay technique. Crucial mea-
surement parameters affecting the accuracy of the gamma-spectrometric ^{235}U iso-
tope abundance determination are discussed in detail and, wherever possible,
evaluated quantitatively. The correction terms and tolerance limits given refer
both to physical and chemical properties of the samples under assay and to rele-
vant parameters of typical measurement systems such as counting geometry, signal
processing, data evaluation and calibration.

(1)   ditto, KfK-Report 3752 (1985)

6.4.8 PLUTONIUM ISOTOPIC ANALYSIS BY GAMMA SPECTROMETRY IN REPROCESSING PRODUCT
SOLUTIONS

H. Eberle, H. Ottmar

The KfK K-edge densitometer, which has been primarily designed for the accurate
determination of the uranium and plutonium concentration in reprocessing product
solutions by means of X-ray absorptiometry at the K-absorption edge (1), provides
as an additional option the possibility to measure also the isotopic composition
of the plutonium product (2).

The plutonium isotopic composition is obtained from a passive gamma count-
ing of the plutonium samples. The analysis makes use of the low-energy 39-, 43-,
45- and 51-keV gamma rays from ^{239}Pu, ^{238}Pu, ^{240}Pu and ^{239}Pu, respectively. A se-
cond spectral region used in the analysis includes the 129-, 148- and 153-keV
gamma rays from ^{239}Pu, ^{241}Pu and ^{238}Pu. The respective isotopic gamma rays are
marked in the gamma spectrum from a typical reactor-grade plutonium sample shown
in Fig. 1. The isotope ^{242}Pu, which does not emit a detectable gamma-ray signa-
ture, is estimated from an isotopic correlation between the isotopes ^{239}Pu, ^{240}Pu
and ^{241}Pu.

The adopted scheme of analysis permits the determination of the isotopic
composition from freshly separated plutonium samples. Aged samples with an appre-
ciable Am content ($\gtrsim$ 0.2 %) cannot be reliably analysed, because in this case the
low-energy gamma rays below 60 keV are masked by the Compton tailing of the abun-
dant 60 keV gamma ray from ^{241}Am.
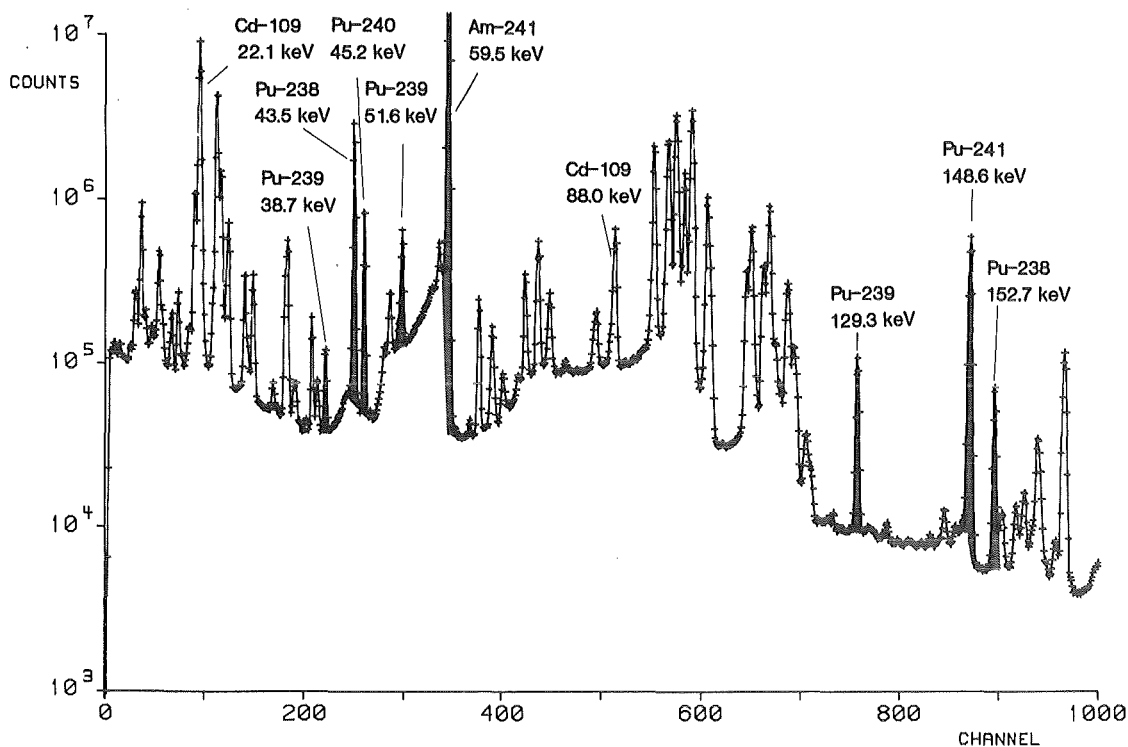
Fig. 1 Low-energy part of the passive gamma spectrum from a plutonium product
solution. Gamma rays used for the isotopic analysis are marked by hatched
areas.

The gamma-spectrometric technique has been successfully demonstrated by
measurements on plutonium product solutions from the Karlsruhe Reprocessing Plant
over a period of about one year. The results so far obtained can be summarized as
following:

-The inherent precision from a 2000 s gamma counting are 0.8 % for ^{238}Pu,
0.15 % for ^{239}Pu, 0.35 % for ^{240}Pu and 0.7 % for ^{241}Pu. The actually ob-
served precisions for ^{239}Pu and ^{240}Pu were lower by about a factor of 2
due to a small systematic measurement bias of the ^{239,240}Pu results from
samples with high (> 30 %) ^{240}Pu abundance.

-The average deviations from mass-spectrometric reference values are $\leq$ 0.3%
for the measured isotopes 238, 239, 240 and 241.

-The potential precisions and accuracies for a complete isotopic analysis
are basically limited by the relatively poor ^{242}Pu estimates ($\pm$ 10 %) from
the isotopic correlation, which at larger counting times ($\geq$ 2000 s) affect
the assay performance for the major isotopes ^{239}Pu and ^{240}Pu.

-The use of reactor-specific isotopic correlations for ^{242}Pu, obtained from
historical reactor fuel data, could probably improve significantly the
overall performance of the plutonium isotopic assay from gamma spectro-
metry.

(1)   H. Eberle, H. Ottmar, Report JOPAG/06.85-PRG-116, Kernforschungszentrum Karlsruhe (1985)
(2)   H. Eberle, H. Ottmar, P. Matussek, Report JOPAG/04.85-PRG-113, Kernforschungszentrum Karlsruhe (1985)

6.4.9   AN X-RAY SPECTROMETER FOR PRECISE URANIUM AND PLUTONIUM ANALYSIS IN DISSOLVED SPENT NUCLEAR FUELS

H. Ottmar, H. Eberle

One of the most important and difficult analytical determination for nuclear materials accountancy within the nuclear fuel cycle exists at the reprocessing headend, where uranium and plutonium have to be quantitatively analyzed with high accuracy after the dissolution of the spent nuclear fuels. In the highly radioactive dissolver solution, containing all the fission products with a total β,γ-activity of up to a few 10^{12} Bq/l, the major element uranium is usually present at a concentration level of about 200 g/l, while the plutonium concentration is lower by a factor of 100 - 200 for light water reactor fuels.

The analytical technique commonly used for this purpose is Isotope Dilution Mass Spectrometry (IDMS). It is a fairly elaborate and accurate method, but requires a number of remote sample handlings and treatments in a hot cell environment. As an alternative, we have developed an X-ray spectrometer, which permits a direct quantitative uranium and plutonium analysis with a minimum of operator interactions (1).

The instrument makes use of two proven nondestructive X-ray techniques: energy-dispersive K-edge X-ray absorptiometry ('K-edge densitometry'), and energy-dispersive X-ray fluorescence (XRF) analysis of K X-rays. The layout and measurement geometry of the spectrometer is shown in Fig. 1.

The interrogating X-rays are obtained from an X-ray tube with a tungsten target, which is operated at 150 kV/15 mA. K-edge densitometry for the major element uranium is performed in the direct X-ray beam through a 2 cm thick solution sample. The minor element plutonium is determined from the simultaneously performed XRF analysis on a smaller sample vial, containing 1 ml of the dissolver solution. A major feature of the assay approach is the fact, that the whole assay process for analysis of uranium and plutonium is reduced to the measurement of two ratios: the X-ray transmsssion ratio at the K-edge of uranium, and the intensity ratio of fluorescence K X-rays from uranium and plutonium. This adds great reliability to the measurement.

The spectrometer has been installed in a hot cell of the European Institute for Transuranium Elements (TUI), Karlsruhe, for performance evaluation. The

K-XRF Analysis

XRF Detector

Filters

Cavity for External Sample

Reference Foil

K-Edge Detector

K-Edge Densitometry

Tube Shielding

X-Ray Tube

Tube for Sample Transport

[109]Cd Source
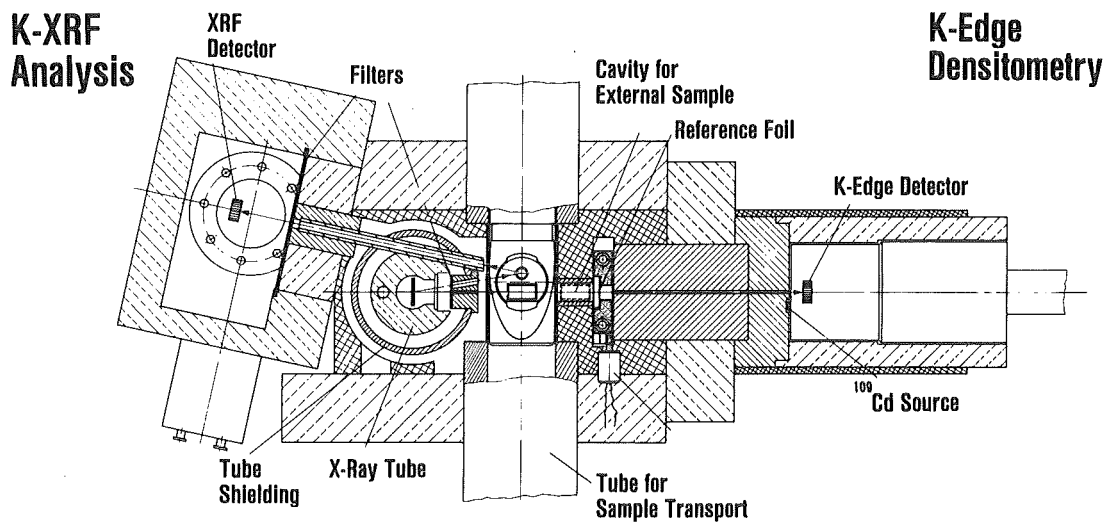
Fig. 1 Cross-sectional plan of the hybrid X-ray spectrometer for uranium and plutonium analysis in dissolver solutions of reprocessed spent nuclear fuels.

dissolver solution samples are directly loaded into the measurement cuvettes in a hot cell, from which they are then mechanically driven by a sample transport system into the shielded spectrometer located outside of the hot cell. During the nondestructive analysis the samples remain safely contained inside a stainless steel tube used for the sample transport.

The projected measurement accuracies (1σ) for a 20-min assay time are 0.3% for uranium and about 1% for plutonium. The plutonium assay error is predominantly determined by counting statistics. The assay time is therefore normally extended to about one hour in order to bring the plutonium assay error down to 0.5%. These figures compare favorably with the performance of the traditional IDMS. The actual performance of the spectrometer is currently being evaluated from measurements on a larger number of real dissolver solutions from the Karlsruhe Reprocessing Plant.

(1)   H. Ottmar, ESARDA Bulletin No. 4 (1983)

6.4.10 A PORTABLE LOW LOST μP-BASED DATA PROCESSING UNIT FOR K-EDGE DENSITOMETRY
OF Th, U, Np, Pu, Am

I. Michel-Piper, P. Matussek

During the past few years we have developed the technique of X-ray absorption
edge spectrometry ('K-edge densitometry') to a proven analytical method for the
precise and reliable determination of heavy element concentrations. A prototype
K-edge densitometer is installed since 1983 at the European Institute for Trans-
uranium Elements (TUI), Karlsruhe, where it is primarily employed for the assay
of uranium and plutonium in the product solutions from the Karlsruhe Reprocess-
ing Plant WAK. The instrument software is presently laid out for the analysis of
the elements Th, U, Np, Pu and Am. Extensions for the analysis of other high Z
elements ($Z \gtrsim 40$) are possible.

Fig. 1 shows a photograph of the densitometer installation at TUI. The ab-
sorption edge spectra are recorded and processed on a fixed installed disk-based
ND 6600 computer system (A).
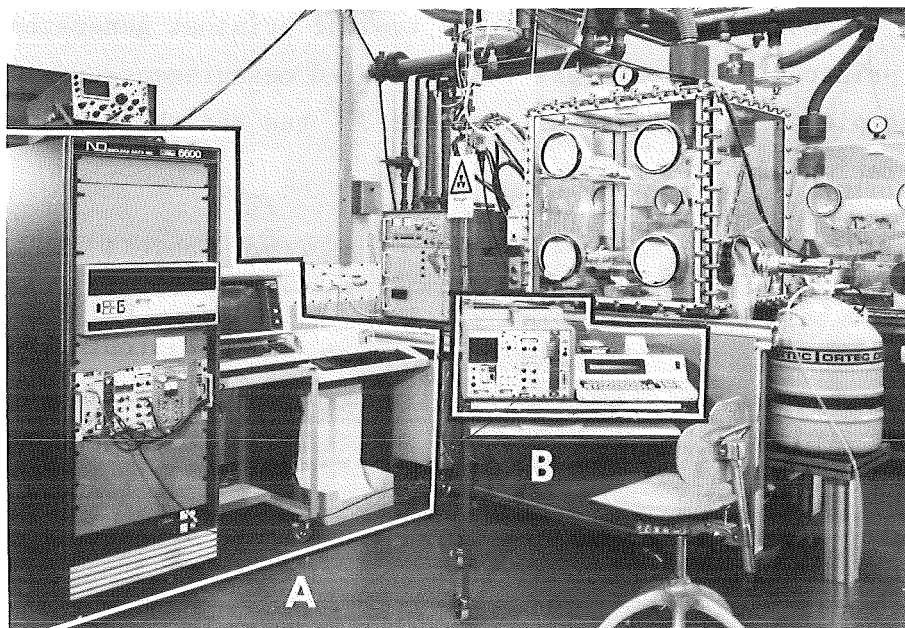
Fig. 1 K-edge densitometer at TUI with both computer systems in comparison:
The fixed system (A) and the μP-system (B).

Alternatively, spectrum accumulation and analysis is also possible on a
compact microprocessor-based data processing unit (B), which has been recently
developed and tested (1). The major incentive to the development of the latter
system arises from the request of International Safeguards Authorities for pos-
sibilities to verify independently measurement data from installed assay sys-
tems, which are used for accountancy measurements of fissile nuclear materials.
One of the proposed procedures includes the collection of measurement data to

the Safeguards inspector with own electronics in parallel to the measurement of the plant operator. An inspector shall be able to accumulate spectra on his own MCA, to save them on a portable storage medium and to evaluate them with his own software package. The validation of the measured data can be done by the inspector, measuring, e.g., an inspector-owned test material in the operator's instrument, which at the same time is also connected to the inspector's MCA.

The microprocessor-based system consists of a portable NIM-modular multichannel analyser (model Silena) comprising a 400 MHz ADC, a digital stabilizer, a 2K memory and a display with detector HV-supply unit. A general purpose µP-module (1/2 NIM width) controls the MCA, a dedicated program module (1/12 NIM) for the special user firmware, and the "IRIS"-terminal equipped with an own µP for independent recording of spectra. The keyboard of the terminal serves for data and command input on the basis of a display dialogue. The terminal is also equipped with a twenty column printer and an ECMA 34 cassette recorder. The user program "K-Edge" fits into four 2732-EPROMS and was developed using an INTEL MDS 800 system.

Table 1 shows an extraction of the typical printout generated by the µP-system. The printout example refers to 3 repeated measurements of 1000 s each on an uranium sample, giving the result for the 3rd run and the mean value and standard deviation of all 3 runs.

```
K-EDGE ABSORPTION        DELTAMU :       3.3130
KFK KARLSRUHE IK3        ************************
06/11/85      11:47      ** U **
                         CONC(G/L):      195.465
                         ERROR (%):         .151
 3. RUN OUT OF  3        ERROR-ABS:         .296
   06/11/85    12:41     ************************
FILENAME:       U2CA03
CELL(CM):        2.200
ANALYSIS:            3   MEANVALUE FOR FW-END
ELTIM(S):         1000   CONC(G/L):      195.435
PRTIM(S):         1000     SD(G/L):        0.597
SAMPLE: ** U **            RSD(%):         0.350
```

Table 1

Extraction of a µP-printout. The left column is recorded to cassette as spectrum header.

The compact portable µP-based data processing unit is simple to operate and has successfully passed an in situ test.

(1)   I. Michel-Piper, P. Matussek, Report JOPAG/06.85-PRG-117, Kernforschungs-zentrum Karlsruhe (1985)

6.4.11 STATISTICAL ANALYSIS OF MEASUREMENT DATA FROM THE KfK K-EDGE DENSITOMETER

R. Beedgen[+], H. Ottmar (1)

The KfK K-edge densitometer has been adopted as one of the instruments used for verification measurements in the international safeguarding of nuclear materials. In order to ensure continuous measurement quality under routine operation, appropriate measures for effective measurement control and assurance have to be incorporated into the standard measurement procedures. Some of these measures include, for example, regular control measurements on reference or normalization samples, and the continuous control of important instrument parameters.

The generation of the respective control data generally does not represent problems with advanced instrumentations. However, the more difficult question is, how to actually convert the informations obtained from those data into improved measurement quality and assurance. As an example the set of data, which resulted from control measurements with the K-edge densitometer during a 1-year demonstration period, has been statistically analyzed using known statistical procedures. The statistical analyses aimed at deriving quantitative informations about systematic measurement biases arising in the long-term operation, and to develop possible procedures for a measurement control program.

(1)   ditto., Proc. ESARDA/INMM Joint Specialist Meeting on NDA Statistical Problems. ESARDA 18 (1984) 27, ed. by JRC Ispra, Italy.

+   Institut für Datenverarbeitung in der Technik, Kernforschungszentrum Karlsruhe

6.4.12 K-EDGE JUMP OF THE TOTAL PHOTON MASS ATTENUATION COEFFICIENT OF ACTINIDE ELEMENTS

H. Eberle, I. Michel-Piper, H. Ottmar, O. Cromboom[+]

The quantitative analysis of heavy elements from K-edge densitometry with an X-ray continuum (Fig. 1) requires accurate values for the change of the total photon mass attenuation coefficient, $\Delta\mu \, [cm^2 \cdot g^{-1}]$, across the K-absorption edge. The $\Delta\mu$-values enter as calibration constant into the densitometry equation $\rho = \ln R/(\Delta\mu \cdot d)$, which relates the concentration $\rho \, [g \cdot cm^{-3}]$ of the element to be determined in glass cells of thickness d [cm], with the measured X-ray transmission change R across its K-absorption edge.

Very little experimental data are available on accurate $\Delta\mu$-values for most elements. The values derived from different compilations of theoretically calculated photon cross sections (1,2,3) differ by several percent, which is about one order of magnitude worse than the potential accuracy of the K-edge densitometry technique for quantitative analysis.

We have determined the $\Delta\mu$-values at the K-absorption edge for the actin-

ide elements Th, U, Np, Pu and Am. The determinations for U and Pu were made
on sets of internationally characterized calibration solutions, having an uncer-
tainty of 0.15 % for the U and Pu concentrations. For the measurements on Th,
Np and Am the European Institute for Transuranium Elements (TUI), Karlsruhe, has
prepared carefully characterized reference solutions, each containing about
185 mg/ml of the respective element. The accuracy of the chemically determined
reference concentrations were estimated to 0.2 % for Np, 0.3 % for Am, and 0.4 %
for Th. During the measurements the solutions were kept in glass cells, where
the transmission length of 20 mm was known to 0.05 %.

The experimental results, obtained with the KfK K-edge densitometer instal-
led at TUI, are summarized in Table 1. They are compared with $\Delta\mu$-values derived
from 3 different compilations of theoretically calculated photon cross sections.
For some elements the theoretical values differ significantly from each other.
However, when taking mean values of the theoretical data, fairly good agreement
with the experimental results is obtained.
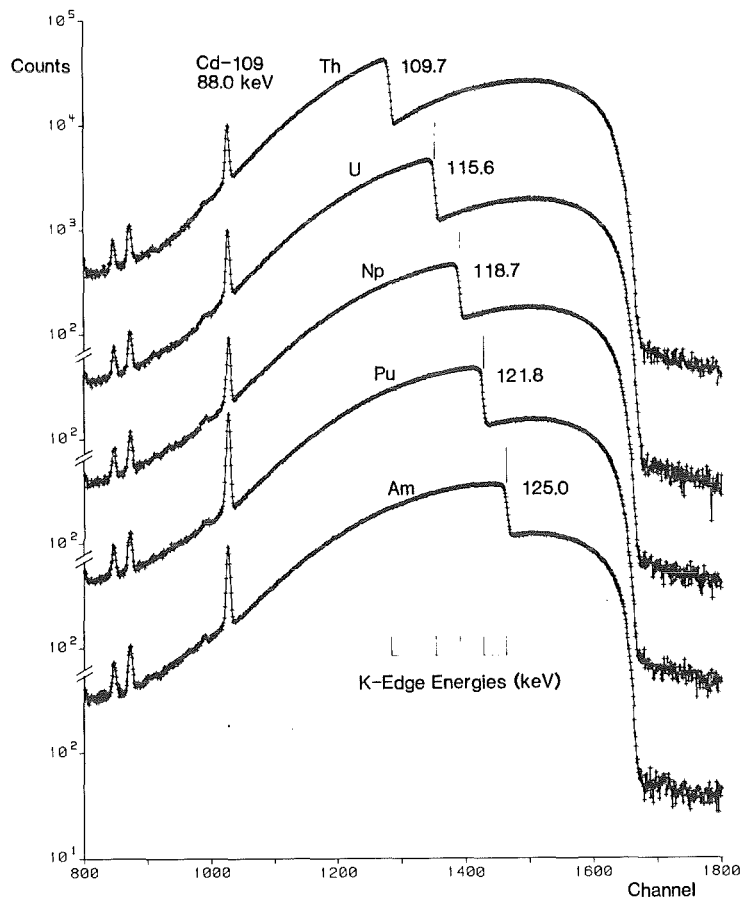
Fig. 1 Examples of K-edge densitometry measurements on actinide elements.

Table 1 $\Delta\mu$-Values for the K-absorption edge of 5 actinide elements

Element	K-Edge Jump $\Delta\mu$ $[cm^2 \cdot g^{-1}]$				Exp.-Theory Mean
	Experiment	Theory(1)	Theory(2)	Theory(3)	Exp. (%)
Th	3.812+0.035	3.848	3.882	3.926	- 1.92
U	3.546+0.025	3.501	3.605	3.651	- 1.13
Np	3.427+0.024	3.407	3.842*	3.466	- 0.29
Pu	3.272+0.021	3.193	3.223	3.397	+ 0.03
Am	3.100+0.025	3.053	-	3.190	- 0.71

* Omitted from theoretical mean.

(1)   E. Storm, H. Israel, Nucl. Data Tables 7 (1970) pp. 565-688
(2)   W.M.J. Veigele, Atomic Data Tables 5 (1973) pp. 51-111
(3)   E.F. Plechaty, D.E. Cullen, R.J. Howerton, Report UCRL-50400, Vol. 6
      Revision 1 (1975)

+   European Institute for Transuranium Elements (TUI), Karlsruhe

6.4.13 ENERGY DEPOSITION SPECTRA CALCULATED FOR A BEAM FROM A BIOMEDICAL PION CHANNEL

G. Büche and H. Hilgendorff

The work on the transport code for negatively charged pions called PIONDOSE was terminated at the end of 1984 by a comparison of results to distributions of absorbed dose that were deduced from measurements. The parameters of the irradiation channel PIOTRON at the Swiss Institute for Nuclear Research for the cases of two typical pion momenta and a water phantom were used for the calculations. It was found that the calculated data agree remarkably well with the measured isodoses (1). From this outcome together with earlier results we conclude that most of the physical data are known which are needed to do realistic transport calculations for negatively charged pions within materials containing the biologically relevant elements C, H, O, and N.

Parallel to this work energy deposition spectra were worked out for various positions and directions across the dose fields. Spectra of this kind are needed to estimate the quality and to quantify the relative biological efficiency (RBE) of an absorbed dose. Fig. 1 shows energy deposition spectra for several positions along a direction perpendicular to the beam axis originating at a depth within the stopping region of pions. The spectra given for the pairs of positions X = -2,75/+5,25 cm and X = -0,25/2,57 cm correspond to cases where the absorbed doses
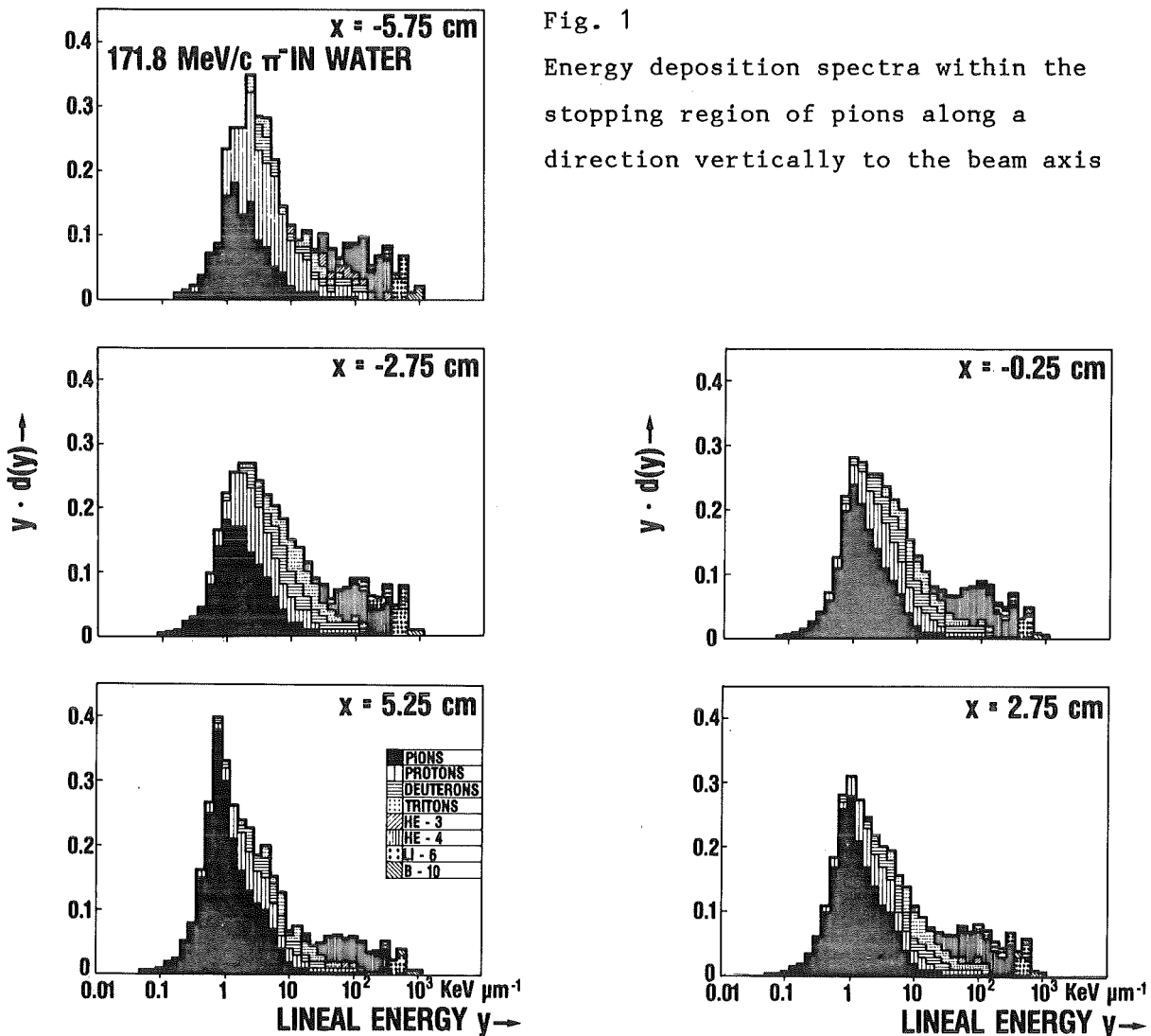
Fig. 1

Energy deposition spectra within the
stopping region of pions along a
direction vertically to the beam axis

are equal in pairs as well (about 40% and 85% of the peak dose). But the numbers
of crossing and stopping primary pions are different because of the dispersive
character of the beam configuration. Consequently, the contributions to the
absorbed dose given from primary pions and their secondary particles vary along
the considered isodoses and are expected to result in a variation of RBE, too.
A similar behaviour of the energy deposition spectra was observed experimentally
at the PIOTRON by H. Schuhmacher et al. who intend now to use our Monte Carlo
code and continue the work described in this context (2).

(1)   H. Hilgendorff, Berechnung von Dosisverteilungen für π^--Mesonen aus einem
        magnetischen Bestrahlungskanal und Vergleich mit experimentellen Daten,
        Technical Report KfK 3908 (März 1985)

(2)   H. Schuhmacher, private communication (May 1985)

7. LIST OF PUBLICATIONS

7.1 PUBLICATIONS AND REPORTS

ANSELMENT, M.
Laserspektroskopische Untersuchungen der optischen Isotopieverschiebung und Hyperfeinstruktur bei stabilen und radioaktiven Blei- und Zinn-Nukliden.
KfK-3797 (August 84)

ALBINSKA, M.; ALBINSKI, J.; BUSCHMANN, J.; GILS, H.J.; KLEWE-NEBENIUS, H.; REBEL, H.; ZAGROMSKI, S.
Projectile break up associated with gamma rays from interactions of the non-spectator fragment with the nucleus.
Machner, H. [Hrsg.]
Coincident Particle Emission from Continuum States in Nuclei,
Bad Honnef, June 4-7, 1984
Singapore: World Scientific Publ., 1984. - S.326-27

ARNOULD, M.; TAKAHASHI, K.; YOKOI, K.
On the validity of the local approximation for the s-process in the Os region, and implications for the $^{187}Re-^{187}Os$ cosmochronology.
Astronomy and Astrophysics, 137(1984) S.51-57

AURES, R.; HEERINGA, W.; KLAGES, H.O.; MASCHUW, R.; SCHMIDT, F.K.; ZEITNITZ, B.
A brute-force polarised proton target as an application of a versatile brute-force polarisation facility.
Nuclear Instruments and Methods, 224(1984) S.347-54

BACHER, R.; GOTTA, D.; SIMONS, L.M.; MISSIMER, L.; MUKKOPADHYAY, N.G.
Muonic atoms with vacant electron shells.
Physical Review Letters, 54(1985) S.2087

BACKENSTOSS, G.; CIERJACKS, S.; FURIC, M.; IZYCKI, M.; LJUNGFELT, S.; PETKOVIC, T.; STEINACHER, M.; WEBER, P.; WEYER, H.J.
S-wave pion absorption in ^{3}He.
SIN Newsletter, (1985) No. 17

BALZER, R.; HENNECK, R.; JACQUEMART, C.; LANG, J.; NESSI-TEDALDI, F.; ROSERT, T.; SIMONIUS, M.; HAEBERLI, W.; JACCARD, S.; REICHART, W.; WEDDIGEN, CH.
Parity violation in proton-proton scattering at 45 MeV.
Physical Review C, 30(1984) S.1409-30

BECK, R.; DICKMANN, F.; KRUPPA, A.
Cluster model with breathing clusters: dynamical distortion effects in ^{6}Li.
Physical Review C, 30(1984) S.1044-54

BEEDGEN, R.; OTTMAR, H.
Statistical analysis of measurement data from the KfK K-edge densitometer.
Proc.of the ESARDA/INMM Joint Specialists' Meeting on NDA Statistical Problems, Ispra, I, September 12-14, 1984
ESARDA, 18(1984) S.27

BEER, H.; WALTER, G.; MACKLIN, R.L.; PATCHETT, P.J.
Neutron capture cross sections and solar abundances of supra(160,161)Dy, supra(170,171)Yb, supra(175,176)Lu and supra(176,177)Hf for the s-process analysis

of the radionuclide ^{176}Lu.
Physical Review C, 30(1984) S.464-78

BUSCHMANN, J.; GILS, H.J.; JELITTO, H.; KRISCH, J.; LUDWIG, G.; MANGER, D.; REBEL, H.; SEITH, W.; ZAGROMSKI, S.
The vaccum system of the Karlsruhe magnetic spectrograph 'Little John'.
KfK-3681B (Februar 85)

CBC-COLLABORATION
Study of the antiproton-proton annihilation at LEAR with a 4π neutral detector.
CERN/PSCC/85-26, CERN(1985)

CELLO-COLLABORATION
Search for new heavy quarks in e^+e^- collisions up to 46.78 GeV C.M. energy.
22nd Internat.Conf.on High Energy Physics, Leipzig, DDR, July 19-25, 1984
DESY-84-051 (Juni 84)
Physics Letters B, 144(1984) S.297-301

CELLO-COLLABORATION
An investigation of the process $e^+e^- \rightarrow \mu^+\mu^-\gamma$.
DESY-84-101 (Oktober 84)

CELLO-COLLABORATION
Observation of a multiparticle event with 2 isolated energetic muons in e^+e^- interactions.
DESY 84-024 (March 1984)
Physics Letters B, 141(1984) S.145-52

CELLO-COLLABORATION
A study of final states with four charged leptons in e^+e^- interactions.
DESY-84-103 (Oktober 84)

CHRIEN, R.E.; [HRSG.]; MICHAUDON, A.; CIERJACKS, S.; CHRIEN, R.E.
[GENERAL EDITORS]
Neutron radiative capture.
Neutron Physics and Nuclear Data in Science and Technology. A Nuclear Energy Agency Nuclear Data Commettee Series. Vol. 3
Oxford [usw.]: Pergamon Pr. 1984

CIERJACKS, S.; HINO, Y.; RAUPP, F.; FILGES, D.; CLOTH, P.; ARMSTRONG, T.W.
Nuclear data research in the Institut fuer Kernphysik, Kernforschungszentrum Karlsruhe.
In: Quaim, S.M. [Hrsg.]
Progress Report on Nuclear Data Research in the Federal Republic of Germany for the Period April 1, 1983 to March 31, 1984
NEANDC(E)-252 U Vol. 5(June 1984)
INDC(Ger)-27/LN + Special

CIERJACKS, S.; ULLRICH, H.
Energy dependence of pion absorption.
SIN News-Letter, (1984) Nr. 16

DAMMERTZ, G.; PIOSCZYK, B.
Development work on H⁻-ion sources.
Knoepfel, H.; Sindoni, E. [Hrsg.]
Proc.of the 4th Internat.Symp.on Heating in Toroidal Plasmas, Roma, I, March 21-28, 1984
Rom: ENEA 1984 S.1087-93

DEMBCZYNSKI, J.; REBEL, H.
Perturbation of the configurations $5s^25pn's$ and $5s^25pn''d$ by the configuration $5s5p^3$ in

the spectrum Sn I.
KfK-3703 (Februar 84)
Physica C, 125(1984) S.341-52

DOERR, M.; FETSCHER, W.; GOTTA, D.; REICH,
J.; ULLRICH, H.; BACKENSTOSS, G.; KOWALD, W.;
WEYER, H.J.
Composite particle emission following
π⁻-absorption in ⁶Li.
Machner, H. [Hrsg.]
Coincident Particle Emission from Continuum
States in Nuclei,
Bad Honnef, June 4-7, 1984
Singapore: World Scientific Publ., 1984. -
S.555, S.573

EBERLE, H.
Extended software for the KfK K-edge
densitometer.
JOPAG/04.85-PRG-110

EBERLE, H.; OTTMAR, H.; MATUSSEK, P.
Plutonium isotopic assay of reprocessing
product solutions in the KfK K-edge
densitometer.
JOPAG/04.85-PRG-113

EBERLE, H.; OTTMAR, H.
Operations manual for the KfK K-edge
densitometer. Task C.2.
JOPAG/06.85-PRG-116

ENGLER, J.
Perspectives in calorimetry.
Meeting on Physics in Collision IV,
Santa Cruz, Calif., August 21-24, 1984
Proc.of the Topical Seminar on Perspectives
for Experimental Apparatus at Future High
Energy Machines, St.Miniato, I, May 21-25,
1984
Nuclear Instruments and Methods A, 235(1985)
S.301-09

ENGLER, J.
Status and perspectives of liquid argon
calorimeters.
Nuclear Instruments and Methods, 225(1984)
S.525-29

ENGLER, J.; KEIM, H.
A liquid ionization chamber using
tetramethylsilane.
Nuclear Instruments and Methods, 223(1984)
S.47-51

ESCHNER, W.; SCHMIDT-OTT, W.D.; GIPPERT,
K.L.; RUNTE, E.; BEER, H.; WALTER, G.;
KIRCHNER, R.; KLEPPER, O.; ROECKL, E.;
SCHARDT, D.
Measurement of the β-decay branch in ¹⁸⁰Lu to
supra(180m)Hf for investigation of the
r-process nucleosynthesis of supra(180m)Ta.
Zeitschrift fuer Physik A, 317(1984) S.281-86

FETSCHER, W.; GERBER, H.J.; GOERING, K.;
KLEIN, U.; KLUGE, W.; MATTHAEY, H.; METZLER,
M.; PEDRONI, E.; WIEDNER, U.
Coulomb nuclear interference in π⁺⁻p
scattering at 55 MeV.
SIN Newsletter, (1985) Nr. 17 S.NL25

FILGES, D.; CIERJACKS, S.; HINO, Y.;
ARMSTRONG, T.W.; CLOTH, P.
Validation of the
intra-nuclear-cascade-evaporation model for
particle production.
Juel-1960 (November 84)
KfK-3779 (November 84)

FORSTBAUER, B.
Messungen zum Szintillationslicht aus
Fluessigargon.
KfK-3774B (Juli 84)

FLUEGGE, G.
Upgrading the CELLO track detector.
KfK-3858 (Januar 85)

FRIES, D.C.; MATUSSEK, P.; WEDDIGEN, CH.;
[HRSG.]
Annual report on nuclear physics activities,
July 1, 1983 - June 30, 1984.
KfK-3815 (Oktober 84)

GARCILAZO, H.
Mass and range dependence in the binding
energy of the three-body system.
Physical Review C, 30(1984) S.765

GARCILAZO, H.
Completeness relation for energy dependent
separable potentials.
Journal of Mathematical Physics, 26(1985)
S.1380

GARCILAZO, H.
Angular momentum effects in the π⁻ nn
bound-state problem.
Physical Review C, 31(1985) S.257-58

GILS, H.J.; FRIEDMAN, E.
Combined analysis of pionic atoms and elastic
scattering of alpha particles.
Journal of Physics G, 11(1985) S.85-93

GILS, H.J.
Untersuchung der radialen Verteilung der
Nukleonen in Atomkernen der 1fsub(7/2)-Schale
mit Hilfe der elastischen
Alpha-Teilchen-Streuung.
KfK-3765 (Dezember 84)
Habilitationsschrift, Universitaet Tuebingen
1984

GYLES, W.; MATHIE, E.L.; OTTERMANN, C.R.;
SMITH, G.R.; BOSCHITZ, E.T.; KONTER, J.A.;
MANGO, S.; MATSUYAMA, A.; JOHNSON, R.R.;
OLSZEWSKI, R.
Polarization effects in the π⁺d→π⁺np
reaction.
SIN Newsletters, (1985) No. 17 S.29

HECK, D.
The Karlsruhe ion microprobe setup and its
applications.
Atomkernenergie-Kerntechnik, 46(1985)
S.187-92

HECK, D.
Die Ionenmikrostrahlanlage und ihre
Anwendungsmoeglichkeiten.
KfK-Nachrichten, 16(1984) S.145-50

HECK, D.; ROKITA, E.
Matrix correction for PIXE in biomedical
samples.
KfK-3909 (Maerz 85)

HEERINGA, W.
Static nuclear polarisation and polarised
targets.
KfK-3851 (Dezember 84)

HEERINGA, W.; KLAGES, H.O.; DOBIASCH, H.;
FISCHER, R.; HAESNER, B.; SCHWARZ, P.;
WILCZYNSKI, J.; ZEITNITZ, B.
Neutron polarisation from the reactions
¹³C(p,n₀)¹³N and ¹⁵N(d,n₀)¹⁶O.
Nuclear Instruments and Methods, 227(1984)
S.509-11

HILGENDORFF, H.
Berechnung von Dosisverteilungen fuer
π⁻-Mesonen aus einem magnetischen
Bestrahlungskanal und Vergleich mit
experimentellen Daten.
KfK-3908 (Maerz 85)
Diplomarbeit, Universitaet Karlsruhe 1985

HINTERBERGER, F.; EVERSHEIM, P.D.; KLAGES,
H.O.; ABDEL-WAHAB, M.S.; DOBIASCH, H.;
HAESNER, B.; SCHMALZ, G.; SCHWARZ, P.;
WILCZYNSKI, J.
^{20}Ne+n$\rightarrow^{21}$Ne(T=3/2) resonances.
Nuclear Physics A, 424(1984) S.200-20

HUETTEN, L.; HABFAST, C.; POTH, H.; WOLF, A.;
GIRARDINI, M.; PONCET, A.
The ultra-high-vacuum system of the
electron-cooling device of LEAR.
KfK-3816 (Mai 85)

JOEDICKE, B.
Ueber die Bestimmung von Roentgenenergien
antiprotonischer Atome durch kritische
Absorption an Kanten und die theoretische
Deutung von Ergebnissen.
KfK-3933 (Juni 85)
Diplomarbeit, Universitaet Karlsruhe 1985

KAELBER, W.
Optogalvanische Spektroskopie am Europium.
KfK-3945 (Juni 85)
Diplomarbeit, Universitaet Karlsruhe 1985

KAEPPELER, F.; WALTER, G.; MATHEWS, G.J.
Stellar neutron capture rates for ^{46}Ca and
^{48}Ca.
The Astrophysical Journal, 291 (1985)
S.319-27

KRUPP, H.; HIEBERT, J.C.; KLAGES, H.O.; DOLL,
P.; HANSMEYER, J.; PLISCHKE, P.; WILCZYNSKI,
J.; ZANKEL, H.
^{4}He(n,n)^{4}He analyzing power in the energy
range from 15 to 50 MeV.
Physical Review C, 30(1984) S.1810-21

LJUNGFELT, S.
Pionabsorption in flight on ^{3}He.
KfK-3792 (Februar 85)

MATUSSEK, P.
Accurate determination of the ^{235}U isotope
abundance by gamma spectrometry. User's
manual for the certified reference material
EC-NRM-171/NBS-SRM-969.
KfK-3752 (Mai 85)

MATHIE, E.L.; SMITH, G.R.; BOSCHITZ, E.T.;
GYLES, W.; OTTERMANN, C.R.; MANGO, S.;
KONTER, J.A.; MATSUYAMA, A.; JOHNSON, R.R.;
OLSZEWSKI, R.
First measurements of iT$_{11}$ in the
pion-deuteron breakup reaction.
Physics Letters B, 154(1985) S.28-32

MAYER, B.; BERTINI, R.; CAMERON, J.M.; CATZ,
H.; DURAUD, J.M.; GERVINO, G.P.; GLASHAUSER,
C.M.; LUGOL, J.C.; WHITTEN, C.A.; YAVIN,
A.I.; ARVIEUX, J.; BAKER, S.D.; FARVAQUE, L.;
HUTCHEON, D.A.; CATILLON, P.; SMITH, G.R.
Angular and energy dependence of the cross
section and analyzing power of the reaction
pp→dπ$^+$ between 725 and 100 MeV.
Nuclear Physics A, 437(1985) S.630

MICEK, S.; MAJKA, Z.; REBEL, H.; GILS, H.J.;
KLEWE-NEBENIUS, H.
The optical potential for ^{6}Li-^{6}Li elastic
scattering at 156 MeV.
KfK-3798 (Oktober 84)
Nuclear Physics A, 435(1985) S.621-34

MICHEL-PIPER, I.; MATUSSEK, P.
Software development in PLIM for the partable
microprocessor equipment: KfK K-edge
densitometer for quantitative determination
of Th, Np, U, Pu, Am in solutions.
JOPAG/06.85-PRG-117

MISSIMER, J.; SIMONS, L.M.
The neutral weak current in muonic atoms.
Physics Reports, 118(1985) S.179-238

OCHS, A.; HECK, D.; KRATT, C.; SCHNEIDER, G.;
MAIER, K.P.
Protoneninduzierte Roentgenemission zur
Spurenelementanalyse in menschlichen
Lebergewebsproben.
Verhandlungen der Deutschen Gesellschaft fuer
Innere Medizin Bd. 90
Muenchen: Bergmann, 1984. - S.1531-34

OTTERMANN, C.R.; MATHIE, E.L.; BOSCHITZ,
E.T.; SMITH, G.R.; GYLES, H.; MANGO, S.;
KONTER, J.A.; VAN DEN BRANDT, B.; OLSZEWSKI,
R.; JOHNSON, R.R.
Study of the vector analyzing power iT$_{11}$ in
the π$^+$d→2p reaction.
SIN Newsletter, (1985) No. 17 S.28

OTTMAR, H.
Roentgenabsorptiometer fuer die
Praezisionsbestimmung Schwerer Elemente.
KfK-Nachrichten, 17(1985) S.83-93

PILKUHN, H.; POTH, H.
Eine Ionenstrahllampe fuer Roentgenstrahlen.
KfK-3764 (September 84)

POTH, H.
ECOOL 84: Elektronenkuehlung und ihre
Anwendung.
Physikalische Blaetter, 41(1985) S.21-22

SCHATZ, G.; OEHLSCHLAEGER, J.
Ein Programm zur Berechnung der
Ansprechwahrscheinlichkeit eines
4π-Szintillationszaehlers.
KfK-3710 (Juli 84)

SCHWEICKERT, H.
Das Karlsruher Kompaktzyklotron - ein
Beschleuniger im Dienste der Medizin und
Technik.
KfK-Nachrichten, 16(1984) S.204-13

SEEGERT, G.; PFEIFFER, A.; GRABMAYR, P.;
KIHM, TH.; KNOEPFLE, K.T.; MAIRLE, G.;
WAGNER, G.J.; BECHTOLD, V.; FRIEDRICH, L.
Study of deeply-bound hole states in the
Zr-region via the (d,^{3}He) reaction.
Internat.Symp.on Highly Excited States and
Nuclear Structure, Orsay, F, September 5-8,
1983
Journal de Physique, Colloque C4, Suppl.au no
3, 45(1984) S.C4/85-C4/89

SMITH, G.R.; MATHIE, E.L.; BOSCHITZ, E.;
OTTERMANN, C.R.; MANGO, S.; KONTER, J.A.;
DAUM, M.; MEYER, M.; OLSZEWSKI, R.; VOGLER,
F.
Measurements of the vector analyzing power
iT$_{11}$ in the πd elastic scattering reaction
between 117 and 325 MeV.
Physical Review C, 29(1984) S.2206-21

SMITH, G.R.; MATHIE, E.L.; BOSCHITZ, E.;
OTTERMANN, C.R.; GYLES, W.; LIST, W.; MANGO,
S.; KONTER, J.A.; VAN DEN BRANDT, B.;
OLSZEWSKI, R.; JOHNSON, R.R.
Vector analyzing power iT$_{11}$ in the πd→2p
reaction between 112 and 325 MeV.
Physical Review C, 30(1984) S.980-88

SMITH, G.R.; MATHIE, E.L.; BOSCHITZ, E.T.;
OTTERMANN, C.R.; GYLES, W.; LIST, W.; MANGO,
S.; KONTER, J.A.; VAN DEN BRANDT, B.;
OLSZEWSKI, R.; VOGLER, F.
Search for dybarions in measurements of the
πd (pol) system.
Mischke, R.E. [Hrsg.]
AIP Conference Proceedings No. 123 (July
1984) S.1072

SPIEKER, C.; HECK, D.; ZIDEK, W.; KERENY, G.;
LOSSE, H.; VETTER, H.
The evaluation of tissue Ca^{2+} by proton
induced X-ray emission in the arteries of
spontaneously hypertensive and normotensive
rats.
Klinische Wochenschrift, 63(1985)
(Suppl.III), S.74-77

STEIGER, A.
Aufbau eines Messgeraetes zur schnellen und
genauen Bestimmung der Wellenlaenge
sichtbarer Laserstrahlung.
KfK-3820 (Oktober 84)
Diplomarbeit, Universitaet Karlsruhe 1984

TRAUTVETTER, H.P.; KAEPPELER, F.
Destruction of ^{26}Al via the
$^{26}Al(n,p)^{26}Mg$-reaction.
Zeitschrift fuer Physik A, 318(1984) S.121-22

WALTER, G.; BEER, H.
Measurement of neutron capture cross sections
of s-only isotopes: ^{70}Ge, ^{86}Sr, and ^{87}Sr.
Astronomy and Astrophysics, 142(1985)
S.268-72

WILCZYNSKI, J.
Untersuchung der
Neutron-Proton-Wechselwirkung im
Energiebereich von 20 bis 50 MeV.
KfK-3781 (Juli 84)
Dissertation, Universitaet Karlsruhe 1984

WILCZYNSKI, J.; HANSMEYER, J.; BRADY, F.P.;
DOLL, P.; HEERINGA, W.; HIEBERT, J.C.;
KLAGES, H.O.; PLISCHKE, P.
Measurements of the neutron-proton analyzing
power in the energy range from 17 to 50 MeV.
Nuclear Physics A, 425(1984) S.458-68

WINTERS, R.R.; KAEPPELER, F.; WISSHAK, K.;
REFFO, G.; MENGONI, A.
Stellar neutron capture rates of

supra(148,149,150)Sm.
KfK-3827 (November 84)

WISSHAK, K.; KAEPPELER, F.; SCHATZ, G.
Calculated efficiency of a 4π detector of BGO
or BaF_2 for monoenergetic gamma rays and
gamma cascades following neutron capture.
Nuclear Instruments and Methods, 221(1984)
S.385-92

WISSHAK, K.; KAEPPELER, F.
Large barium fluoride detectors.
Nuclear Instruments and Methods, 227(1984)
S.91-96

WISSHAK, K.; KAEPPELER, F.
Neutron capture in s-wave resonances of ^{56}Fe,
and supra(58,60,64)Ni.
Cullen, D.E. [Hrsg.]
Nuclear Data for Structural Materials:
Proc.of the IAEA Consultants' Meeting, Wien,
A, November 2-4, 1983
Wien: IAEA, 1984. - S.46-56

WISSHAK, K.; KAEPPELER, F.; REFFO, G.
The capture width of the 34.8-keV s-wave
neutron resonance in ^{27}Al.
Nuclear Science and Engineering, 88(1984)
S.594-98

YOKOI, K.; TAKAHASHI, K.
Beta-decay rates for the s-process.
KfK-3849 (Februar 85)

ZEITNITZ, B.
Few body problems in physics. Considerations
after the tenth international conference.
Comments on Nuclear and Particle Physics,
13(1984) S.97-102

ZEITNITZ, B.
Low energy neutrino physics at high intensity
pulsed proton accelerators.
Progress in Particle and Nuclear Physics,
13(1985) S.445-78

7.2 CONFERENCE CONTRIBUTIONS

Colloquium on Cold Stars with Excess of Heavy
Elements, Strasbourg, F, July 3-6, 1984

BEER, H.; WALTER, G.
Analysis of isotopic Zr abundances from
S-stars using the s-process with an
exponential distribution of neutron
exposures.

22nd Internat.Conf.on High Energy Physics,
Leipzig, DDR, July 19-25, 1984

APEL, W.D.
Recent result from Cello.

CELLO-COLLABORATION
High Psub(t) lepton production in hadronic
events in e^+e^- annihilation up to 46.78 GeV
C.M. energy.

CELLO-COLLABORATION
Search for scalar electrons and neutralinos
in e^+e^- interactions.

CELLO-COLLABORATION
Evidence for hard scattering in untagged
photon-photon collisions.

CELLO-COLLABORATION
Investigation of $e^+e^-e^+e^-$ and $e^+e^-\mu^+\mu^-$ final
states in e^+e^- interactions.

4th Internat.Conf.on Clustering Aspects of
Nuclear Structure and Nuclear Reactions,
Chester, GB, July 23-27, 1984

BECK, R.; DICKMANN, F.; LOVAS, R.G.
Effects of the Pauli principle in
quasi-elastic cluster knockout reactions.

PLANETA, R.; NEUMANN, B.; REBEL, H.;
ALBINSKA, M.; ALBINSKI, J.; BUSCHMANN, J.;
GILS, H.J.; GROTOWSKI, K.; KLEWE-NEBENIUS, H.
Investigation of the inelastic break up of
the projectile in ^{6}Li induced reactions at
156 MeV.

SRIVASTAVA, D.K.; REBEL, H.
A plane-wave matrix approach for exact finite
range treatment of break-up of light ions.

10th Internat.Conf.on Particles and Nuclei,
Heidelberg, July 30 - August 3, 1984

BACKENSTOSS, G.; CIERJACKS, S.; FURIC, M.;
IZYCKI, M.; LJUNGFELT, S.; MANKIN, U.;
PETKOVIC, T.; STEINACHER, M.; ULLRICH, H.;
WEBER, P.; WEYER, H.J.
πsupra(+/-) absorption in flight on ^{3}He.

BACKENSTOSS, G.; GOTTA, D.; IZYCKI, M.;
KOWALD, W.; LJUNGFELT, S.; SCHMIDT, G.;
ULLRICH, H.; WEYER, H.J.
S-wave absorption of stopped π^- on ^{3}He.

BAUER, TH.S.; AMANDRUZ, P.; DOMINGO, J.;
INGRAM, Q.; KYLE, G.; RENKER, D.; STAMMINGER,
R.; SMITH, G.R.
(π^{+-},π^{+-}) and (π^{+-},π^{-+}) on ^{16}O and ^{18}O at
240, 163 and 115 MeV.

DOERR, M.; FETSCHER, W.; GOTTA, D.; REICH,
J.; ULLRICH, H.; BACKENSTOSS, G.; KOWALD, W.;
WEYER, H.J.
Composite particle emission following
π^--absorption in ^{6}Li.

GILS, H.J.; FRIEDMAN, E.; REBEL, H.
Nuclear sizes and densities of
1fsub(7/2)-nuclei from pionic atoms and
elastic scattering of α particles.

GYLES, W.; MATHIE, E.L.; OTTERMANN, C.R.;
SMITH, G.R.; BOSCHITZ, E.; KONTER, J.A.;
MANGO, S.; JOHNSON, R.R.; OLSZEWSKI, R.
Polarisation effects in the $\pi^+d\rightarrow\pi^+np$
reaction.

OLSZEWSKI, R.; HOFMANN, A.; KRELL, S.;
ORTNER, H.W.; SCHMIDTLEIN, G.; VOGLER, F.;
GYLES, W.; LIST, W.; MATHIE, E.L.; SMITH,
G.R.; DEHNHARD, D.
$(\pi,\pi'\gamma)$ angular correlations in the region of
the (3,3)-resonance.

OTTERMANN, C.R.; MATHIE, E.L.; BOSCHITZ, E.;
SMITH, G.R.; GYLES, W.; MANGO, S.; KONTER,
J.A.; OLSZEWSKI, R.; VAN DEN BRANDT, B.
Study of the vector analyzing power iT11 in
the $\pi-d\rightarrow2p$ reaction between 112 and 325 MeV.

POTH, H.; BUECHE, G.; HANCOCK, A.D.; KOCH,
H.; KOEHLER, TH.; KREISSL, A.; RAICH, U.;
ROHMANN, D.; FINDEISEN, C.; REPOND, J.;
TAUSCHER, L.; NILSSON, A.; CARIUS, S.;
SUFFERT, M.; CHARALAMBUS, S.; CHARDALAS, M.;
DEDOUSSIS, S.; EGIDY, T.VON; HARTMANN, F.J.;
KANERT, W.; REIDY, J.J.
Study of antiprotonic X-ray and γ spectra at
LEAR.

Internat.Meeting on Nuclear Orientation and
Nuclei far from Stability, Leuven, B, August
27-31, 1984

HEERINGA, W.
Static nuclear polarisation and polarised
targets.

Workshop on Polarized Target Materials and
Techniques, Bonn, September 3-6, 1984

HEERINGA, W.
A brute-force polarized proton target.

5th Internat.Symp.on Capture Gamma-Ray
Spectroscopy and Related Topics, Knoxville,
Tenn., September 10-14, 1984

BEER, H.; WALTER, G.; MACKLIN, R.L.
The ^{163}Dy-^{163}Ho branching: an s-process
barometer.

KAEPPELER, F.
Neutron capture reactions in astrophysics.

ESARDA/INMM Joint Specialists' Meeting on NDA
Statistical Problems, Ispra, I, September
12-14, 1984

BEEDGEN, R.; OTTMAR, H.
Statistical analysis of measurement data from
the KfK K-edge densitometer.

ECOOL 1984, Workshop on Electron Cooling and
Related Applications, Karlsruhe, September
24-26, 1984

BROUET, M.; GIRARDINI, M.; PONCET, A.; WOLF,
A.; HUETTEN, L.; POTH, H.; HABFAST, C.
An ultra-high vacuum system for coolers.

HASEROTH, H.; HILL, C.E.; VALLET, J.L.;
HABFAST, C.; HUETTEN, L.; POTH, H.; WOLF, A.
The LEAR electron cooler.

PILKUHN, H.; POTH, H.
An ion beam lamp for monochromatic X-rays.

POTH, H.
Review of electron cooling experiments.

Workshop on Nuclear Physics with Stored
Cooled Beams, Bloomington, Ind., October
15-17, 1984

POTH, H.
Laser application in electron cooling.

21st European Cyclotron Progress Meeting,
Juelich, November 8-9, 1984

BECHTOLD, V.; ERNST, R.; FRIEDRICH, L.;
HUTTEL, E.; SCHULZ, F.
Development of an ECR-Li^{+++}ion source for the
Karlsruhe cyclotron.

EHRET, H.P.; SCHWABE, J.; SCHWEICKERT, H.;
STARZEWSKI, G.; WIERBA, W.
Modification of the Karlsruhe insochronous
cyclotron to an energy variable machine.

Workshop on Production and Application of
Light Negative Ions, Paris, F, November 21,
1984

DAMMERTZ, G.; PIOSCZYK, B.
Properties of an H$^-$ beam extracted from a
volume source.

6th Internat.ECR Ion Source Workshop,
Berkeley, Calif., January 17-18, 1985

BECHTOLD, V.; ERNST, R.; FRIEDRICH, L.;
HUTTEL, E.; SCHULZ, F.
LISKA, the Karlsruhe ECR ion source for fully
stripped lithium ions.

3rd LEAR Workshop on Physics with Low Energy
Cooled Antiprotons, Tignes, F, January 19-26,
1985

HABFAST, C.; POTH, H.; SELIGMANN, B.;
HASEROTH, H.; HILL, C.E.; VALLET, J.L.; WOLF,
A.
Status and perspectives of the electron
cooling device under construction at LEAR.

KOCH, H.
CsI crystal ball at LEAR.

24.Internat.Universitaetswochen fuer
Kernphysik der Universitaet Graz -
Nucleon-Nucleon and Nucleon-Antinucleon
Interactions - from Low to High Energies,
Schladming, A, February 20 - March 1, 1985

KLAGES, H.O.; DOLL, P.; GARRETT, R.;
HANSMEYER, J.; HEERINGA, W.; HOFMANN, K.;
KRUPP, H.; WILCZYNSKI, J.
np scattering experiments at POLKA.

FINK, G.; DOLL, P.; GARRETT, R.; HEERINGA,
W.; HOFMANN, K.; KLAGES, H.O.; KRUPP, H.
Measurement of the np differential cross
section.

KRUPP, H.; KLAGES, H.O.; WILCZYNSKI, J.
NN phase shift analyses up to 50 MeV.

49.Physikertagung gemeinsam mit der
Fruehjahrstagung DPG, Kern- und
Hochenergiephysik, Didaktik der Physik,
Energietechnik - Physikalische Grundlagen,
Vakuumtechnik, Computer in der Technischen
Physik, Gravitation und Relativitaetstheorie,
Muenchen, 11.-15.Maerz 1985
Verhandlungen der Deutschen Physikalischen
Gesellschaft, R.6, Bd.20(1985)

ALBINSKI, J.; WIKTOR, S.; BUDZANOWSKI, A.;
REBEL, H.
Nuclear matter sizes and isoscalar transition
rates of supra(58,60,62,64)Ni from 172.2 MeV
alpha-particle scattering.

ANSELMENT, A.; CHONGKUM, S.; HANSER, A.;
GOERING, S.; MEISEL, G.; REBEL, H.; SCHATZ,
G.
Laserspektroskopische Untersuchungen von
Strontium-Isotopen.

APEL, W.D.
Neue Ergebnisse von PETRA.

BACHER, R.; BLUEM, P.; GOTTA, D.; KUNOLD, W.;
MISSIMER, J.; SCHNEIDER, M.; SIMONS, L.M.
Ionisationsgrad in myonischem Neon und Argon.

BECHTOLD, V.; ERNST, R.; FRIEDRICH, L.;
HUTTEL, E.; SCHULZ, F.
Entwicklung einer ECR-Quelle am Karlsruher
Zyklotron fuer Li^{3+}.

BECK, R.; DICKMANN, F.; KRUPPA, A.T.; LOVAS,
R.G.
Decomposition properties of ^{6}Li.

BECK, R.; DICKMANN, F.; LOVAS, R.G.
Quantifications of the clustering properties
of nuclear states.

BECKER, H.W.; HEINEMANN, U.; ROLFS, C.;
TRAUTVETTER, H.P.; GELTENBORT, P.;
GOENNENWEIN, F.; KAEPPELER, F.; BAUMANN, M.;
FREIESLEBEN, H.
Die ^{26}Al-Isotopenanomalie und
die^{26}Al(n,p)^{26}Mg Reaktion.

BERG, G.P.A.; GAUL, G.; HACKER, U.;
HAGEDOORN, H.; HARDT, A.; HINTERBERGER, F.;
JAHN, R.; KOEHLER, M.; MARQUARDT, N.; MARTIN,
S.A.; MAYER-KUCKUK, T.; MEISSBURGER, J.;
OSTERFELD, F.; PAETZ GEN. SCHIECK, H.; POTH,
H.; PRASUHN, D.; RIEPE, G.; ROGGE, M.;
ROSSEN, P.VON; TUREK, P.
Planungsstand des Kuehler-Speicherrings COSY.

CELLO-COLLABORATION; GROSSE WIESMANN, P.
Dalitz Plot Analyse der Reaktionen ee→µµγ und
ee→eeγ bei PETRA.

CELLO-COLLABORATION; GROSSE WIESMANN, P.
Suche nach angeregten Leptonen bei PETRA.

CELLO-COLLABORATION; HOPP, G.
Energy dependence of αsub(s).

CELLO-COLLABORATION; KUESTER, H.
Suche nach SUSY-Teilchen bei PETRA.

DOLL, P.; FINK, G.; GARRETT, R.; HEERINGA,
W.; HOFMANN, K.; JANY, P.; KLAGES, H.O.;
KOIKE, Y.; KRUPP, H.; NITZ, W.; WILCZYNSKI,
J.
n-d scattering experiments up to 50 MeV and
Faddeev calculations using different
NN-potentials.

DOLL, P.; FINK, G.; GARRETT, R.; HEERINGA,
W.; HOFMANN, K.; KLAGES, H.O.; KRUPP, H.
Measurement of the differential cross section
of the elastic np scattering at backward
angles.

DOLL, P.; FINK, G.; GARRETT, R.; KLAGES, H.O.
A ΔE-E telescope system for the detection of
charged particles from neutron induced
reactions.

DOLL, P.; GARRETT, R.; HEERINGA, W.; HOFMANN,
K.; KLAGES, H.O.; KRUPP, H.; WILCZYNSKI, J.
Measurement of the spin correlation parameter
A sub(yy) of the elastic n-p scattering
between 20 and 50 MeV.

DOLL, P.; GARRETT, R.; KLAGES, H.O.; KRUPP,
H.
Test of MWPC's for detection of charged
particles produced in neutron induced
reactions.

DOLL, P.; HALE, G.M.; HEERINGA, W.; HOFMANN,
K.; JANY, P.; KLAGES, H.O.; KRUPP, H.; MAIER,
CHR.; WILCZYNSKI, J.
Analyzing power of the elastic nsupra(+)-^{3}He
scattering and phase shift analyses in the
n-^{3}He system at low energies.

DREXLIN, G.; KIONTKE, S.; MASCHUW, R.;
PLISCHKE, P.; REUSCHER, M.; SCHULZ, R.;
WOCHELE, J.
Prototypuntersuchungen fuer den
KARMEN-Detektor.

EYRICH, W.; GILS, H.J.; GOTTSCHALK, G.;
HOFMANN, A.; REBEL, H.; MUEHLDORFER, B.;
SCHLOESSER, H.
Untersuchung der Riesenresonanzen der
Sn-Isotope mit Hilfe von ^{6}Li-Streuung.

GEMMEKE, H.; GRANDEGGER, W.; MASCHUW, R.;
PLISCHKE, P.
n-Nachweis mit Gadolinium im
Neutrino-Detektor.

GEMMEKE, H.; GRIMM, A.; KLEINFELLER, J.;
MASCHUW, R.; MOMAYEZI, M.; RAUPP, F.
Eigenschaften des ν-Detektors KARMEN.

GEMMEKE, H.; KIONTKE, S.; MASCHUW, R.;
REMANE, E.; SCHMIDT, F.K.
Untersuchungen von fluessigen Szintillatoren
fuer grossvolumige Detektoren.

GILS, H.J.; BUSCHMANN, J.; ZAGROMSKI, S.;
JELITTO, H.; REBEL, H.; SCHLOESSER, H.
Erste Ergebnisse mit dem Karlsruher
Magnetspektrographen 'Little John'.

GIORGINIS, G.; MASCHUW, R.; OTTMANN, H.K.;
ZEITNITZ, B.
Ein LAr-Testmodul fuer den ν+e
KARMEN-Detektor.

GYLES, W.; BOSCHITZ, E.T.; MATHIE, E.L.;
OTTERMANN, C.R.; SMITH, G.R.; MANGO, S.;
KONTER, J.A.; MATSUYAMA, A.; JOHNSON, R.R.;
OLSZEWSKI, R.
First measurements of iT$_{11}$ in the pion
deuteron breakup reaction.

HABFAST, C.; GIRARDINI, M.; HUETTEN, L.;
PONCET, A.; POTH, H.; SELIGMANN, B.; WOLF, A.

Das Ultrahochvakuumsystem des
Elektronenkuehlers fuer LEAR.

HARMS, V.; GABELMANN, H.; KRATZ, K.L.; LEIST,
B.; WIESCHER, M.; KAEPPELER, F.; GOERRES, J.
Untersuchung p-ungebundener Zustaende in ^{22}Mg
und ^{26}Si.

HUELSMANN, B.; STAUBER, K.; VOETISCH, D.;
BOETTCHER, J.; FINCKH, E.; KRETSCHMER, W.;
MASCHUW, R.
Entwicklung des Antizaehlers fuer das
KARMEN-Projekt.

KANERT, W.; HARTMANN, F.J.; DANIEL, H.;
EGIDY, T.VON; MOSER, E.; SCHMIDT, G.;
NICHOLAS, M.; REIDY, J.J.; LEON, M.; BUECHE,
G.; HANCOCK, A.D.; KOCH, H.; KOEHLER, TH.;
POTH, H.; KREISSL, A.; RAICH, U.; ROHMANN,
D.; CHARDALAS, M.; DEDOUSSIS, S.; SUFFERT,
M.; NILSSON, A.
Antiprotonisches Molybdaen:
E2-Kernresonanzeffekt und Restkernverteilung
nach Antiprotonannihilation im Kern.

KHAN, S.; KIHM, TH.; KNOEPFLE, K.T.; MAIRLE,
G.; BECHTOLD, V.; FRIEDRICH, L.
Die (d, ^{3}He)-Reaktion an supra(32,34,36)S und
eine Systematik der Bindungsenergien in der
(s,d)-Schale.

KOZIK, T.; BUSCHMANN, J.; GILS, H.J.;
GROTOWSKI, K.; KLEWE-NEBENIUS, H.; PLANETA,
R.; REBEL, H.
Experimental study of massive transfer to the
projectile in ^{6}Li induced reactions at
Esub(Li) = 156 MeV.

KREISSL, A.; BUECHE, G.; HANCOCK, A.D.; KOCH,
H.; KOEHLER, TH.; POTH, H.; ROHMANN, D.;
RAICH, U.; FINDEISEN, CH.; TAUSCHER, L.;
NILSSON, A.; SUFFERT, M.; CHARDALAS, M.;
DEDOUSSIS, S.; EGIDY, T.VON; HARTMANN, F.J.;
KANERT, W.; SCHMIDT, C.; REIDY, J.J.; WOLF,
A.
Bestimmung des magnetischen Momentes und der
Masse des Antiprotons und LS-Effekte der
starken Wechselwirkung in antiprotonischem Ba
138.

LIEWEHR, W.; KAELBER, W.; BECK, K.; MEISEL,
G.; REBEL, H.
Isotopieverschiebung und Hyperfeinstruktur
von Am- und Eu-Isotopen mittels
optogalvanischer Laserspektroskopie.

LIST, W.; BOSCHITZ, E.T.; GARCILAZO, H.;
GYLES, W.; OTTERMANN, C.R.; TACIK, T.;
JOHNSON, R.R.; SMITH, G.R.
Messung des differentiellen
Wirkungsquerschnittes in der elastischen π⁺-d
Streuung unter Rueckwaertswinkel.

MASCHUW, R.; PLISCHKE, P.; REUSCHER, M.;
ZEITNITZ, B.
Empfindlichkeit des KARMEN Detektors auf
Oszillation.

MICEK, S.; MAJKA, Z.; REBEL, H.; GILS, H.J.;
KLEWE-NEBENIUS, H.
Das optische Potential fuer die elastische
Streuung von ^{6}Li-Ionen an ^{6}Li bei 156 MeV.

MUEHLDORFER, B.; EYRICH, W.; FUCHS, K.;
HOFMANN, A.; REBEL, H.; SCHEIB, U.;
SCHLOESSER, H.
Untersuchung des n-Zerfalls der
Riesenresonanzen in ^{90}Zr nach ^{6}Li-Anregung.

OLSZEWSKI, R.; BARAN, R.; HOFMANN, A.; KRELL,
S.; ORTNER, H.W.; ORZECHOWSKY, J.;
SCHMIDTLEIN, G.; VOGLER, F.; DEHNHARD, D.;
LIST, W.; SMITH, G.R.

(π,π',γ)-Winkelkorrelationen im Bereich der (3,3)-Resonanz.

OTTERMANN, C.R.; BOSCHITZ, E.T.; GYLES, W.; LIST, W.; MATHIE, E.L.; SMITH, G.R.; MANGO, S.; KONTER, J.A.; VAN DEN BRANDT, B.; JOHNSON, R.R.; OLSZEWSKI, R.
Untersuchung der Vektoranalysierstaerke iT_{11} in der $\pi d \rightarrow 2p$ Reaktion zwischen 112 und 325 MeV.

POTH, H.; SOERENSEN, A.H.; WOLF, A.
Computer-Simulation zur Abschaetzung der Leistungsfaehigkeit der Elektronenkuehlung in Speicherringen.

ROESCH, W.; BRENDEL, C.; RICHTER, A.; SCHRIEDER, G.; GENTNER, R.; KELLER, K.; LASSEN, L.; LUECKING, W.; SCHRECK, R.; GEMMEKE, H.; SCHUELL, D.
Praeaequilibriumsemission von Nukleonen fuer das System $^{40}Ar + {}^{40}Ca$ bei 20 MeV/amu.

ROHMANN, D.; BUECHE, G.; HANCOCK, A.D.; KOCH, H.; KOEHLER, TH.; KREISSL, A.; POTH, H.; RAICH, U.; FINDEISEN, CH.; TAUSCHER, L.; NILSSON, A.; SUFFERT, M.; CHARDALAS, M.; DEDOUSSIS, S.; EGIDY, T.VON; HARTMANN, F.J.; KANERT, W.; SCHMIDT, G.; REIDY, J.J.; WOLF, A.
Starke Wechselwirkungseffekte an leichten antiprotonischen Atomen.

SRIVASTAVA, D.K.; REBEL, H.
A prior-interaction distorted waves Born approximation theory for break-up of light ions.

SRIVASTAVA, D.K.; REBEL, H.; DICKHOFF, W.H.; MUETHER, H.
Evidence for a dynamic density dependence of the alpha-nucleon force in excitations of collective nuclear states by alpha-particle scattering.

TACIK, R.; GYLES, W.; LIST, W.; OTTERMANN, C.R.
Search for the two step pion absorption mechanism $^{12}C(\pi^+,\pi^+p) \rightarrow {}^{11}B(\pi^+,2p)$.

VAN DEN BRANDT, B.; KONTER, J.A.; MANGO, S.; OTTERMANN, C.R.
A polarized target for π-d experiments.

WALTER, G.; LEUGERS, B.; KAEPPELER, F.; BEER, H.; REFFO, G.; FABBRI, F.
Die s-Prozess-Verzweigungen am ^{79}Se und ^{85}Kr.

1st Internat.Symp.on Calcium and Hypertension, Siena, I, March 15-16, 1985

SPIEKER, C.; HECK, D.; ZIDEK, W.; LOSSE, H.; VETTER, H.
Ca-metabolism in arteries of spontaneously hypertensive rats - assessment by proton induced X-ray emission (PIXE).

Moriond Meeting on Nucleosynthesis: its Implications on Nuclear and Particle Physics, Les Arcs, F, March 17-23, 1985

BEER, H.
s-process nucleosynthesis below A=90.

KAEPPELER, F.
s-process nucleosynthesis - stellar aspects and the classical model.

Fruehjahrstagung DPG, Molekuelphysik, Massenspektrometrie, Oberflaechenphysik,

Kurzzeitphysik, Plasmaphysik, Quantenoptik, Bayreuth, 25.-29.Maerz 1985.
Verhandlungen der Deutschen Physikalischen Gesellschaft, R.6, Bd.20(1985)

SCHULTHEISS, C.; ROGNER, A.
Die 'Rutherford-Shadowbox' - ein neues Hilfsmittel zur Strahldiagnose.

Workshop on Nuclear and Particle Physics at Intermediate Energies with Hadrons, Trieste, I, April 1-3, 1985

KOCH, H.; BLUEM, P.; SCHAFFER, G.; SCHECK, F.
Towards an European hadron facility.

2nd European Conf.on Atomic and Molecular Physics, Amsterdam, NL, April 14-19, 1985

ANSELMENT, M.; CHONGKUM, S.; HANSER, A.; GOERING, S.; MEISEL, G.; REBEL, H.
Laserspectroscopy of stable and unstable strontium isotopes.

LIEWEHR, W.; KAELBER, W.; BEKK, K.; MEISEL, G.; REBEL, H.
Optogalvanic laserspectroscopy of ^{243}Am.

91.Tagung der Deutschen Gesellschaft fuer Innere Medizin, Wiesbaden, 16.-18.April 1985

SPIEKER, C.; HECK, D.; ZIDEK, W.; VETTER, H.; LOSSE, H.
Ca^{2+} in der Arterienwand spontanhypertoner Ratten - Nachweis durch PIXE (Protonen-induzierte Roentgenstrahlung).

General Meeting of the American Physical Society, Washington, D.C., April 25-27, 1985

MARTOFF, C.J.; POCANIC, D.; WHITLOW, L.W.; HANNA, S.S.; ULLRICH, H.; CIERJACKS, S.; FURIC, M.; PETKOVIC, T.
Search for emission of nucleons and nucleon pairs following muon capture in selected light nuclei.

Internat.Conf.on Nuclear Data for Basic and Applied Science, Santa Fe, N.M., May 13-17, 1985

DIERCKX, R.; KLEY, W.; VERGA, A.; BENTON, E.V.; BUSCHMANN, J.
The interaction of deuterons with lithium.

KLAGES, H.O.
Few-nucleon experiments with fast polarized neutrons.

KLAGES, H.O.
Neutron-deuteron studies in the energy range up to 50 MeV.

KLAGES, H.O.
The Karlsruhe polarized neutron facility POLKA.

WISSHAK, K.; KAEPPELER, F.
A 4π barium-fluoride detector for high precision measurements of neutron capture cross sections in the keV range.

Workshop on Nuclear Astrophysics, Ringberg Castle, Tegernsee, May 20-24, 1985

BEER, H.
Analysis of branchings with a pulsed s-process model.

3rd Internat.Symp. 'Mesons and Light Nuclei',
Rez/Prag, CSSR, May 27 - June 1, 1985

BOSCHITZ, E.
The interaction of pions with deuterons.

MARTOFF, C.J.; POCANIC, D.; WHITLOW, L.W.;
HANNA, S.S.; ULLRICH, H.; CIERJACKS, S.;
FURIC, M.; PETKOVIC, T.; WEYER, H.J.
Search for emission of nucleons and nucleon
pairs following muon capture in selected
light nuclei.

WEYER, H.J.; BACKENSTOSS, G.; IZYCKI, M.;
SALVISBERG, P.; STEINACHER, M.; WEBER, P.;
CIERJACKS, S.; LJUNGFELT, S.; ULLRICH, H.;
FURIC, M.; PETKOVIC, T.
π-absorption in ^{3}He.

19th Annual Conf.on Trace Substances in
Environmental Health, Columbia, Mo., June
3-6, 1985

SPIEKER, C.; HECK, D.; ZIDEK, W.; ZUMKLEY,
H.; LOSSE, H.; VETTER, H.
The assessment of trace-elements in organic
tissue by proton-induced X-ray-emission
(PIXE).

Internat.Conf.on Analytical Chemistry in
Nuclear Technology, Karlsruhe, June 3-6, 1985

OTTMAR, H.; EBERLE, H.; MATUSSEK, P.;
MICHEL-PIPER, I.
How to simplify the analytics for
input-output accountability measurements in a
reprocessing plant.

10th European Symp.on the Dynamics of Few
Body Systems, Balatonfuered, H, June 3-7,
1985

BECK, R.; DICKMANN, F.; LOVAS, R.G.
Appraisal of macroscopic cluster models.

BECK, R.; DICKMANN, F.; KRUPPA, A.T.; LOVAS,
R.G.
Decomposition properties of ^{6}Li.

BRADY, F.P.; DOLL, P.; FINK, G.; GARRETT, R.;
HEERINGA, W.; HOFMANN, K.; KLAGES, H.O.;
KRUPP, H.; WILCZYNSKI, J.
Status of n-p measurements and phase-shift
analyses up to 50 MeV neutron energy.

DOLL, P.; GARRETT, R.; HEERINGA, W.; HOFMANN,
K.; KLAGES, H.O.; KOIKE, Y.; KRUPP, H.;
NITZ, W.
Neutron-deuteron experiments in the energy
range up to 50 MeV.

2nd European Meeting on Hypertension, Milano,
I, June 9-12, 1985

SPIEKER, C.; HECK, D.; ZIDEK, W.; LOSSE, H.;
VETTER, H.
Ca^{2+} analysis in arteries of spontaneously
hypertensive rats by proton induced X-ray
emission.

4th Internat.Conf.on Nuclear Reaction
Mechanisms, Varenna, I, June 10-15, 1985

PLANETA, R.; KLEWE-NEBENIUS, H.; BUSCHMANN,
J.; KOZIK, T.; GILS, H.J.; REBEL, H.;
GROTOWSKI, K.
The nonelastic projectile break up cross
section associated with γ-ray emission in ^{6}Li
+ ^{40}Ca collisions at 156 MeV.

SRIVASTAVA, D.K.; REBEL, H.
A prior interaction DWBA for direct break-up
of light-ions.

Workshop on Advanced Methods in the
Evaluation of Nuclear Scattering Data,
Berlin, June 18-20, 1985

GILS, H.J.
Impact of Fourier-Bessel analyses on studies
of composite particle scattering.

NN-N⁻ Interaction Workshop,
Bad Honnef, June 18-21, 1985

POTH, H.
Recent results from antiprotonic atoms at
LEAR.

8.   PERSONNEL

Head of the Institute IK I: Prof.Dr.Bernhard Zeitnitz

Scientific and Technical staff:

Apel, W.-D., Dr.	Lutz, R., Ing.
Beiner, A.	Maier, Chr.,DP
Deutsch, G.	Mann, D.
Dittmann, R.	Maschuw, R., Dr.
Doll, P., Dr.	Momayezi, M.
Drexlin, G.	Müller, C.
Eberhard, V.	Müller, H., Dr.
Engler, J., Dr.	Nitz, W.
Flügge, G., Prof.Dr.	Ottmann, K.H.
Fries, D.C., Dr.	Panter, M., Dr.
Gamerdinger, K., DP	Plischke, P., Dr.
Gemmeke, H., Dr.	Ranitzsch, K.H., Dr.
Giorginis, G., Dr.	Raupp, F., DP
Grandegger, W.	Reppenhagen, D.
Grimm, A.	Reuscher, M., DP
Grosse-Wiesmann, P., DP	Schmalz, G., DI
Gumbsheimer, R., DI(FH)	Schmidt, F.K., Dr.
Hagert, H.	Schneider, H., Dr.
Hansmeyer, J., DP	Schnell, R.
Henkes, Th., DP	Schulz, R.
Heeringa, W., Dr.	Skacel, H.
Hesselbarth, J.	Spohrer, G.
Hofmann, K., DP	Völker, G.
Hopp, G., Dr.	Wild, B.
Hucker, H.	Wild, P.
Husson, L., Ing.	Wochele, J., DP
Jany, P.	Wolf, J.
Jung, J.	Ziegler, P.
Keim, H., Ing.	
Kiontke, S., DP	Guest scientists:
Klages, H.O., Dr.	Garrett, R., Prof.Dr.
Kleinfeller, J., Dr.	Univ. of Auckland, New Zealand
Knapp, J., DP	
Krüger, M., DP	
Krupp, H., DP	
Küster, H., DP	

Head of the Section IK II: Prof. Dr. Anselm Citron

Scientific and Technical staff:

Aker, E., DP

Bacher, R., DP

Barth, H.

Blüm, P., Dr.

Boschitz, E., Prof. Dr.

Budig, H.

Büche, G., Dr.

Bürker, L.

Cierjacks, S., Dr.

Engelhardt, D., Prof. Dr.

Garcilazo, H., Prof. Dr.

Göring, K. P.

Gotta, D., Dr.

Gyles, W., Dr.

Habfast, C., DP

Heitlinger, K.

Hilgendorff, H.

Höhne, A.

Jödicke, B.

Kärcher, K.

Klein, U., DP

Kluge, W., Prof. Dr.

Kunze, M.

Koch, H., Prof. Dr.

Köhler, T., DP

Kreissl, A., DP

List, W., DP

Matthäy, H., Dr.

Metzler, M.

Ottermann, C.R., Dr.

Poth, H., Dr.

Rohmann, D., Dr.

Rohrbach, W., Dr.

Rzehorz, R.

Schneider, M., DP

Schott, W., DP

Seligmann, B., DP

Simons, L. M., Dr.

Stoll, M.

Tacik, R.

Ullrich, H., Prof. Dr.

Walther, D., DP

Weddigen, Ch., Prof. Dr.

Wiedner, U., DP

Wolf, A., DP

Zach, G.

Guest scientists:

Furić, M., Prof. Dr., U. of Zagreb, YU

Petković, T., U. of Zagreb, YU

Powers, R., Dr., Arete Assoc., Pasadena, USA

Simicevic, N., DP, U. of Zagreb, YU

Head of the Section IK III: Prof. Dr. Gerhard Schatz

Scientific and Technical staff:

Anselment, M., DP

Beck, R., Dr.

Beer, H., Dr.

Bekk, K., Dr.

Buschmann, J., Dr.

Dennerlein, H.-D.

Dickmann, F., Dr.

Dürrschnabel, D.

Eberle, H., Ing.

Feurer, B.

Friederich, H.M.

Gils, H.J., Dr.

Göring, S., Dr.

Hanser, A., Dr.

Heck, D., Dr.

Jelitto, H., DP

Käppeler, F., Dr.

Kiener, J.

Liewehr, W., DP

Lingenfelder, B.

Matussek, P., DP

Meisel, G., Dr.

Michel-Piper, I. DI(FH)

Müller, H.

Oehlschläger, J., D.-Math.

Ottmar, H., Dr.

Rebel, H.G., Prof. Dr.

Rupp, G.

Schmidt, K.A., DP

Voss, F., Dr.

Walter, G., DP

Wisshak, K., Dr.

Zagromski, S., DI(FH)

Guest scientists:

Bao, Z., Dr.

Chongkum, S., DP

Daniels, T.

Dembczyński, J., Prof.Dr.

Kozik, T., Dr.

Krivec, R.

Samanta, S., Dr.

Srivastava, D.K., Dr.

Head of the Cyclotron Laboratory: Dr. Hermann Schweickert

Scientific and Technical staff:

Acharja, H.

Assmus, K.

Augstein, S.

Bauer, G.

Bechtold, V., Dr.

Bialy, J., DP

Biber, J.

Blank, R.

Bollmann, E., DP

Daniels, T.

Dohrmann, H., Ing.

Dressen, R.

Ehret, H.-P.

Erbe, D.

Erdel, E.

Ernst, R.

Fehsenfeld, P., Dr.

Fischböck, Th.

Foßhag, E., Dr.

Franz, J.

Friedrich, L., Dr.

Gegenheimer, B.

Günther, O.

Haßpacher, G.

Haushahn, G., DP

Heger, V.

Heidenreich, K.

Heneka, C.

Heinzmann, H., DI

Heitz, E.

Herrmann, P.

Hirth, W.

Holler, H.

Hüfner, R., Dr.

Huttel, E., Dr.

Jänisch, M.

Kaltenbaek, J.

Kappel, W.-R., Ing.

Kauther, P.

Kernert, N., DP

Kessel, M.

Kirste, E.

Kleinrahm, J., Dr.

Klinger, G.

Kögel, B.

Konrad, J.

Krieg, U.

Lang, R.

Maier, W.

Mangold, D.

Mayl, R.

Mirasch, U.

Möck, W.

Möllenbeck, J., Ing.

Peters, J., DP

Pfeifer, R.

Pfeiffer, B., Dr.

Rämer, Ch., Ing.

Reißle, S.

Ripp, H.

Roth, H.

Sahm, U., Dr.

Seidel, H.

Seidler, M.

Seitz, J.

Seufert, H.

Sheikh, S.

Schimpf, P.

Schmitt, M.

Schönstein, E.

Schüssler, B.

Schütz, R.

Schulz, F., Ing.

Schweickert, H., Dr.

Schwindt, E.

Stöbener, E., Ing.

Tischer, M.

Thouw, Th., Dr.

Uchatius, R.

Uhlemann, S.

Wild, H.

Wiss, L.

Ziegler, P.

Zimmermann, H.

Zimmermann, U.